Hawaii Ocean Time-series

Data Report 2

1990

Christopher Winn
Stephen Chiswell
Eric Firing
David Karl
Roger Lukas

School of Ocean and Earth Science and Technology
University of Hawaii
1000 Pope Road
Honolulu, Hawaii 96822
U. S. A.

SOEST-92-1

Preface

The Hawaii Ocean Time-series (HOT) project has been making repeated observations of the hydrography, chemistry, and biology at a station north of Hawaii since October 1988, with the objective of describing the oceanography at a site representative of the central north Pacific Ocean. Cruises are made approximately once a month to the HOT deep-water station (22° 45'N, 158°W) located about 100 km north of Oahu, Hawaii. Measurements of the hydrography, water column chemistry, primary production, and particle sedimentation rates are made over three days.

This document reports the data collected during 1990; however, we have included some data from 1988 and 1989 in order to place the data collected in 1990 within the context of our time-series observations. The data reported here are a screened subset of the complete data set. Summary plots are given for CTD, biogeochemical, optical, meteorological, and ADCP observations.

In order to conserve paper and to provide easy computer access to our data, CTD data at NODC standard pressures for temperature, potential temperature, salinity, oxygen, and potential density are provided in ASCII files on the enclosed diskette. Chemical measurements are summarized in a set of Lotus 1-2-3™ files on the enclosed diskette. A more complete data set resides on a Sun workstation at the University of Hawaii. These data are in ASCII format, and can easily be accessed using anonymous ftp via Internet. Instructions for using the Lotus files and for obtaining the data from the network are presented in Section 7. The entire data set will also be submitted to the National Oceanographic Data Center (NODC) and will be available through that service.

Acknowledgements

Many people have participated in cruises sponsored by the HOT program. They are listed in Table 3.3. We gratefully acknowledge their involvement and support.

Special thanks are due to John Dore, Dale Hebel, Ricardo Letelier, Stewart Reid, Marc Rosen, and Jefrey Snyder for participating in most of the cruises and for the tremendous amount of time and effort they have put into the program. In addition, we would like to acknowledge the contributions made by Sharon DeCarlo for programming and data management, Willa Zhu and Julie Ranada for ADCP processing, and Lance Fujieki for programming and data processing. Fernando Santiago-Mandujano computed the final CTD calibration coefficients. Toshiaki Shinoda helped with the quality controlling of the WOCE bottle data. Carl Chun and Nava Zvaig provided additional computer support. Ursula Magaard performed many routine chemical analyses, including Winkler titrations. Ted Walsh and Gerald Akiyama performed the salinity and nutrient analyses. Without the assistance of these people, the data presented in this report could not have been collected, processed and analyzed. We would like to thank Anne Shure for producing this document.

Oxygen data obtained by Dr. Steve Emerson from the University of Washington on HOT-14 were used to calibrate CTD 0_2.

We also would like to thank the captains and crew members of the R/V MOANA WAVE, SSP KAIMALINO, and R/V WECOMA for their efforts.

This data set was acquired under National Science Foundation (NSF) grants OCE-8717195 (WOCE), OCE-8800329 (JGOFS), and OCE-9016090 (JGOFS). Ship time on the SSP KAIMALINO was partially supported by the National Oceanic and Atmospheric Administration (NOAA).

1. Introduction

In 1987, the National Science Foundation established a special-focus research initiative termed 'The Global Geosciences Program.' This program is intended to support studies of the earth as a system of interrelated physical, chemical, and biological processes that act together to regulate the habitability of our planet. The stated goals of this program are two-fold. The first goal is to understand the earth-ocean-atmosphere system and how it functions. The second goal is to describe, and eventually predict, major cause-and-effect relationships. Two of the components of the Global Geosciences Program are the World Ocean Circulation Experiment (WOCE) and the Joint Global Ocean Flux Study (JGOFS) programs. The former is focused on physical oceanographic processes and the latter on biogeochemical processes.

The Hawaii Ocean Time-series (HOT) project has been funded under the sponsorship of the WOCE and JGOFS programs to make repeated observations of the hydrography, chemistry, and biology for five years at a station north of Hawaii. The objectives of HOT are to describe the physical oceanography, and to identify and quantify the processes controlling biogeochemical cycling in the ocean at a site representative of the central North Pacific Ocean.

The HOT deep-water station, also known as Station ALOHA (A Long-term Oligotrophic Habitat Assessment), is about 100 km north of Kahuku Point, Oahu, Hawaii (Figure 1.1). The nominal deep-water station is at 22°45' N, 158°W, and is defined as a 10-km radius circle centered on this position. Every effort is made to sample within this circle, especially during the 36-

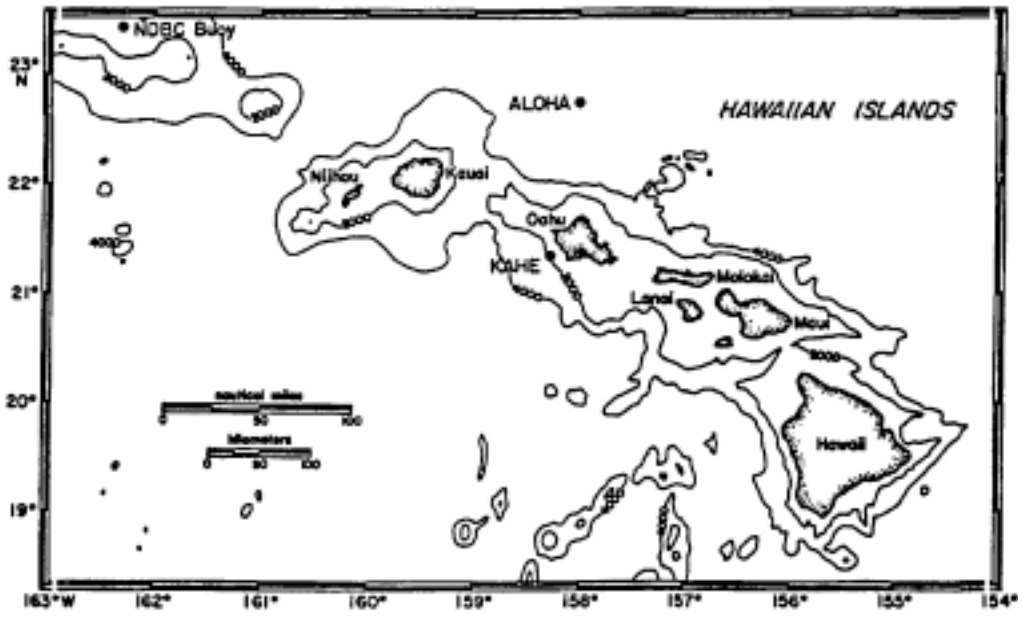

Figure 1.1: Map of Hawaiian Islands, showing Station ALOHA, the Kahe Point Station and NDBC Buoy. Isobaths are in meters.

hour burst of CTD sampling. The maximum depth at Station ALOHA is 4750 m. A station is also occupied at 21°20.6' N, 158°16.4' W, near Kahe Point, Oahu, during the transit from Honolulu to Station ALOHA. The Kahe Point station is used primarily to test the CTD and other equipment, but it also provides additional time-series data at a near-shore site. The Kahe Point station is located in approximately 1500 m of water about 16 km from shore.

Time-series cruises are made at approximately monthly intervals. Approximately 3 to 4 hours are spent at the Kahe Point Station, and about 72 hours are spent at Station ALOHA during each cruise. The cruise length is dictated by the minimum time necessary to obtain reasonable estimates of particle flux using the free-floating sediment traps deployed at Station ALOHA. The JGOFS and WOCE components of the program measure a variety of parameters during the regular monthly sampling work at Station ALOHA (Table 1.1). JGOFS sampling work includes primary production, particle flux, a variety of chemical determinations at discrete depths, as well as continuous profiles of optical parameters. WOCE sampling includes a 36-hour burst of CTD casts at roughly 3-hour intervals to obtain temperature, salinity, and oxygen profiles from O-1000 dbars. WOCE sampling also includes a monthly deep CTD cast as close to the bottom as possible within safe operating conditions. Current velocity measurements are made on HOT cruises using a shipboard Acoustic Doppler Current Profiler (ADCP) when a ship having the necessary equipment is used for monthly cruises. In addition, lowered ADCP measurements have been made on several HOT cruises.

This report presents data collected during the second year of the HOT Program (January-December 1990). During this period, 10 cruises were conducted using four research vessels (Table 3.1). The R/V MOANA WAVE and R/V WECOMA are UNOLS vessels operated by the University of Hawaii and Oregon State University, respectively. The SSP KAIMALINO is a U.S. Navy vessel operated by a private contractor, and the NA'INA is a privately-owned vessel home-ported in Honolulu.

2. Sampling Procedures and Analytical Methods

2.1. CTD Profiling

CTD data were collected with a Sea-Bird SBE-09 CTD, which has an internal Digiquartz pressure sensor and external temperature, conductivity, and oxygen sensors. The Sea-Bird temperature-conductivity duct, which is used to circulate seawater through both the temperature and conductivity sensors, was used on all cruises during 1990. The CTD was mounted in a rosette sampler, and the package was deployed on a conducting cable, which allowed for real-time data acquisition and data display. Water samples were taken on the upcasts for chemical analyses, and for calibration of the conductivity and oxygen sensors. A Sea-Tech flash fluorometer was also incorporated in the CTD package during 1990.

Table 1.1: Time-series Parameters Measured at Station ALOHA

Parameters	Depth Range (m)	Analytical Procedure
I. CTD Measurements		
Temperature	0-4750	Thermistor on Sea-Bird CTD package with frequent calibration
Salinity	0-4750	Conductivity sensor on Sea-Bird CTD package, standardization with AGE inductive Salinometer against Wormley water
Oxygen	0-4750	Polarographic sensor on Sea-Bird CTD package with Winkler standardization
Fluorescence	0-1000	Sea-Tech Flash Fluorometer on Sea-Bird CTD package
II Optical Measurements		
solar radiance (PAR)	Surface	Licor Cosine Collector and Biospherical 2 pi Collector
underwater irradiance (PAR)	0-150	Biospherical Profiling Natural Fluorometer 4 pi Collector
solar stimulated fluorescence	0-150	Biospherical Profiling Natural Fluorometer
III Water Column Chemical Measurements		
Oxygen	0-4750	Winkler Titration
total dissolved carbon dioxide	0-4750	Coulometry
dissolved inorganic nitrate plus nitrite	0-4750	Autoanalyzer
total dissolved phosphorus	0-4750	Autoanalyzer
total dissolved silica	0-4750	Autoanalyzer
dissolved organic carbon	0-1000	Persulfate wet oxidation
total dissolved nitrogen	0-1000	U.V. oxidation
total dissolved phosphorus	0-1000	U.V. oxidation
particulate carbon	0-1000	High temperature combustion
particulate nitrogen	0-1000	High temperature combustion
Particulate phosphorus	0-1000	High temperature combustion
IV. Water Column Biomass Measurements		
chlorophyll *a* and phaeopigiments	0-200	Fluorometric Analysis / High Pressure Liquid Chromatography
adenosine 5'-triphospate	0-1000	Firefly Bioluminescence
picoplankton / nanoplankton	0-1000	Epifluorescence Microscopy
V. Carbon Assimilation and Particle Flux		
primary production	0-200	"clean" ^{14}C incubations
carbon, nitrogen, phosphorus, and mass flux	150,300,500	Free-Floating Particle Interceptor Traps
VI. Currents		
acoustic Doppler Current Profiler	0-300	Hull mounted
acoustic Doppler Current Profiler	0-4750	Lowered

A CTD cast to approximately 1000 dbar was made at the Kahe Point Station on each cruise. At Station ALOHA, a burst of consecutive CTD casts to 1000 dbar was made over 36 hours to span the local inertial period (~31 hours) and three semi-diurnal tidal cycles. This sampling was designed so that energetic tidal and near-inertial variability during each cruise could be averaged to prevent these components from aliasing the longer time-scale signals. In order to satisfy WOCE requirements, one deep cast to near the bottom was made on each cruise. When cruises were made on a ship equipped with a 12-kHz echo sounder, a Benthos acoustic pinger attached to the rosette was used to make the cast to within 50 m of the sea floor (approximately 4750 in). When the research platform was not equipped with an echo sounder, this cast was made to 4500 dbar.

2.1.1. CTD Data Acquisition and Processing

CTD data were acquired at the instrument's highest sampling rate of 24 samples per second. Digital data were stored on a PC-compatible computer and, for redundancy, the analog CTD signal was recorded on VHS video tapes.

A flowchart of the CTD processing is shown in Figure 2.1. The raw data from various sensors (pressure, pressure-sensor temperature, temperature, conductivity, oxygen-sensor current, oxygen-sensor temperature, and fluorescence) were recorded as voltages or frequencies. The first step was to convert these to scientific units (dbar, C, C, S m^{-1}, mA, C, respectively) using laboratory calibrations. The data were then subjected to quality control procedures and preliminary processing. First they were screened for spikes or missing data using a 9-point median filter. After screening, the correct alignment of temperature and conductivity time-series was computed since the lag between temperature and conductivity can change from cruise to cruise, depending on the placement of the sensors. The data were then averaged to half-second values, and the pressure, temperature, conductivity, and oxygen calibration corrections were applied. Salinity and oxygen were then computed in units of psu and μmol kg^{-1}, respectively. Details of these corrections are described in the following sections.

Eddy shed wakes, caused when the rosette entrains water, introduce salinity spikes in the CTD profile data. These contaminated data were handled using an algorithm which eliminated data collected when the CTD's speed was less than 0.25 m s^{-1} or its acceleration was greater than 0.25 m s^{-2} . Finally, the data were averaged into 2 dbar pressure bins.

Temperature is reported here in the ITS-90 scale. Salinity and all derived units were calculated using the UNESCO (1981) routines.

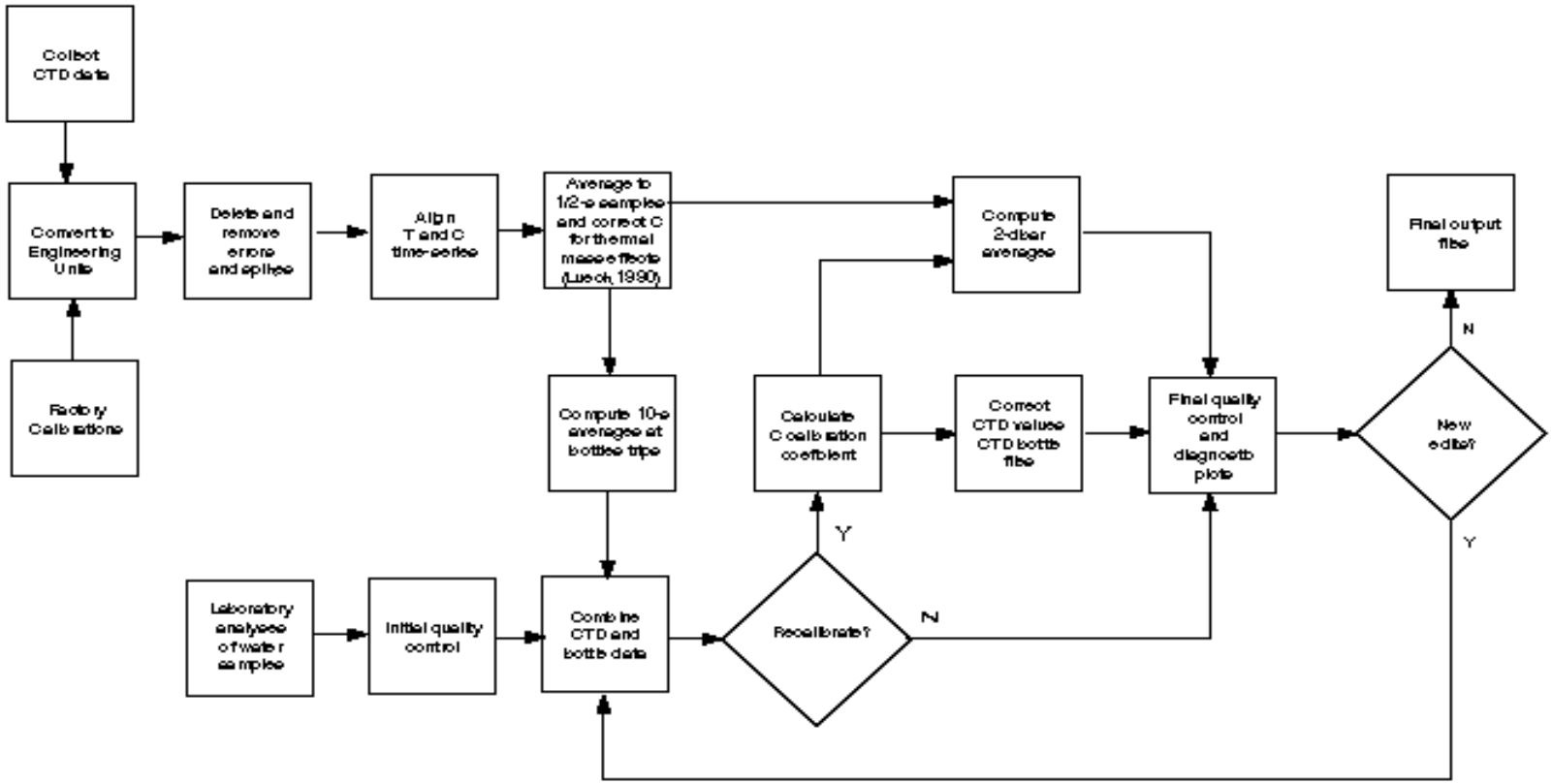

Figure 2.1: Flowchart of CTD data processing.

2.1.2. CTD Sensor Corrections and Calibration

2.1.2.1. Pressure

The pressure calibration strategy employed a high-quality quartz pressure transducer as a transfer standard. Periodic recalibrations of this lab standard were performed with a primary pressure standard. A Russka precision dead-weight pressure tester with weights meeting National Bureau of Standards specifications, operated under environmentally-controlled conditions, was used as a primary standard. The transfer standard was used to check the CTD pressure transducers at six-month intervals.

Pressure Standard Calibration

We used a Paroscientific Model 760 pressure gauge, which has a 10,000 psi Digiquartz pressure transducer, as a transfer standard This instrument was purchased in March 1988, and the original calibration was done at Paroscientific against a primary standard in their laboratory.

Our transfer standard was recalibrated by the Oceanographic Data Facility at Scripps Institution of Oceanography against their primary standard on 16 May 1991. The offset at 0 dbar from the original calibration was 0.3 dbar, and there was a 0.6 dbar increase in the pressure difference (our standard reading high) over the range 0-4500 dbar. (There is some reason to believe that this change in offset and slope of the pressure standard occurred as a result of shipping from Honolulu to San Diego. The changes with time of the offset and slope of both our primary and backup CTD pressure transducers are consistent with this interpretation, as discussed below.) Hysteresis was less than 0.1 dbar throughout the entire range.

JIMAR Laboratory Calibrations

In-house calibrations for pressure were done using a dead-weight pressure tester and a manifold to apply pressure simultaneously to the CTD pressure transducer and to the transfer standard. All of our laboratory calibrations had at least 6 points over the pressure range, which is from 0 dbar to between 4500 and 5000 dbar. In addition, recent calibrations include more points taken during the removal of pressure in order to estimate hysteresis.

The internal pressure transducer in our CTD #1 (Sea-Bird #91361; pressure transducer #26448) was calibrated at the NOAA Northwest Regional Calibration Center (NWRCC) at the time of manufacture in 1987. Subsequent calibrations against the transfer standard using this original calibration are given in Table 2.1. These results show that the bias of this pressure transducer changed by between 0.7 and 1.0 dbar over one year, with the uncertainty due to the unknown shape of the transfer standard drift. The change in calibration of the transfer standard seems to have occurred during the shipping to Scripps; if the bias and slope changes are applied to the standard only for the June 1991 calibration at JIMAR, the difference in slope between lab standard and CTD pressure transducer is consistent with that measured in February 1991, and with the trend over all calibrations.

The external pressure transducer on our CTD #2 (Sea-Bird #92859; pressure transducer #39217) was calibrated at NWRCC at the time of manufacture in 1989. This instrument has been sea-tested, but never used for primary data acquisition. Calibrations against our lab standard are given in Table 2.1. Note again that the consistency between the 26 June 1991 lab calibration and those previous is best when it is assumed that the transfer standard shifted during shipping to Scripps.

Table 2.1: CTD Pressure Calibrations
(all units are in decibars)

Sea-Bird SBE-09 #91361 / Pressure Transducer #26448

Calibration Date	Offset @ 0 dbar	Slope offset @ max pressure	Hysteresis
10 May 1989	-1.1	-0.6 @ 4500	N/A
10 July 1990	-1.65	-0.8 @ 5000	0.2
20 February 1991	-2.15	-0.9 @ 4800	0.25
27 June 1991	-2.7	-0.3 @ 4600	0.2
	-2.4*	-0.9 @ 4600*	0.2

Sea-Bird SBE-09 #92859 / Pressure Transducer #39217

Calibration Date	Offset @ 0 dbar	Slope offset @ max pressure	Hysteresis
20 July 1990	-1.05	-0.1 @ 5000	N/A
22 February 1991	-0.8	-0.5 @ 4800	N/A
26 June 1991	-0.6	0.0 @ 4500	0.8
	-0.9*	-0.6 @ 4500*	0.8

*Adjusted for shift in lab pressure standard calibrated 16 May 1991 at SIO/ODF.

Dynamic Calibration

As described by Chiswell (1991), the indicated pressure from each profile was corrected for errors due to thermal disequilibrium during profiling. While the pressure error from this source can reach 7 dbar for sensor #91361, the correction is good to better than 0.5 dbar. In September and October 1991, Sea-Bird upgraded our pressure transducers, virtually eliminating the thermal disequilibrium problem.

2.1.2.2. Temperature

Our strategy for CTD temperature calibration also relied upon the use of a transfer standard periodically recalibrated at a primary calibration center using techniques traceable to the National Bureau of Standards. We used three Sea-Bird SBE-3-02/F temperature transducers, serial numbers 741, 886, and 961. These transducers are returned to Sea-Bird approximately once per year (recently increased to twice per year) for calibration by the NWRCC. The frequency of recalibration is a trade-off between confidence in the behavior of the sensor with time versus the risk of damage or loss during shipping to and from the calibration center.

Sensor #961 was used only as a transfer standard during intercomparison runs with the other two sensors, both used at sea. These intercomparisons were done between each cruise to provide a check on the nature of the drift of each sensor relative to the transfer standard

Primary calibrations

The calibrations at NWRCC typically have an RMS residual of 0.25—1.0 m°C (Table 2.2). The quality of these calibrations can also be estimated by repeated calibration runs on the same sensor, see the discussion of sensor #961 which follows. Consistent with the extensive experience of Sea-Bird (N. Larson, personal communication, 1991), our sensors have exhibited a tendency towards higher temperature readings with time. Table 2.2 gives the calibration coefficients which were determined by NWRCC measurements.

Sensor #961

Sensor #961 was calibrated on 3 and 10 November 1989, and then again on 12 and 21 December 1990. Within each pair of calibrations, the mean difference between the calibrations over the 0-30°C range was 0.6 and 0.4 m°C, respectively, which is within the uncertainty of the calibrations. The maximum deviations in this temperature range associated with the slope and nonlinear terms in the calibration equation for these calibration pairs were 1.7 and 0.6 m°C, respectively. The comparison of the 13 and 20 October 1989 calibrations shows differences up to 4 m°C, with a mean of 2.8 m°C. This large calibration shift is due to the replacement of an electronic component in the transducer. The quality of prior temperature measurements was not compromised by this shift.

Over the 13 months separating the calibration groups, the sensor drifted by 6.3 m°C. We modeled the drift of sensor #961 as a linear function of time as per the experience of Sea-Bird over many years of working with these sensors. We used the 10 November 1989 calibration as the baseline for 1990 intercomparisons. We corrected temperatures measured at other times by subtracting 1.62×10^{-5} C day^{-1} to estimate the true temperature. Maximum error from changes in the slope and nonlinear terms in the frequency to temperature conversion is estimated to be less than 1 m°C during 1990.

Table 2.2: Calibration Coefficients for Sea-bird Temperature Transducers Determined at Northwest Regional Calibration Center. RMS Residuals from Calibration Give an Indication of Quality of the Calibration.

SN	YYMMDD	f_0	a	b	c	d	**RMS** (m°C)
961	901221	6596.33	3.67427E-3	6.00296E-4	1.50788E-5	1.90332E-6	0.28
961	901212	6555.62	3.67800E-3	6.00590E-4	1.54925E-5	2.33356E-6	0.27
961	891110	6593.31	3.67448E-3	6.00431E-4	1.54701E-5	2.26236E-6	1.42
961	891103	6570.80	3.67652E-3	6.00440E-4	1.54579E-5	2.39329E-6	0.48
961	891020	6584.74	3.67527E-3	6.00530E-4	1.60085E-5	2.99272E-6	0.80
961	891013	6569.50	3.67662E-3	6.00261E-4	1.45637E-5	1.50324E-6	0.26
961	890728	6585.62	3.67515E-3	6.00522E-4	1.58721E-5	2.82023E-6	0.81
886	910621	5734.40	3.67513E-3	5.95897E-4	1.39470E-5	1.18908E-6	0.71
886	901108	5736.72	3.67482E-3	5.95946E-4	1.44577E-5	1.86031E-6	0.72
886	891103	5720.16	3.67652E-3	5.96265E-4	1.52177E-5	2.50123E-6	0.57
886	891013	5719.06	3.67662E.3	5.96299E-4	1.50921E-5	2.19843E-6	0.30
886	881007	5738.95	3.67443E-3	5.96117E-4	1.52143E-5	2.58644E-6	0.42
741	910614	6242.89	3.67392E-3	6.01617E-4	1.44529E-5	1.67976E-6	0.96
741	891103	6215.18	3.67652E-3	6.01685E-4	1.44771E-5	1.74730E-6	0.26
741	870821	6233.01	3.67465E-3	6.01498E-4	1.43227E-5	1.70525E-6	0.37
741	870305	6227.60	3.67516E-3	6.01775E-4	1.52878E-5	2.58641E-6	0.48

Sensor #886

Sensor #886 was calibrated on the dates given in Table 2.2. Relative to the 7 October 1988 original calibration of this sensor, the 0-30°C average offset was 8.4 m°C on 13 October 1989, 10.1 m°C on 3 November 1989, 13.3 m°C on 8 November 1990, and 19 m°C on 21 June 1991. A linear fit to these offsets gives an intercept of 1.2 m°C, with a slope of 1.778 x 10^{-5} °C day^{-1}. The RMS deviation of the offsets from this fit was 1.2 m°C. The baseline calibration was selected by taking the coefficients from each of the calibration runs and applying the linear drift interpolated to 1 June 1990 (the midpoint between HOT cruises 15 and 22 for which this sensor was used). The deviation of each estimate from the ensemble mean was calculated for the temperature range 0-5°C, where accuracy requirements are greatest The June 1991 calibration run had the smallest offset in this range, with less than 1 m°C deviation from the mean over 0-5°C.

The 3 November 1989 calibration was considered to be an outlier because of its relatively large deviation (nearly 2 m°C) from the ensemble mean, and the fit was recomputed. The final intercept and slope for the linear drift are 0.49 m°C and 1.824 x 10^{-5}° C day^{-1}, with an RMS residual of 0.85 m°C. Using the June 1991 calibration as the baseline, interpolating back to 1 June 1990 gives a mean deviation of 0.19 m°C from the 0-5°C range ensemble mean of all the calibrations used, with less than 1 m°C deviation within that range. The November 1990 calibration has a mean deviation of -1.45 m°C in the 0-5°C range, while the October 1989

calibration has a mean deviation of 1.6 m°C. Thus, for the HOT cruises conducted in 1990, we place an error bound of 1.5 m°C on deep water temperatures measured with this sensor.

Sensor #741

The same procedure as used for sensor #886 was applied to sensor #741. The offsets over the range O-30°C from the original calibration of this sensor in March 1987 were 1.6 m°C (21 August 1987), 11.8 m°C (3 November 1989), and 16.8 m°C (14 June 1991). Computing a linear fit to this drift yields an intercept of 8.4 x 10^{-5}° C, a drift of 1.104 x 10^{-5}° C day^{-1}, with an RMS residual of 0.58 m°C. Using each of the calibrations as the baseline, and interpolating to 2 March 1990 (the midpoint between the HOT-13 and -14 cruises for which this sensor was used), estimates of temperature in the range O-5°C were made. The deviation of each calibration from the ensemble mean over this range was less than 1 m°C, with the June 1991 calibration being closest to the mean over most of the range. Thus, we used that calibration as the baseline for 1990 HOT cruises that employed sensor #741. For deep water temperatures, our measurements of temperature with this sensor during 1990 are estimated to be accurate to better than 1 m°C.

Laboratory calibrations

Our laboratory temperature sensor intercomparisons were done in an insulated water bath, using the CTD for data acquisition and sensor power. There was a strong circulation system which draws water from the bottom of the tank and spreads it across the top of the water column. It is unlikely that there were persistent temperature variations within the bath greater than 1 m°C, though we have not made exhaustive tests of this assertion. Short-term variations in temperature differences between sensors were less than ± 0.5 m°C. The bath was initially chilled down to near 0C, the CTD and sensors were inserted, the bath was closed, and over a period of 2 days the system slowly warmed to the lab temperature of 23-25C. An initial period when the temperature of the CTD was coming into equilibrium with the bath (and was acting as heat source) was readily identified. Averaging temperature transducer output over several minutes gave exceptionally stable temperature differences at a variety of bath temperatures.

Using sensor #961 as a reference, with the linear drift correction as described earlier, sensor #886 showed a drift of 1.5 x 10^{-5}° C day^{-1}, with an RMS residual of 0.74 m°C for 8 laboratory intercomparisons. This is compared to the 1.8 x 10^{-5}° C day^{-1} linear drift estimated from the NWRCC calibrations.

Using the corrected #961 as a reference, 4 intercomparisons with sensor #741 showed a linear drift of 1.074 x 10^{-5} °C day^{-1} which is to be compared with the 1.104 x 10^{-5} °C C day^{-1} estimated from the NWRCC calibrations. The corrections applied to sensors #741 and #886 used during the 1990 HOT cruises are given in Table 2.3.

Dynamic comparisons

Temperature sensors #886 and #741 were installed simultaneously on the CTD for tests during HOT-14 in February 1990. There was a mean offset of about 0.2 m°C below 1500 m, with peak-to-peak noise of about 2 m°C. This noise was likely related to horizontal inhomogeneities in the water column, as well as to turbulence created by the rosette frame and instrumentation. Above 1500 m, #741 was cold relative to #886, as much as -7 m°C near 350 m. This offset appeared to be mostly due to a slight physical offset in the vertical, though a variation in response time between the sensors could also have contributed.

Deep water temperature

The calibrated average CTD potential temperature between 4400 and 4500 dbar at the HOT site is given in Figure 2.2 for individual HOT cruises. (The HOT-20 CTD trace did not go this deep.) This pressure range is at least 200 m above the sea floor, so geothermal heating would not be expected to produce a temporal signal, although other natural variations could exist The mean potential temperature is 1.118°C, and the standard deviation is 2.1 m°C. The range is 7 m°C, which seems large for the deep water. However, we believe that our calibrations are good to better than 1.5 m°C (see sections on sensors #886 and #741 in Section 2.1.2.2), and the warming trend from HOT-13 through HOT-17 would appear real. In fact, an increase in temperature from HOT-l0 through HOT-12 is consistent with this trend (Chiswell *et al.*, 1990).

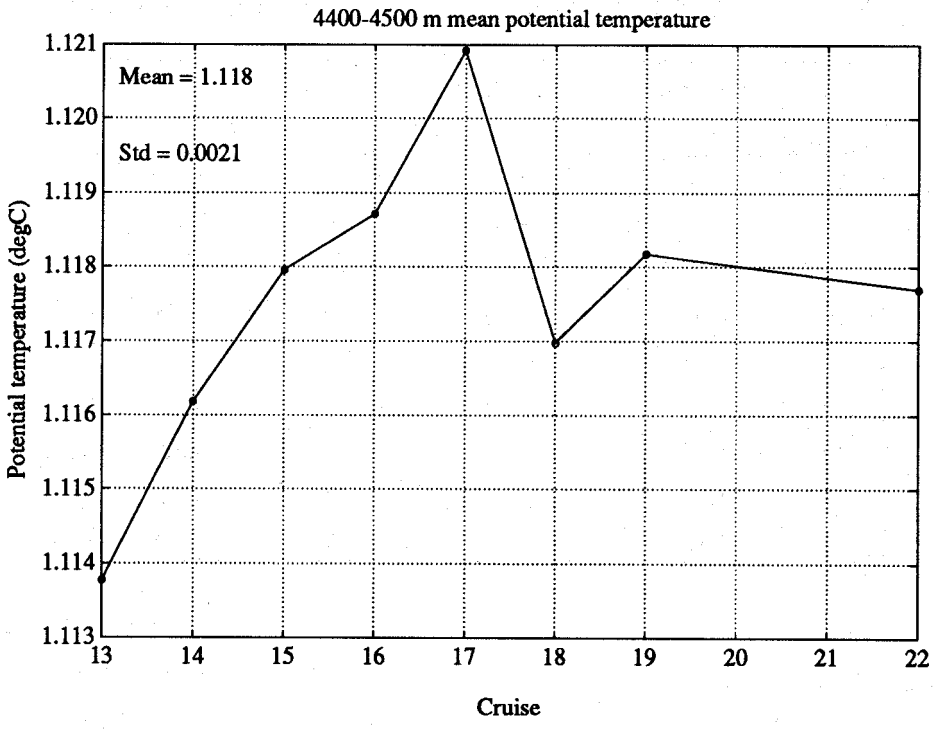

Figure 2.2: Average CTD potential temperature between 4400 and 4500 dbar at the HOT site.

2.1.2.3 Conductivity

The conductivity cell was calibrated periodically at the NWRCC by varying the temperature of a saltwater bath. This was done at two salinities and a variety of temperatures, which allowed for a determination of the explicit temperature dependence of the cell. These calibrations were only used as nominal calibrations for real-time display during data acquisition, and for preliminary quality control. Final calibration was determined empirically by comparison with the salinities of discrete water samples acquired during each cast. Conductivity cells #527 and #679 were used during 1990. Cell #527 was calibrated at NWRCC on October 28, 1988, and again on May 2, 1991. Cell #679 was calibrated on October 13, 1989, and on October 20, 1990.

Conductivity cells were flushed with distilled water and kept wet between casts as recommended by Sea-Bird. We did not notice any consistent drift within a cruise, but we did see a cruise-to-cruise freshening associated with a gradual coating of the inside of the cell. Periodic cleaning of the cell and NWRCC recalibration prevented a substantial deviation from the nominal calibration that we used.

Prior to the empirical calibration of conductivity data with water bottle salinities, conductivity was corrected for the thermal inertia of the glass conductivity cell as described by Chiswell *et al*. (1990). Table 2.3 lists the value of a used for each cruise. No drift corrections were necessary during 1990.

Table 2.3: Temperature and Conductivity Sensor Corrections

HOT	**Temp #**	**T Correction** °C	**Cond #**	**α**
13	741	-0.0057	679	0.045
14	741	-0.0054	679	0.037
15	886	-0.0085	679	0.028
16	886	-0.0080	679	0.028
17	886	-0.0075	679	0.028
18	886	-0.0068	679	0.028
19	886	-0.0061	679	0.028
20	886	-0.0051	679	0.028
22	886	-0.0034	527	0.028

Water sample analysis

Salinity was determined on discrete water samples as described in Section 2.2.1.

Screening of bottle samples

Preliminary screening of the water sample salinities was done by comparing against all previous data deemed good which had been collected at the particular site (Kahe Point or ALOHA). The nominally-calibrated CTD salinity trace was also used to identify questionable discrete samples. Potential rosette mistrip problems were resolved where possible before data were excluded from use in the calibration of the conductivity cell.

After an initial calibration of the conductivity cell using all casts within a cruise, the deviations between CTD salinity and bottle salinity were tested against limits within 4 pressure ranges (3 standard deviations of the ensemble of 'good' data). Bottles were marked as 'suspicious' when the difference exceeded 3 standard deviations, and 'bad' when greater than 4. These bottles were not used in further iterations of the calibration. For HOT-13 to -22 the standard deviations are: 0.0047 psu (0—150 dbar), 0.0061 psu (151—500 dbar), 0.0034 psu (501—1000 dbar), and 0.0012 psu (1001—5000 dbar)

Empirical calibration

Calibration of the conductivity cell was performed empirically by comparing its nominally calibrated output against the calculated conductivity values obtained from water sample salinities using the calibrated pressure and temperature of the CTD at the time of bottle closure. An initial estimate of bias and slope corrections to the nominal calibration were determined from a linear least squares fit to the ensemble of bottle-CTD conductivity differences as a function of conductivity, from all stations and casts during a particular cruise. As mentioned earlier, this calibration was then used to screen suspect water samples.

The second iteration allowed for the possible addition of a quadratic term in the correction to conductivity, as well as a revised estimate of slope and bias. The quadratic term was only included when the residuals from the regression showed a parabolic character when plotted against conductivity and there was a noticeable reduction of the RMS residuals from the fit. Only HOT-14 needed the addition of a quadratic term. The final conductivity calibration coefficients are given in Table 2.4.

The quality of the CTD calibration is illustrated by Figure 2.3, which shows the differences between the corrected CTD salinities and the bottle salinities as a function of pressure for each cruise. Typically, the calibrations are best below 500 dbar, because the weaker vertical salinity gradients at depth lead to less error if the bottle and CTD pressures are slightly mismatched.

The final step of the calibration was to perform a profile-dependent bias correction, to allow for a drift of the conductivity cell with time during each cruise, or for sudden offsets due to fouling. This offset was determined by taking the median value of CTD-bottle salinity differences for each profile at temperatures below 5°C. Very few profiles collected during 1990 required adjust-

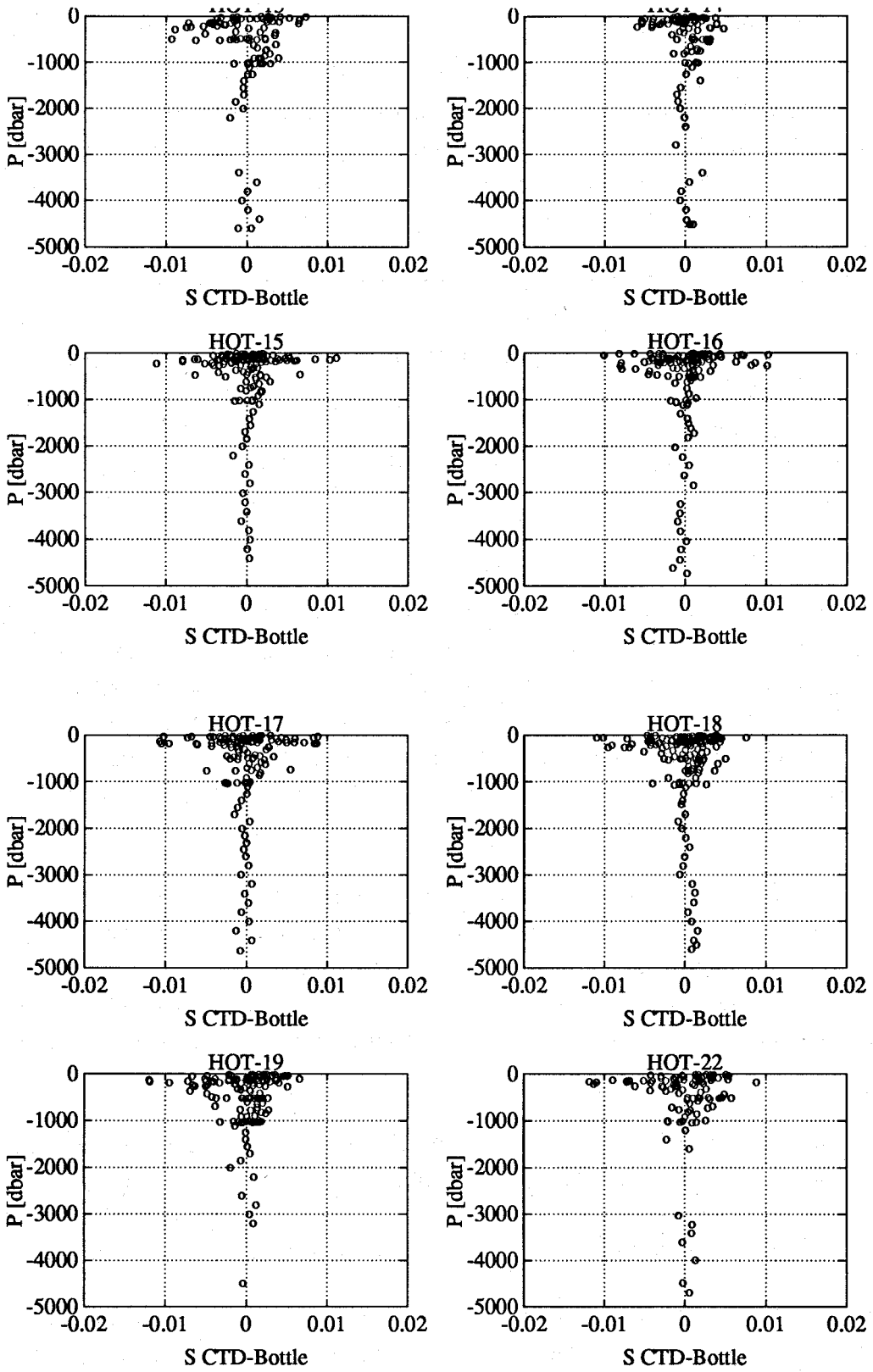

Figure 2.3 : Difference between calibrated CTD salinities and bottle salinities for Station 2, HOT-13 to Hot -22.

in this way (Table 2.5.) . Note that a change of 1 x 10^{-4}s m^{-1} in conductivity is approximately equivalent to 0.001 psu in salinity. Table 2.6. gives the mean and standard deviation for the final calibrated CTD values minus the water sample values. These values are comparable to the precision (0.001 psu) and accuracy (0.003 psu) estimated for the water sample salinities.

Table 2.4: Table of Conductivity Calibration Coefficients

Cruise	a	b	c
HOT-13	0.001335508	-0.000974088	
HOT-14	0.008356415	-0.004456943	0.000425137
HOT-15	0.000781481	-0.000793605	
HOT-16	0.001212221	-0.000885503	
HOT-17	0.001485549	-0.001000618	
HOT-18	0.001384305	-0.000943037	
HOT-19	0.001145888	-0.000870217	
HOT-20	0.000848886	-0.000777994	
HOT-22	0.002439196	-0.001097936	

Table 2.5: Individual Cast Conductivity Offsets. Units are Siemens m^{-1} x 10^{-4}.

Cruise	Station	Cast	Offset
Hot-13	2	1	0.4
	2	4	1.8
	2	7	-1.8
	2	8	-0.8
	2	14	1.1
Hot-14	2	9	-1.0
	2	12	-0.1
Hot-15	2	3	0.5
Hot-16	1	1	1.7
	2	13	-2.0
	2	15	-2.0
Hot-18	2	1	-0.1
	2	9	-0.7
Hot-19	2	1	1.0
Hot-22	1	1	3.0
	2	10	-3.3
	2	11	-0.9

Table 2.6: CTD-Bottle Salinity (psu) Comparison for Each Cruise

	0 < P < 4700		500 < P < 4700	
Cruise	Mean	St. Dev.	Mean	St. Dev.
HOT-13	-0.0002	0.0032	0.0004	0.0019
HOT-14	0.0001	0.0023	0.0004	0.0012
HOT-15	-0.0001	0.0031	0.0003	0.0011
HOT-16	0.0000	0.0032	0.0002	0.0010
HOT-17	0.0000	0.0032	0.0000	0.0017
HOT-18	0.0001	0.0028	0.0005	0.0015
HOT-19	-0.0001	0.0031	0.0002	0.0014
HOT-19	0.0000	0.0021	0.0008	0.0004
HOT-22	-0.0001	0.0035	0.0006	0.0018

Deep water salinity

The average calibrated CTD salinity between 4400 and 4500 dbar at the HOT site is given in Figure 2.4 for individual HOT cruises. The mean salinity is 34.689 psu, with a standard deviation of 1.2 mpsu. The range is nearly 4 mpsu. Given the uncertainties in our empirical calibration and in the water sample analyses discussed above, the salinity variability in the deep water at the HOT site for cruises 13-22 seems to be insignificant. It is worth noting, however, that the fresh-

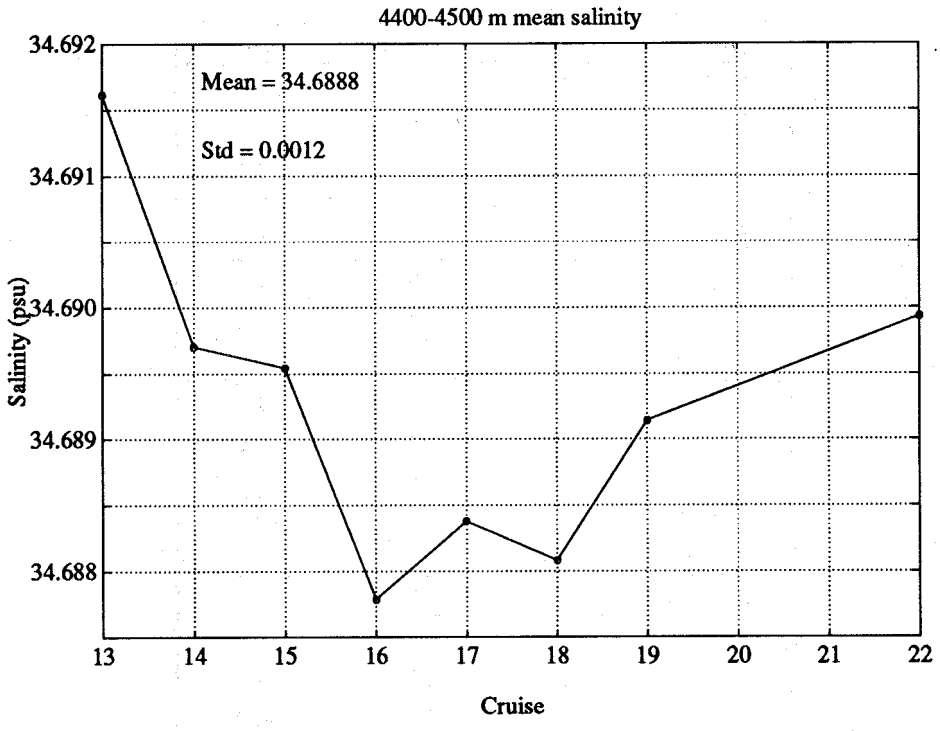

Figure 2.4: Average CTD salinity between 4400 and 4500 dbar at the HOT site.

ening trend from cruises 13-16 corresponds to the warming trend observed in this depth range (Figure 2.3). Also, the salinities in this depth range for HOT cruises 10-12 are close to the value for HOT-13. There was a change in batches of standard seawater from P110 to P111 between HOT-12 and HOT-13, but P111 was used through HOT-19, so this trend cannot be due to a change in standard seawater. The variation in deep water salinity appears to be non-random.

2.1.2.4 Oxygen

The Beckman polarographic oxygen sensor is notoriously difficult to calibrate, primarily because of its nonlinear sensitivity to pressure and temperature changes (cf. Owens and Millard, 1985). Difficulty in calibration also arises because the response characteristics of the membrane are sensitive to fouling, and the electrolyte in the cartridge may become depleted or breakdown with time. Laboratory calibrations of the oxygen sensor are not useful except to provide a nominal calibration for use during data acquisition.

For these reasons, we viewed the oxygen sensor data as being useful primarily to assist in quality controlling water sample oxygens, and for interpolating between the discrete samples. We 'calibrated' the sensor to the ensemble of bottle data taken during the so-called WOCE deep and shallow casts. These were the only casts where the distribution of bottle samples with pressure and temperature were adequate to determine those coefficients in the calibration fit to the discrete oxygen data.

We then used this calibration for all other casts, using any available discrete samples (usually only in the upper 200 m) to visually check for shifts. Because the behavior of the Beckman sensor in the top 100 m or so appears to be poor, the shape of the O_2 profile often did not resemble the distribution suggested by the bottles. (Experiments with the version of this sensor produced by YSI, and integrated into a transducer by Sea-Bird, show that this is a particular characteristic of the Beckman version of the membrane and cartridge. We are switching over to the YSI version for operational use.)

Water sample analysis

Water samples are analyzed for oxygen as described in Section 2.2.2.

Screening of bottle samples

Bottle O_2 data were screened against the historical data base, which is rapidly accumulating for the Kahe Point and HOT sites. Bottle data were overplotted on the ensemble of all 'good' data collected from each site. Both O_2 vs. pressure and O_2 vs. θ were inspected for suspicious values. Apparent rosette problems were investigated by looking at other water properties and resolved if possible.

The continuous O_2 profile from the CTD was also used for screening the bottle data. It is our experience that there is considerable finestructure in O_2, not always correlated with T-S finestructure. This is partly due to the biological processes which make O_2 a nonconservative tracer. Without the continuous profile to reveal this structure, and depending on the distribution of bottle samples, one might reject bottle oxygen values that are accurate. Thus, even though the sensor has some undesirable characteristics, it still provides useful information on the variability of O_2 on scales smaller than or comparable to the bottle spacing.

Empirical calibration

CTD O_2 calibration was performed following Owens and Millard (1985). Six parameters (B_{oc}, S_{oc}, tcor, pcor, τ, w_T) are fitted to the CTD oxygen current (O_c), oxygen temperature (O_T), and O_c time variation (dO_c/dt) by the equation:

$$OX = [S_{oc} (O_c + \tau(dO_c/dt)) + B_{oc}] * OXSAT(T,S) * \exp[tcor[T+ w_T \quad (T_o -T)] + \quad pcor * (p)$$

where the oxygen saturation (OXSAT) is calculated from the CTD temperature and bottle salinity (or calibrated CTD salinity if the bottle salinity is absent or of suspect quality).

The bottle values of O_2 and the downcast CTD observations at the potential density of each bottle trip were grouped together for each cruise and used to find the best set of parameters with a nonlinear least squares algorithm based on the Levenberg-Marquardt method (Press *et al*., 1988).

Two sets of parameters were obtained per cruise, corresponding to the casts of Station 1 (Kahe Pt.) and Station 2 (ALOHA). At Station 2 only WOCE casts were used for the fitting. Data deeper than 1000 m were assigned extra weight given that only one deep cast was obtained per cruise. This weighting was done by duplicating the data below 1000 m as many times as shallow (< 1000 m) casts were available for the calibration. The set of parameters obtained was used to calculate oxygen (OX) for all the CTD casts of this station.

In some of the cruises τ was kept constant (τ = 20, nominal in cruises 16, 17 and 18, station 2), rather than allowing it to be a negative value. This did not noticeably affect the results of the calibrations.

In cruises 19, 20, and 22, the CTD traces in the upper 100 dbar showed large deviations from the O_2 bottle data, leading to a lack of fit of the whole cast during the calibration. The fit largely improved after neglecting the upper 100 dbar. The CTD O_2 was flagged as bad or suspicious in the upper 100 dbar of these casts.

The quality of the O_2 sensor calibration can be accessed from table 2.7.

Table 2.7: CTD-Bottle O_2 (µmol kg^{-1}) Comparison for Each Cruise

Station 1, Kahe Point			Station 2, ALOHA			
0 < P < 1100			0 < P < 4700		500 < P < 4700	
Cruise	**Mean**	**St. dev**	**Mean**	**St. dev**	**Mean**	**St. dev**
HOT-13	*	*	0.0703	1.4637	0.1883	1.4488
HOT-14	-0.0080	2.52	0.0446	1.3260	0.2343	1.4603
HOT-15	**	**	**	**	**	**
HOT-16	0.0142	2.27	0.3808	3.8675	0.0931	1.9505
HOT-17	-0.1160	3.21	-0.4669	3.4928	-0.7486	2.3599
HOT-18	-0.2543	2.87	-1.1226	4.0878	-0.8825	3.1559
HOT-19	0.0010	2.91	-1.5143	4.3535	-1.1510	4.2183
HOT-20	-0.0257	2.68	***	***	***	***
HOT-22	-0.2022	1.55	0.2881	3.4285	-0.0664	3.5480

* No 02 sensor during this station
** No 02 sensor on CTD during this cruise
*** CTD lost during Station 2, cast 1

2.1.2.5. Fluorescence

Stimulated *in situ* fluorescence was measured using a flash fluorometer manufactured by Sea Tech, Inc., having an excitation wavelength of 425 nm and an emission wavelength of 625 nm. Fluorometer voltage was recorded and averaged into 2 dbar pressure bins as described in Section 2.1.1. Although fluorescence data were generally collected on as many casts as possible, fluorescence data were always collected on the cast used for the collection of water samples for the fluorometric determination of chlorophyll *a*. This cast was always obtained at night in order to avoid the variable light-dependent inhibition of fluorescence in the upper water column during daylight hours, and to facilitate the comparison of fluorescence traces between monthly cruises.

2.2. Water Column Chemical Measurements

Samples for water column chemical analyses were collected at both Kahe Point and Station ALOHA. Most of the samples were collected in the upper 1000 m. As much as possible, depth profiles of specific chemical constituents were collected on consecutive casts in order to minimize the effects of time-dependent variation within the water column. In addition, samples were collected near the same density horizons or depth each month in order to facilitate comparisons between monthly profiles. Our HOT program sampling protocols call for approximately 20% of the discrete chemical samples to be collected and analyzed in triplicate.

A detailed description of our sampling procedures and analytical methods has been given in a separate report (Karl *et al.*, 1990). Abbreviated descriptions of these procedures were given in

Chiswell *et al*. (1990). Beyond a general description of our analytical methods, only changes in the procedures described by Chiswell *et al*. (1990) will be given in this report.

During 1990, water samples were collected using a 24-place aluminum rosette manufactured by Scripps Institution of Oceanography's Oceanographic Data Facility (ODF). Twelve-liter polyvinylchloride sampling bottles, also made by ODF, were used on this rosette. These sample bottles were equipped with Buna-N rubber 0-rings, Teflon-coated steel springs and standard General Oceanics sampling valves.

The primary objective of the Hawaii Ocean Time-series program is to assess variability in the central Pacific Ocean on annual and interannual time scales. One of our most important concerns, therefore, is to ensure that the highest possible precision and accuracy is consistently maintained for all water column chemical measurements. In order to achieve the highest possible data quality, we have instituted a quality-assurance/quality-control program with the HOT program (see Karl *et al*., 1990), and have attempted to collect all ancillary information necessary to ensure that our data are not biased by sampling artifacts.

Although approximately 20% of our chemical analyses are analyzed in replicate (see Karl *et al*., 1990), only mean values are reported in the data sets provided with the report (see Section 7). To assist in the interpretation of these data and to save users the time needed to estimate the precision of individual chemical analyses, we have summarized precision estimates from replicate determinations for each constituent on each HOT cruise during 1990. Whenever possible, we have also monitored the consistency of our analytical results between cruises by maintaining reference materials and by monitoring the concentration of the chemical of interest in the deep sea where month-to-month variability is believed to be small.

2.2.1. Salinity

Salinity samples were collected in 250 ml polyethylene bottles and stored at room temperature in the dark for subsequent analysis in our shore-based laboratories. The time between sample collection and analysis was about one week. Prior to analysis, each sample was allowed to equilibrate to laboratory temperature. All water samples for HOT-13 to -22 were run on an AGE Minisal using the same procedures as described in Chiswell *et al*. (1990) for HOT-1 to -12. For HOT cruises 13-19, IAPSO standard seawater from batch Pill was used. For HOT cruise 20, batch P112 was used. For HOT-22, a switchover from P112 to batch P114 was made, with an interleaving of the two standards. Station 1 was run with P114, along with casts 2, 4, 5, 10, 11, 13, and 14 from Station 2. Casts 1, 3, 6-9, and 12 of Station 2 were run with P112. No significant differences were observed between casts run with the two standards. Typical precision (one standard deviation of triplicate samples from the same Niskin bottle) during 1990 was about 0.001 psu.

2.2.2 Oxygen

Samples for oxygen were drawn as soon as possible after the rosette arrived on deck into pre-calibrated 125-ml iodine flasks, and were fixed immediately for subsequent analysis in the laboratory. Oxygen concentrations were determined using the Winkler titration method of Carpenter (1965) as described by Chiswell *et al*. (1990).

The precision of our oxygen analysis during 1990 was typically 0.1% (Table 2.8). Oxygen concentrations measured on HOT- 13 through HOT-22 are plotted at constant pressure and density horizons in the deep ocean in Figure 2.5. Oxygen analyses differed by no more than 4 μmol kg^{-1} in deep water, indicating that analytical consistency was maintained throughout 1990.

Table 2.8: Precision of Winkler Titration

CV(%) Average of All Triplicate Measurements		
Cruise	CV(%)[a]	N[b]
13[c]	0.25	11
14[c]	0.16	12
14[c]	0.09	7
16[c]	0.04	7
17	0.12	9
18	0.19	8
19	0.15	7
20	0.06	24
21[d]	-	-
22	0.07	19

a Coefficient of variation of differences between replicates expressed as a percentage of the mean when duplicate samples were collected, and as standard deviation as a percentage of the mean for samples collected in triplicate.

b Number of depths from which replicates were collected. Only replicates from depths where oxygen concentrations exceed 100 μmol kg^{-1} were included in the analysis.

c Triplicates analyzed at each depth. On all other cruises duplicates were analyzed.

d Extremely rough weather prevented sample collection on HOT-2 I.

Oxygen concentrations are reported in the 1990 data set in units of μmol kg^{-1}. These concentrations were computed assuming that the samples come to the surface adiabatically (i.e., they were collected at their *in situ* potential temperature). As has been described previously (Chiswell *et al*., 1990), this procedure introduces a systematic error in oxygen concentration because the water sample warms en route to the surface.

Figure 2.5: Oxygen versus time at three density levels.

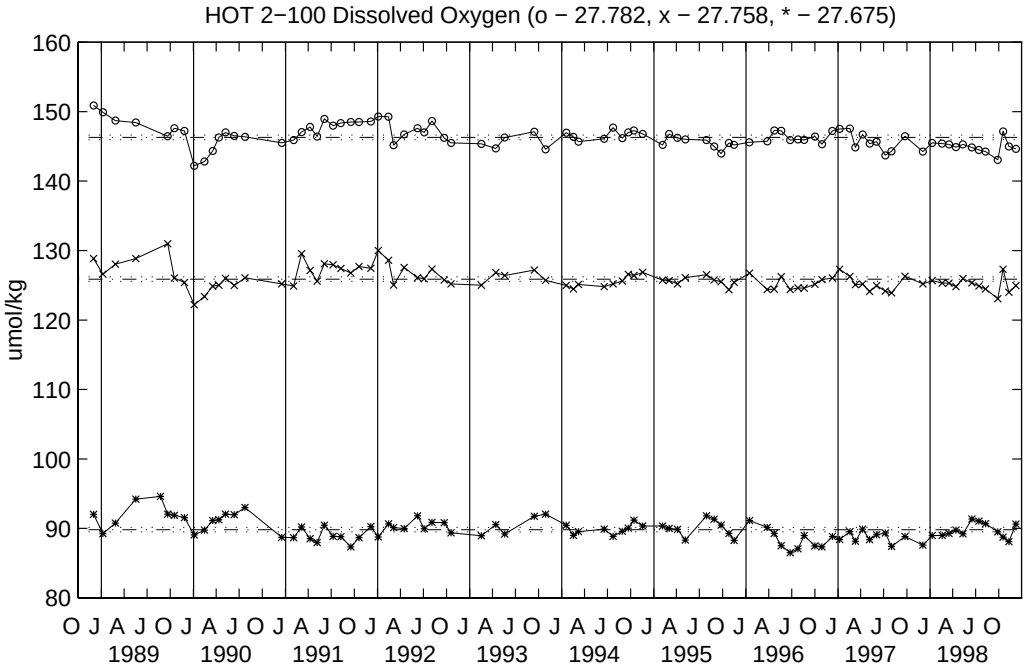

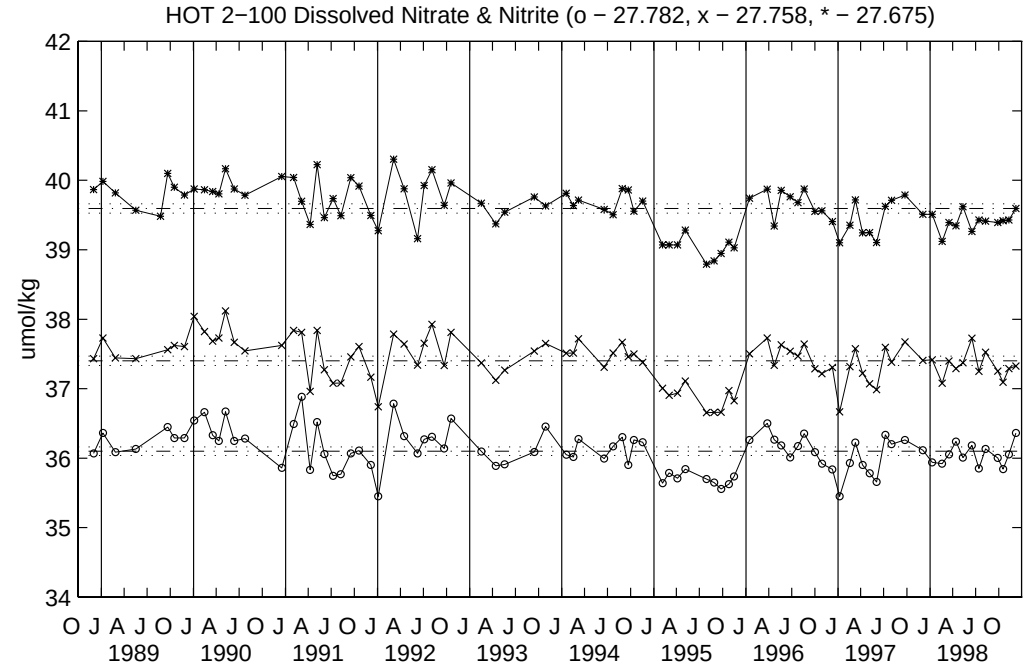

Figure 2.7 : Nitrate plus nitrite versus time at three density levels.

In order to evaluate the magnitude of this error and to allow for the calculation of oxygen concentrations with the greatest accuracy, we measured the temperature of the seawater sample within individual Niskin bottles at the time that the iodine flask was filled (i.e., on-deck temperature). On-deck temperatures were measured on all HOT cruises during 1990 using a standard glass mercury thermometer or a digital thermistor. Because of the rough sea-state frequently encountered at the time-series site, the precision of on-deck temperatures measured as described above was about ± 1°C.

A plot of the difference between on-deck temperature and potential temperature computed from *in situ* temperature at the time of bottle trip versus pressure for all data collected during 1990 is shown in Figure 2.6. The large degree of scatter observed below approximately 500 dbars was due primarily to the speed with which the CTD was brought up through the thermocline. The large scatter indicated that a uniform correction for all samples collected from a single depth could not be applied and confirmed the need to measure temperature of the time of sample collection in order to avoid this variable source of systematic error. The largest temperature differences were observed between 500 and 1000 dbars where the CTD was brought slowly through the thermocline for high-resolution sampling in this portion of the water column. Smaller temperature differences were often observed on deep casts where samples were collected between the sea floor and 2000 dbars and the CTD package was then raised rapidly through the thermocline.

A plot of the difference between oxygen concentrations computed using on-deck and potential temperatures is also shown in Figure 2.6. The difference in oxygen concentrations computed from the two temperatures below about 200 dbars varied between 0.02 and 0.18 μmol kg^{-1}. Although this difference is small, and only approaches the precision of the analysis at high oxygen concentrations, this error is systematic and should be eliminated for the most accurate work. The difference in oxygen concentrations computed from the two temperature estimates shows an interesting pattern when plotted against pressure (Figure 2.6), with the largest differences being observed near 500 dbars, a minimum at approximately 800 dbars, and differences rising from this minimum as the sea floor is approached. This pattern is a result of the oxygen profile found at Station ALOHA and the sampling employed on the time-series cruises. The low oxygen concentrations at 750 dbars generate the relatively small differences observed in oxygen concentrations computed using on-deck and potential temperatures at this depth. The maximum in Δ oxygen observed at approximately 500 m was generated on the 1000 dbar casts where water samples were taken frequently and the CTD moved slowly through the thermocline. Slightly lower A oxygen values were generated on deep casts where water samples were collected from the sea floor to about 2000 dbar and the CTD was then moved quickly through the main thermocline.

2.2.3. Dissolved Inorganic Carbon

As described by Chiswell *et at*. (1990), samples for dissolved inorganic carbon (DIC) were measured using a commercial coulometer modified for high-precision work.

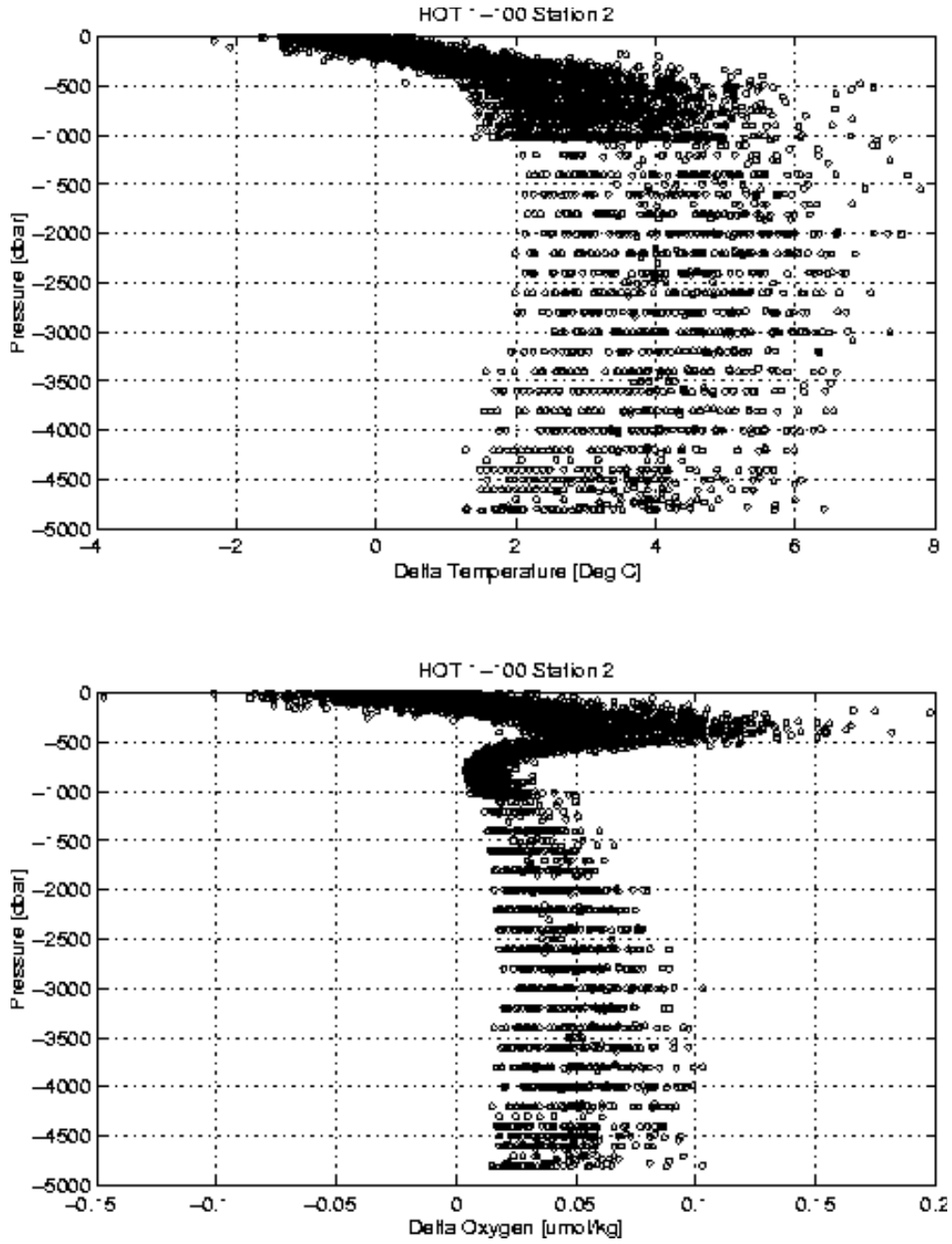

Figure 2.6: Upper Panel: Difference between sample temperature at the time of sample collection and potential temperature calculated from *in situ* temperature at the time of bottle trip. Lower Pannel: Difference in oxygen concentration in units of μmol kg^{-1} using temperatures measured at the time of sample collection and potential temperature computed from *in situ* temperature.

2.2.4 Inorganic and Organic Nutrients

Samples for the determination of nutrient concentrations were collected in acid-washed 125-

ml polyethylene bottles, and immediately frozen for transport to the laboratory. Analyses were conducted at room temperature on a four-channel Technicon Autoanalyzer II continuous flow system, using slight modification of the Technicon procedures for the analysis of seawater samples (Chiswell *et al*., 1990; Karl *et al*., 1990).

A summary of the precision of our dissolved nutrient analyses during HOT- 13 through HOT-22 is shown in Table 2.9. In Figures 2.7-2.9, nutrient concentrations measured during 1990 at constant deep water pressure horizons are presented. Nitrate plus nitrite (Figure 2.7) and phosphate (Figure 2.8) plotted at constant pressure show little cruise-to-cruise variability, indicating that analytical consistency was maintained for these analyses as well. Deep-water silicate values (Figure 2.9) show larger cruise-to-cruise variability, up to 5 μmol kg^{-1} at 3000 m. However, this variability represents less than 4% of the absolute value at this depth, indicating that reasonably good analytical consistency was also maintained for this analyses. Analytical precision for the other water column measurements made in 1990 are presented in Tables 2.9—2.12.

Table 2.9: Precision of Dissolved Nutrient Analyses

	Phosphorus		Nitrate + Nitrite		Silicate	
Cruise	Analytical[a]	Field[b]	Analytical[a]	Field[b]	Analytical[a]	Field[b]
13	0.2	0.0	0.6	0.4	0.5	2.5
14	0.5	0.2	0.6	0.1	0.2	1.6
15	0.4	0.0	0.7	0.1	1.7	1.7
16	0.1	0.0	0.3	0.1	0.3	1.0
17	0.3	0.8	0.4	0.2	0.4	2.1
18	0.2	0.0	0.7	0.7	0.1	9.3
19	0.1	0.0	0.1	0.0	0.0	4.1
20	0.7	0.0	0.4	0.4	0.1	0.0
22	0.9	2.5	0.3	1.6	1.5	8.3

a Average coefficient of variation (i.e., standard deviation as a percentage of the mean) for analytical replicates (i.e., replicate analysis of a single sample) for phosphate concentrations ≥ 0.4 μM, nitrate plus nitrite concentrations ≥ 0.2 μM, and silicate concentrations ≥ 0.2 μM.

b Average coefficient of variation for field replicates (i.e., analysis of replicate samples from the same Niskin) for the above concentration ranges.

Figure 2.8 : Phosphate versus time at three density levels. Concentrations at these levels are interpolated from the two nearest pressures.

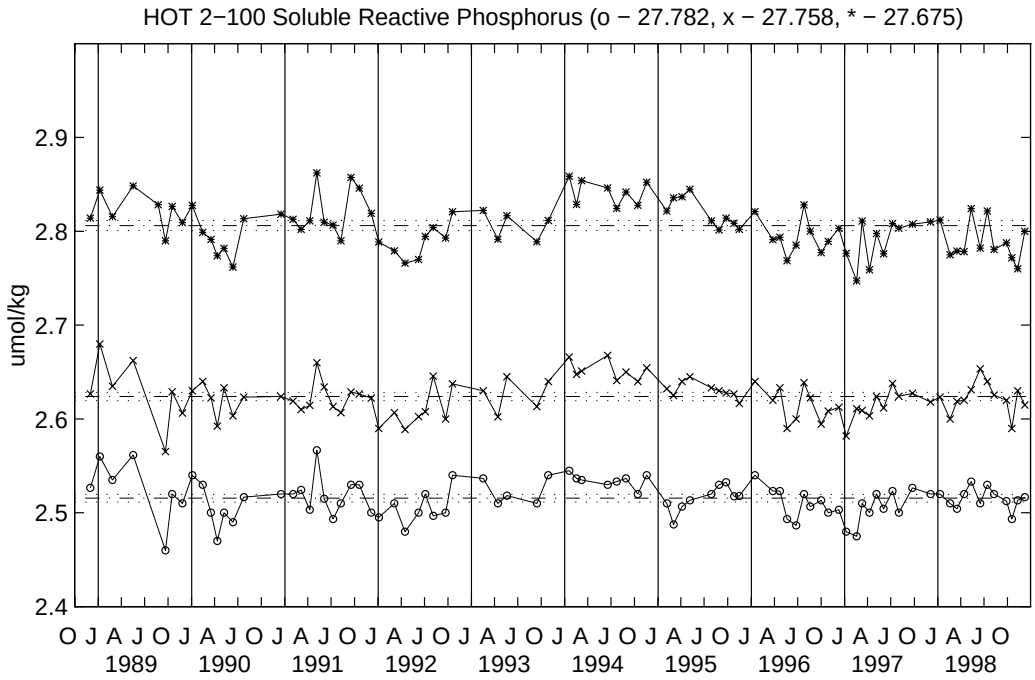

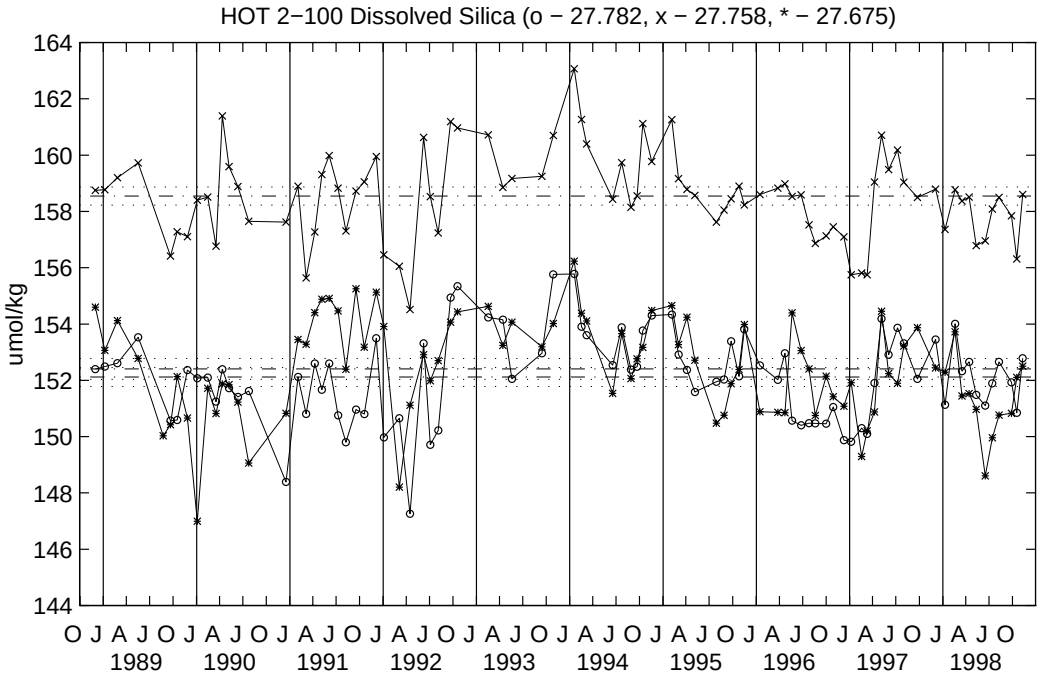

Figure 2.9 : Silicate versus time at three density levels. Concentrations at these levels are interpolated from the two nearest pressures.

Table 2.10: Precision of Dissolved Organic Nutrient Analyses

CV (%) Dissolved Organic Nutrients						
	DOC		DON		DOP	
Cruise	cv(%)	N	cv(%)	n	cv(%)	n
13	0.8	3	13.9	3	15.3	3
14	4.1	2	11.3	2	10.8	2
15	3.9	3	10.1	3	27.1	3
16	3.4	3	20.4	3	7.6	3
17	4.7	3	3.3	3	13.1	3
18	2.7	4	4.1	4	16.7	4
19	2.0	2	8.2	2	20.4	2
22	nd	Nd	3.4	3	4.6	3

2.2.4.1. Nitrate plus Nitrite and Dissolved Organic Nitrogen

Inorganic nitrogen was measured as the sum of nitrate plus nitrite with nitrate being quantitatively reduced to nitrite in a copperized cadmium reduction column on the autoanalyzer.

Total dissolved nitrogen (TDN) was determined by using ultraviolet (UV) light oxidation (Armstrong *et al*., 1966; Walsh, 1989). Dissolved organic nitrogen (DON) was measured as the difference between TDN and the sum of nitrate plus nitrite.

2.2.4.2. Orthophosphate and Total Dissolved Phosphorus

Orthophosphate (soluble reactive phosphorus) was measured by reaction with acidified molybdate reagent and potassium antimonyl tartrate, followed by the subsequent reduction with ascorbic acid. Total dissolved phosphorus was measured by photo-oxidation, followed by analysis of the oxidation products as described above. Dissolved organic phosphorus is measured as the difference between TDP and orthophosphate.

2.2.4.3. Silicate

Soluble reactive silicate was measured by reaction with ammonium molybdate at low pH,followed by reduction with ascorbic acid.

2.2.4.4. Dissolved Organic Carbon

Dissolved organic carbon was determined with the persulfate oxidation method (Menzel and Vacarro, 1964) using an O.I. Model 700 automated TOC analyzer. In this procedure, 0.4 ml of 6% phosphoric acid and 1.0 ml of sodium persulfate (25 g/250 ml distilled deionized water) were added to 2.7 ml of seawater sample. The sample was first purged with N_2 gas in order to remove the CO_2 generated from the acidification of the inorganic carbon. The sample was then heated to 100°C and oxidized with persulfate. The $C0_2$ evolved from the oxidation of dissolved organic

material was quantified with a non-dispersive infrared analyzer. The coefficient of variation on replicate field samples averaged 3% in 1990.

In April 1991 an NSF-sponsored DOC/DON intercomparison study was conducted at Station ALOHA. The persulfate method described above was compared with several high-temperature techniques employing platinum catalysts. On average, the high-temperature methods yielded DOC concentrations that were 2- to 3-fold higher than the persulfate oxidation technique. Consequently, we have begun to use a commercially available high-temperature instrument for DOC analyses.

2.2.5. Particulate Carbon and Nitrogen

Samples for particulate carbon (PC) and particulate nitrogen (PN) were prefiltered through a 202-μm Nitex mesh, and analyzed using a commercial CHN analyzer (Chiswell *et al*., 1990). The coefficient of variation for water column field replicates of both PC and PN averaged approximately 12% in 1990

2.2.6. Particulate Phosphorus

Samples for particulate phosphorus (PP) were prefiltered through a 202-μm Nitex mesh, organic compounds were then oxidized by high temperature ashing, and the resultant orthophosphate was measured spectrophotometrically.

Table 2.11: Precision of Fluorometric Analyses of Chlorophyll a and Phaeopigment

Cruise	Chl a CV(%)	Phaeo CV(%)
13	7.39	16.30
14	9.45	9.10
15	8.03	11.12
16	5.58	11.38
17	4.31	7.19
18	1.85	4.67
19	1.76	4.94
20	1.91	5.04
22	3.00	6.34

HOT-20 has only duplicate values from Go-flo cast from Station ALOHA
Coefficient of variation is the mean of all triplicate determinations on each cruise.

2.2.7. Chlorophyll *a* and Phaeopigments

Chlorophyll a and phaeopigments were measured fluorometrically using standard techniques (Strickland and Parsons, 1972). Integrated values for pigment concentrations were calculated

using the trapezoid rule. In addition to the fluorometric determination of pigments, we also measured chlorophyll *a* by high-performance liquid chromatography (HPLC; Chiswell *et al*., 1990). Analytical precision for fluorometric chlorophyll *a* determinations in 1990 are summarized in Table 2.11.

2.2.8. Adenosine 5'-Triphosphate

Samples for the determination of adenosine 5'-triphosphate (ATP) were extracted in boiling TRIS buffer and measured by photometry using the firefly bioluminescence reaction. The coefficient of variation on replicate samples drawn from the same Niskin bottle in 1990 are summarized in Table 2.12.

Table 2.12: Precision of ATP analyses

Cruise	ATP CV(%)*
13	11.6
14	10.6
15	11.2
16	14.3
17	13.2
18	11.0
19	10.2
22	17.1

Coefficient of variation is the mean of all triplicate determinations on each cruise.

2.3. Primary Productivity

Photosynthetic production of organic matter was measured by the carbon-14 method using trace metal clean methods, as described in Chiswell *et al*. (1990). During the first year of sampling, primary production measurements were made in an on-deck incubation system which simulated *in situ* light and temperature (Chiswell *et al*., 1990). During the second year, *in situ* incubation procedures were employed. In order to evaluate the influence of these incubation methods on the measured rates of primary production, replicate subsamples were incubated using both procedures on most of the cruises in 1990.

Deck incubations were done in a specially designed on-deck incubator which *simulates in situ* light quality and quantity, as well as *in situ* temperature. *In situ* incubations were conducted using a free-floating array equipped with a VHF transmitter and a strobe light. Twelve-hour in situ incubations were conducted during 1990 on all cruises on which it was possible to do primary production experiments. In addition, on several cruises during this period, 12- and 24-

hour incubations were conducted using the on-deck incubation system. On HOT-22, simultaneous 12- and 24-hour incubations were conducted *in situ*. Triplicate bottles were deployed at each incubation depth. The coefficient of variation for carbon assimilation rates derived from triplicate determinations averaged 19.7% in 1990. Carbon uptake for either 12 or 24 hour incubations was calculated as described in Chiswell *et al*. (1990). Integrated carbon assimilation rates were calculated using the trapezoid rule. In all cases, the shallowest values were extended to 0 m, Primary production rates were extrapolated to zero at 200 m.

2.4. Particle Flux

Particle flux was measured using sediment traps deployed on a free-floating array which was deployed for approximately 72 hours each month. Sediment trap design and sample collection methods, as well as sample analysis, were performed as previously described in Chiswell *et al*. (1990).

2.5. ADCP Measurements

Shipboard ADCPs were available and used on the MOANA WAVE cruises (HOT-13, -20, -22) and on the WECOMA cruises (HOT-16, -18). The profiling depth range obtained from the two ships was similar when on station. Underway, the range was typically better from the WECOMA because of lower acoustic noise levels and perhaps because of a smaller tendency to entrain bubbles in the water flowing under the transducer. ADCP data were collected and processed as described in Chiswell *et al*. (1990).

There were no major gaps in the ADCP data, but navigation data were not obtained at the end of HOT-13, south of 22°15’ N. Navigation was almost entirely by GPS, except on HOT-13 when GPS gaps of about 8 hours per day were filled with Transit fixes. A few Transit fixes also helped fill shorter GPS gaps on HOT- 16. The raw reference layer velocity estimates were much noisier on the WECOMA data sets than on the MOANA WAVE data During periods with GPS coverage, the difference was primarily caused by less accurate position information on the WECOMA relative to the MOANA WAVE. Position fixes were recorded at fixed 2-minute intervals on the WECOMA, independent from the ADCP data, whereas on the MOANA WAVE a fix was recorded at the end of each ADCP data record. Transit fixes were of higher quality on the MOANA WAVE than on the WECOMA because a dual-channel receiver was used on the former, a single-channel receiver on the latter. Transit fixes were also less numerous on the WECOMA because the data logging system missed some of the fixes that were received.

2.6. Meteorology

Meteorological data were collected at four-hour intervals while on station. Wind speed and direction, atmospheric pressure, wet- and dry- bulb air temperature, sea surface temperature, cloud cover, and sea state were recorded as described in Chiswell *et al*. (1990).

2.7. XBT

XBT casts were generally made spaced seven minutes of latitude apart during the transit to or from the deep-water site. Sippican T-7 probes having a maximum depth of 750 m were used. The files were screened for bad and missing data, and no corrections have been applied.

2.8. Optical Measurements

Incident irradiance at the sea surface was measured on each HOT cruise with a Licor LI-200 data logger and cosine collector. Irradiance levels are averaged over 10-minute intervals and integrated over the daylight period during the primary production experiment. Vertical profiles of Photosynthetically Available Radiation (PAR) were also obtained on most cruises during 1990 with a Biospherical Instruments model PNE-300 optical profiler.

3. Cruise Summaries

3.1. HOT-13; C. Winn, Chief Scientist

HOT-13 departed Snug Harbor at 0800 on 3 January 1990, aboard the R/V MOANA WAVE. Approximately 3 hours were spent on station at Kahe Point on both the transit to ALOHA and the return to Snug Harbor, and about 72 hours were spent at Station ALOHA. Because of problems with the CTD deck box, no CID data were collected at Kahe Point on the outbound leg. The station was reoccupied on our return transit to Snug Harbor.

WOCE and JGOFS Sampling

All WOCE and JGOFS chemical sampling was completed on HOT- 13.

CTD and XBT Operations

In general, CTD operations were successful on this cruise. However, problems with the deck box prevented the collection of CID data at Kahe Point on the outbound transit, and oxygen sensor problems prevented the collection of continuous oxygen profiles on most of the CID casts collected at Station ALOHA. The Kahe Point data was collected on the return leg. In spite of sensor problems, CID oxygen sensor data was collected at Kahe Point and on three casts, including the WOCE deep cast, at Station ALOHA. XBTs were deployed on the return leg to Snug Harbor.

Primary Production and Sediment Trap Measurements

Primary production and particle flux measurements were made at Station ALOHA. Primary production was measured *in situ* for 12 hours using the free-floating array and 24-hour incubations were conducted using the on-deck incubator system. Several bottles from the upper three incubation depths were lost during the recovery of the *in situ* array when the array drifted under the ship. However, some replicate samples incubated at each of these depths were recovered. The sediment trap samples were collected without problems.

Optical Measurements

Surface irradiance measurements were collected with both the 2 pi and cosine collectors. Underwater PAR profiles were collected with the submersible 4 pi collector.

ADCP Measurements

Current measurements were made with the hull-mounted ADCP. In addition, test casts were conducted with an ADCP attached to the 12-place rosette. Several ADCP calibration runs were made in the vicinity of the HOT site.

Ancillary projects

In addition to the regular JGOFS sampling, samples for dissolved gases were collected for Charles Keeling of Scripps Institution of Oceanography and for Steve Emerson and Paul Quay of University of Washington. Samples for dissolved organic compounds were collected by Robert Chen of the Scripps Institution of Oceanography.

3.2. HOT-14; S. Chiswell, Chief Scientist

HOT-14 departed Snug Harbor on the SSP KAIMALINO at 0800 on 13 February 1990. HOT-14 returned to Snug Harbor on 19 February.

WOCE and JGOFS Sampling

All water column chemical sampling was completed on HOT-14. The WOCE deep cast and CID burst sampling were completed. JGOFS primary production experiment and sediment trap sampling were completed.

CTD and XBT Operations

The oxygen sensor was particularly noisy on this cruise and failed on the WOCE deep cast. Following this cast, the oxygen sensor was removed from the CID package. Since the oxygen sensor was removed from the CID before the regular time-series oxygen sampling was conducted, oxygen traces that were obtained were calibrated with oxygen analyses conducted by Steve Emerson's group from the University of Washington. XBTs were dropped on the return transit from Station ALOHA.

Primary Production and Sediment Trap Measurements

Primary production was measured on-deck and *in situ* for 12 hours. Sediment trap samples were collected without significant problems.

Optical Measurements

Optical casts were completed at Kahe Point.

Ancillary projects

Samples for dissolved gases were collected for Charles Keeling of Scripps and for Steve Emerson and Paul Quay of the University of Washington.

3.3. HOT-15; C. Winn, Chief Scientist

This cruise left Snug Harbor on the SSP KAIMALINO at 0800 on 14 March 1990. Samples were collected at Kahe Point, but rough seas encountered upon rounding the northeast end of Oahu forced the ship to return to Snug Harbor to wait for calmer weather.

A second leg left Snug Harbor on 18 March 1990 after local weather conditions became more favorable. Rough seas were not a problem on this second trip, and the Kahe Point station was not revisited on this leg. HOT-15 returned to Snug Harbor on 21 March 1990.

WOCE and JGOFS Sampling

All sampling was completed on HOT-15.

CTD and XBT Operations

The CID cable needed to be reterminated once during this cruise. This required about 5 hours of station time and produced a gap of about 6 hours in the WOCE CID burst sampling. Oxygen sensor problems prevented the collection of continuous oxygen profiles on this cruise. No XBTs were deployed on this cruise.

Primary Production and Sediment Trap Measurements

In addition to the standard 12-hour *in situ* measurement of primary production using Go-Flo bottles, *in situ* primary production was also measured on water samples collected with the PVC bottles mounted on the rosette system. Comparisons of primary production estimates taken from rosette sampling and Go-Flo bottles were obtained on dim separate 12-hour *in situ* incubation experiments. No 24-hour or on-deck incubations were conducted on this cruise.

Optical Measurements

Optical casts were completed at Kahe Point.

Ancillary projects

Samples for dissolved gases were obtained for Charles Keeling of Scripps and for Steve Emerson and Paul Quay of the University of Washington). Samples for dissolved DNA were collected by Karen Selph (U. Hawaii).

3.4. HOT-16; D. Karl, Chief Scientist

HOT-16 departed Snug Harbor at 0900 on 11 April 1990 aboard the *R/V WECOMA*. Samples were collected at Kahe Point and regular sampling work was conducted at Station ALOHA. The ship returned to Snug Harbor at approximately 1800 on 15 April. The Kahe Point station was moved approximately 9 km north of the usual station site on this cruise because of

WOCE and JGOFS Sampling

All WOCE and JGOFS primary sampling was completed on this cruise.

CTD and XBT Operations

There were no CTD problems on this cruise. No XBTs were deployed.

Primary Production and Sediment Trap Measurements

Primary production was measured during 12-hour *in situ* incubations and during 24-hour ondeck incubations. Sediment trap samples were obtained without significant problems.

Optical Measurements

Optical casts were completed at Kahe Point.

Ancillary Projects

Samples for dissolved gases were collected for Charles Keeling of Scripps and for Steve Emerson and Paul Quay of the University of Washington.

3.5. HOT-17; C. Winn, Chief Scientist

HOT-17 departed Snug Harbor on the SSP KAIMALINO on 7 May 1990 and returned to Snug Harbor at 1700 on 10 May 1990.

WOCE and JGOFS Sampling

All primary sampling work was completed at both Kahe Point and Station ALOHA on this cruise.

CTD and XBT Operations

There were some problems with the flash fluorometer on this cruise, due to a corroded connector. Otherwise, CTD operations were completely successful. No XBTs were deployed on this cruise.

Primary Production and Sediment Trap Measurements

Primary production was measured *in situ* for 12 hours and on-deck for 24 hours; sediment trap collections were successful.

Optical Measurements

Optical casts were completed at Kahe Point

Ancillary Projects

Samples for dissolved gases were collected for Charles Keeling of Scripps and for Steve Emerson and Paul Quay of the University of Washington.

3.6. HOT-18: D. Karl, Chief Scientist

HOT- 18 departed Snug Harbor at 12:00 on 11 June 1990 aboard the R/V WECOMA. Kahe Point was visited en route to Station ALOHA, and HOT-18 returned to Snug Harbor at 0800 on 14 June. As on HOT-16, the Kahe Point Station was moved approximately 9 km north of the usual location.

WOCE and JGOFS Sampling

All WOCE and JGOFS sampling was completed on HOT-18.

CTD and XBT Operations

There were no CID problems on this cruise. XBTs were dropped en route to Station ALOHA.

Primary Production and Sediment Trap Measurements

Primary production was measured *in situ* for 12 hours. Sediment trap measurements were made as usual with no significant problems.

Optical Measurements

Optical casts were completed at Kahe Point.

Ancillary projects

Samples were collected for Charles Keeling of Scripps and for Steve Emerson and Paul Quay of the University of Washington.

3.7. HOT-19; C. Winn, Chief Scientist

HOT-19 departed Snug Harbor at 0900 aboard the SSP KAIMALINO on 23 July 1990. We returned to Snug Harbor at 2100 on 27 July. Kahe Point was occupied on the outbound transit and approximately 72 hours was spent at Station ALOHA.

WOCE and JGOFS Sampling

The WOCE deep cast and the CID burst sampling was obtained on HOT-19.

CTD and XBT Operations

Although there were no serious problems with CTD operations on HOT-19, there were several minor problems with the pylon. During the cruise, pylon positions 4, 12, and 18 were removed from service. Also, the flash fluorometer trace was somewhat noisier than usual, apparently due to the fluorometer cable which was showing signs of corrosion. XBTs were dropped en route to Station ALOHA.

Primary Production and Sediment Trap Measurements

Primary production was measured *in situ* for 12 hours. No on-deck incubations were conducted. Sediment traps were deployed and recovered without problems.

Optical Measurements

Optical casts were completed at Kahe Point

Ancillary projects

Samples for dissolved gases were collected for Charles Keeling of Scripps and for Steve Emerson and Paul Quay of the University of Washington. Samples were also collected for UH researchers Lisa Campbell and Daniel Vaulot and UH graduate students Peter Sedwick, Ricardo Letelier, and John Dore. REU (Research Experience for Undergraduates) students Dave Rose and Ian Gilbert also obtained samples for their work.

3.8. HOT-20; D. Karl, Chief Scientist

HOT-20 departed Snug Harbor aboard the R/V MOANA WAVE at 0800 on 13 September 1990. Kahe Point was visited en route to Station ALOHA, and XBTs were dropped after leaving the Kahe Point Station.

Upon arriving at Station ALOHA the time-series sediment trap array was deployed. In addition, an experimental sediment trap array was deployed for scientists at the University of Southern Mississippi.

The hydrowire parted on the first cast at Station ALOHA and the CTD was lost. The science party returned to Snug Harbor immediately to collect grappling gear with which to recover the array. After returning to Station ALOHA, both the time-series' and USM traps were recovered.

The CTD was eventually recovered using grappling gear and HOT-20 returned to Snug Harbor at approximately 2200 on 17 September. Other than the sediment trap data and the downcast data from the WOCE deep cast, no data were collected at Station ALOHA on HOT-20.

3.9. HOT-21; C. Winn, Chief Scientist

The NA'INA, a 110' vessel, was chartered from a private contractor for HOT-21. A test cruise conducted on the NA'INA demonstrated that the ship's crane was too long to safely deploy the CID. It was therefore decided that CID operations would be cancelled on HOT-21 and that sampling would be restricted to work not requiring the CID.

HOT-21 departed Snug Harbor at 1030 on 17 November 1990 after solving some last minute electrical problems. An XBT was dropped, and an optical profile was obtained at the Kahe Point Station. XBTs were dropped en route to Station ALOHA.

Rough conditions at Station ALOHA (30 kn winds and 12-15' seas) prevented the planned primary production and sediment trap work. After holding station for approximately 12 hours, forecasts for increasing seas and gale force winds forced HOT-21 to return to Snug Harbor. We returned at 2200 on 18 November.

3.10. HOT-22; C. Winn, Chief Scientist

HOT-22 departed Snug Harbor at 0800 aboard the R/V MOANA WAVE on 16 December. Samples were collected en route to Station ALOHA. HOT-22 returned to Snug Harbor at about 1700 on 20 December.

WOCE and JGOFS Sampling

All sampling was completed on HOT-22.

CTD and XBT Operations

Few CTD problems were encountered on HOT-22. However, the hydrowire kinked during an early cast, producing a gap in our planned CID burst sampling. Also, the tensiometer was not working on HOT-22. The CTD descent speeds were therefore decreased to avoid additional hydrowire kinks. Consequently, the CTD burst sampling interval was increased. XBTs were deployed on the return leg from Station ALOHA to Snug Harbor.

Primary Production and Sediment Trap Measurements

Primary production was measured on HOT-22 with 12-hour *in situ* incubations. Sediment traps were deployed and recovered on HOT-22 without significant problems.

Lowered ADCP Operations

Four lowered ADCP casts were conducted on HOT-22.

Optical Measurements

Optical casts were completed at Kahe Point.

Ancillary projects

Samples for dissolved gases were collected for Charles Keeling of Scripps and for Steve Emerson and Paul Quay of the University of Washington.

Table 3.1: Summary of HOT Cruises, 1990

HOT	Ship	Depart	Return
13	R/V MOANA WAVE	3 January 1990	7 January 1990
14	SSP KAIMALINO	13 February 1990	17 February 1990
15	SSP KAIMALINO	17 March 1990	21 March 1990
16	R/V WECOMA	11 April 1990	15 April 1990
17	SSP KAIMALINO	7 May 1990	11 May 1990
18	R/V WECOMA	11 June 1990	15 June 1990
19	SSP KAIMALINO	23 July 1990	27 July 1990
20	R/V MOANA WAVE	13 September 1990	17 September 1990
21	NA'INA	17 November 1990	19 November 1990
22	R/V MOANA WAVE	16 December 1990	20 December 19%

Table 3.2: Ancillary Projects Supported by HOT

HOT	Principal Investigator	Institution Program
13-22	Charles Keeling	Scripps Inst. of Oceanography
13-22	Steve Emerson	University of Washington
13-22	Paul Quay	University of Washington
13-22	Daniel Vaulot and Lisa Campbell	University of Hawaii

Table 3.3: University of Hawaii Cruise Personnel

	13	14	15	16	17	18	19	20	21	22
S. Chiswell, P. I.		■	▒					▒	▒	▒
E. Firing, P. I.	▒							▒		▒
D. Karl, P. I.				■		■		■		
R. Lukas, P. I.				▒						
C. Winn, P. I.	■		■		■		■		■	■
F. Dobbs, Scientist			▒	▒						
P. Flament, Scientist	▒									
D. Hebel, Scientist	▒	▒	▒	▒	▒	▒		▒	▒	▒
K. Constantine, Technician					▒					
E. Loucks, Technician					▒					
R. Müller, Technician		▒								
M. Rosen, Technician	▒		▒	▒	▒	▒	▒	▒	▒	▒
J. Snyder, Technician	▒	▒	▒	▒	▒	▒	▒	▒	▒	▒
G. Tien, Technician		▒								
J. Christian, Graduate Student								▒		▒
M. Cremer, Graduate Student			▒	▒			▒			
J. Dore, Graduate Student		▒	▒	▒		▒	▒		▒	▒
R. Letelier, Graduate Student	▒	▒	▒	▒	▒	▒	▒	▒	▒	▒
R.-C. Lien, Graduate Student								▒		
G. Parrish, Graduate Student				▒			▒			
E. Parnell, Graduate Student								▒		
S. Reid, Graduate Student	▒	▒	▒	▒	▒		▒	▒	▒	▒
C. Sabine, Graduate Student	▒		▒							
K. Selph, Graduate Student			▒							
T. Shinoda, Graduate Student						▒				
P. Troy, Graduate Student		▒								
	13	14	15	16	17	18	19	20	21	22

Shaded area = cruise participant Solid area=Chief Scientist

4. Results

4.1. Hydrography

4.1.1. 1990 CTD Profiling Data

Continuous profiles of temperature, salinity, oxygen and sigma-theta collected at both Kahe Point and Station ALOHA are, presented in Figures 6.1.1-18. The results of bottle determinations of oxygen, salinity, and inorganic nutrients are also shown on these figures. In addition, stack plots of CTD temperature and salinity profiles for all 1000 m casts conducted at Station ALOHA are pre-sented. The temperature, salinity, and oxygen profiles obtained from the deep casts at Station ALOHA during 1990 are presented in Figures 6.1.19-21. In general, data results are similar to those collected in 1988 and 1989 (Chiswell *et al*, 1990).

4.1.2. Time-series Hydrography, 1988-1990

The hydrographic data collected during the first two years of the time-series program are presented in a series of contour plots (Figures 6.2.1-14). These figures show the data collected in 1990 within the context of the larger time-series database. The CTD data used in these plots are averages of the data collected by monthly burst sampling. Therefore, much of the variability which would otherwise be introduced by tidal and near inertial oscillations in the upper ocean has been removed. Figures 6.2.1 and 6.2.2 show the contoured time series of potential temperature and density for the upper 1000 dbar for all HOT cruises through 1990. Seasonal variation of the temperature of the upper ocean is apparent in the maximum of near-surface temperature of about 26°C that occurs in the early fall, and the minimum of approximately 23°C which occurs in late winter. Oscillations in the depth of the 5°C isotherm are relatively large with displacements up to 75 m. The only other remarkable year-to-year change in the thermal structure at this point is the lack of any 4°C water in 1990 in this pressure range. The main pycnocline is observed between 100 and 600 dbar, with a seasonal pycnocline occurring between June and December in the 50-100 dbar range (Figure 6.2.2). The cruise-to-cruise changes between February and July 1989 in the upper pycnocline illustrate that month-to-month variations in density are not always resolved by our quasi-monthly sampling.

Figures 6.2.3-6 show the contoured time series of salinity for the upper 1000 dbar for all HOT cruises through 1990. The plots show both the CTD and bottle results plotted against pressure and sigma-theta. Most differences between the contoured sections of bottle salinity and CTD salinity are due to the coarse distribution of bottle data in the vertical as compared to the CTD observations. CTD salinities are available for HOT-20, but there are no bottle data for the HOT site due to the loss of the rosette and CTD. Some of the bottles in Figure 6.2.6 are plotted at density values lower than the indicated sea surface density. This is due to surface density changing from cast to cast within each cruise, and even between the downcast and upcast during a single cast.

The surface layer has relatively low salinity, but it is variable from cruise-to-cruise, with no obvious seasonal cycle. The salinity maximum is generally found between 50 and 150 dbars, and within the potential density range 24-25 kg m^{-3}. The salinity maximum region extends to the sea surface in the latter part of 1988 and 1990, as indicated by the 35.1 psu contour reaching the surface. This contour nearly reaches the surface late in 1989. The maximum value of salinity in this feature is subject to short-term variations of about 0.1 psu, which are probably due to the proximity of the HOT site to the region where this water is formed at the sea surface (cf Tsuchiya, 1968). The salinity minimum is found between 400 and 600 dbar (26.35-26.85 kg m^{-3}). There is no obvious seasonal variation of this feature, but there are distinct periods of higher than normal minimum salinity in early 1989 and in the fall of 1990. These variations are related to the episodic appearance at the HOT site of energetic finestructure and submesoscale water mass anomalies (Lukas and Chiswell, 1991).

Figures 6.2.7 and 6.2.8 show contoured time series for oxygen in the upper 1000 dbars at the HOT site. The oxygen data show a strong oxycline between 400 and 625 dbar (26.25-27.0 kg m^{-3}), and an oxygen minimum centered near 800 dbar (27.2 kg m^{-3}). During 1988-89, there was a persistent oxygen maximum near 300 dbar (25.75 kg m^{-3}). which appeared only weakly and intermittently during 1990. The oxygen minimum exhibited some interannual variability as well, with values less than 30 μmol kg^{-1} during the last half of 1989 and the first half of 1990. The surface layer shows a seasonality in O_2 concentrations, with highest values in the winter. This roughly corresponds to the minimum in surface layer temperature (Figure 6.2.1).

Figures 6.2.9-14 show nitrate plus nitrite, phosphate, and silicate at the HOT site plotted against both pressure and potential density. The nitrocline is found between about 200 and 600 dbar (25.75-27 kg m^{-3}; Figures 6.2.9-10). Most of the variations seen in these data are associated with vertical displacements of the density structure, and when nitrate plus nitrite is plotted versus potential density, most of the contours are level. One exception is some variation in the upper thermocline (150-200 dbar, 25.25 kg m^{-3}) which may be associated with biological activity. Another is a relative maximum of nitrate (exceeding 42 μmol kg^{-1}) centered near 27.6 kg m^{-3} during March-May of 1990. It should be noted, however, that this feature is not observed in the phosphate data, and may therefore be the result of a previously undetected error in sampling or analysis. A third exception is found during March-April 1990 when elevated levels of nitrate are seen between 25.5 and 26.25 kg m^{-3}.

Phosphate (Figures 6.2.11-12) is consistent with nitrate plus nitrite. The largest vertical gradient is between about 200 and 600 dbar. Most of the variability in phosphate is also associated with vertical displacements of isopycnals. However, Figure 6.2.12 shows that the variability near 27.6 kg m^{-3} is much less in phosphate than in nitrate. Given analytical precision as discussed in Chiswell et al. (1990), the nitrate variations appear significant, and seem to be related to variations in oxygen (Figure 6.2.8) that occur at slightly lower density. The elevation of phosphate near 26 kg m^{3} in March—April 1990 corresponds to the increased nitrate mentioned above, and to decreased oxygen.

The silicate data (Figures 6.2.13—14) show patterns very similar to those observed in the nitrate plus nitrite and phosphate data. The considerable temporal variation in silicate versus pressure largely disappears in potential density coordinates. Silicate is slightly elevated in the same

densities as noted for phosphate and nitrate in March—April 1990.

4.2.Biogeochemistry

Biogeochemical data collected during 1990 are summarized in Figures 6.3.1-15. In some cases the results from the first year of the program have been combined with the 1990 results to produce these figures.

4.2.1. Fluorescence

In situ fluorescence profiles show the deep pigment maximum, characteristic of the central North Pacific Ocean. Stack plots of flash fluorescence collected at night on cruises conducted during 1990 are shown in Figures 6.3.1 and 6.3.2. In general, fluorescence peaks observed during 1990 were centered at about 100 m and at potential densities between 24 and 25.

Figure 6.3.4 shows contours of fluorescence collected over the entire length of the time-series program plotted against pressure. Considerable variability is observed in the fluorescence over time, and it appears that variability in fluorescence is not being completely resolved with our current sampling frequency. No clear seasonal cycle in fluorescence is observed, although increased fluorescence is observed in April and May in both 1989 and 1990. High surface winds encountered in December 1988 deepened the mixed layer to approximately 105 m (*Chiswell et al.*, 1990). This event mixed the chlorophyll maximum layer upward producing high concentrations of chlorophyll, and high fluorescence yields, within the upper 50 m of the water column during this period.

4.2.2. Primary Productivity

The results of the carbon-14 incubations and pigment determinations made on samples collected on Go-Flo casts in 1990 are presented in Tables 4.1 and 4.2. Table 4.1 presents the primary production and pigment measurements made at individual depths on all 1990 cruises. Table 4.2 presents integrated values for irradiance, pigment concentrations, and primary production rates per m^2 of ocean surface. The pigment concentrations and carbon-14 incorporation rates reported are the average of triplicate determinations. Integrated primary production values for 12-hour incubations conducted both on deck and *in situ* are shown in Figure 6.3.4. The results of 12- and 24-hour incubations are shown in Figure 6.3.5. Primary production data collected during the

Table 4.1: Primary Production and Pigment Summary

Cruise[a]	Depth (m)	Chl a[b] mg m^{-3} Avg	Chl a mg m^{-3} SD[c]	Pheo mg m^{-3} Avg	Pheo mg m^{-3} SD[c]	Light "24h"[d] mg C m^{-3} Rep #1	Light "24h" mg C m^{-3} Rep #2	Light "24h" mg C m^{-3} Rep #3	Light "12h"[d] mg C m^{-3} Rep #3	Light "12h" mg C m^{-3} Rep #3	Light "12h" mg C m^{-3} Rep #3	Dark "12h"[d] mg C m^{-3} Rep #3	Dark"12h" mg C m^{-3} Rep #3	Dark "12h" mg C m^{-3} Rep #3
13 IS	2	0.12	0.01	0.03	0.01				4.68					
13 IS	10	0.11	0.02	0.05	0.02				4.59					
13 IS	40	0.13			0.04					3.97				
13 IS	80	0.19			0.06					2.04	1.60		0.13	
13 IS	95	0.17			0.10					1.61	1.48		0.13	
13 IS	120	0.12			0.04					0.71	0.69		0.11	
13 IS	145	0.06	0.00	0.10	0.03				0.12	0.17		0.11		
13 IS	175	0.01	0.00	0.01	0.00				0.09	0.08		0.13		
13 OD	2	0.12	0.01	0.03	0.01	3.85	4.33		3.28	3.88		0.36		
13 OD	10	0.11	0.02	0.05	0.02	5.60	5.78		7.42	6.64		0.20		
13 OD	40	0.13			0.04		2.54	3.14		3.54	2.54		0.16	
13 OD	80	0.19			0.06		1.32	1.41		0.52	0.80		0.17	
13 OD	95	0.17			0.10		0.85	1.13		0.86	0.59		0.15	
13 OD	120	0.12			0.04		0.42	0.34		0.30	0.40		0.10	
13 OD	145	0.06	0.00	0.10	0.03	0.13	0.15		0.10	0.10		0.17		
13 OD	175	0.01	0.00	0.01	0.00	0.08	0.10		0.08	0.07		0.09		
14 IS	4	0.08	0.02	0.03	0.01				2.53			0.09		
14 IS	10	0.10	0.00	0.03	0.00				5.18	5.88		0.20		
14 IS	30	0.11	0.01	0.03	0.00				3.08			0.23		
14 IS	70	0.22	0.00	0.11	0.01				2.89	3.70		0.16		
14 IS	88	0.33	0.01	0.23	0.01					2.63				
14 IS	115	0.22	0.02	0.26	0.01					0.83				
14 IS	135	0.11	0.06	0.29	0.07				0.26			0.17		
14 IS	160	0.04	0.00	0.06	0.00							0.10		
14 OD	4	0.08	0.02	0.03	0.01	2.92	3.75		4.26	4.67		0.17		
14 OD	10	0.10	0.00	0.03	0.00	5.17	5.30		6.79	7.28		0.22		
14 OD	30	0.11	0.01	0.03	0.00	2.70	2.38		2.69	2.60	0.24	0.24		
14 OD	70	0.22	0.00	0.11	0.01	0.89	0.86		1.05	1.03	0.18	0.18		
14 OD	88	0.33	0.01	0.23	0.01	0.86	0.81		1.36	1.16	0.12	0.12		
14 OD	115	0.22	0.02	0.26	0.01	0.30	0.36		0.28	0.25	0.09	0.09		
14 OD	135	0.11	0.06	0.29	0.07	0.18	0.18		0.17	0.17	0.10	0.10		
14 OD	160	0.04	0.00	0.06	0.00	0.10	0.10		0.12	0.08	0.11	0.11		
15 IS	5	0.09			0.05					4.26	4.37	3.98		
15 IS	25	0.11			0.04					4.14	3.70	3.09		
15 IS	45	0.10			0.05					4.93	4.65	4.41		
15 IS	75	0.17			0.08					4.77	4.95	4.80		
15 IS	100	0.20			0.15					3.71	3.44	3.34		
15 IS	125	0.27			0.23					1.76	1.63	1.78		
15 IS	150	0.05			0.11					0.30	0.28	0.27		
15 IS	175	0.04			0.05					0.12	0.13	0.15		

Cruise[a]	Depth (m)	Chl a[b] mg m^{-3} Avg	Chl a mg m^{-3} SD[c]	Pheo mg m^{-3} Avg	Pheo mg m^{-3} SD[c]	Light "24h"[d] mg C m^{-3} Rep #1	Light "24h" mg C m^{-3} Rep #2	Light "24h" mg C m^{-3} Rep #3	Light "12h"[d] mg C m^{-3} Rep #3	Light "12h" mg C m^{-3} Rep #3	Light "12h" mg C m^{-3} Rep #3	Dark "12h"[d] mg C m^{-3} Rep #3	Dark"12h" mg C m^{-3} Rep #3	Dark "12h" mg C m^{-3} Rep #3
15 OD	25	0.11			0.04		4.95	4.62		5.39	6.18		0.23	
15 OD	45	0.10			0.05		2.97	3.35		3.50	3.85		0.21	
15 OD	75	0.17			0.08		2.11	2.12		1.08	1.24		0.14	
15 OD	100	0.20			0.15		0.67	0.99		1.50	1.20		0.18	
15 OD	125	0.27			0.23		0.73	0.80		0.64	0.81		0.10	
15 OD	150	0.05			0.11		0.13	0.13		0.14	0.14		0.10	
15 OD	175	0.04			0.05		0.10	0.12		0.12	0.10		0.09	
16 IS	2	0.09	0.00	0.09	0.00				2.36	3.04		0.48		
16 IS	10	0.10	0.00	0.06	0.01				1.22	0.74		0.13		
16 IS	40	0.13	0.00	0.04	0.00				2.91	1.91		0.18		
16 IS	80	0.17	0.01	0.09	0.01				9.94	1.47		0.13		
16 IS	95	0.23	0.06	0.14	0.07				4.75	4.41		0.13		
16 IS	120	0.32	0.02	0.29	0.02				2.29	1.51		0.12		
16 IS	145	0.13	0.01	0.26	0.01				1.13	0.58		0.04		
16 IS	175	0.08	0.01	0.16	0.01				0.14	0.12		0.04		
16 OD	2	0.09	0.00	0.09	0.00	3.75	4.07		3.39	4.91		0.13		
16 OD	10	0.10	0.00	0.06	0.01	2.11	2.52		2.11	3.32		0.15		
16 OD	40	0.13	0.00	0.04	0.00	1.81	2.32		2.33	2.52		0:18		
16 OD	80	0.17	0.01	0.09	0.01	1.40	1.40		1.13	2.01		0.21		
16 OD	95	0.23	0.06	0.14	0.07	1.10	1.52		1.03	1.19		0.07		
16 OD	120	0.32	0.02	0.29	0.02	0.42	0.54		0.32	0.48		0.05		
16 OD	145	0.13	0.01	0.26	0.01	0.33	0.12		0.10	0.10		0.04		
16 OD	175	0.08	0.01	0.16	0.01	0.05	0.06		0.04	0.04		0.03		
17 IS	5	0.03	0.00	0.18	0.01				6.93	5.85		0.10		
17 IS	25	0.10	0.00	0.04	0.00				2.60	3.14		0.13		
17 IS	45	0.11	0.01	0.05	0.01				6.08	5.16				
17 IS	75	0.14	0.01	0.07	0.00				2.37	3.44		0.14		
17 IS	100	0.50	0.00	0.49	0.03				3.82	5.55		0.08		
17 IS	125	0.28	0.01	0.37	0.03				1.17	1.03		0.03		
17 IS	150	0.10	0.00	0.14	0.00					0.17		0.03		
17 IS	175	0.06	0.00	0.12	0.01				0.08	0.06		0.06		
17 OD	5	0.03	0.00	0.18	0.01	5.29	6.37		7.45	7.18		0.09		
17 OD	25	0.10	0.00	0.04	0.00	4.69	4.10		6.78	6.33		0.17		
17 OD	45	0.11	0.01	0.05	0.01	4.24	3.42		4.73	1.06		0.21		
17 OD	75	0.14	0.01	0.07	0.00	2.92	1.42		0.90	1.80		0.19		
17 OD	100	0.50	0.00	0.49	0.03	3.60	4.06		3.42	4.77		0.00		
17 OD	125	0.28	0.01	0.37	0.03	1.07	1.02		0.88	0.60		0.05		
17 OD	150	0.10	0.00	0.14	0.00	0.14	0.12		0.08	0.08		0.07		
17 OD	175	0.06	0.00	0.12	0.01	0.06	0.05		0.04	0.03		0.10		
18 IS	5	0.05	0.00	0.02	0.00	2.41	0.97			3.58	3.04	0.22	0.19	0.18
18 IS	25	0.04	0.00	0.02	0.00		1.62		0.58	1.67	1.62	0.28	0.28	0.16
18 IS	45	0.06	0.00	0.03	0.00	0.72	1.44	0.47	1.55	1.52	0.74	2.01[e]	0.16	0.24
18 IS	75	0.11	0.00	0.06	0.00	1.69	1.52	2.06	2.23	3.43	1.50	0.17	0.18	0.20
18 Is	100	0.22	0.01	0.27	0.01	4.45	3.96		4.15	4.06	4.33	0.10	0.13	0.14
18 IS	125	0.08	0.00	0.12	0.00	0.80	0.66	0.70	0.62	0.57	0.58	0.08	0.08	0.09
18 IS	150	0.02	0.00	0.04	0.00	0.09	0.11	0.11	0.09	0.08	0.09	0.05	0.06	0.06

Cruise[a]	Depth (m)	Chl a[b] mg m^{-3} Avg	Chl a mg m^{-3} SD[c]	Pheo mg m^{-3} Avg	Pheo mg m^{-3} SD[c]	Light "24h"[d] mg C m^{-3} Rep #1	Light "24h" mg C m^{-3} Rep #2	Light "24h" mg C m^{-3} Rep #3	Light "12h"[d] mg C m^{-3} Rep #3	Light "12h" mg C m^{-3} Rep #3	Light "12h" mg C m^{-3} Rep #3	Dark "12h"[d] mg C m^{-3} Rep #3	Dark"12h" mg C m^{-3} Rep #3	Dark "12h" mg C m^{-3} Rep #3
19 IS	5	0.04	0.00	0.02	0.00				1.64	1.36	2.77	0.20	0.18	0.24
19 IS	25	0.04	0.00	0.02	0.00				2.16	0.79	1.37	0.12	0.18	0.18
19 IS	45	0.08	0.00	0.04	0.00				3.45	4.97	4.26	0.18	0.15	0.18
19 IS	75	0.11	0.00	0.06	0.00				3.39	4.10	2.29	0.17	0.19	0.17
19 IS	100	0.20	0.00	0.16	0.00				3.27	3.90	9.56	0.12	0.11	0.11
19 IS	125	0.08	0.00	0.10	0.00				0.37	0.40	0.41	0.08	0.07	0.06
19 IS	150	0.04	0.00	0.08	0.01				0.18	0.16	0.14	0.07	0.07	0.08
19 IS	175	0.02	0.00	0.05	0.00							0.06	0.06	0.07
22 IS	5	0.09	0.00	0.04	0.00				5.10	4.52	5.43	0.12	0.14	0.15
22 IS	25	0.09	0.00	0.04	0.01				4.85	4.63	4.74	0.14	0.15	0.14
22 IS	45	0.09	0.00	0.05	0.00				3.32	2.91	3.12	0.14	0.15	0.14
22 IS	75	0.10	0.00	0.04	0.00				1.07	1.03	1.18	0.14	0.17	0.15
22 IS	100	0.154	0.01	0.22	0.01				0.91	0.88	0.90	0.07	0.08	0.08
22 IS	125	0.05	0.00	0.12	0.01				0.17	0.17	0.17	0.08	0.07	0.07
22 IS	150	0.01	0.00	0.02	0.00				0.36[e]	0.04	0.05	0.05	0.07	0.07
22 IS	175	0.09	0.00	0.03	0.00				0.17	0.23	0.21	0.20	0.13	0.11

No data from HOT-20 and –21.

a OD = on-deck incubation; IS = *in situ* incubation

b Average of 2 or more replicates

c SD (standard deviation) computed only at depths with three replicate subsamples

d Incubation times are approximations only (i.e., half day or full day). Actual incubation time for each measurement is given in Table 4.2.

e Questionable values; not used in integrations compiled in Table 4.2.

first two years of time-series sampling are presented in order to place these 1990 data within the context of our entire data set.

Table 4.2: Primary Production and Pigment Summary
Integrated Values 0-200 m

	Incident Irridiance (E m^{-2} d^{-1})		Pigments (mg m^{-2})		Incubation Duration	Carbon assimilation rates (mgC m^{-2} d^{-1})		
Cruise[a]	cosine[b]	hemi[c]	Chl a	Phaeo	(hrs)	24 hrs	12 hrs	12 hrs (dark)
13 IS	27.7	64	21.02	10.48	13.4		359	23
13 OD	27.7	64	21.02	10.48	11.9		308	29
13 OD					23.9	305		
14 IS	20.7	40	27.8	24.48	12		367	28
14 OD	20.7	40	27.8	24.48	11.7		274	27
14 OD					24.3	227		
15 IS	46.9	81.5	24.71	18.71	13.5		527	
15 OD	46.9	81.5	24.71	18.71	12.8		416	29
15 OD					24.3	360		
16 IS	48.5	84.2	30.54	27.34	12.8		336	23
16 OD	48.5	84.2	30.54	27.34	12.8		240	21
16 OD					23.7	224		
17 IS	55.4	95.8	32.66	34.22	13.7		524	16
17 OD	55.4	95.8	32.66	34.22	13.7		474	23
17 OD					24.2	457		
18 IS	ND[d]	91.4	14.54	14.58	14		296	25
18 IS					24	257		
19 IS	ND	86.3	14.96	13.21	13.2		350	23
20	ND	ND	ND	ND	ND	ND	ND	ND
21	ND	ND	ND	ND	ND	ND	ND	ND
22 IS	17.9	35.5	15.68	13.59	13.8	ND	313	21

a OD = On-Deck incubation; IS = in situ incubation
b Cosine collector
c Hemispherical collector
d Not determined

Variability in rates of primary production integrated over the euphotic zone during the first two years of the time-series program appear to be stochastic with no evidence of a seasonal cycle. Measured rates ranged between approximately 150 and 1100 mgC m^{-2} day^{-1} with the highest rate being observed in August 1989. This high rate of primary production coincided with a

cyanobacterial bloom observed in surface waters near Station ALOHA on this cruise (Chiswell *et al*., 1990). This variability, with a range of almost a factor of 7, is surprisingly large. However, the majority of the primary production estimates ranged between 250 and 550 mgC m^{-2} day^{-1}, and the average rate of primary production was approximately 450 mgC m^2 day'. Although this value is higher than historical measurements for the central ocean basins would suggest (Ryther, 1969), it is consistent with more recent measurements using modem methodology (Martin *et al*., 1987; Knauer *et al*., 1990).

In general, on-deck incubations yield somewhat lower values than *in situ* incubations (Figure 6.3.4). However, the two procedures produced similar temporal trends. Primary production rates measured over 24 hours generally yielded lower values than measurements made over 12 hours. However, the average offset between these measurements is small and on several cruises the 24-hour values were greater than or equal to the 12-hour results (Figure 6.3.5).

4.2.3. Particle Flux

Particulate carbon (PC), nitrogen (PN), phosphorus (PP), and mass fluxes measured at 150 m are presented in Table 4.3. In order to put our 1990 data in the context of the entire time series data set, the first two years of the time series particle flux measurements is plotted in Figures 6.3.6-15.. PC flux at 150 m ranges from approximately 20 mgC m^{-2} day^{-1} to a little more than 60 mgC m^{-2} day^{-1}. This factor of three variability displays what appears to be an annual pattern with peaks in carbon flux in both the early spring and in the late summer months (Figure 6.3.6). With the exception of anomalous high PP fluxes measured on the first two HOT cruises, temporal variability in PN, PP, and mass flux show similar temporal trends, and also vary between cruises by a factor of three or more (Figures 6.3.7-9). Elemental ratios of carbon and nitrogen at 150 m are typically between 6 and 10 at 150 m and show no obvious temporal pattern (Figure 6.3.10). These vertical flux estimates and elemental ratios are consistent with those measured in the central Pacific Ocean by the VERTEX program (Martin *et al*., 1987). Nitrogen flux at 150 m, as a percent of photosynthetic nitrogen assimilation (calculated from carbon-14 primary production values assuming a C:N ratio [by atoms] of 6.6) is shown in Figure 6.3.11. This estimate of 'F ratio' ranges between approximately 2 and 10%. No clear seasonal trend is evident and much of the variability is presumably due to uncertainties in the estimates of primary production and nitrogen flux. The average value (approximately 6.5%) is consistent with the estimate of new production for the oligotrophic central gyres made by Eppley and Peterson (1979) and with field data from the VERTEX program (Knauer *et al*., 1990).

Average fluxes of carbon, nitrogen, phosphorus, and total mass at 150, 300, and 500 m from the first two years of the time-series observations are shown in Figures 6.3.12-15. For carbon, nitrogen, phosphorus, and total mass, the flux declines rapidly with depth, presumably due to the rapid dissolution and remineralization of organic particles sinking through the water column. The flux of carbon at 500 m is less than 50% of the flux at 150 m.

Table 4.3: Station ALOHA Sediment Trap Flux Data

Cruise	Depth (m)	Carbon mg m^{2}day	sd;diff[a]	n	Nitrogen mg m^{2}day	sd;diff[a]	n	Phosphorus mg m^{2}day	sd;diff[a]	n	Mass Flux mg m^{2}day	sd;diff	n
13	150	23.3[b]	2.2	6	3.7	0.3	6	0.30	0.06	3	45.1	3.3	3
13	300	11.1	0.7	6	1.5	0.1	6	0.32	0.13	3	29.4	0.9	3
13	500	8.6	0.7	5	1.3	0.04	5	0.10	0.03	3	33.7	6.5	3
14	150	54.1	3	6	6.8	0.6	6	0.72	0.05	3	117	2.6	3
14	300	28.7	5.3	6	2.7	1	6	0.38	0.15	3	68.5	13.8	3
14	500	17.5	4.2	6	1.1	0.6	6	0.16	0.01	3	42.9	3.7	3
15	150	43.4	4.1	5	6	0.7	5	0.95	0.36	3	85.1	4.3	3
15	300	28.1	1.3	5	2.4	0.3	5	0.35	0.15	3	131	17.6	3
15	500	21.5	2.2	6	1.5	0.2	6	0.32	0.06	3	100	16.5	3
16	150	29.4	6.9	6	3.5	0.6	6	0.48	0.08	3	40.3	9.7	3
16	300	12.4	1.2	6	1.4	0.1	6	0.10	0.07	3	22.1	4.9	3
16	500	9.2	1.6	6	1.2	0.1	6	0.28	0.25	3	19.6	9.3	3
17	150	17.7	3.4	6	2.2	0.1	6	0.28	0.01	3	28.3	1.8	3
17	300	17.2	5.6	6	2	0.4	6	0.21	0.04	3	19.1	2.1	3
17	500	9.3	3.2	6	0.8	0.2	6	0.05	0.05	3	15.3	1.7	3
18	150	36.5	2.9	6	5.4	0.9	6	0.46	0.14	3	70.2	11.6	3
18	300	21.3	3.2	6	1.5	0.2	6	0.36	0.17	3	33.2	8.9	3
18	500	12.9	2.4	6	0.8	0.2	6	0.20	0.11	3	18.8	6.4	3
19	150	40.7	3.2	6	6	0.8	6	0.52	0.16	3	82.3	6.4	8
19	300	28.3	11.3	6	4.2	2	6	0.29	0.03	3	52.4	10.1	3
19	500	6.8	0.5	6	0.7	0.1	6	0.10	0.03	3	29	11.1	3
20	150	46.1	7.3	6	8.3	1.4	6	0.66	0.15	3	90.1	7.6	3
20	300	10.1	1.2	6	1	0.05	6	0.06	0.01	3	37.5	15.2	3
20	500	8.4	1.4	6	0.8	0.1	6	0.07	0.02	3	27.5	11.7	3
22	150	22.2	7.8	6	4.2	1.3	6	0.47	0.17	3	54.2	2	3
22	300	11.9	3.7	6	1.3	0.1	6	0.10	0.05	3	24.2	2.7	3
22	500	6.9	1.2	6	1.2	0.1	6	0.29	0.37	2	21.7	5	3

a When n ≥ 3 or the variability is expressed as std. dev. (sd); when n = 2 variability is expressed as the difference (diff)
b All cruises used on-deck T = 0 blank corrections

4.3. ADCP Measurements

An overview of the shipboard ADCP data set is given by the plots of reference layer velocity and position (Figures 6.4. 1-10). On HOT-13 and -18 the currents on station were dominated by

mean flows to the west and northwest, respectively. HOT- 18 was unusual in that the mean flow was to the southeast The mean flow was very weak on HOT-20 and -22. Like the mean flows, the tidal and inertial components varied widely from cruise to cruise.

4.4. Meteorology

The meteorological data are summarized in Figures 6.5. 1-10. All parameters show slight evidence of annual cycles, although the daily and weekly ranges are nearly as high as the annual range. SST and air and wet-bulb temperatures appear to be loosely correlated, all having lowest values in February, but maximum SST leads maximum air temperatures by between one and two months. Meteorological data collected at NDBC Buoy 51001 (Figure 1.1) during the period covered by this report are presented in Figures 6.5.7-10.

4.5. Light measurements

Integrated irradiance measurements made with the on-deck cosine collector on days that primary production experiments were conducted are presented in Table 4.2. Vertical profiles of PAR as a percent of surface irradiance obtained with the optical profiler on HOT-13 to -22 are presented in Figure 6.6.1. Semilog plots of underwater irradiance as a percent of surface PAR show considerable variability and a fairly uniform exponential decrease to at least 180 m. The noise present in these plots in the upper 40 m is variable between cruises and is due to changes in sea surface roughness. The 1% light level was found at depths between 80 and 100 m, as is typical for this oceanic realm.

5. References

Armstrong, F.AJ., P.M. Williams and J.D.H. Strickland, 1966: Photo-oxidation of organic matter in sea water by ultraviolet radiation, analytical and other applications. *Nature*, **211**, 481-483.

Carpenter, J.H., 1965: The accuracy of the Winkler method for dissolved oxygen analysis. *Limnology and Oceanography*, **10**, 135-140.

Chiswell, S.M., 1991: Dynamic response of CTD pressure sensors to temperature. *Journal of Atmospheric and Oceanic Technology*, **8**, 659—668.

Chiswell, S.M., E. Firing, D. Karl, R. Lukas, C. Winn, 1990: Hawaii Ocean Time-series Program Data Report 1, 1988-1989. School of Ocean and Earth Science and Technology Report 1, University of Hawaii, 269 pp.

Eppley, R.W. and Peterson, B.J., 1979: Particulate organic matter flux and planktonic new production in the deep ocean. *Nature*, **282**, 677—680.

Karl, D.M., C.D. Winn, D.V.W. Hebel and R. Letelier, 1990: Hawaii Ocean Time-series Program Field and Laboratory Protocols. September 1990.

Knauer, G.A., D.G. Redalje, W.G. Harrison and D.M. Karl, 1990: New production at the VERTEX time-series site. *Deep-Sea Research*, **37**, 1121—1134.

Lukas, R. and S. Chiswell, 1991: Submesoscale water mass variations in the salinity minimum of the north Pacific near Hawaii. *WOCE Notes*, 3(1), 1,6—8.

Martin, J.H., G.A. Knauer, D.M. Karl and W.W. Broenkow, 1987: VERTEX: Carbon cycling in the northeast Pacific. *Deep-Sea Research*, 34, 267—285.

Menzel, D.W. and RE Vacarro, 1964: The measurement of dissolved and particulate organic carbon in seawater. *Limnology and Oceanography*, 9, 138—142.

Owens, W.B. and Millard, R.C., 1985: A new algorithm for CTD oxygen calibration. *Journal of Physical Oceanography*, 15, 621—631.

Press, W., B. Flannery, S. Teokolsky, W. Vetterling, 1988: Numerical recipes in C. Cambridge U. Press, 735 pp.

Reid, J.L., 1965: Intermediate waters of the Pacific Ocean. *Johns Hopkins Oceanographic Studies*, 2, 85 pp.

Ryther J. H., 1969: Photosynthesis and fish production in the sea: The production of organic matter and its conversion to higher forms of life vary through the world ocean. *Science*, 166, 72—76.

Strickland, J.D.H. and T.R. Parsons, 1972: A practical handbook of seawater analysis. Fisheries Research Board of Canada, 167 pp.

Talley, L.D. and T.M. Joyce, 1990: Trans-Pacific sections at 47°N and 152°W: Distribution of properties. *Deep-Sea Research*, in press.

Tsuchiya, M., 1968: Upper waters of the intertropical Pacific Ocean. *Johns Hopkins Oceanographic Studies*, **4**, 49 pp.

UNESCO, 1981: Tenth report of the joint panel on oceanographic tables and standards. *UNESCO Technical Papers in Marine Science*, No. 36, UNESCO, Paris.

Walsh, T.W., 1989: Total dissolved nitrogen in seawater: a new high-temperature combustion method and a comparison with photo-oxidation. *Marine Chemistry*, **26**, 295—311.

6. Figures

6.1. CTD Profiles

Figures 6.1.1-9: CTD and nutrient data collected at Kahe Point. Upper left panel: Temperature, salinity, oxygen, and density σ_θ as a function of pressure. Salinity and oxygen water bottle data are also plotted. Upper right panel: Nutrients (NO_3 + NO_2, $P0_4$ and SO_4) and oxygen as a function of potential temperature for all water samples. Lower right panel: Salinity and oxygen from CTD and water samples plotted as a function of potential temperature.

Figures 6.1.10a-18a (left pages): As in Figures 6.1.1—9 except for data collected at Station ALOHA. Lower left panel: Temperature and salinity as a function of pressure to 1000 dbars for all CTD casts.

Figures 6.1.lOb-18b (right pages): Stack plots of temperature and salinity against pressure to 1000 dbar for all CTD casts. Upper panel: Potential temperature versus pressure to 1000 dbars. Lower panel: Salinity versus pressure to 1000 dbars.

Figure 6.1.19: 1990 potential temperature profiles. Upper panel: Potential temperature versus pressure for all deep casts in 1990. Lower panel: Potential temperature for all deep casts in 1990 plotted from 2500 dbar.

Figure 6.1.20: 1990 temperature-salinity plots. Upper panel: Potential temperature versus salinity for all deep casts collected during 1990. Lower panel: Potential temperature versus density on same casts in the 1-5°C range.

Figure 6.1.21: 1990 oxygen profiles. Upper panel: Oxygen values derived from calibrated CTD sensor data versus potential temperature for all deep casts collected during 1990. Lower panel: Oxygen versus potential temperature for 1990 deep casts within the 1-5°C range.

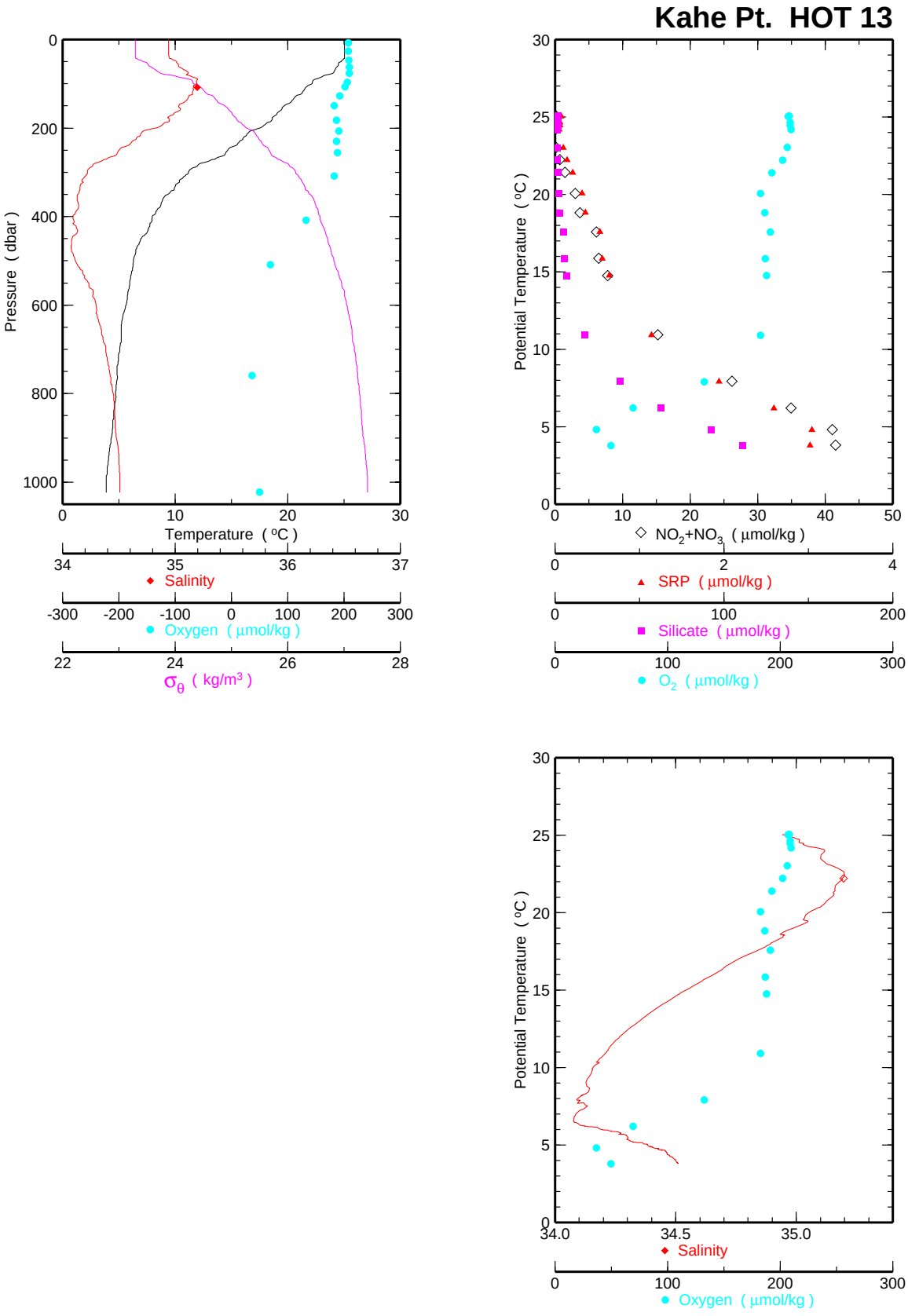
Kahe Pt. HOT 13
Pressure (dbar)
Temperature (°C)
Salinity
Oxygen (µmol/kg)
σθ (kg/m³)
Potential Temperature (°C)
NO2+NO3 (µmol/kg)
SRP (µmol/kg)
Silicate (µmol/kg)
O2 (µmol/kg)
Potential Temperature (°C)
Salinity
Oxygen (µmol/kg)

Figure 6.1.1

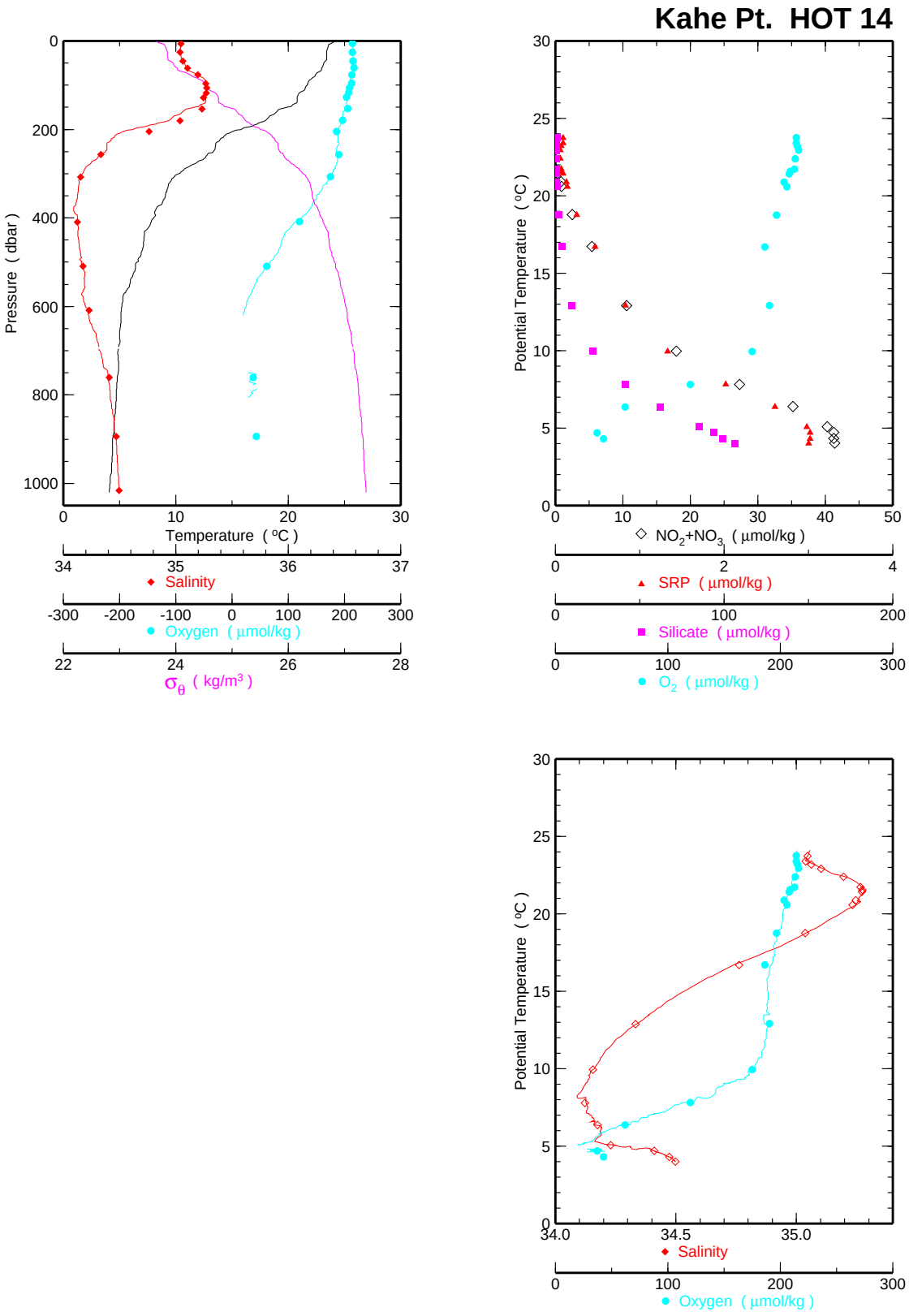
Kahe Pt. HOT 14
Pressure (dbar)
Temperature (°C)
Salinity
Oxygen (µmol/kg)
σθ (kg/m3)
Potential Temperature (°C)
NO2+NO3 (µmol/kg)
SRP (µmol/kg)
Silicate (µmol/kg)
O2 (µmol/kg)
Potential Temperature (°C)
Salinity
Oxygen (µmol/kg)

Figure 6.1.2

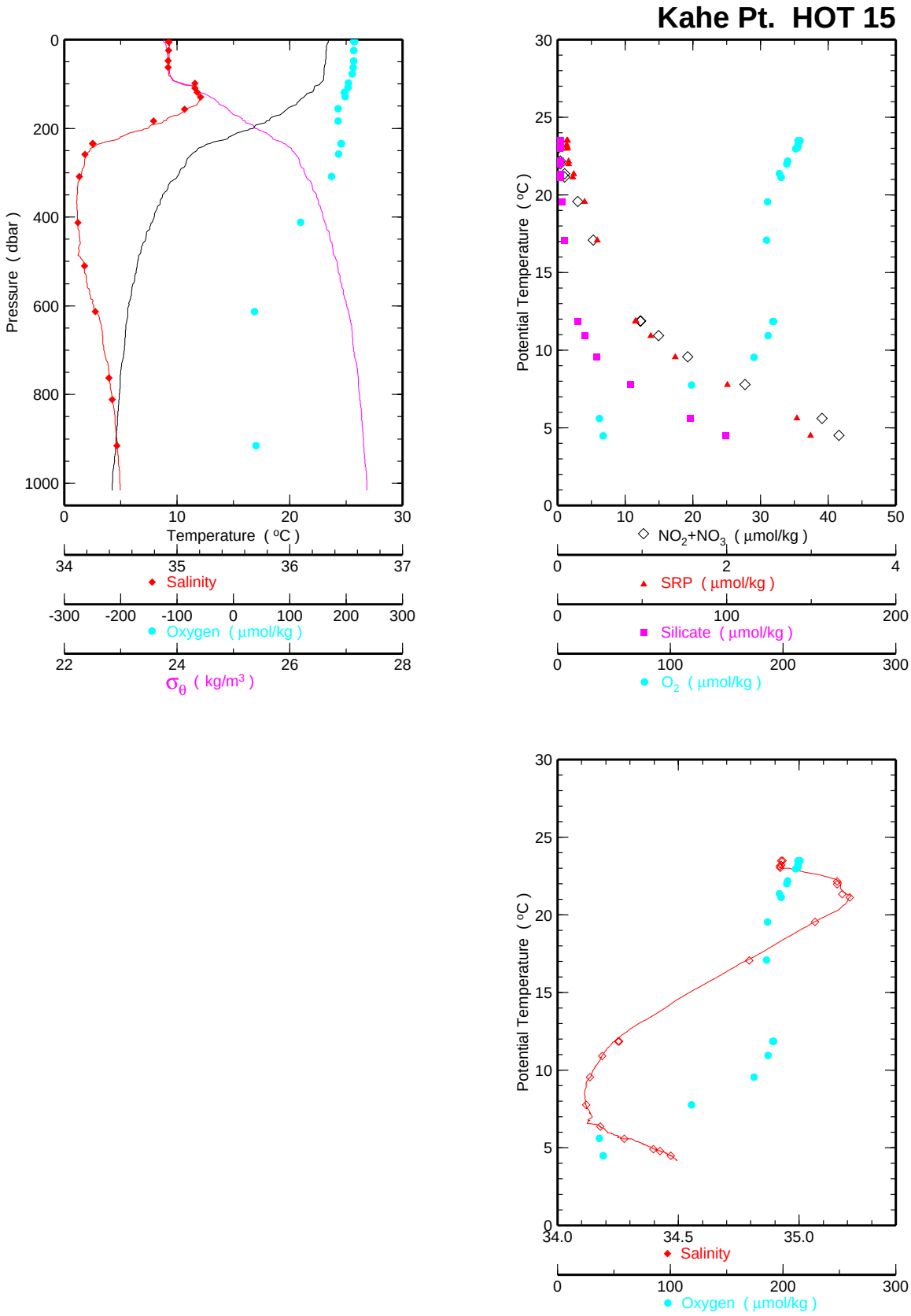
Kahe Pt. HOT 15
Pressure (dbar)
Temperature (ºC)
Salinity
Oxygen (µmol/kg)
σθ (kg/m³)
Potential Temperature (ºC)
NO2+NO3 (µmol/kg)
SRP (µmol/kg)
Silicate (µmol/kg)
O2 (µmol/kg)
Potential Temperature (ºC)
Salinity
Oxygen (µmol/kg)

Figure 6.1.3

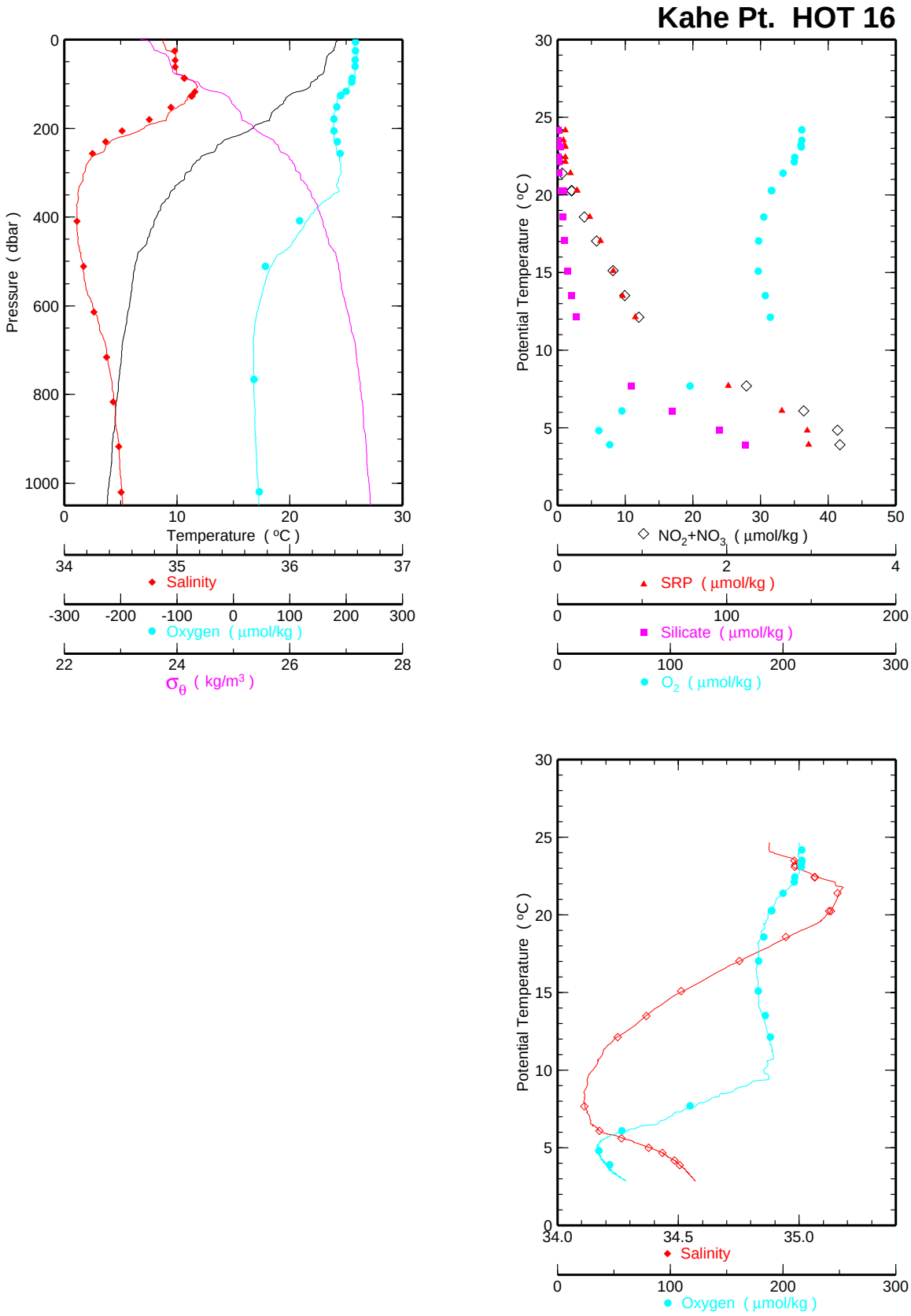
Kahe Pt. HOT 16
Pressure (dbar)
Temperature (ºC)
Salinity
Oxygen (µmol/kg)
σθ (kg/m³)
Potential Temperature (ºC)
NO2+NO3 (µmol/kg)
SRP (µmol/kg)
Silicate (µmol/kg)
O2 (µmol/kg)
Potential Temperature (ºC)
Salinity
Oxygen (µmol/kg)

Figure 6.1.4

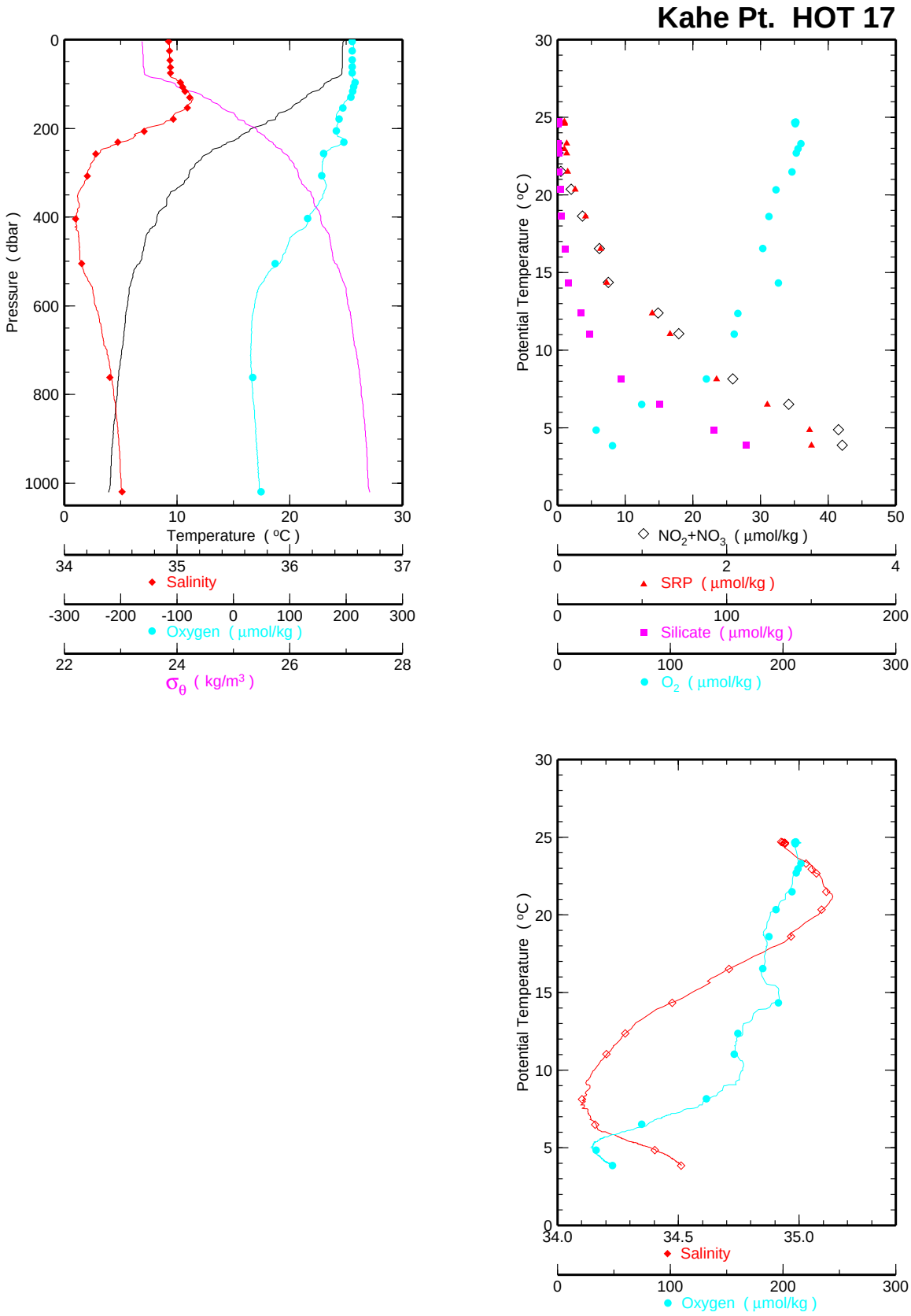
Kahe Pt. HOT 17
Pressure (dbar)
Temperature (ºC)
Salinity
Oxygen (µmol/kg)
σθ (kg/m³)
Potential Temperature (ºC)
NO2+NO3 (µmol/kg)
SRP (µmol/kg)
Silicate (µmol/kg)
O2 (µmol/kg)
Potential Temperature (ºC)
Salinity
Oxygen (µmol/kg)

Figure 6.1.5

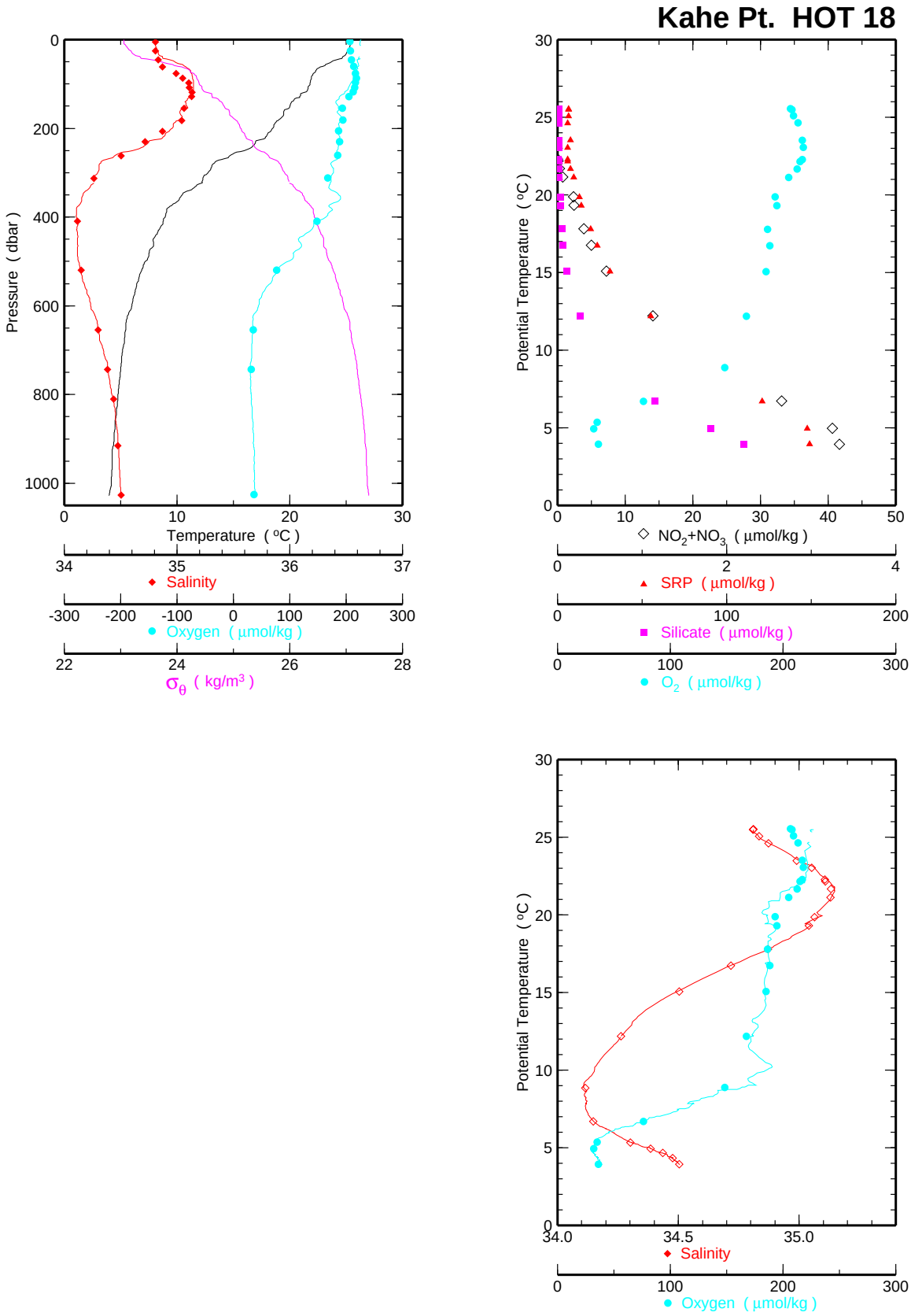
Kahe Pt. HOT 18
Pressure (dbar)
Temperature (ºC)
Salinity
Oxygen (µmol/kg)
σθ (kg/m³)
Potential Temperature (ºC)
NO2+NO3 (µmol/kg)
SRP (µmol/kg)
Silicate (µmol/kg)
O2 (µmol/kg)
Potential Temperature (ºC)
Salinity
Oxygen (µmol/kg)

Figure 6.1.6

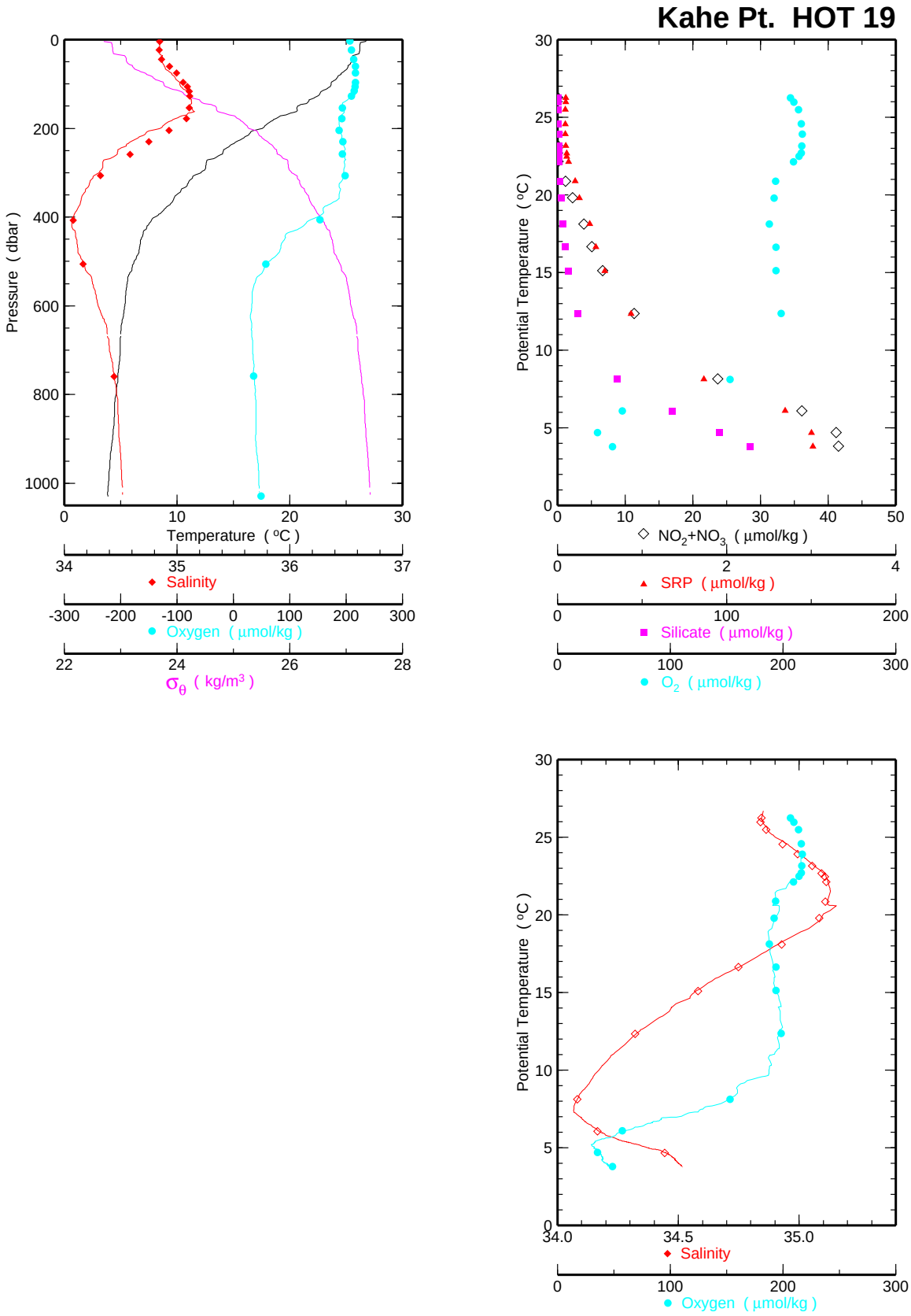
Kahe Pt. HOT 19
Pressure (dbar)
Temperature (ºC)
Salinity
Oxygen (µmol/kg)
σθ (kg/m³)
Potential Temperature (ºC)
NO2+NO3 (µmol/kg)
SRP (µmol/kg)
Silicate (µmol/kg)
O2 (µmol/kg)
Potential Temperature (ºC)
Salinity
Oxygen (µmol/kg)

Figure 6.1.7

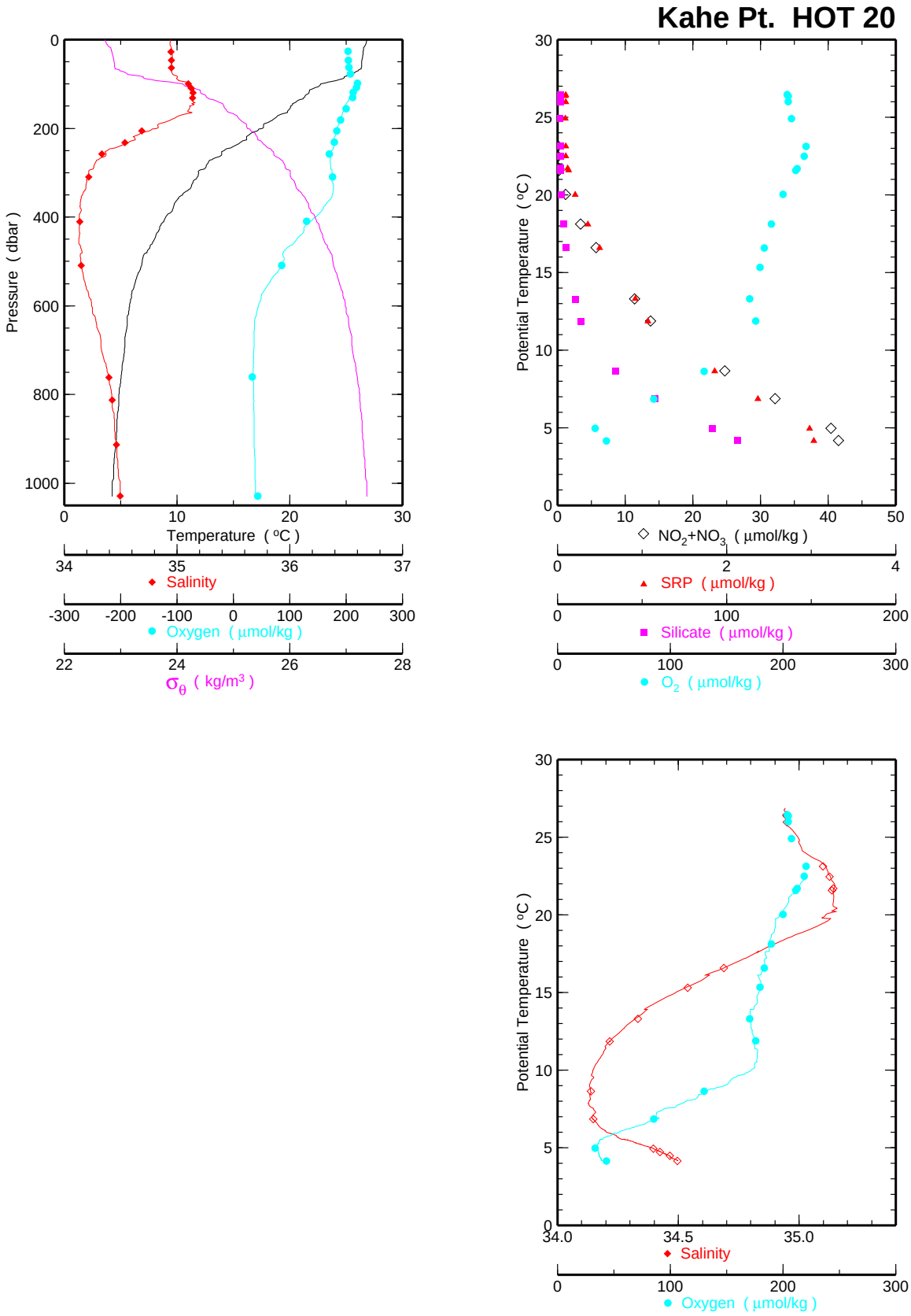
Kahe Pt. HOT 20
Pressure (dbar)
Temperature (ºC)
Salinity
Oxygen (µmol/kg)
σθ (kg/m³)
Potential Temperature (ºC)
NO2+NO3 (µmol/kg)
SRP (µmol/kg)
Silicate (µmol/kg)
O2 (µmol/kg)
Potential Temperature (ºC)
Salinity
Oxygen (µmol/kg)

Figure 6.1.8

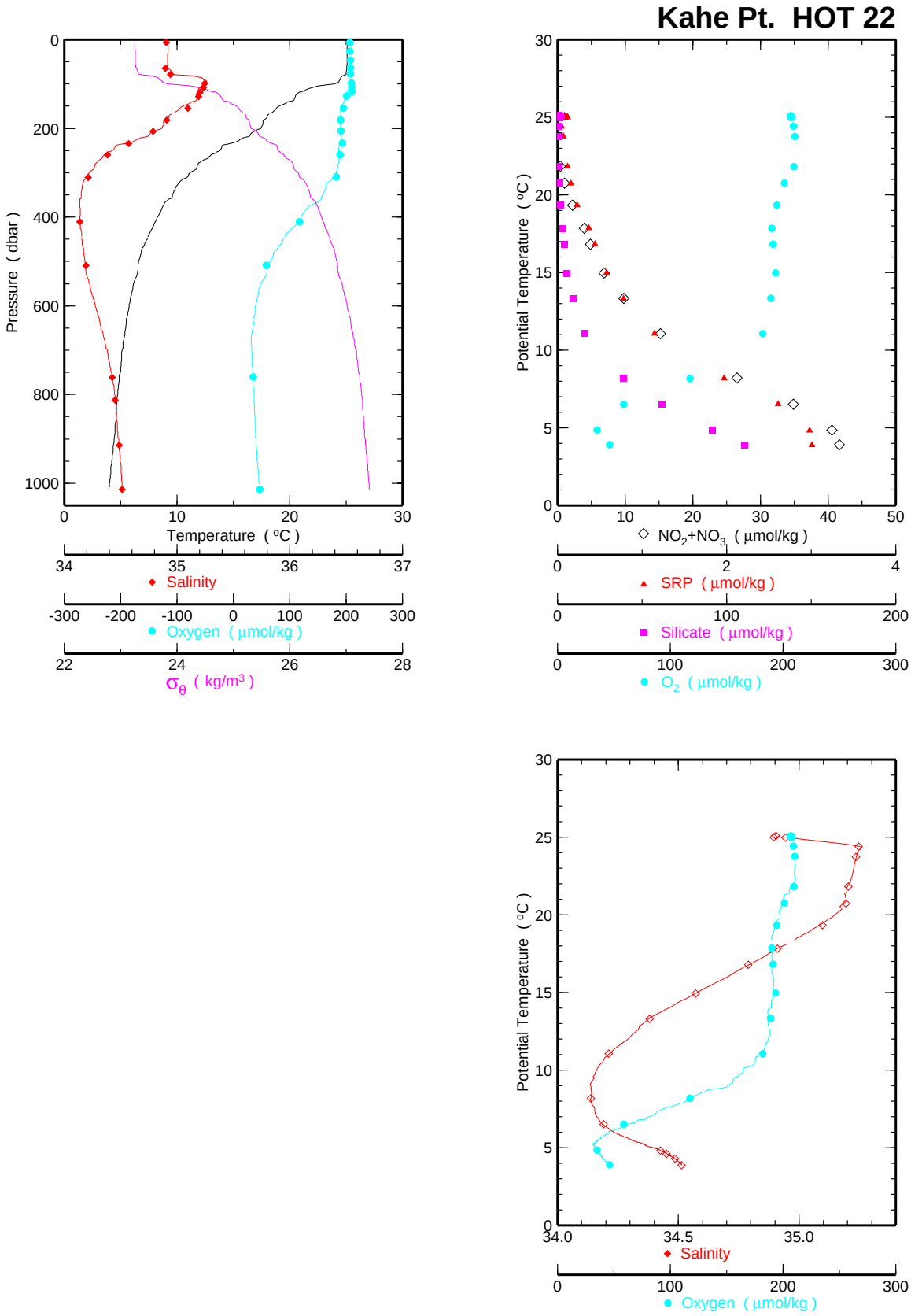
Kahe Pt. HOT 22
Pressure (dbar)
Temperature (ºC)
Salinity
Oxygen (µmol/kg)
σθ (kg/m³)
Potential Temperature (ºC)
NO2+NO3 (µmol/kg)
SRP (µmol/kg)
Silicate (µmol/kg)
O2 (µmol/kg)
Potential Temperature (ºC)
Salinity
Oxygen (µmol/kg)

Figure 6.1.9

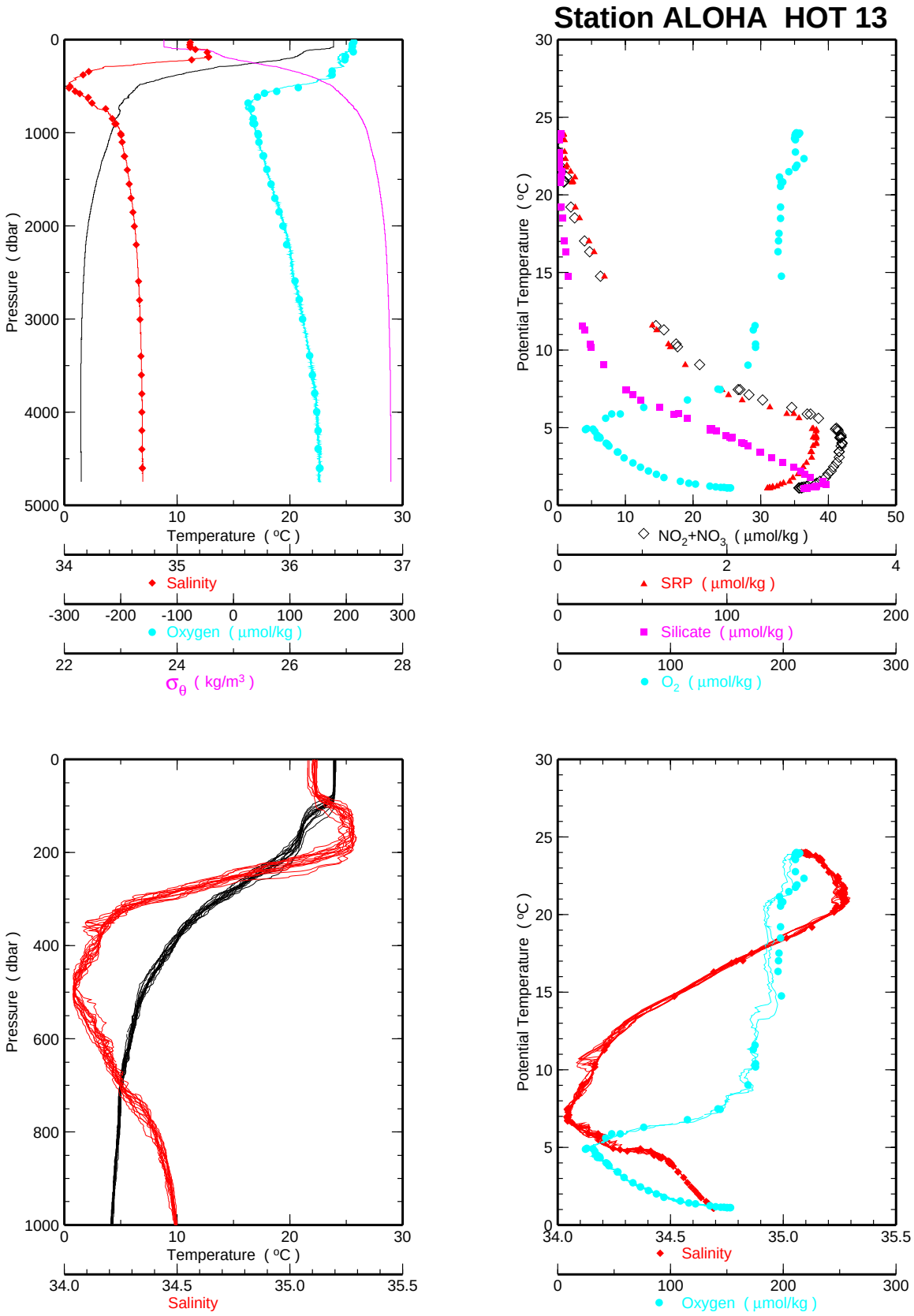

Figure 6.1.10a

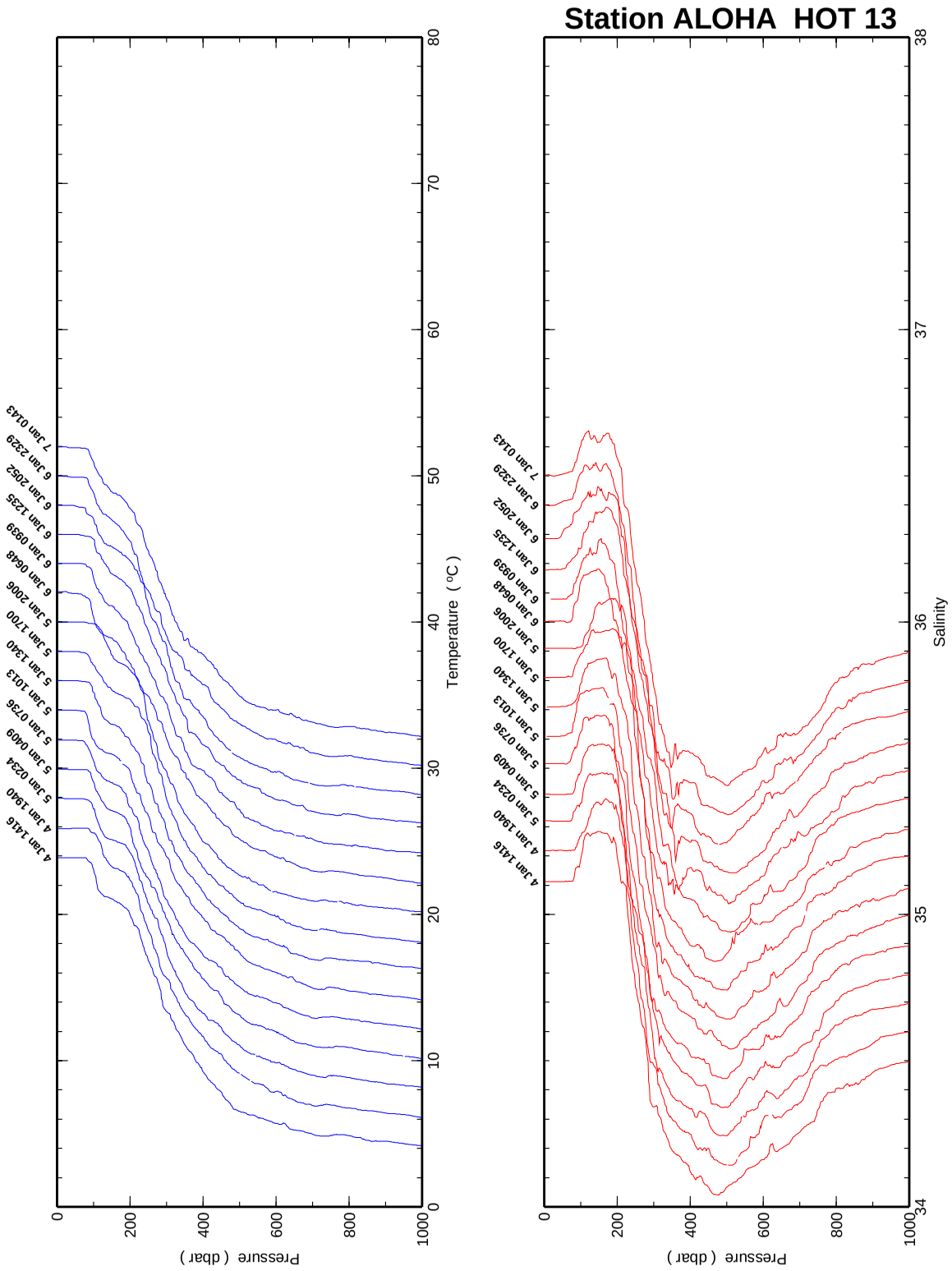

Figure 6.1.10b

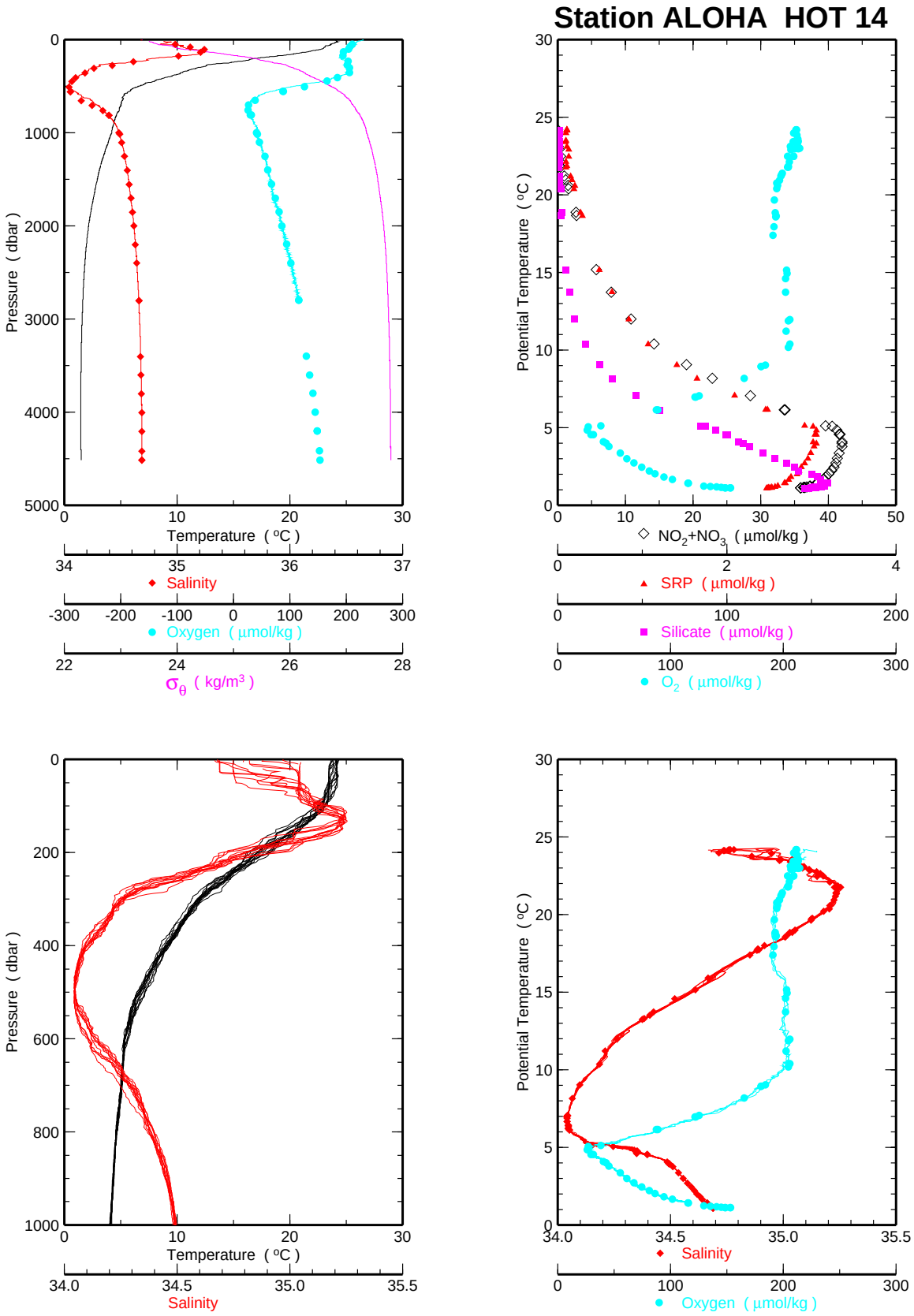

Figure 6.1.11a

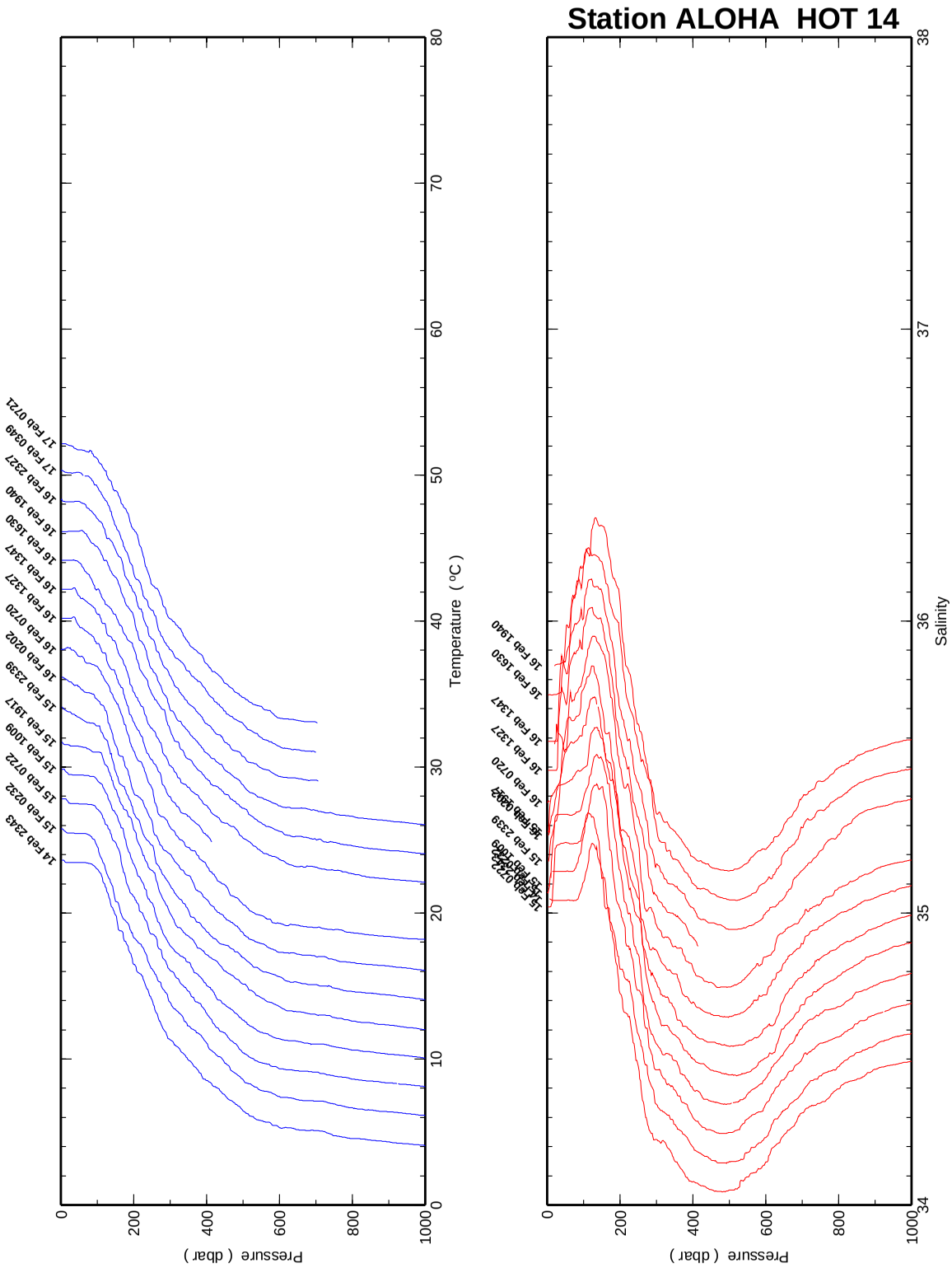

Figure 6.1.11b

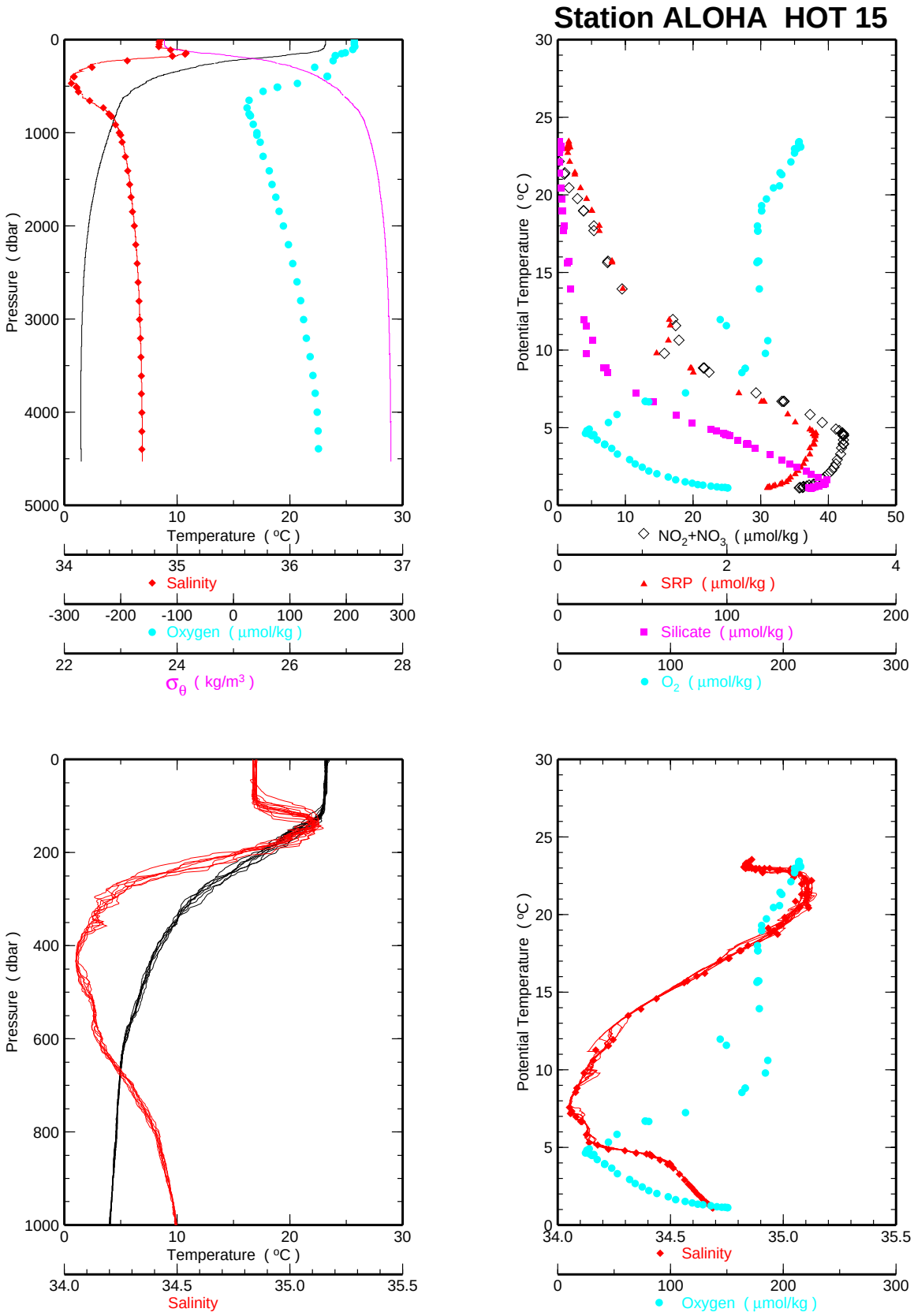

Figure 6.1.12a

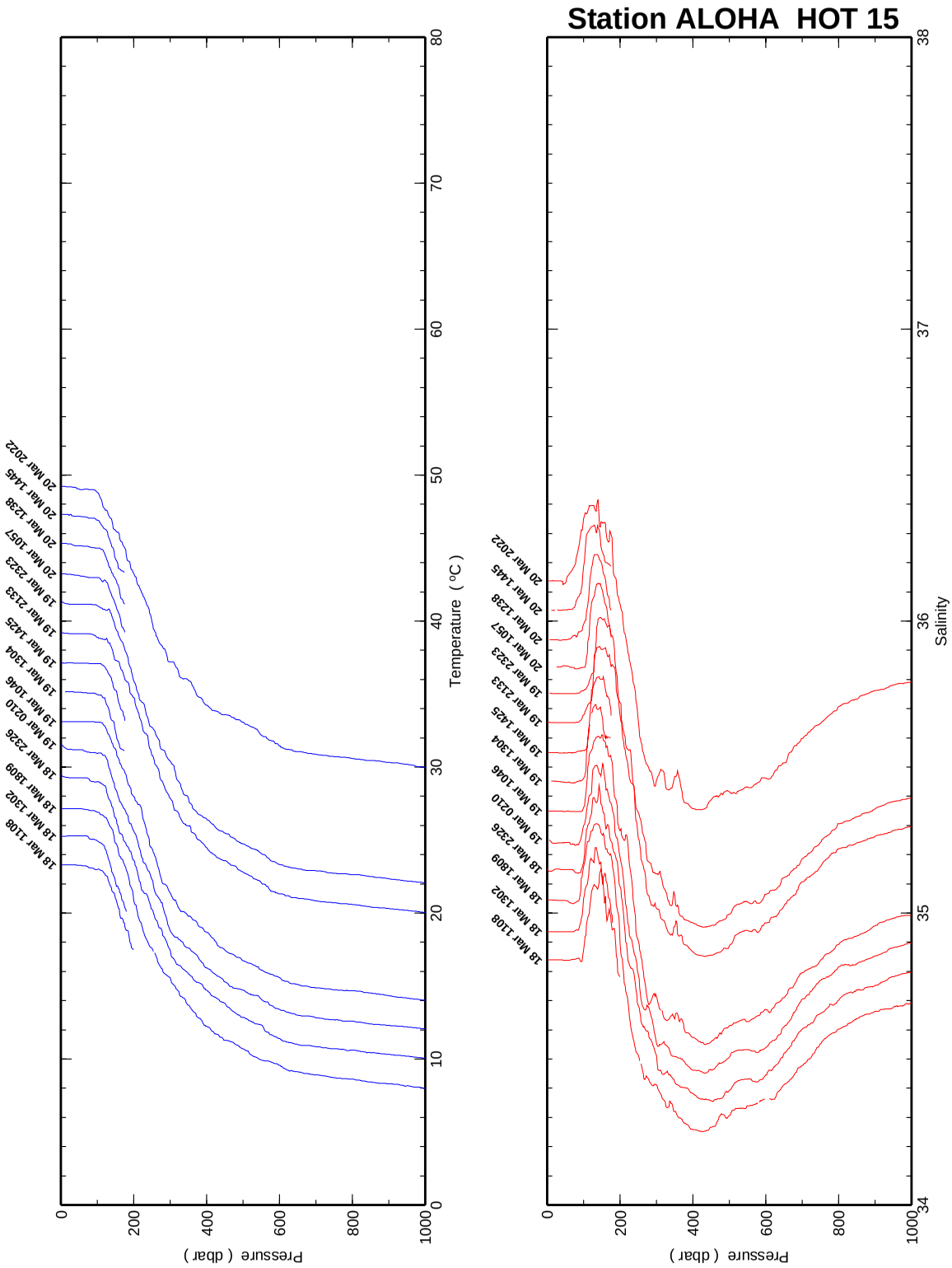

Figure 6.1.12b

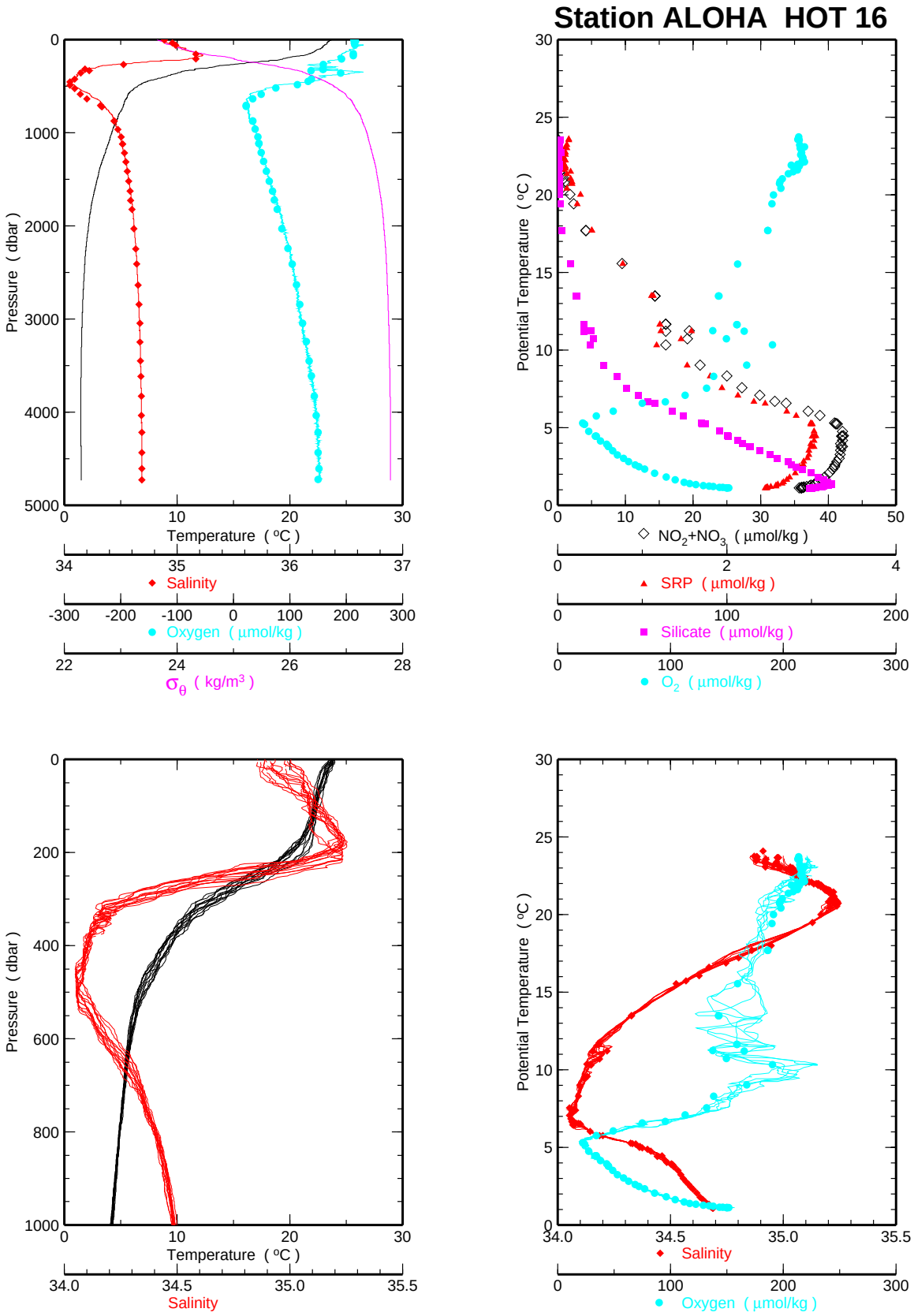

Figure 6.1.13a

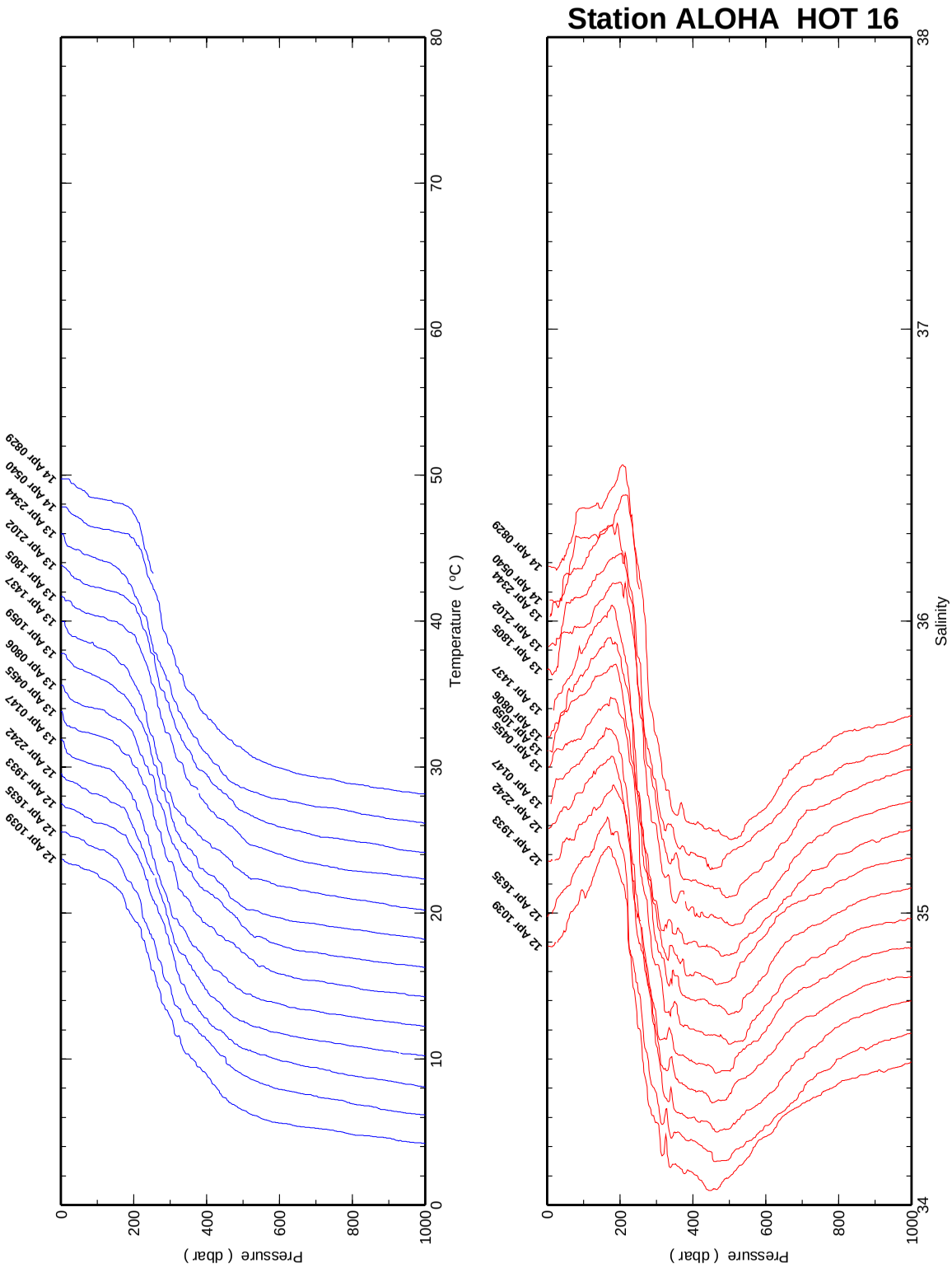

Figure 6.1.13b

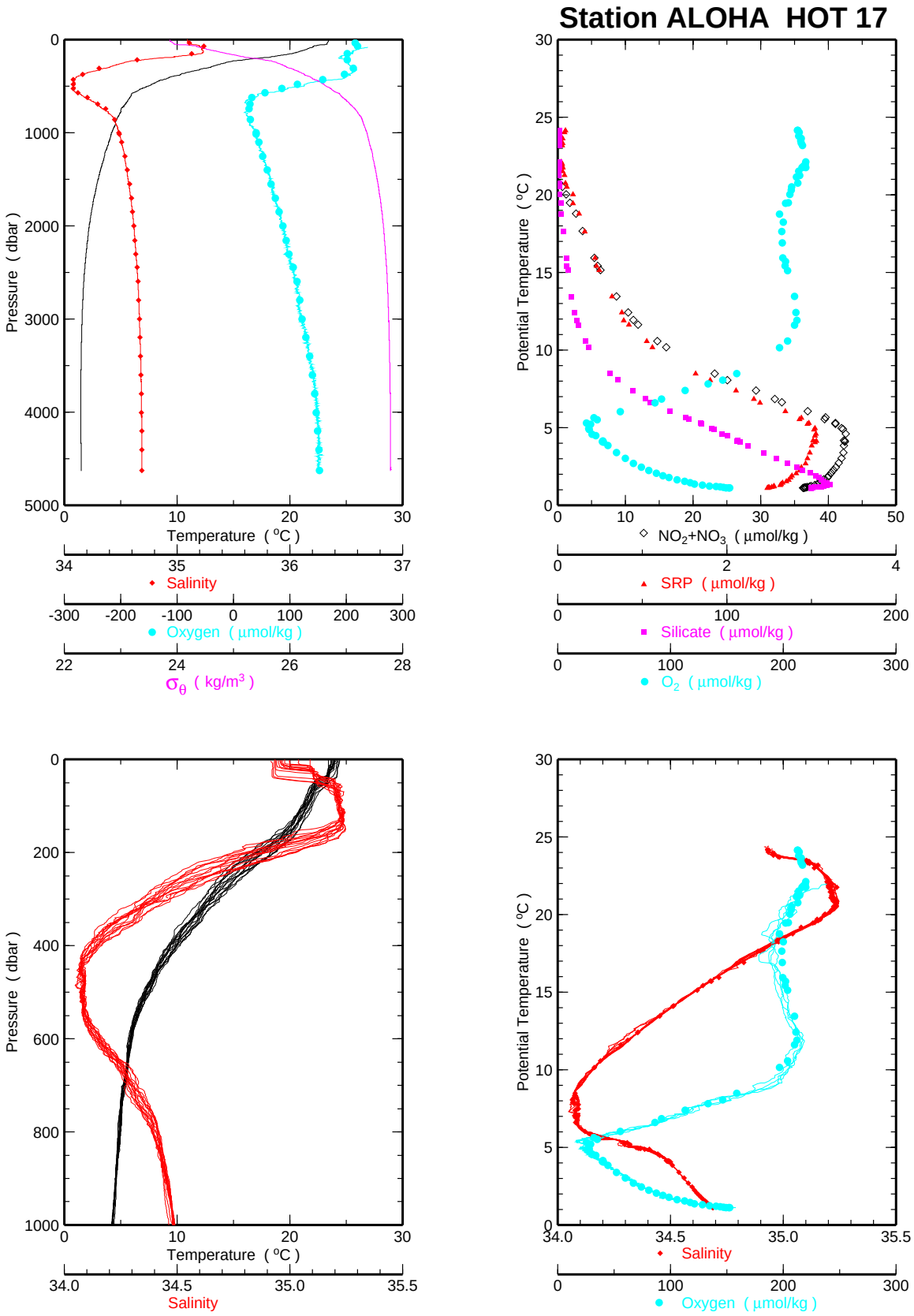

Figure 6.1.14a

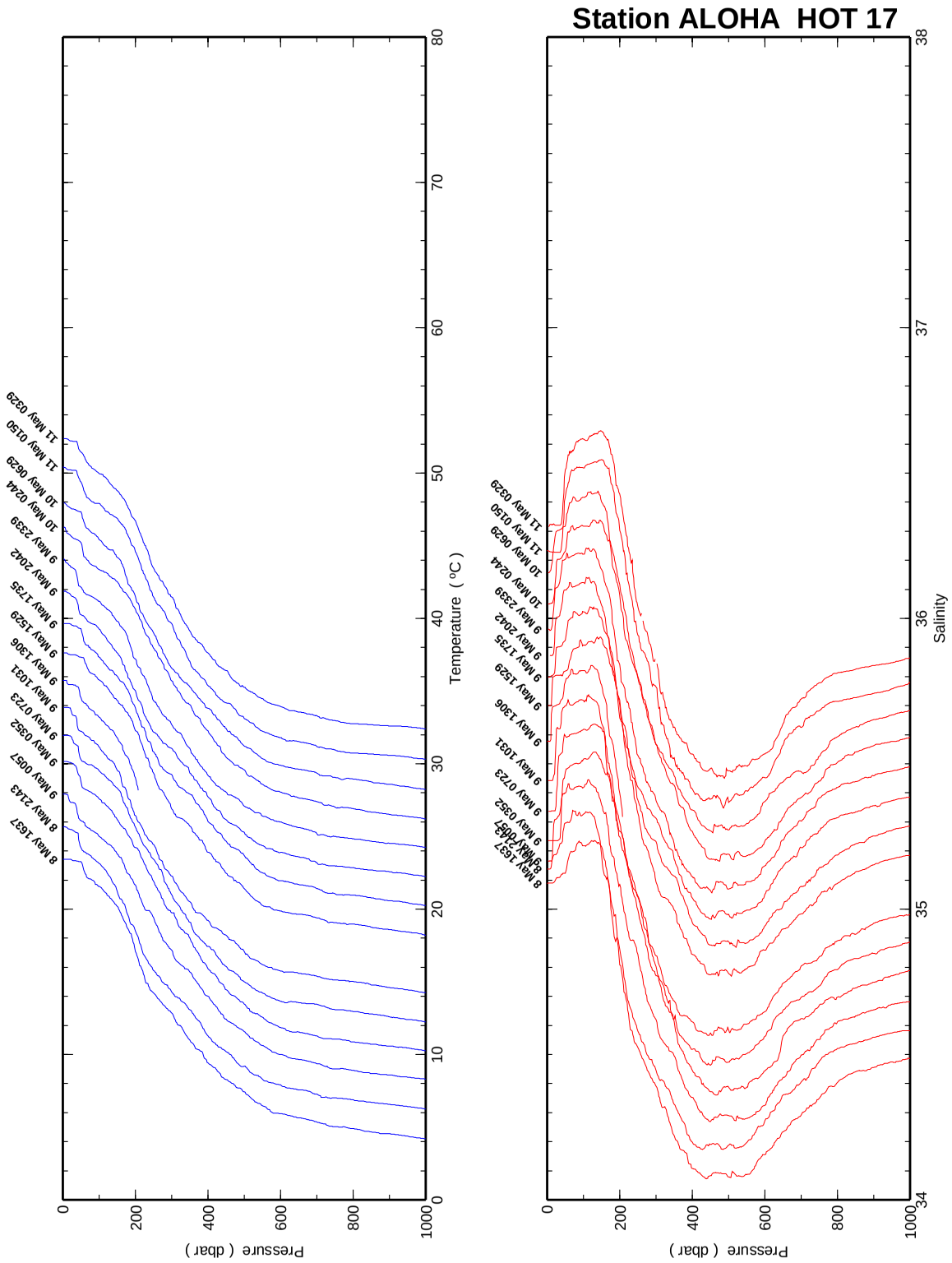

Figure 6.1.14b

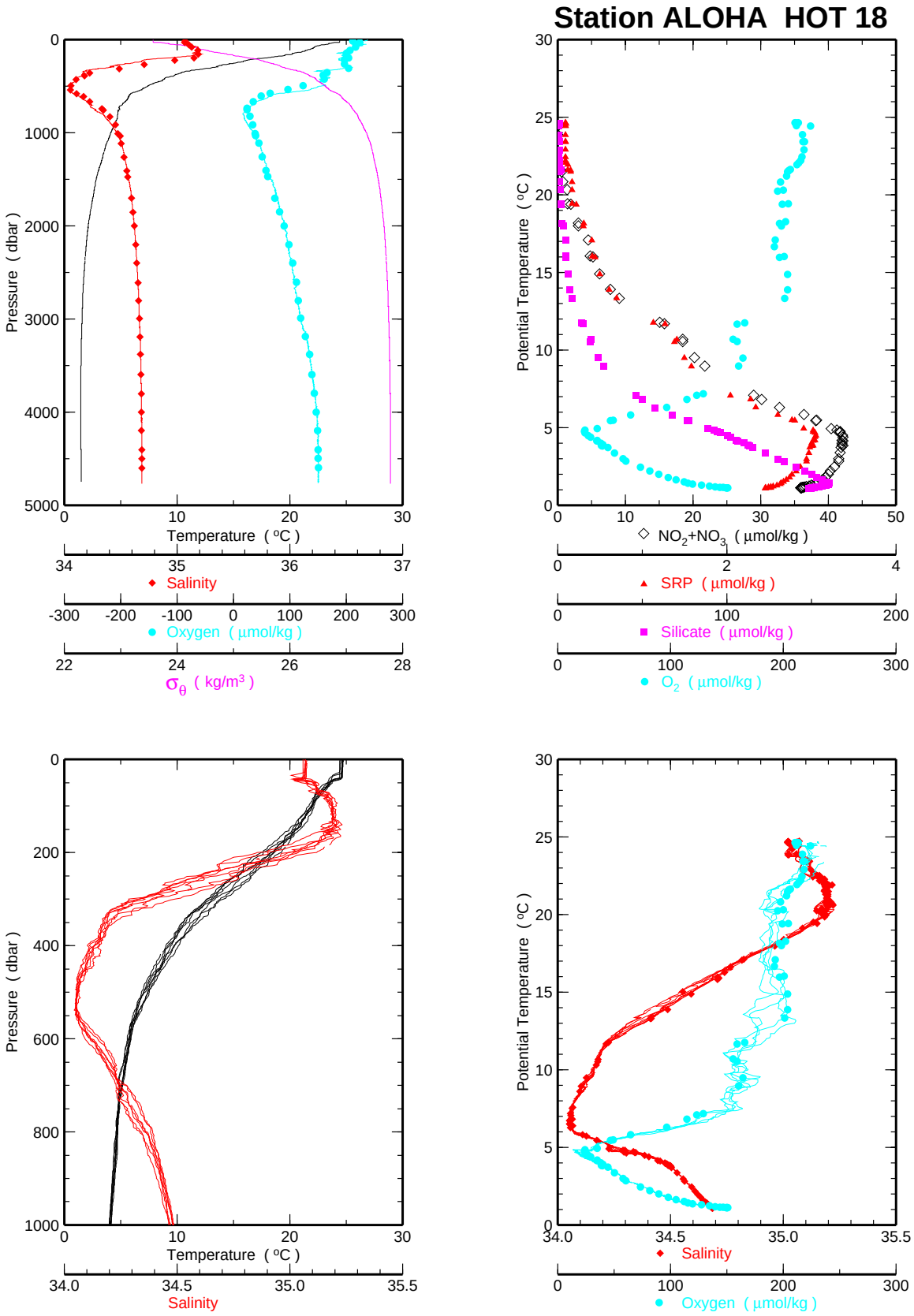

Figure 6.1.15a

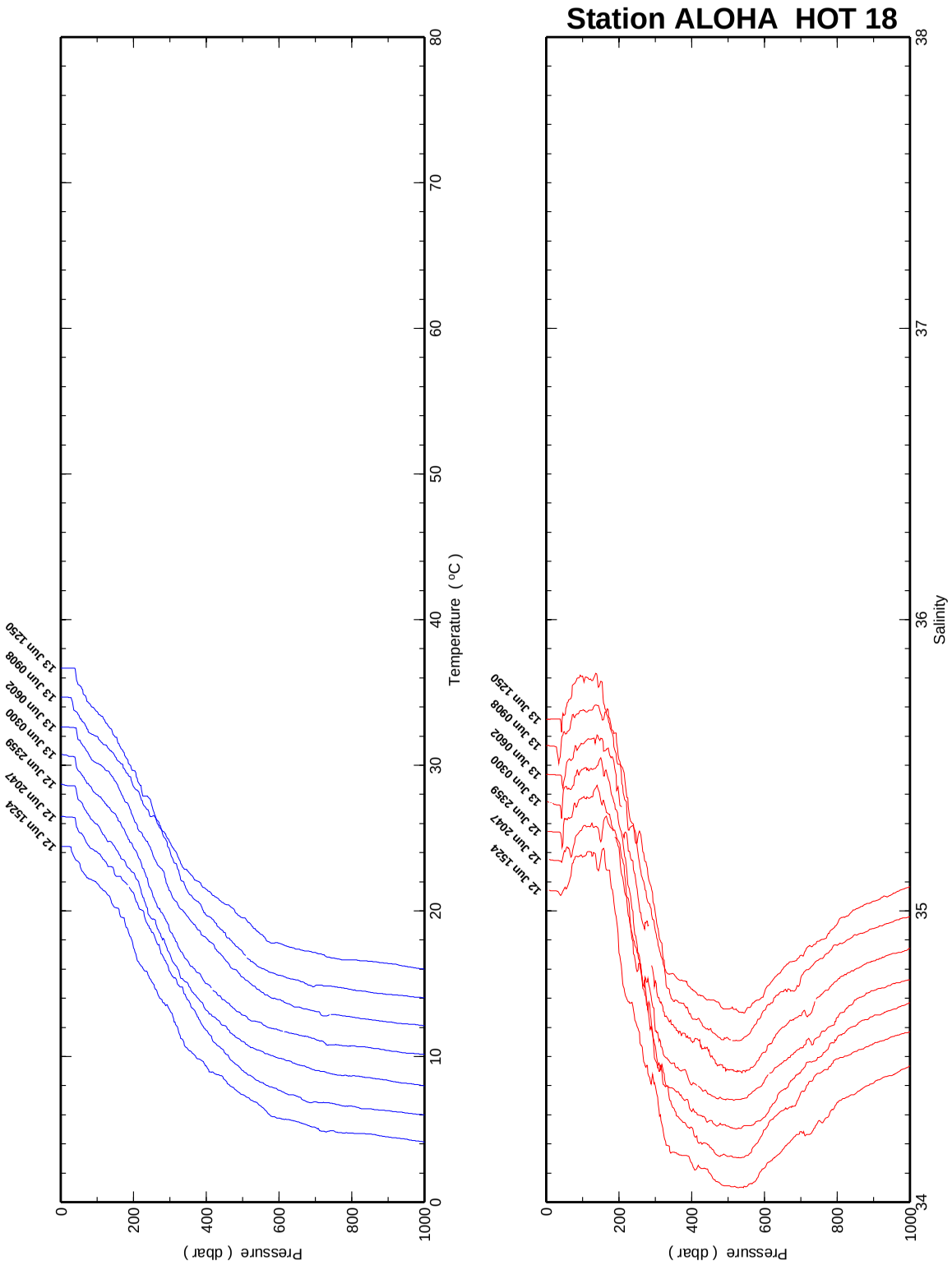

Figure 6.1.15b

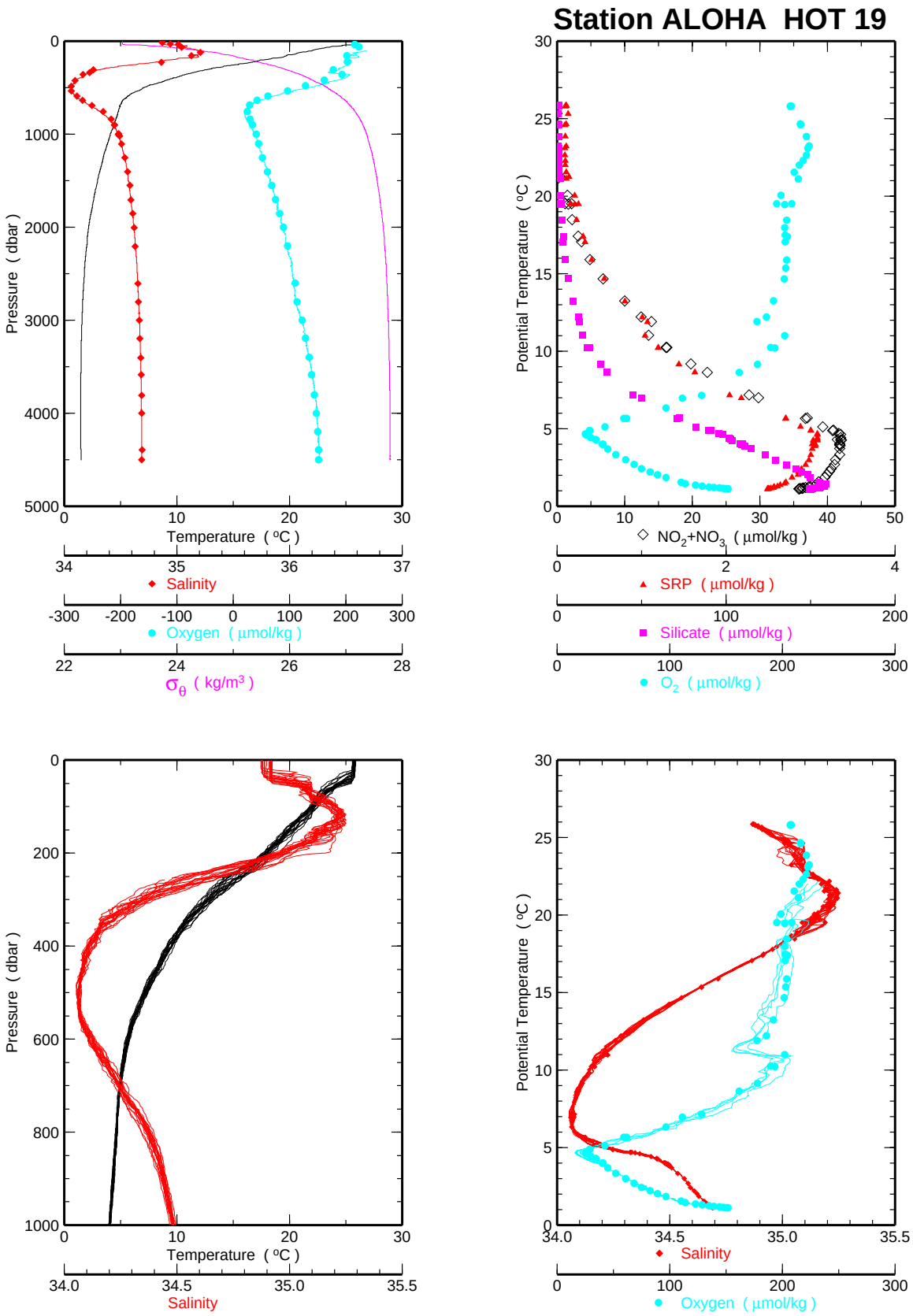

Figure 6.1.16a

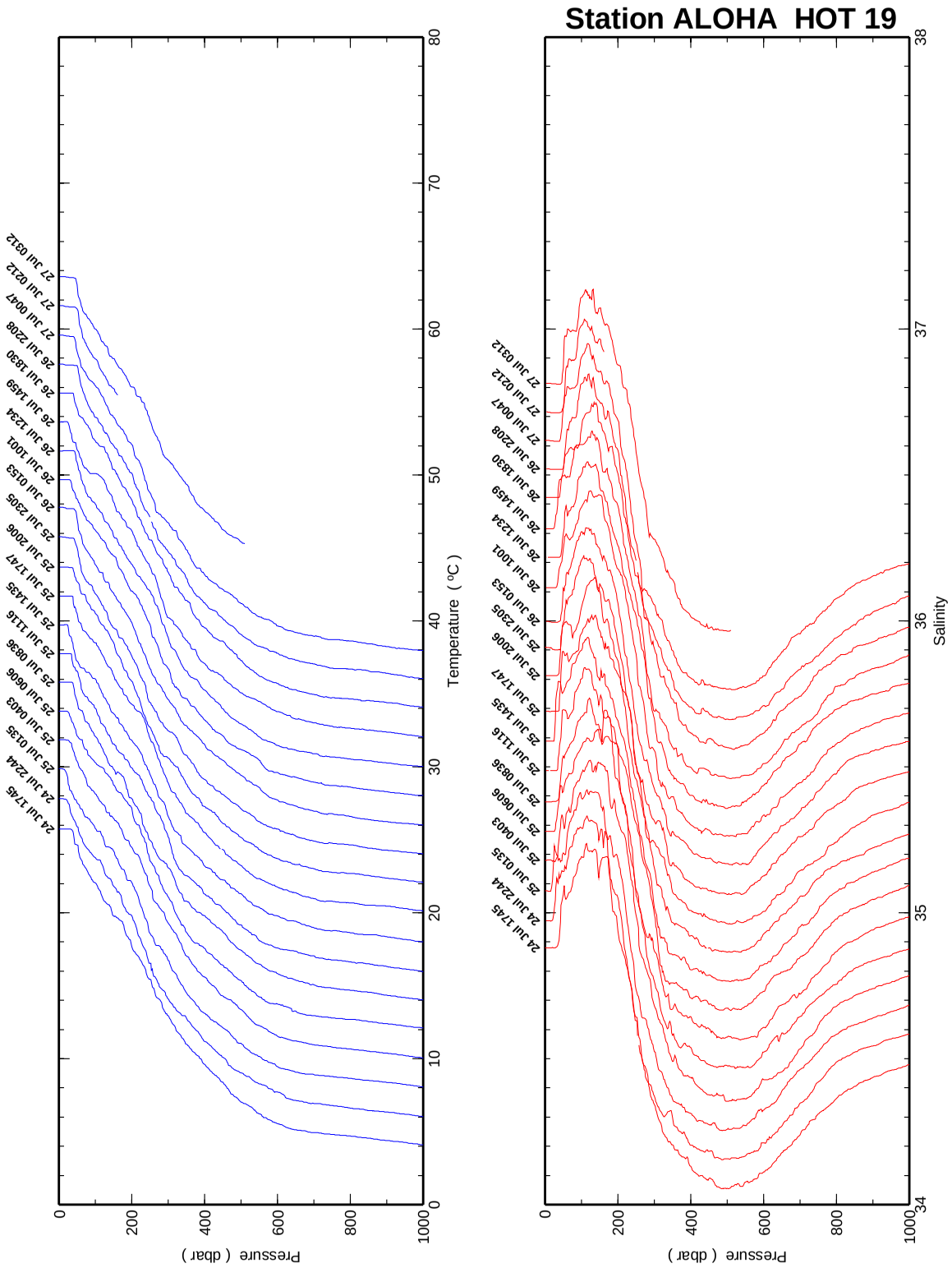

Figure 6.1.16b

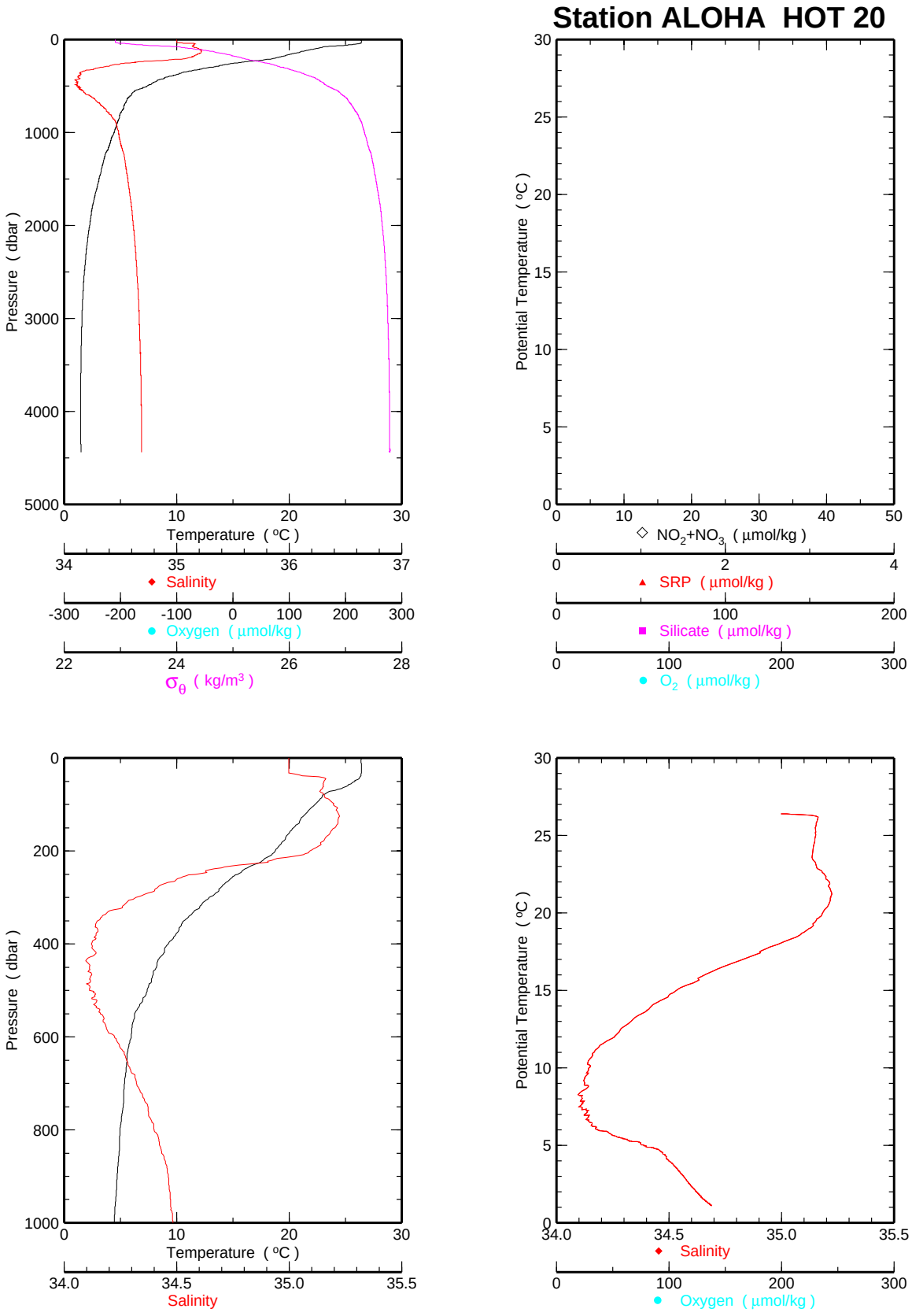

Figure 6.1.17a

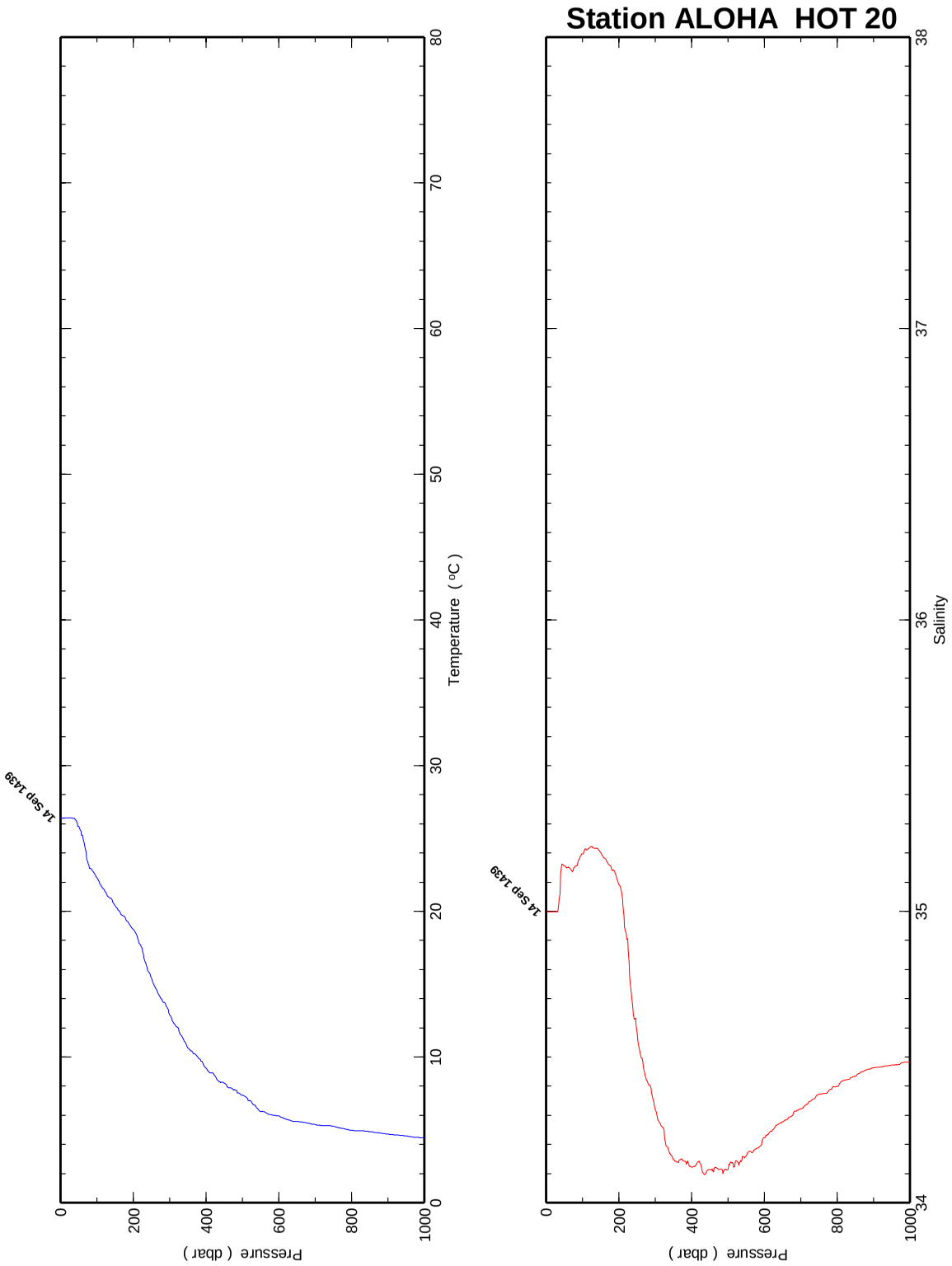

Figure 6.1.17b

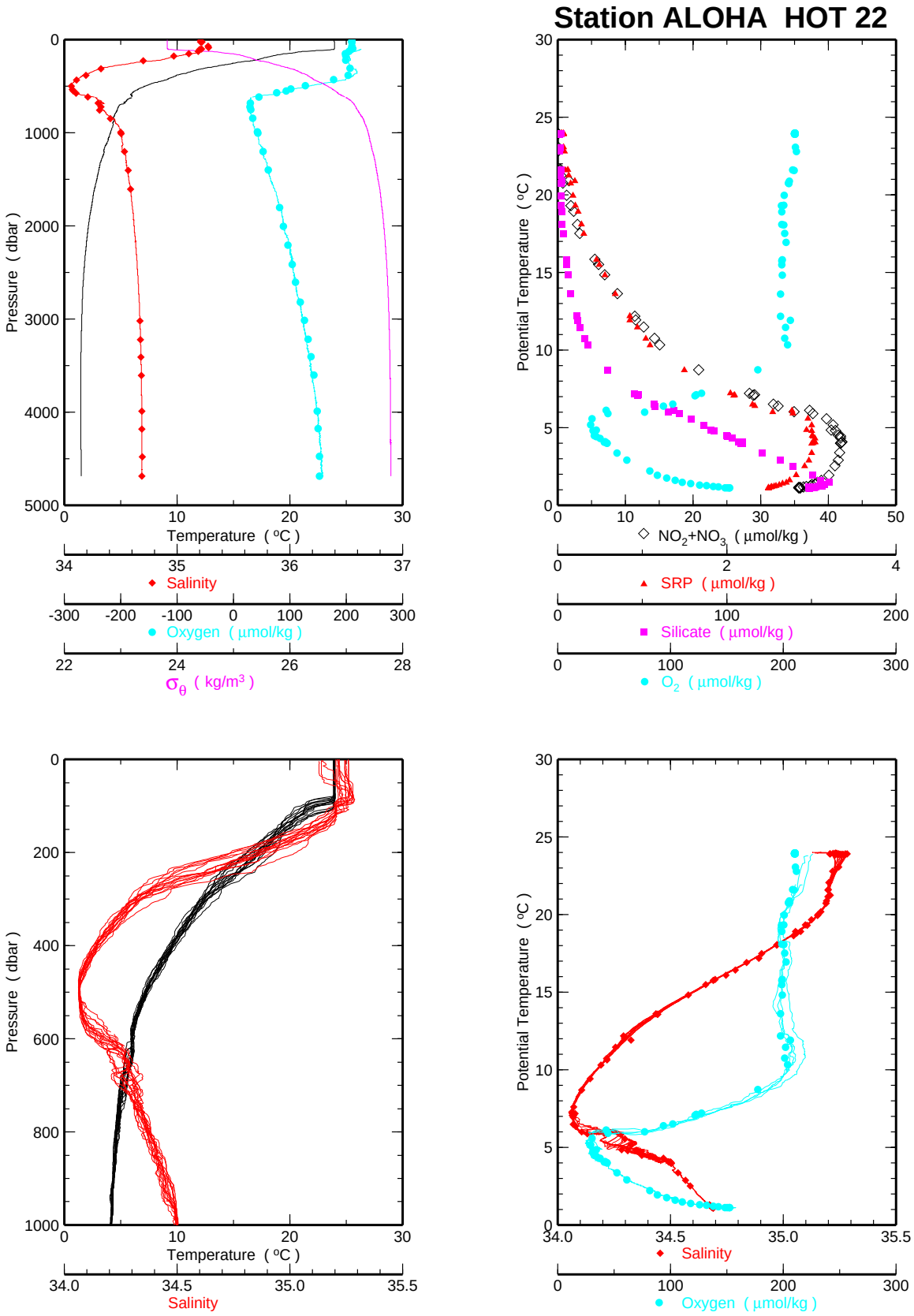

Figure 6.1.18a

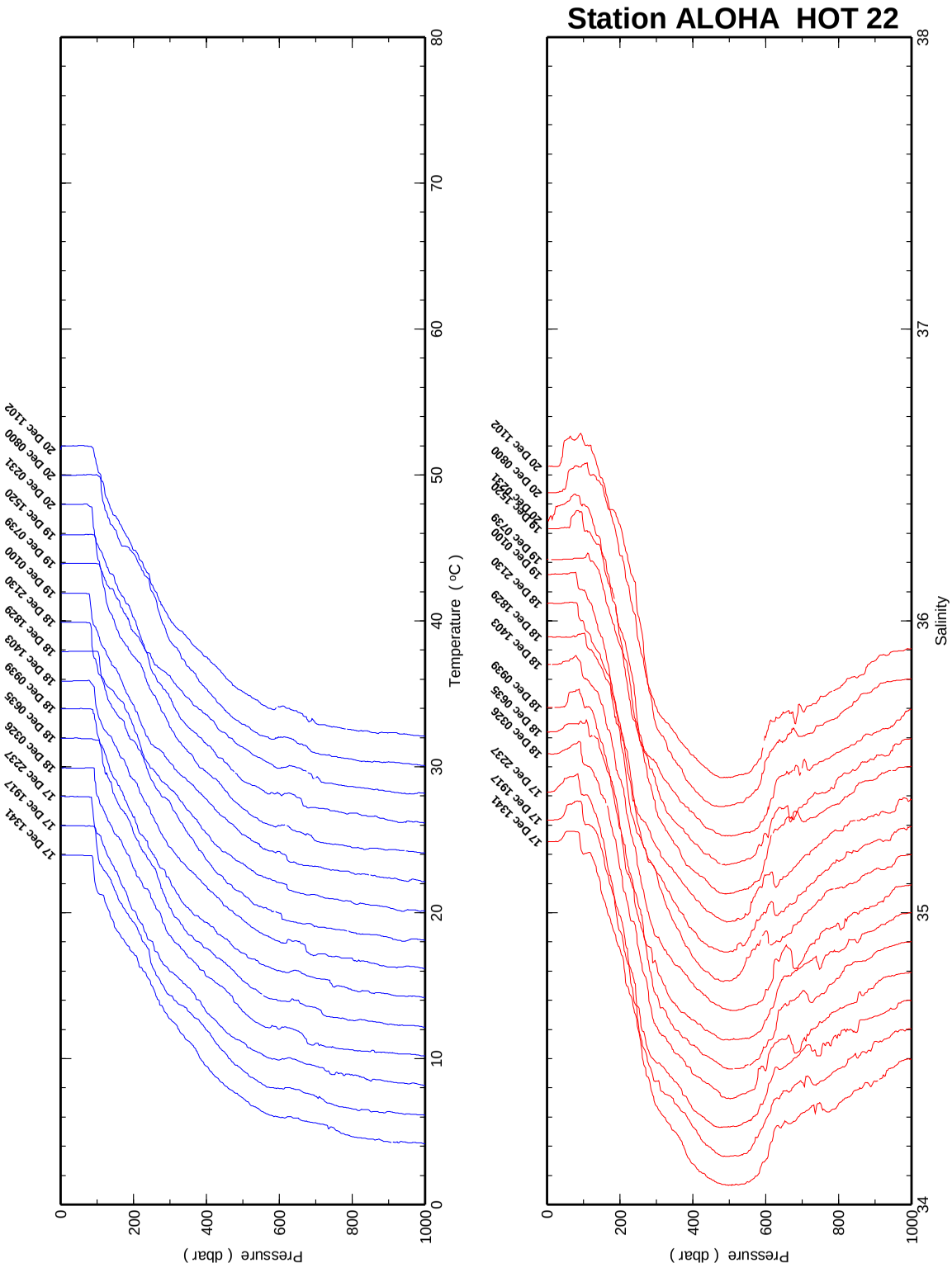

Figure 6.1.18b

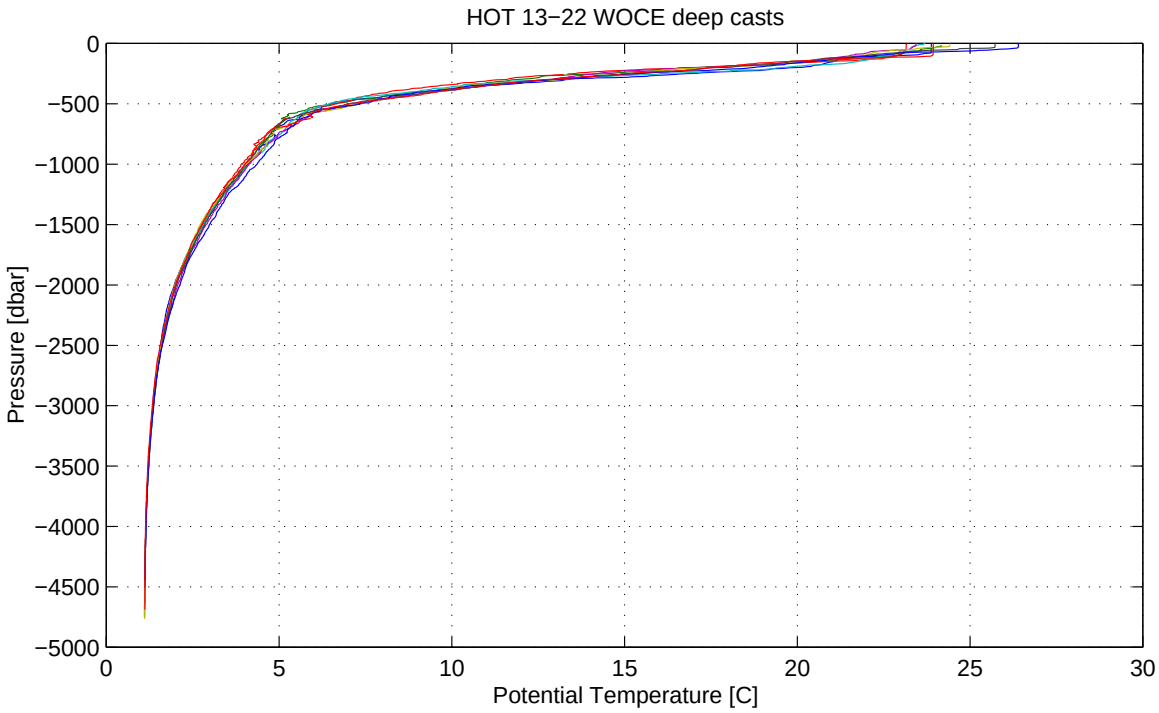
HOT 13−22 WOCE deep casts
Pressure [dbar]
Potential Temperature [C]
0
−500
−1000
−1500
−2000
−2500
−3000
−3500
−4000
−4500
−5000
0
5
10
15
20
25
30

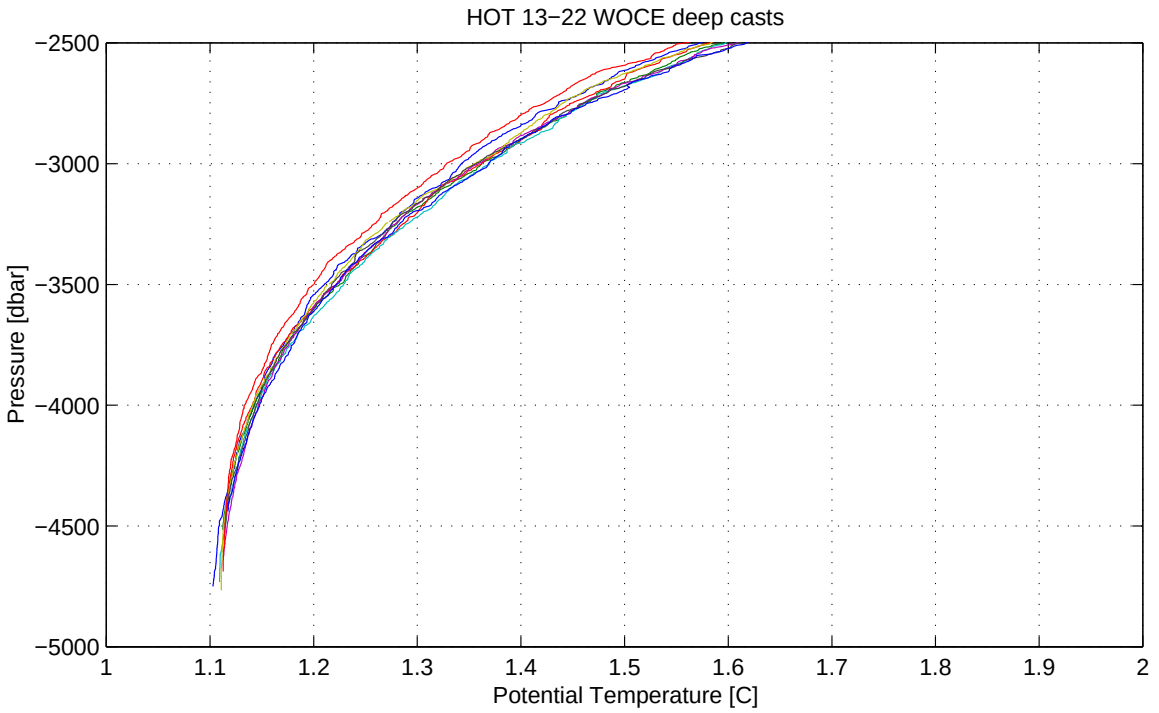
HOT 13−22 WOCE deep casts
Pressure [dbar]
Potential Temperature [C]
−2500
−3000
−3500
−4000
−4500
−5000
1
1.1
1.2
1.3
1.4
1.5
1.6
1.7
1.8
1.9
2

Figure 6.1.19

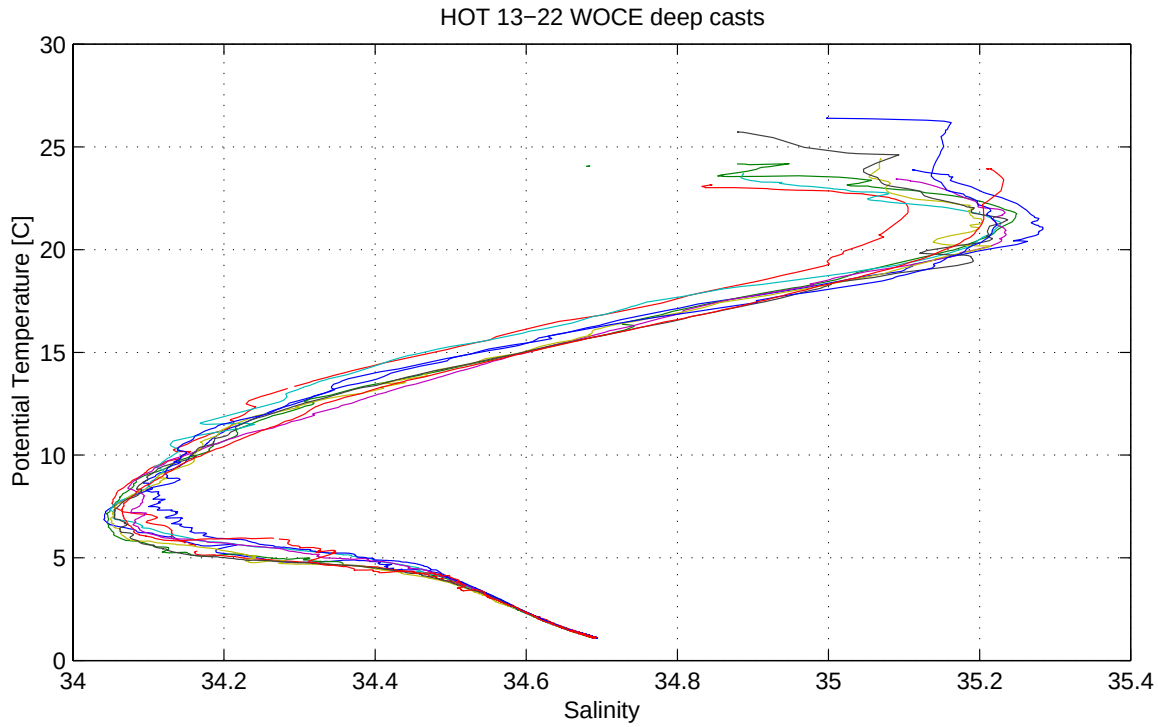
HOT 13−22 WOCE deep casts
Potential Temperature [C]
Salinity
30
25
20
15
10
5
0
34
34.2
34.4
34.6
34.8
35
35.2
35.4

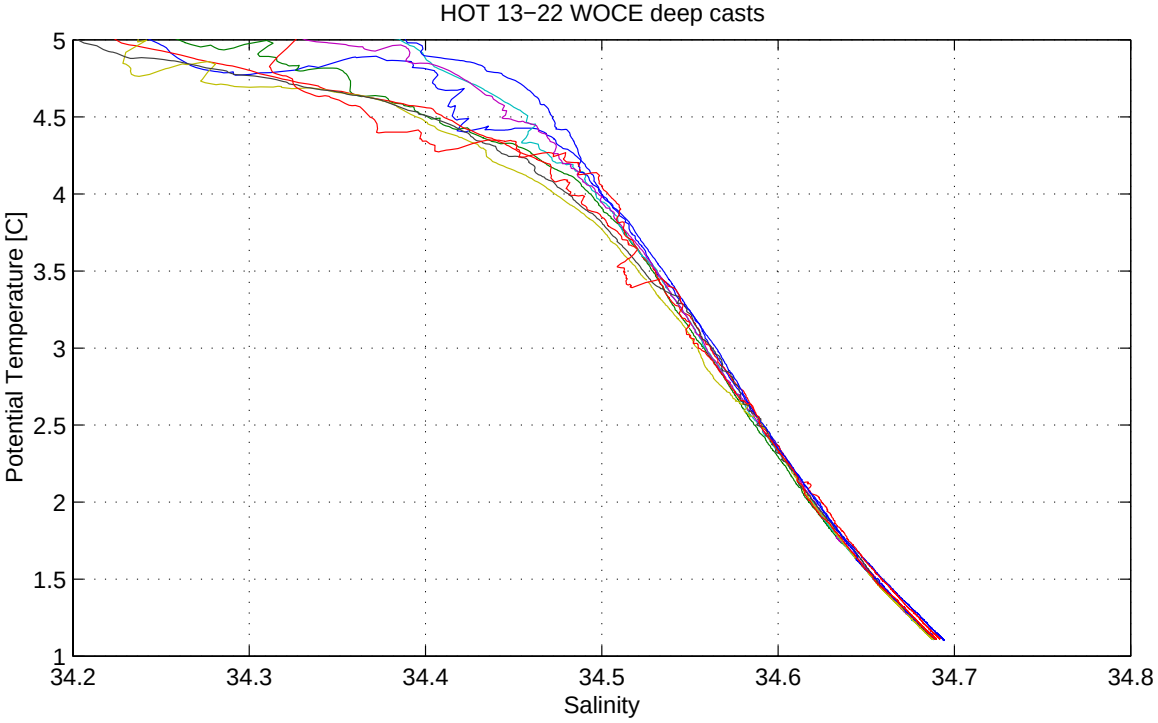
HOT 13−22 WOCE deep casts
Potential Temperature [C]
Salinity
5
4.5
4
3.5
3
2.5
2
1.5
1
34.2
34.3
34.4
34.5
34.6
34.7
34.8

Figure 6.1.20

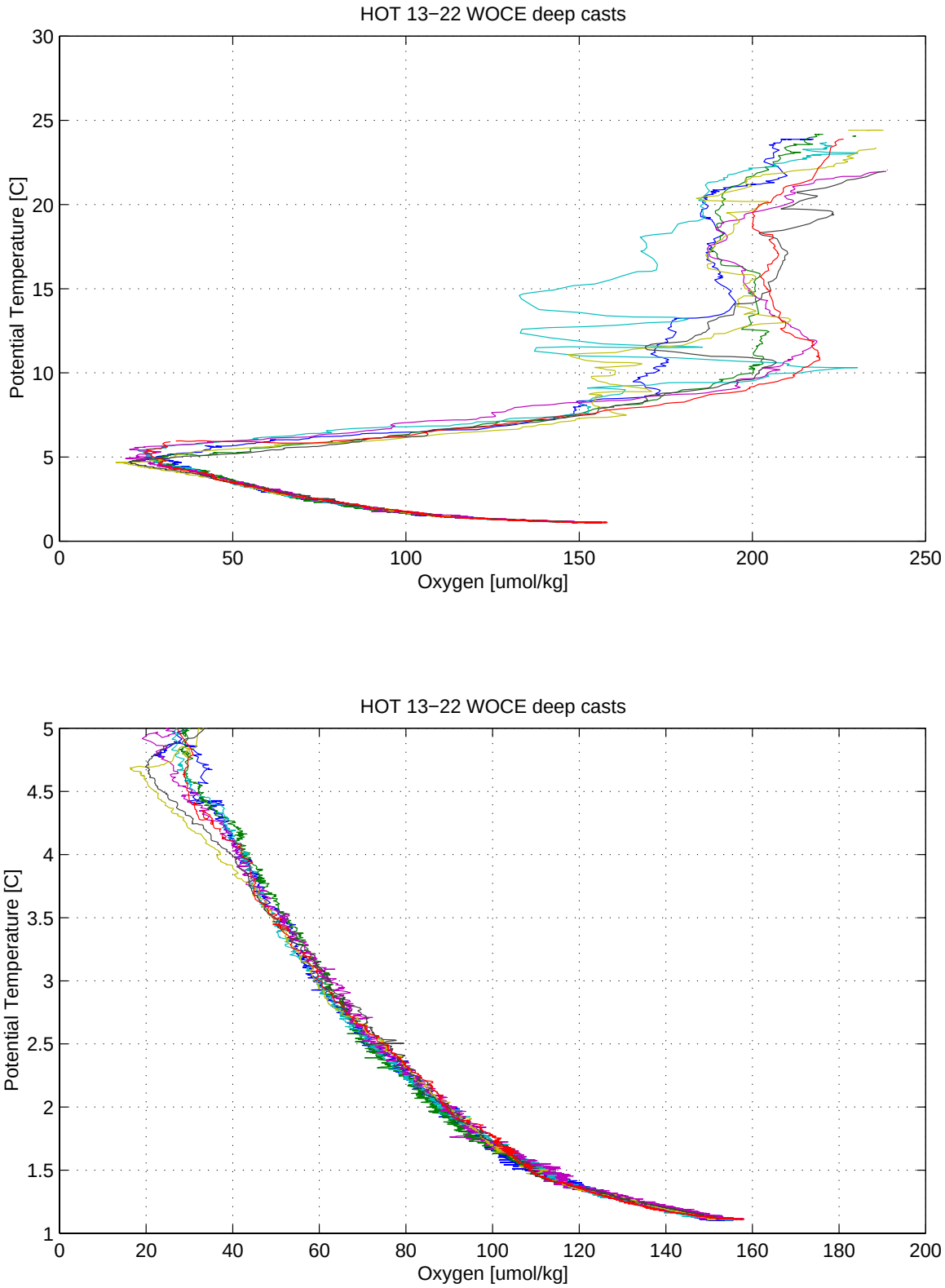
HOT 13−22 WOCE deep casts
Potential Temperature [C]
Oxygen [umol/kg]
0
5
10
15
20
25
30
0
50
100
150
200
250
HOT 13−22 WOCE deep casts
Potential Temperature [C]
Oxygen [umol/kg]
1
1.5
2
2.5
3
3.5
4
4.5
5
0
20
40
60
80
100
120
140
160
180
200

Figure 6.1.21

6.2. Contour Plots

Figures 6.2.1-14 show data from HOT cruises 1-22. Time of each cruise is indicated by a symbol along the time axis.

Figure 6.2.1: Potential temperature measured by CTD plotted against pressure. All casts at the HOT site are averaged for each cruise.

Figure 6.2.2: Potential density, calculated from CTD measurements of pressure, temperature and salinity, plotted against pressure. All casts at the HOT site are, averaged for each cruise.

Figure 6.2.3: Salinity measured by CTD plotted against pressure. All casts at the HOT site are averaged for each cruise.

Figure 6.2.4: Salinity measured by CTD plotted against potential density. All casts at the HOT site are averaged for each cruise. The average density of the sea surface from CTD for each cruise is connected by a heavy line.

Figure 6.2.5: Salinity from discrete water sample analyses plotted against pressure. Locations of bottle closures are indicated by dots.

Figure 6.2.6: Salinity from discrete water sample analyses plotted against potential density. The average density of the sea surface from CTD for each cruise is connected by a heavy line. Locations of bottle closures are indicated by dots.

Figure 6.2.7: Oxygen from discrete water sample analyses plotted against pressure. Locations of bottle closures are indicated by dots.

Figure 6.2.8: Oxygen from discrete water sample analyses plotted against potential density. The average density of the sea surface from CTD for each cruise is connected by a heavy line. Locations of bottle closures are indicated by dots.

Figure 6.2.9: Nitrate plus nitrite from discrete water sample analyses plotted against pressure. Locations of bottle closures are indicated by dots.

Figure 6.2.10: Nitrate plus nitrite from discrete water sample analyses plotted against potential density. The average density of the sea surface from CTD for each cruise is connected by a heavy line. Locations of bottle closures are indicated by dots.

Figure 6.2.11: Phosphate from discrete water sample analyses plotted against pressure. Location of bottle closures are indicated by dots.

Figure 6.2.12: Phosphate from discrete water sample analyses plotted against potential density.The average density of the sea surface from CTD for each cruise is connected by a heavy line. Locations of bottle closures are indicated by dots.

Figure 6.2.13: Silicate from discrete water sample analyses plotted against pressure. Locations of bottle closures are indicated by dots.

Figure 6.2.14: Silicate from discrete water sample analyses plotted against potential density. The average density of the sea surface from CTD for each cruise is connected by a heavy line. Locations of bottle closures are indicated by dots.

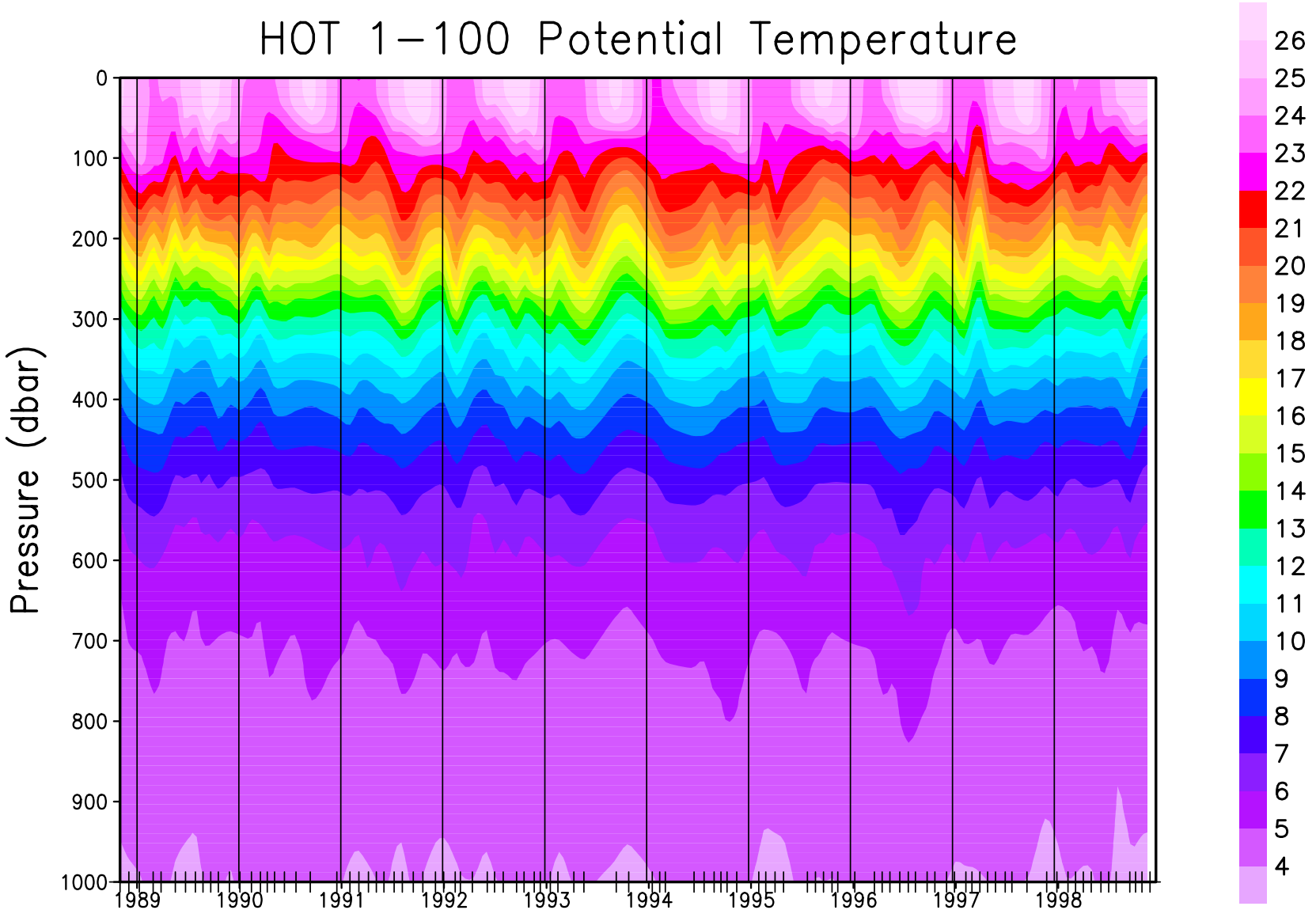

Figure 6.2.1: Contour plot of CTD potential temperature versus pressure for HOT cruises 1-100.

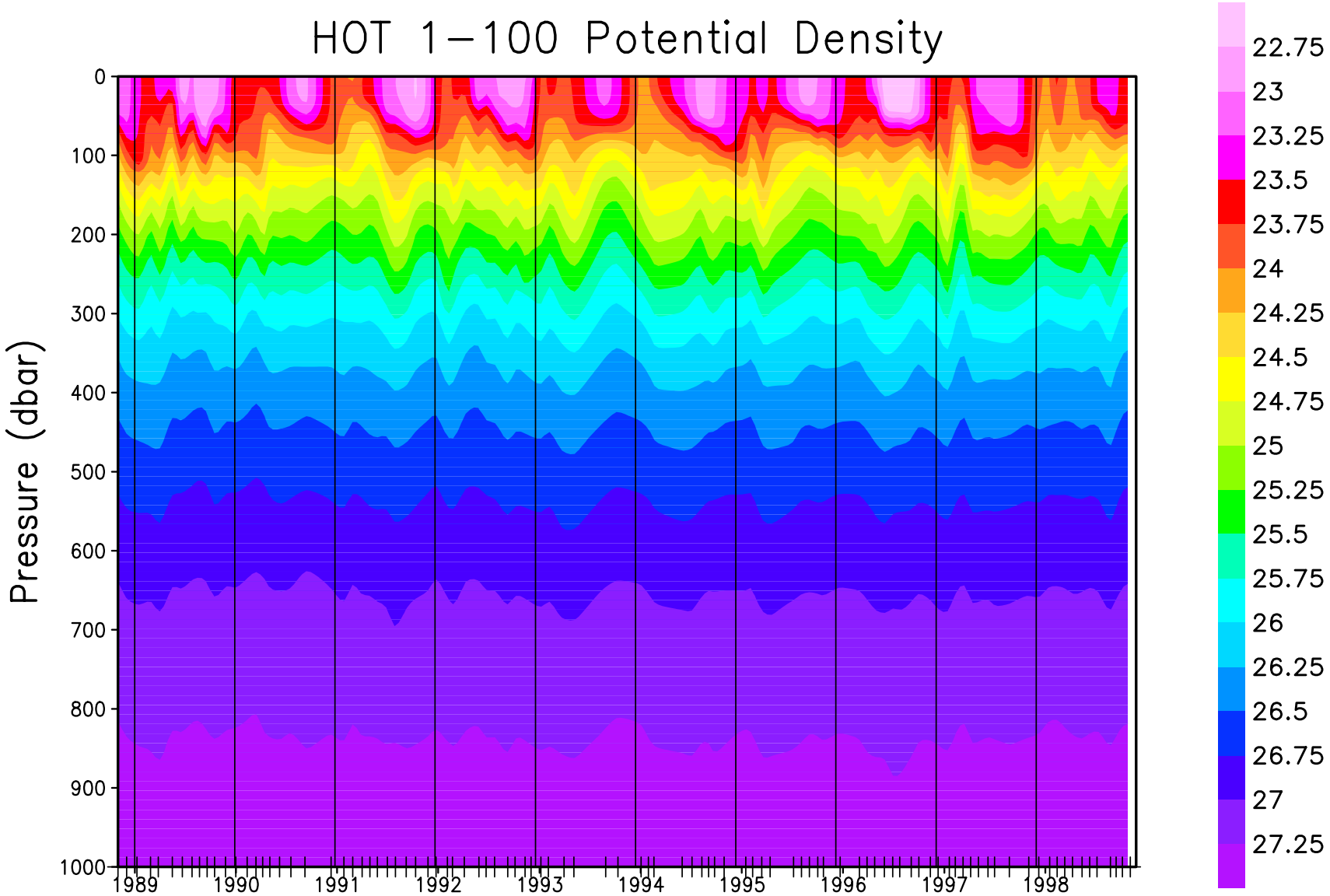

Figure 6.2.2: Contour plot of potential density (σ_θ), calculated from CTD pressure, temperature and salinity, versus pressure for HOT cruises 1-100.

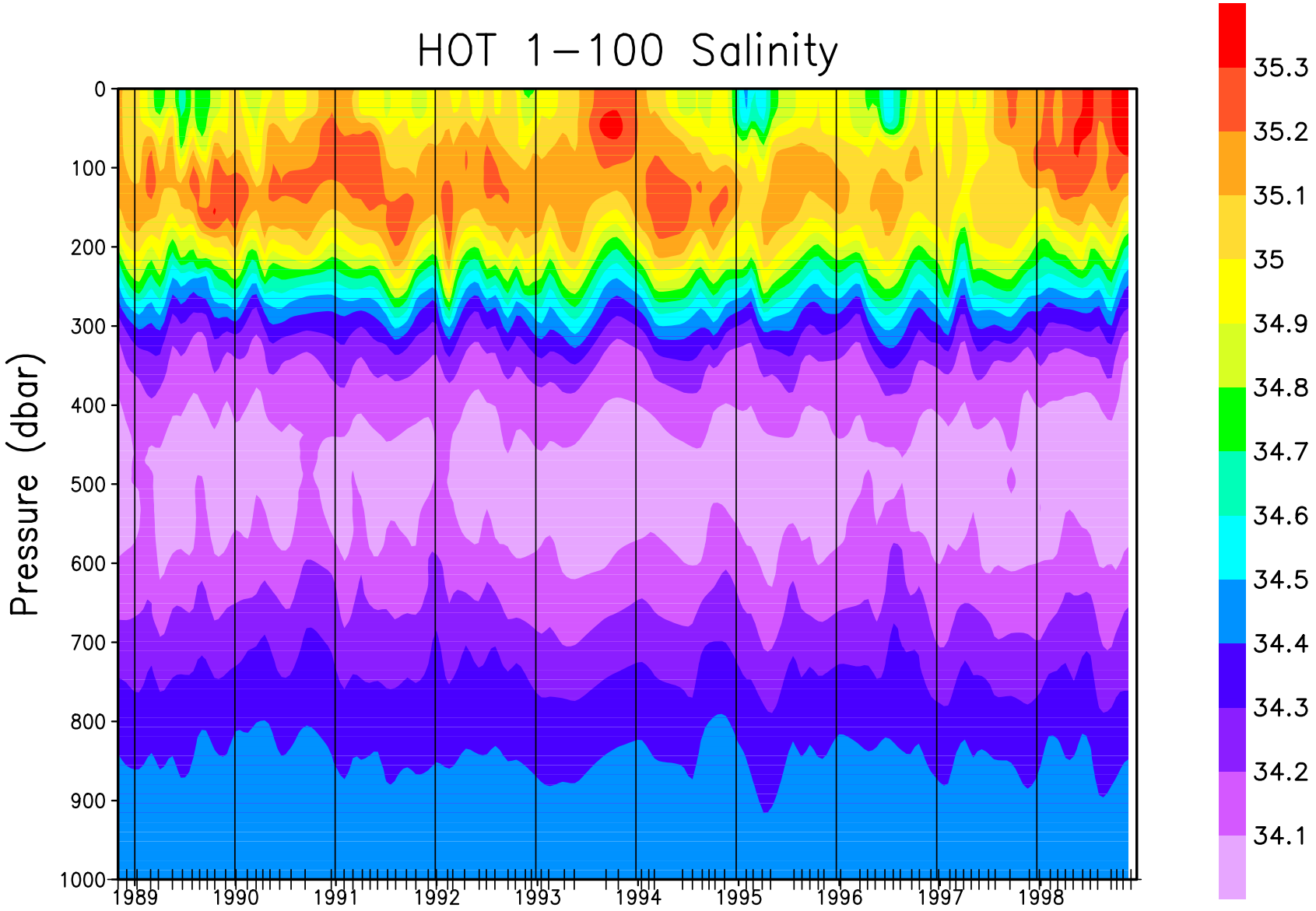

Figure 6.2.3: Contour plot of CTD salinity versus pressure for HOT cruises 1-

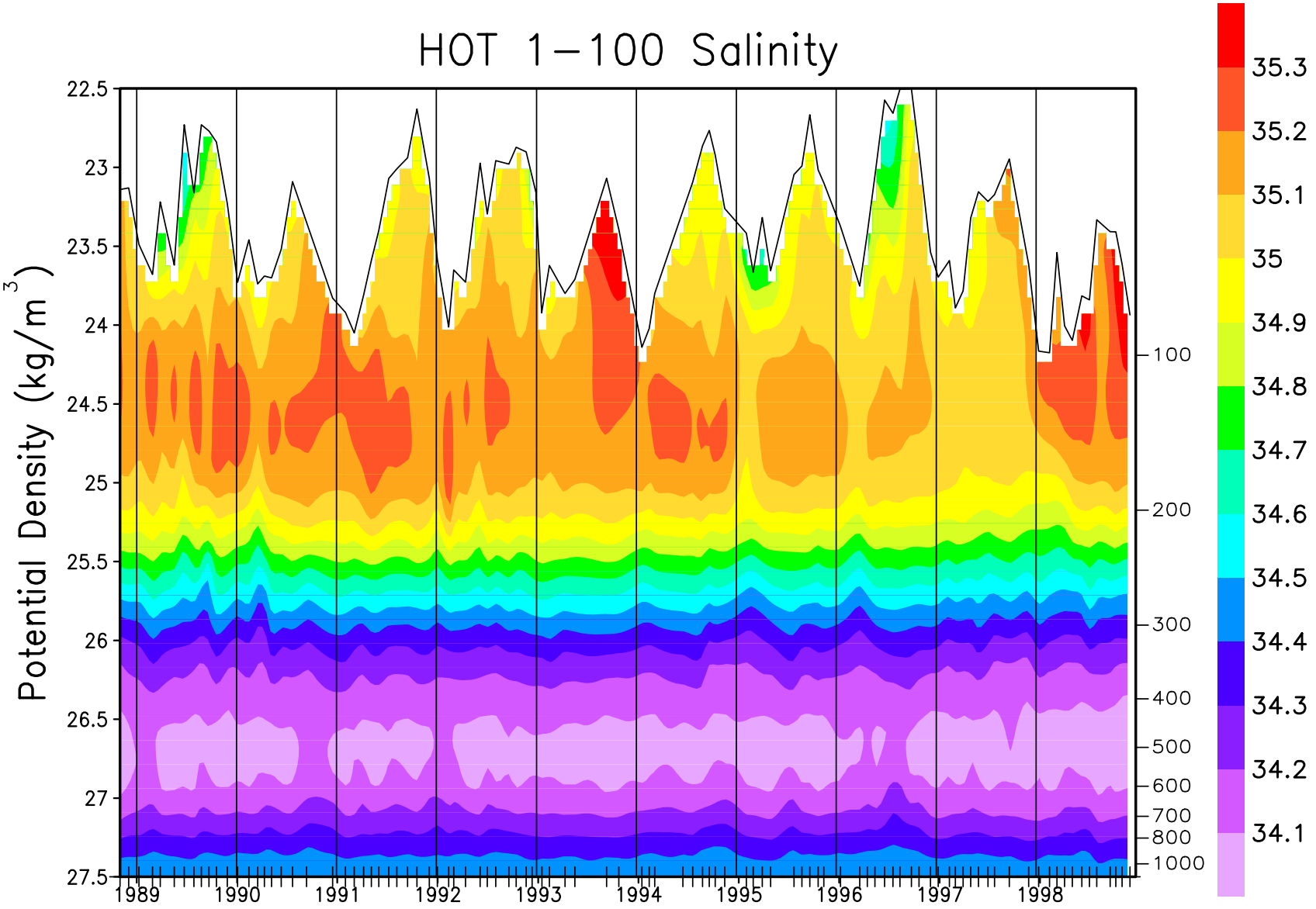

Figure 6.2.4: Contour plot of CTD salinity versus potential density (σ_θ) to 27.5 kg m^{-3} for HOT cruises 1-100. The average density of the sea surface is connected by the heavy line.

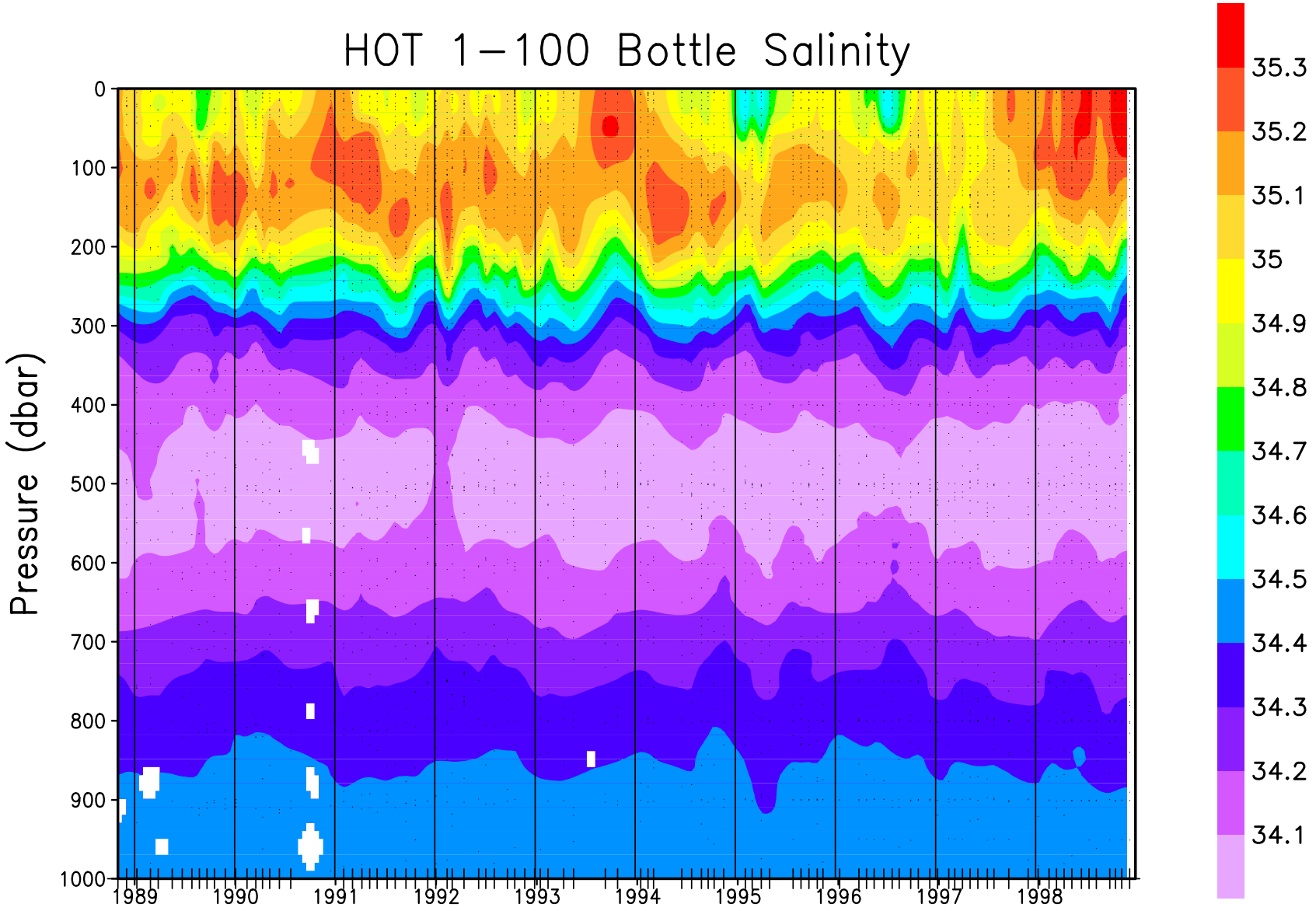

Figure 6.2.5: Contour plot of bottle salinity versus pressure for HOT cruises 1-100. Location of samples in the water column are indicated by the solid circles.

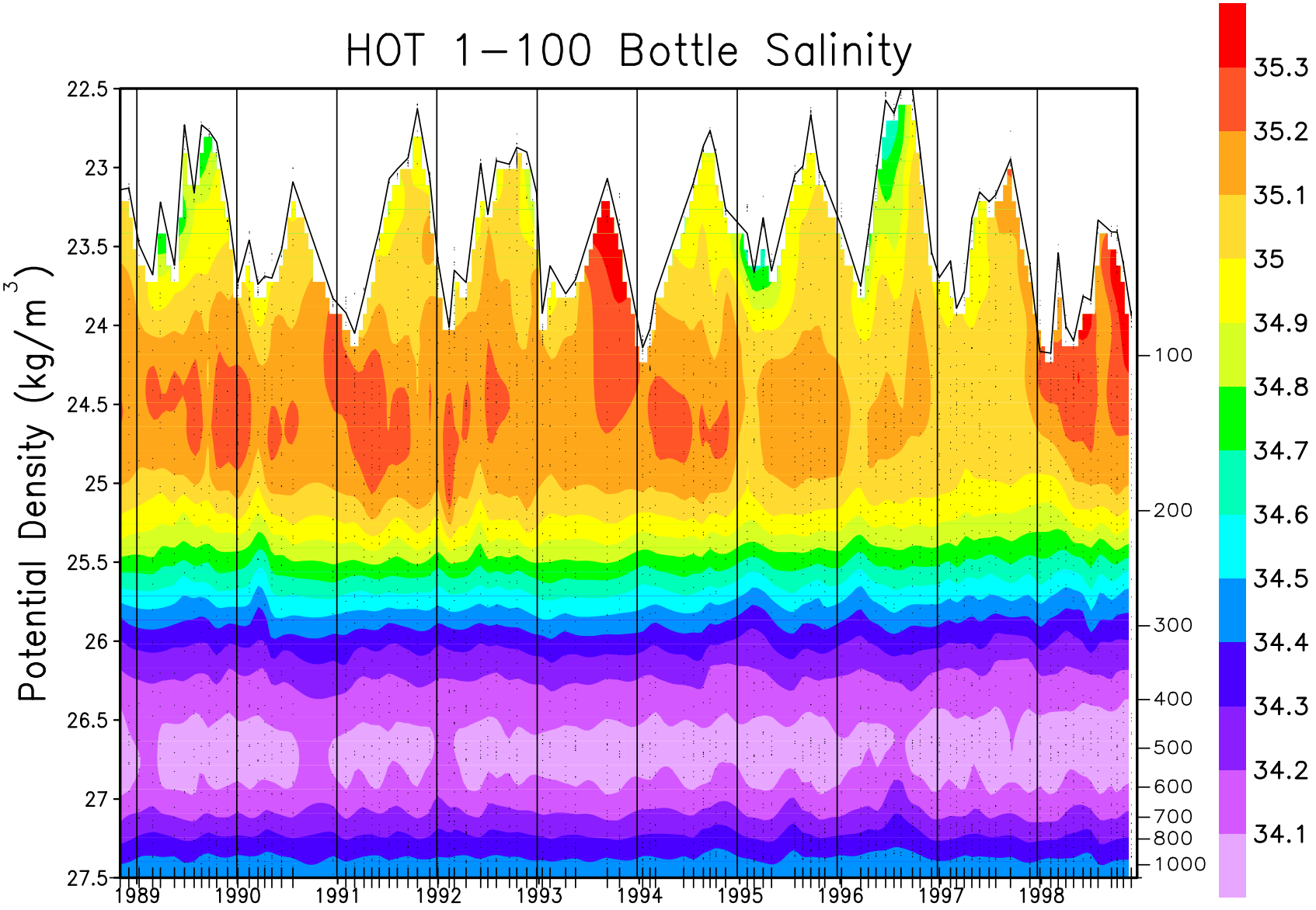

Figure 6.2.6: Contour plot of bottle salinity versus potential density (σ_θ)to 27.5 kg m^{-3} for HOT cruises 1-100. The average density of the sea surface is connected by the heavy line.

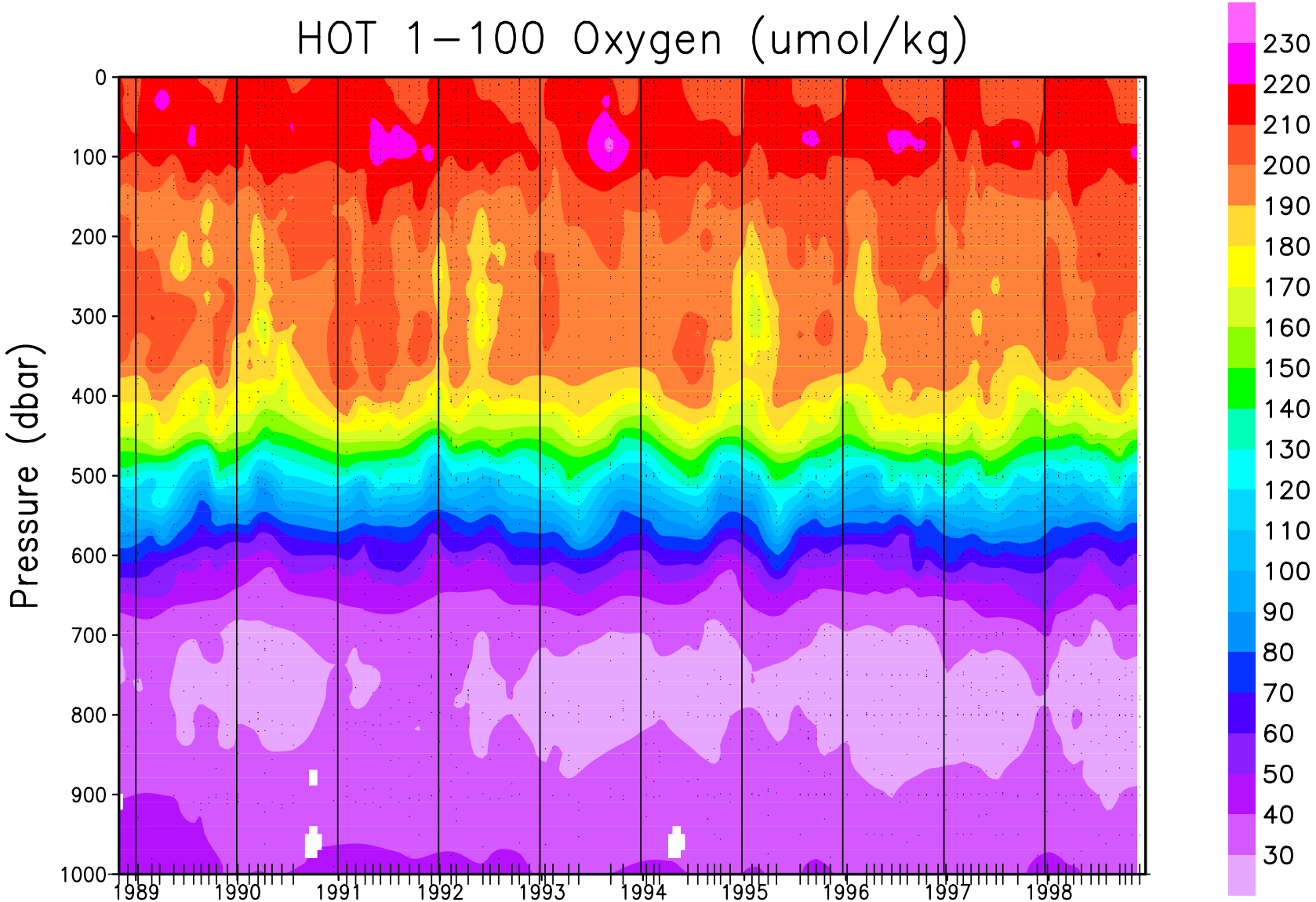

Figure 6.2.7: Contour plot of bottle oxygen versus pressure for HOT cruises 1-100. Location of samples in the water column are indicated by the solid circles.

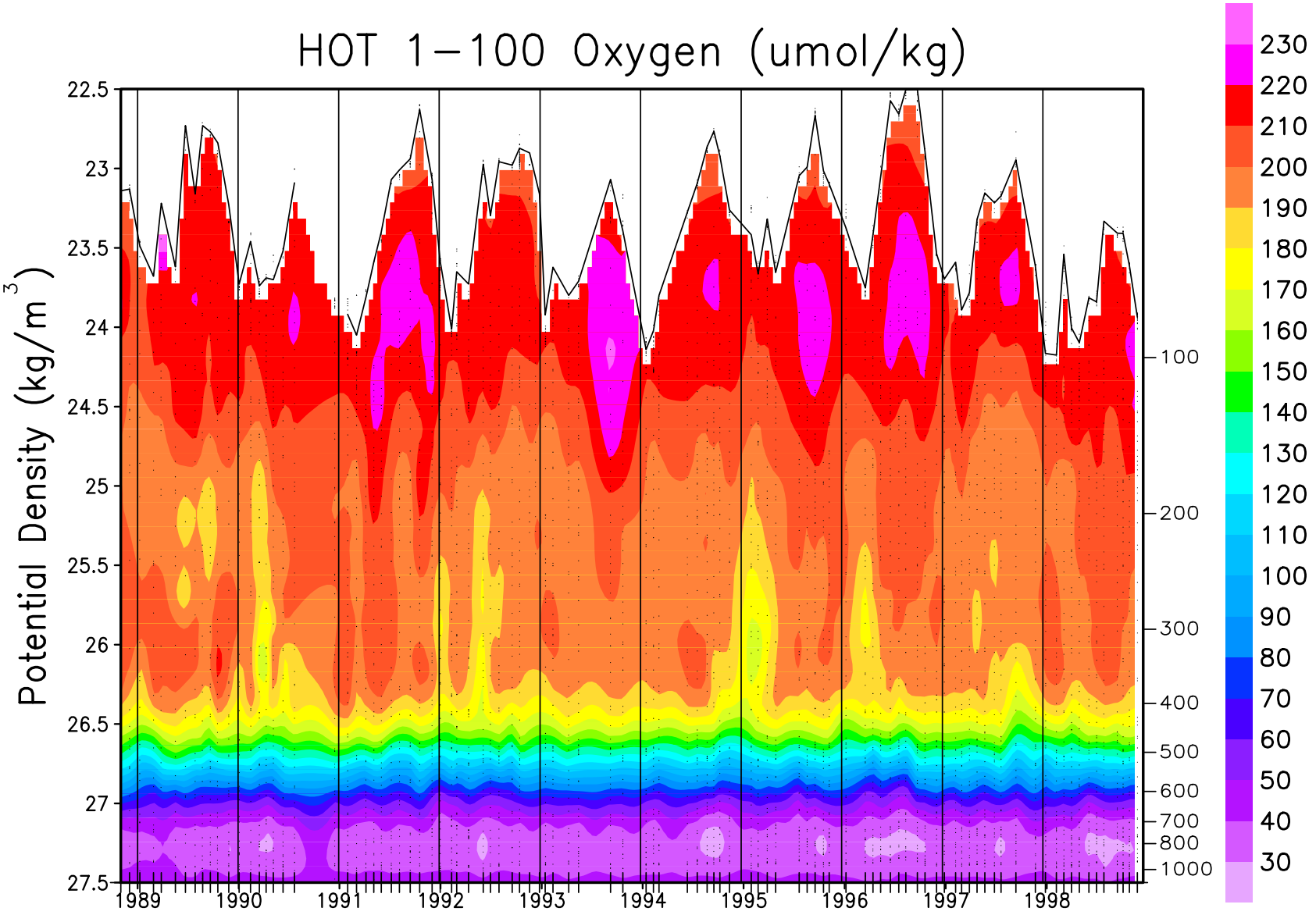

Figure 6.2.8: Contour plot of bottle oxygen versus potential density (σ_θ) to 27.5 kg m^{-3} for HOT cruises 1-100. The average density of the sea surface is connected by the heavy line.

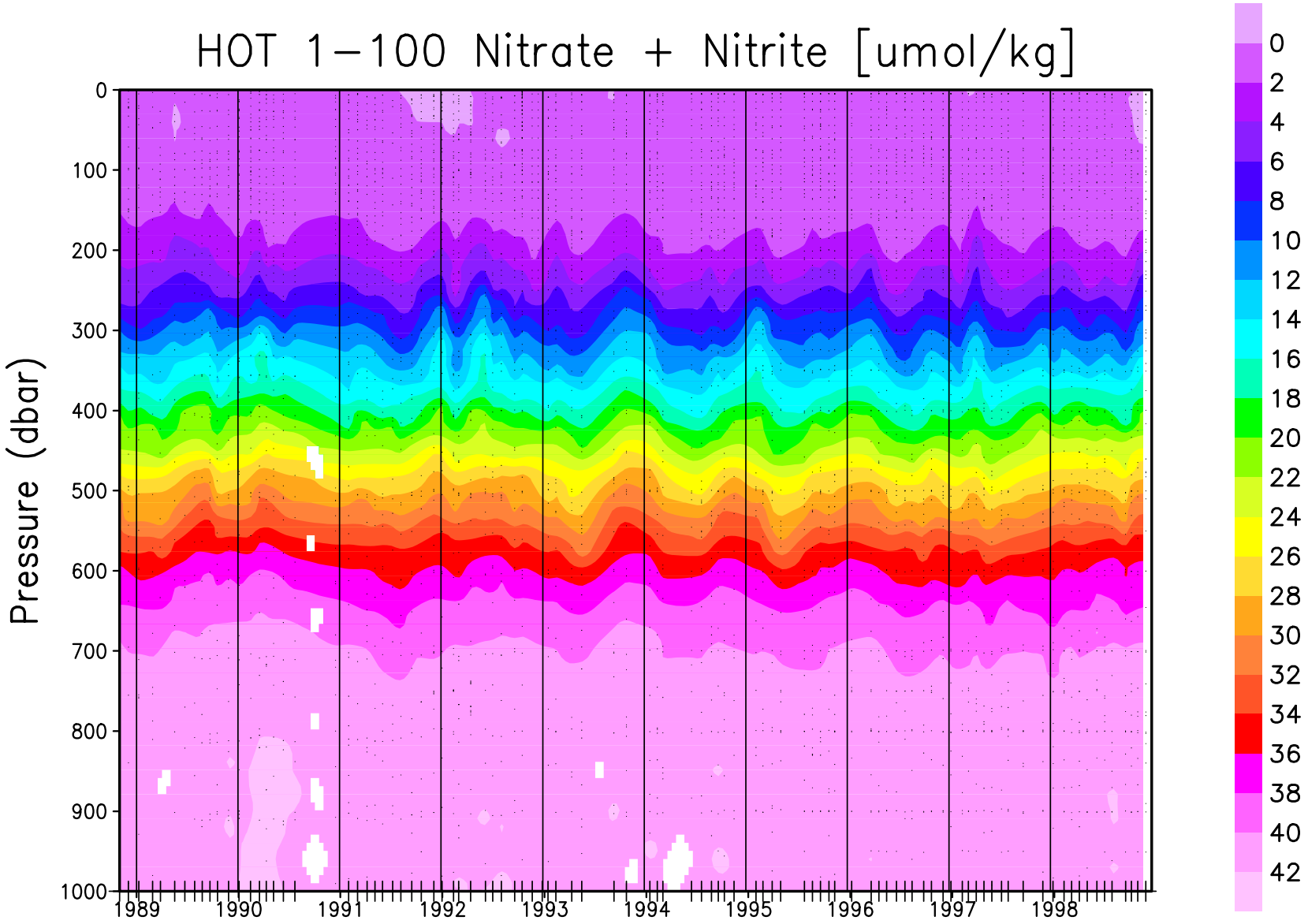

Figure 6.2.9: Contour plot of [nitrate + nitrite] versus pressure for HOT cruises 1-100. Location of samples in the water column are indicated by the solid circles.

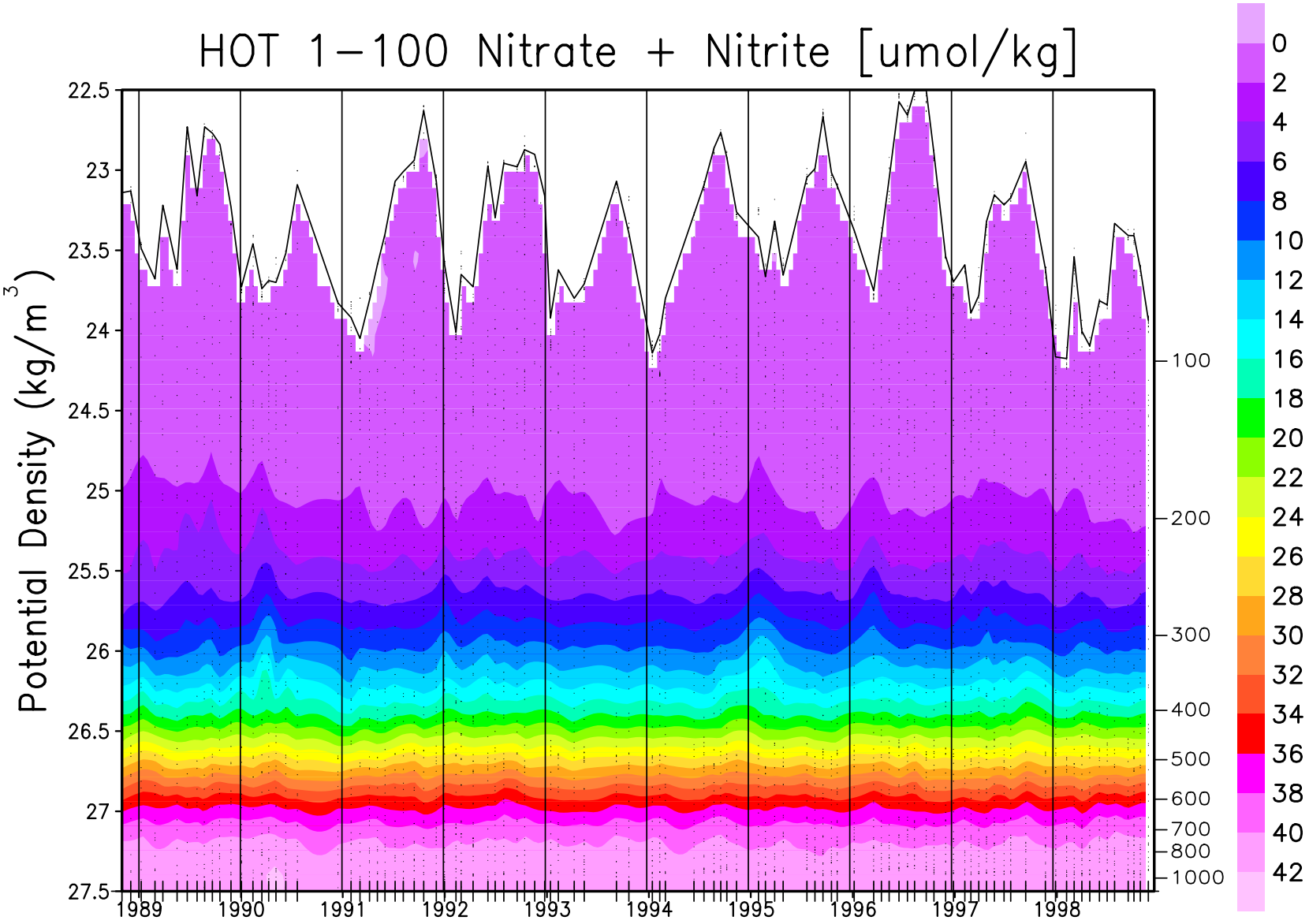

Figure 6.2.10: Contour plot of [nitrate + nitrite] versus potential density (σ_θ) to 27.5 kg m^{-3} for HOT cruises 1-100. The average density of the sea surface is connected by the heavy line.

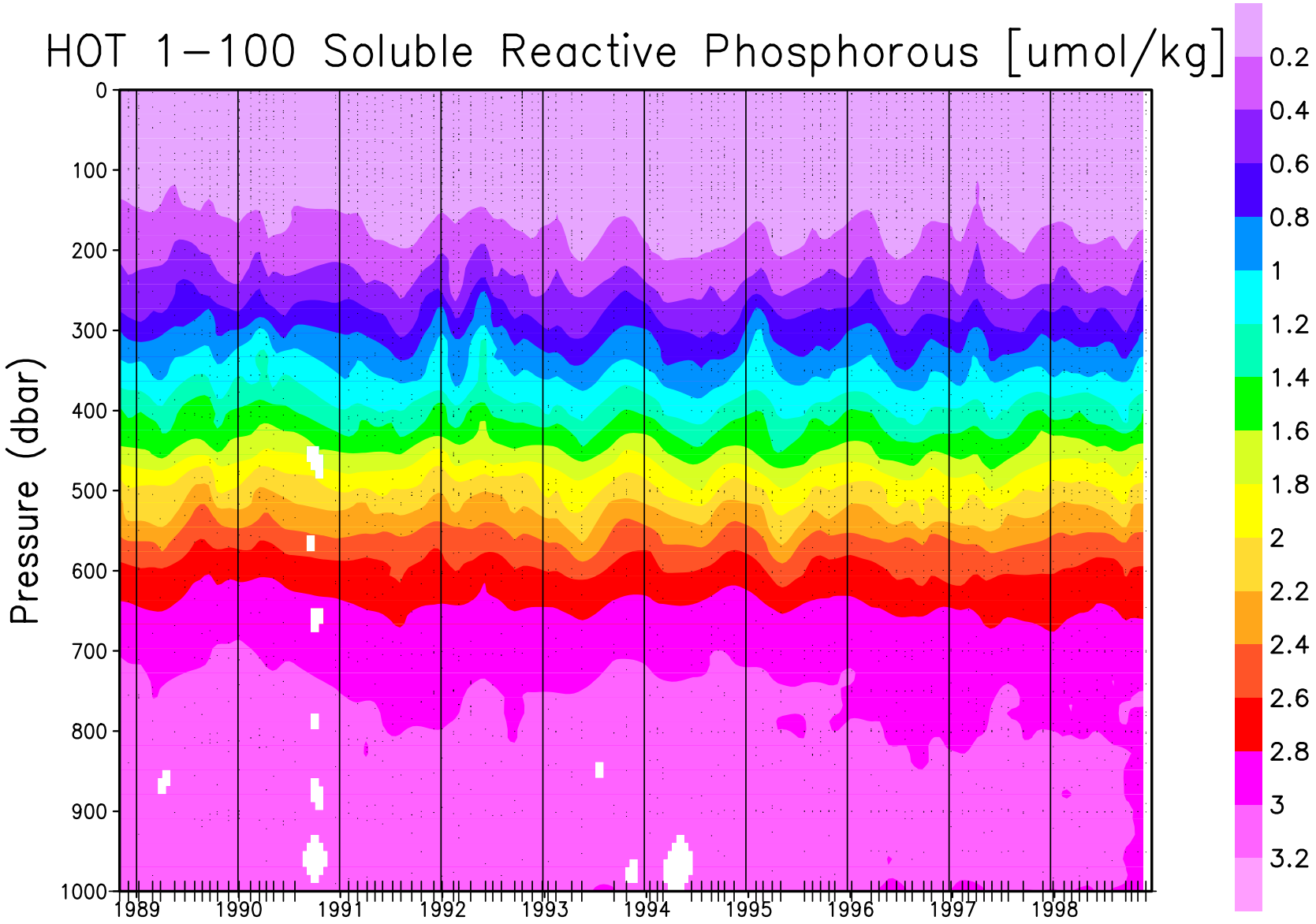

Figure 6.2.11: Contour plot of soluble reactive phosphate versus pressure for HOT cruises 1-100. Location of samples in the water column are indicated by the solid circles.

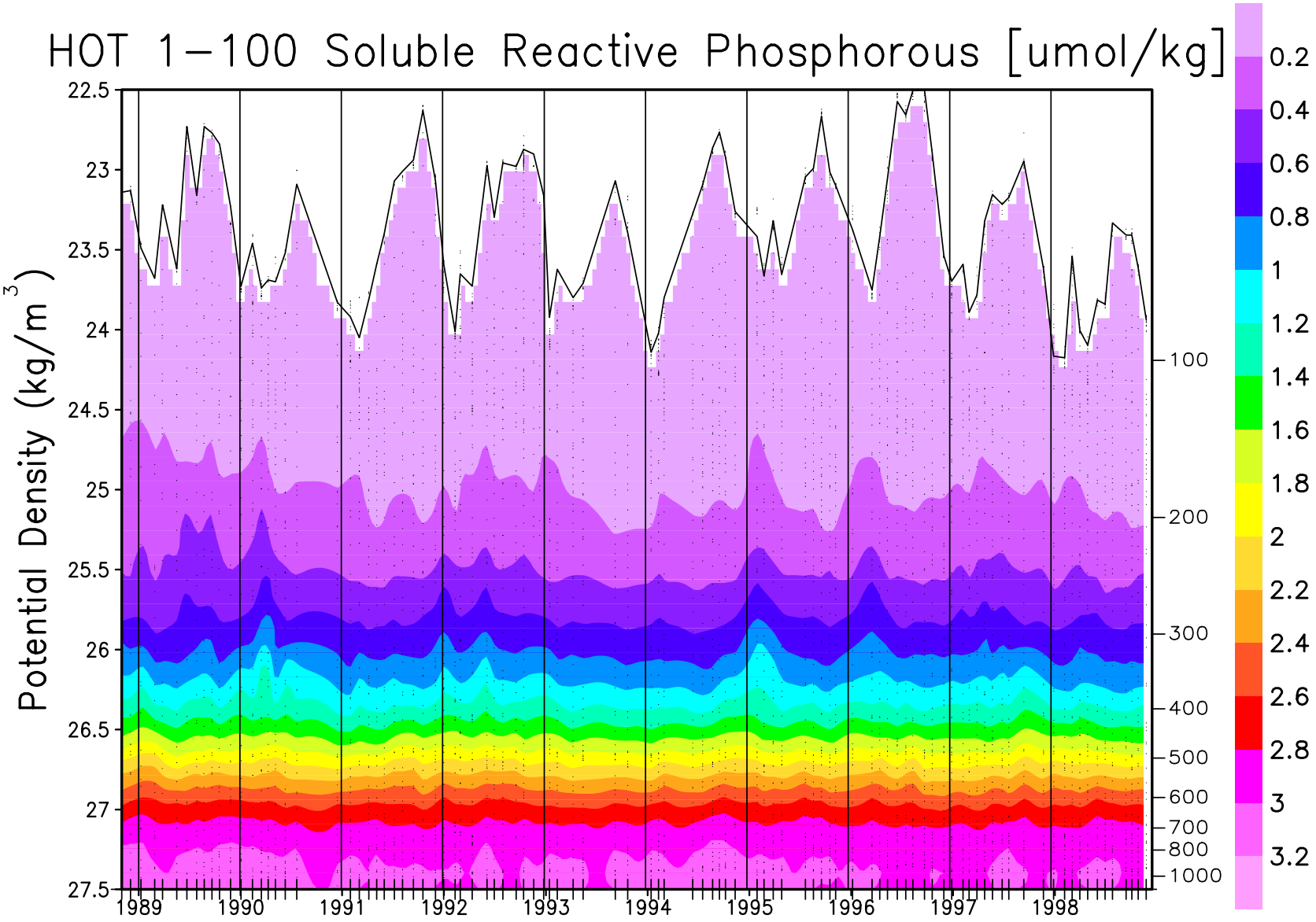

Figure 6.2.12: Contour plot of soluble reactive phosphate versus potential density (σ_θ) to 27.5 kg m^{-3} for HOT cruises 1-100. The average density of the sea surface is connected by the heavy line.

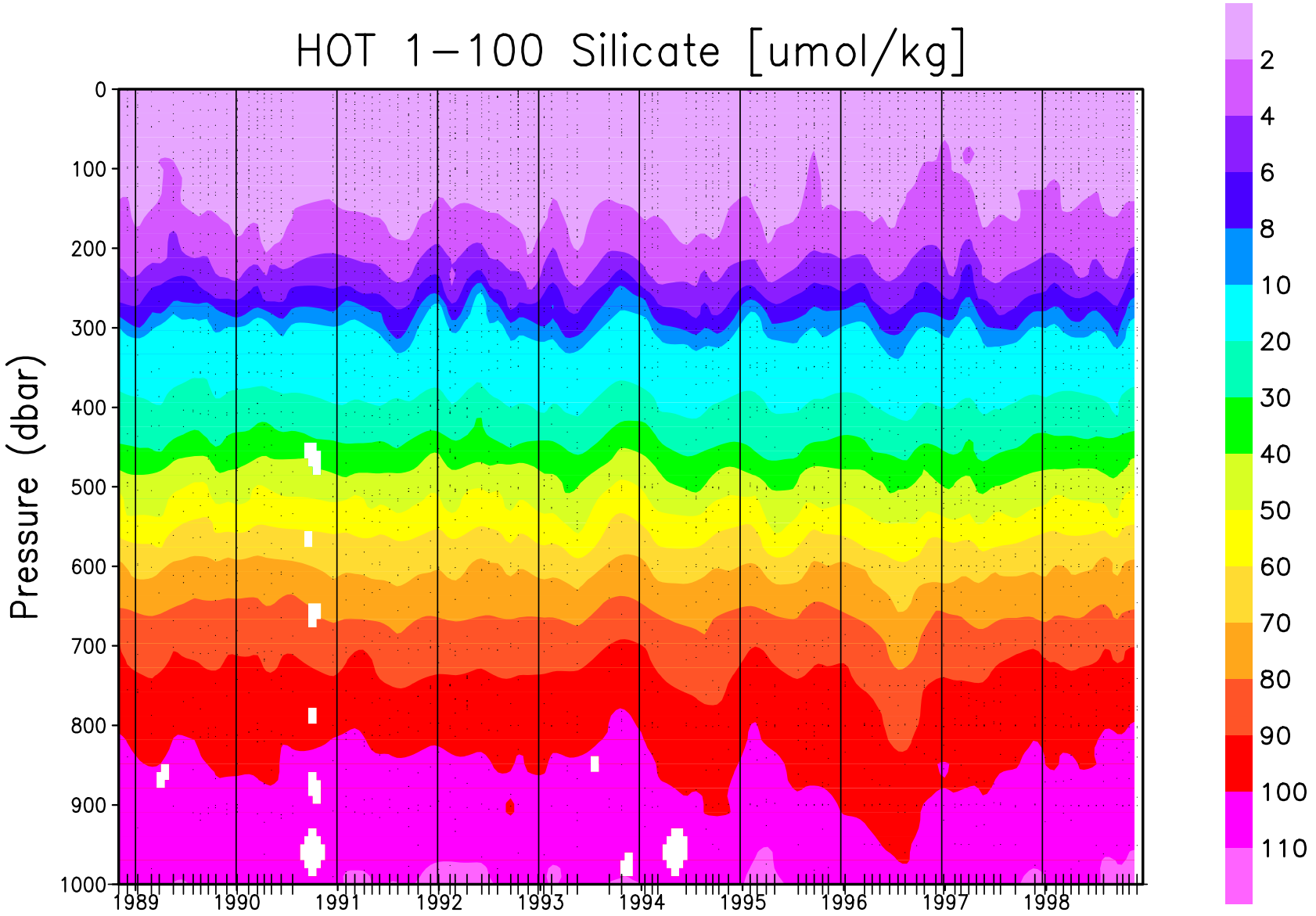

Figure 6.2.13: Contour plot of silicate versus pressure for HOT cruises 1-100. Location of samples in the water column are indicated by the solid circles.

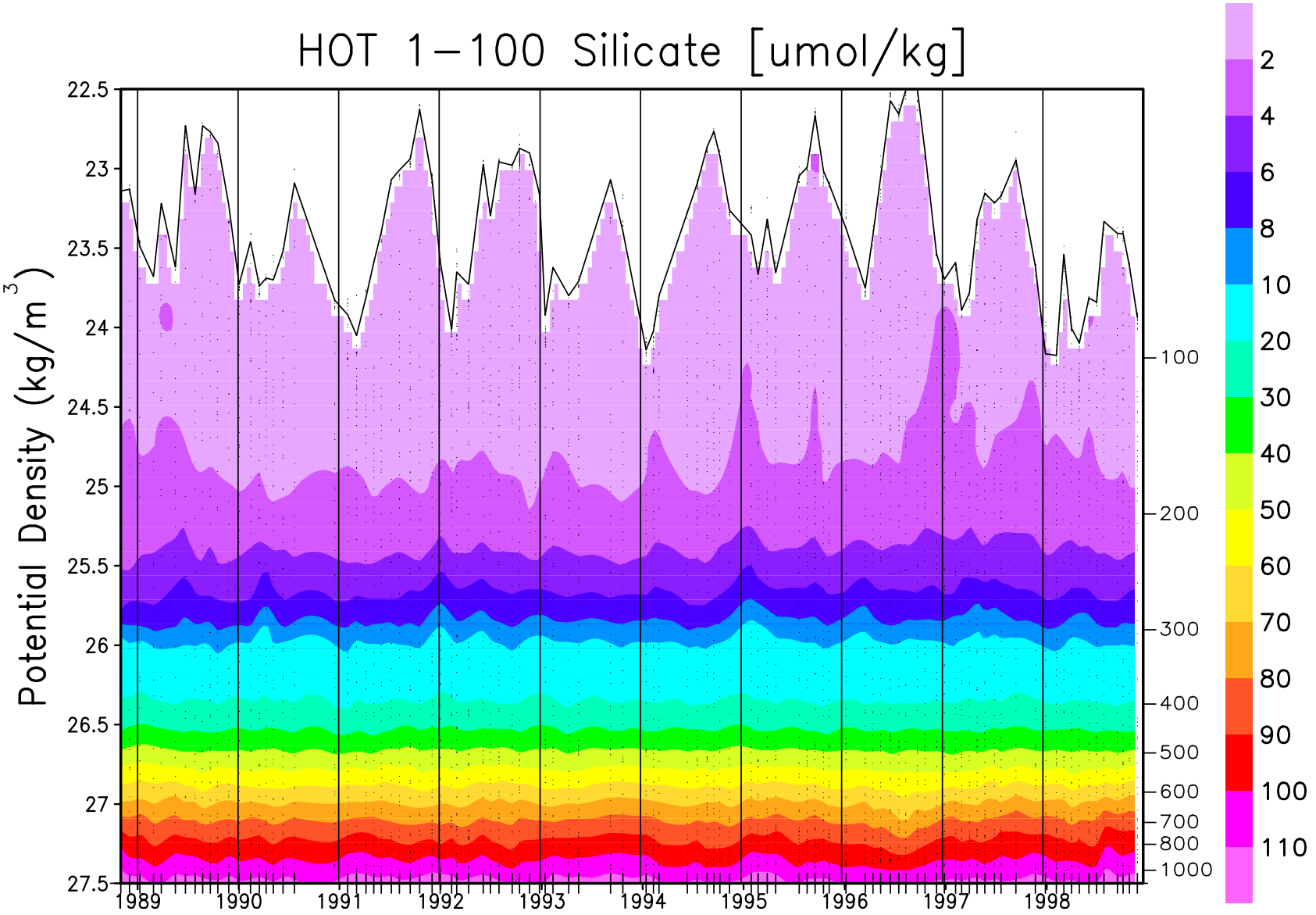

Figure 6.2.14: Contour plot of silicate versus potential density (σ_θ) to 27.5 kg m^{-3} for HOT cruises 1-100. The average density of the sea surface is connected by the heavy line.

6.3 Fluorescence, Primary Production and Particle Flux

Figure 6.3.1: Flash fluorescence profiles collected at night during 1990 plotted against pressure.

Figure 6.3.2: Flash fluorescence profiles collected at night during 1990 plotted against sigma-theta.

Figure 6.3.3: Contour plot of flash fluorescence plotted against pressure for HOT cruises 1-22.

Figure 6.3.4: Integrated primary production rates measured on HOT-1 to -22. Results for simultaneous 12-hour incubations conducted on-deck and *in situ* are shown.

Figure 6.3.5: Integrated primary production rates measured for 12 and 24 hours on HOT-1 to -22. Closed symbols indicate on-deck incubations; open symbols indicate *in situ* incubations.

Figure 6.3.6: Carbon flux measured at 150 m on HOT-1 to -22. Error bars represent the standard deviation of replicate analyses.

Figure 6.3.7: As in Figure 6.4.1, except for nitrogen.

Figure 6.3.8: As in Figure 6.4.1, except for phosphorus.

Figure 6.3.9: As in Figure 6.4.1, except for total mass.

Figure 6.3.10: Carbon:Nitrogen ratio of trap-collected material at 150 m on HOT-1 to -22. Error bars represent estimates by propagating error associated with individual measurements of carbon and nitrogen.

Figure 6.3.11: Nitrogen flux at 150 m as a percent of photosynthetic nitrogen production. Photosynthetic nitrogen production was calculated using primary production rate measurements assuming a C:N incorporation ratio of 106:16 by atoms.

Figure 6.3.12: Average carbon flux at 150, 300, and 500 m using flux data collected on HOT-1 to -22. Error bars are 95% confidence limits on the mean.

Figure 6.3.13: As in Figure 6.4.7, except for nitrogen.

Figure 6.3.14: As in Figure 6.4.7, except for phosphorus.

Figure 6.3.15: As in Figure 6.4.7, except for total mass.

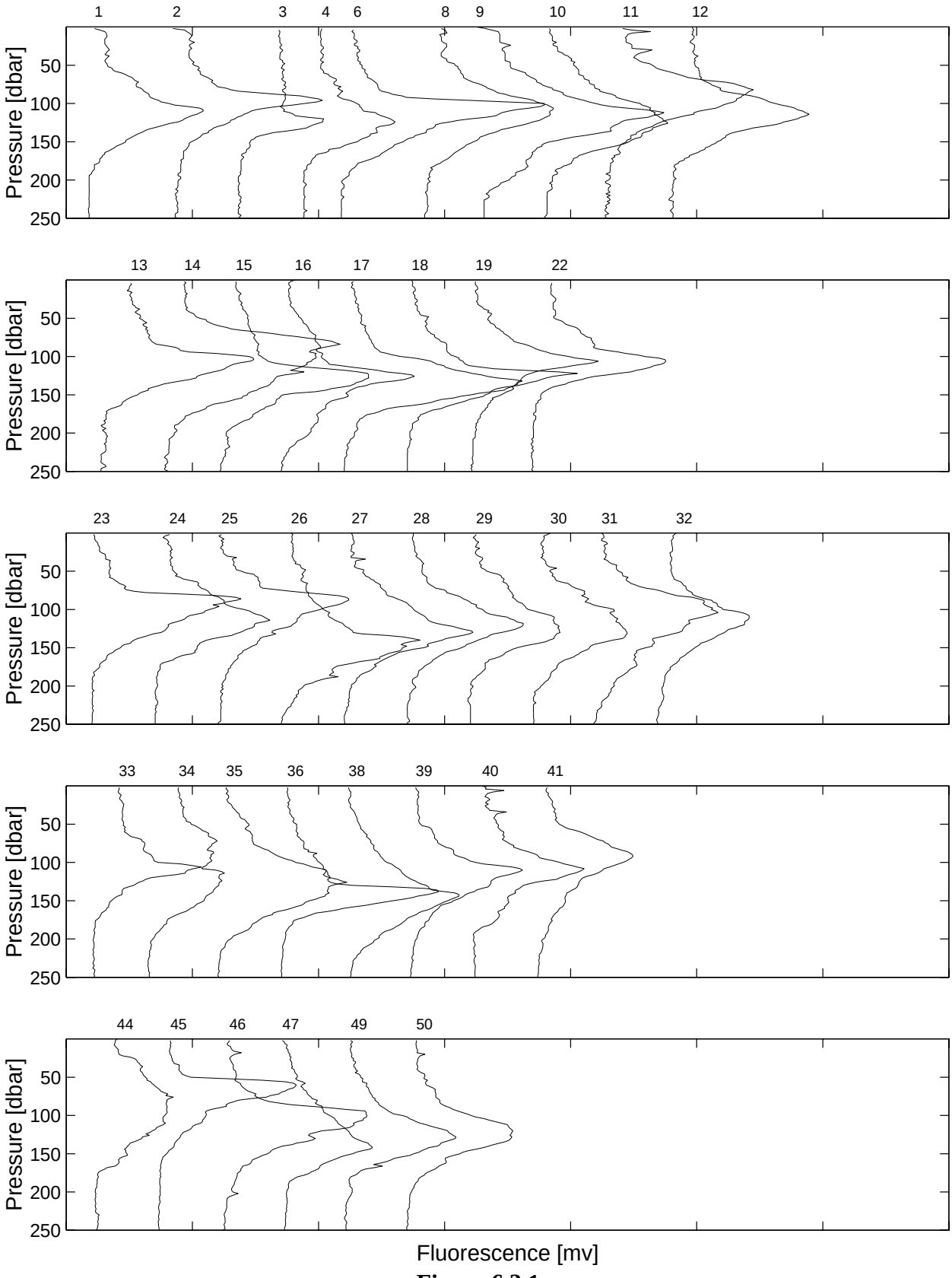
1 2 3 4 6 8 9 10 11 12
13 14 15 16 17 18 19 22
23 24 25 26 27 28 29 30 31 32
33 34 35 36 38 39 40 41
44 45 46 47 49 50
Pressure [dbar]
50
100
150
200
250
Fluorescence [mv]

Figure 6.3.1

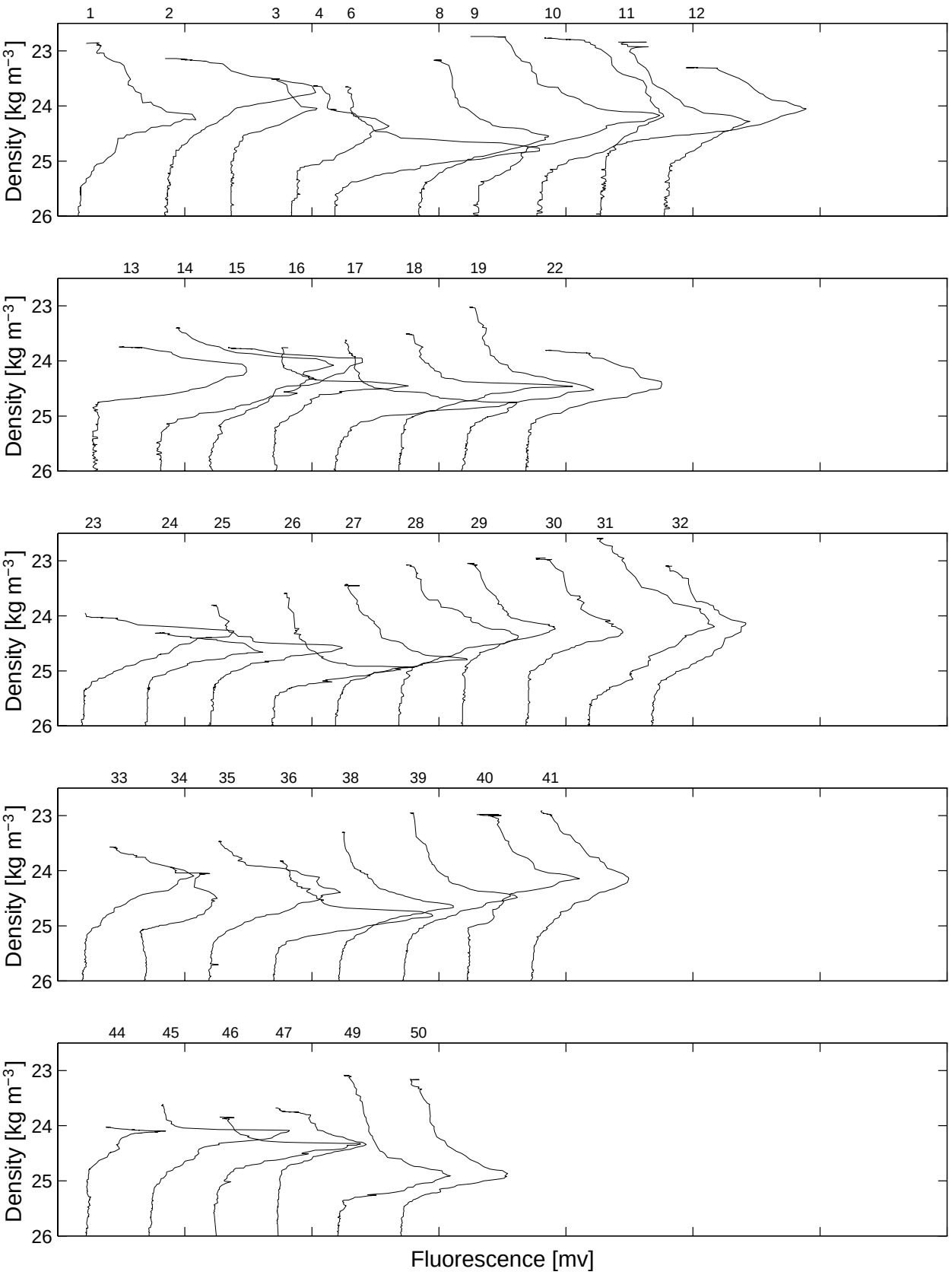
1 2 3 4 6 8 9 10 11 12
13 14 15 16 17 18 19 22
23 24 25 26 27 28 29 30 31 32
33 34 35 36 38 39 40 41
44 45 46 47 49 50
Density [kg m⁻³]
23
24
25
26
Fluorescence [mv]

Figure 6.3.2

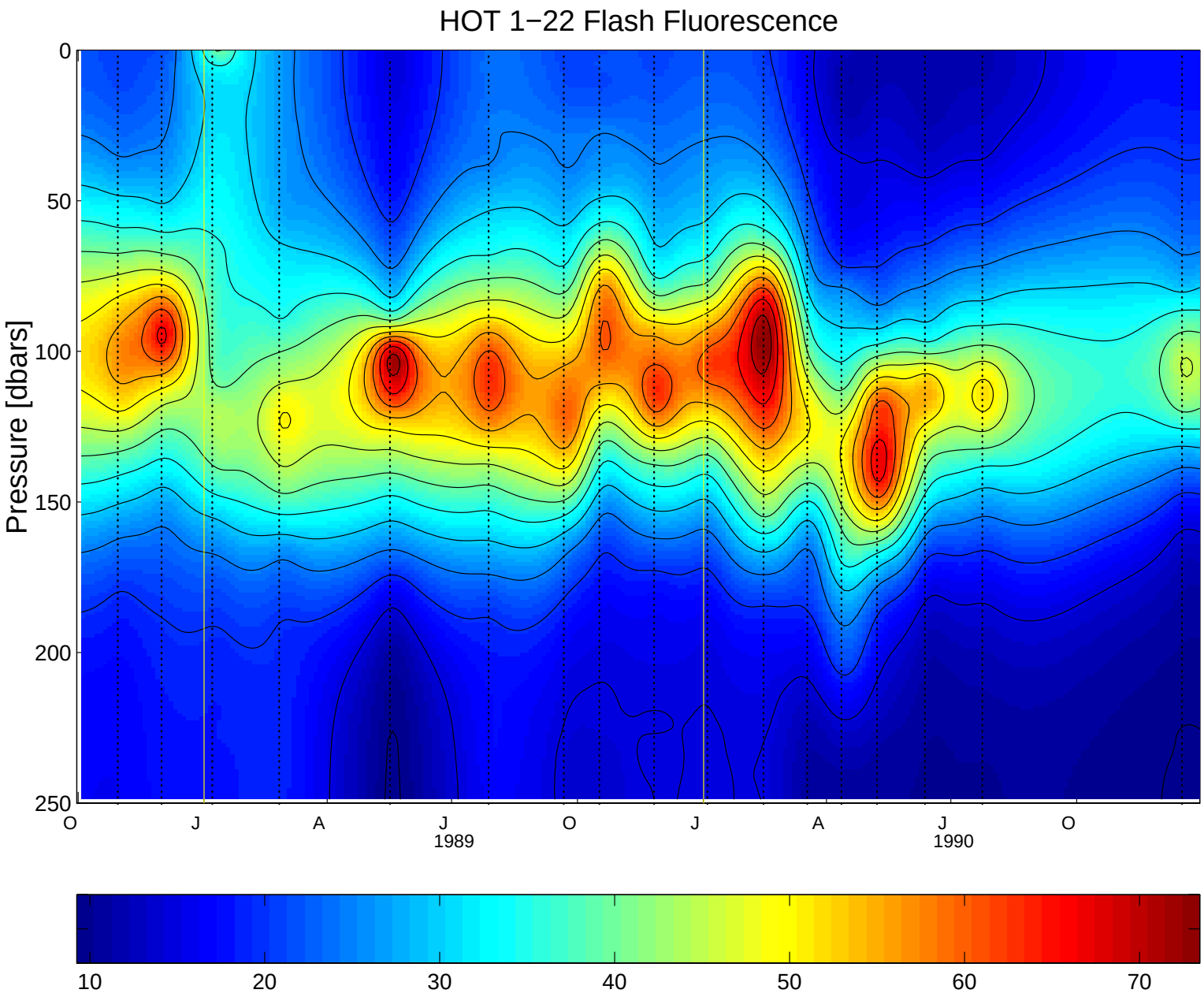
HOT 1−22 Flash Fluorescence
Pressure [dbars]
0
50
100
150
200
250
O
J
A
J
O
J
A
J
O
1989
1990
10
20
30
40
50
60
70

Figure 6.3.3

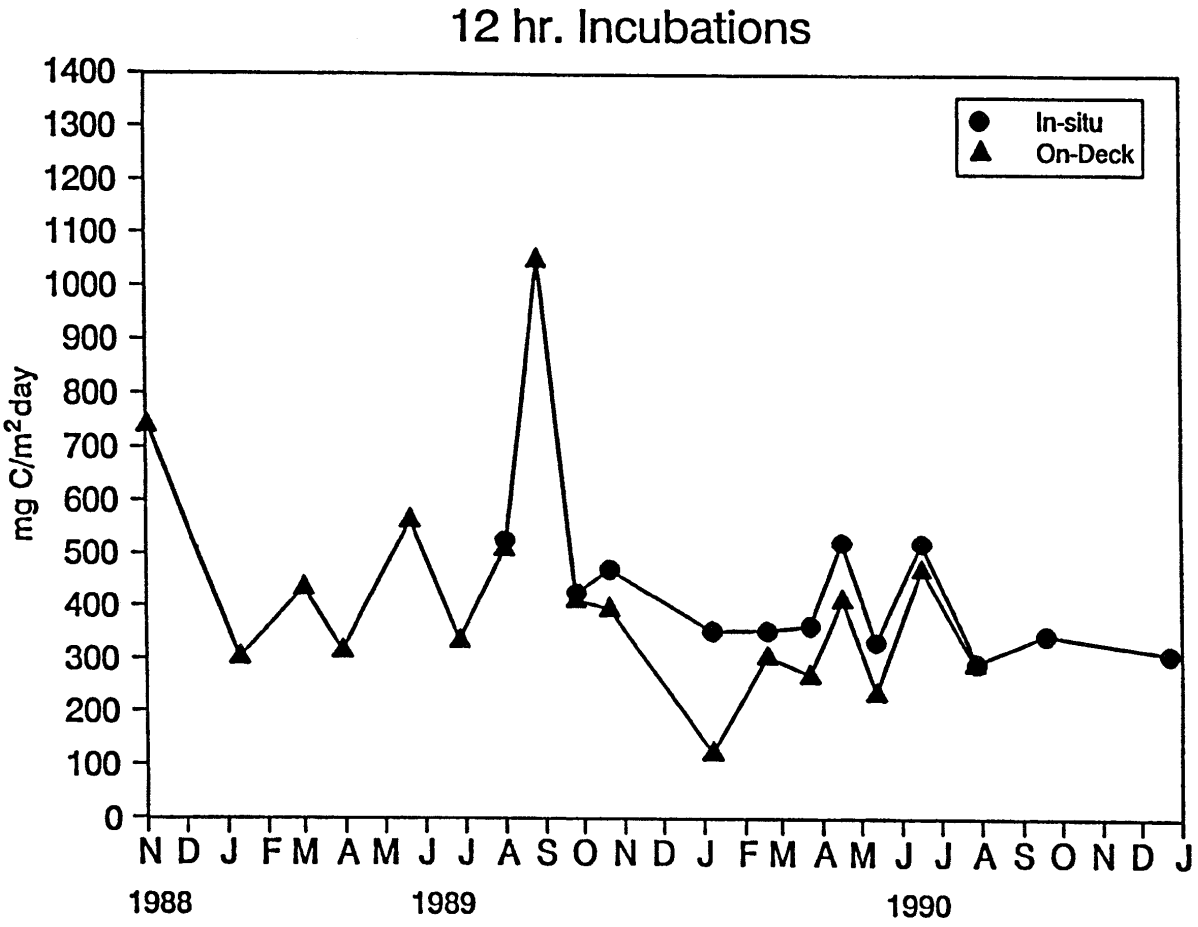
12 hr. Incubations
In-situ
On-Deck
mg C/m²day
1400
1300
1200
1100
1000
900
800
700
600
500
400
300
200
100
0
N D J F M A M J J A S O N D J F M A M J J A S O N D J
1988
1989
1990

Figure 6.3.4

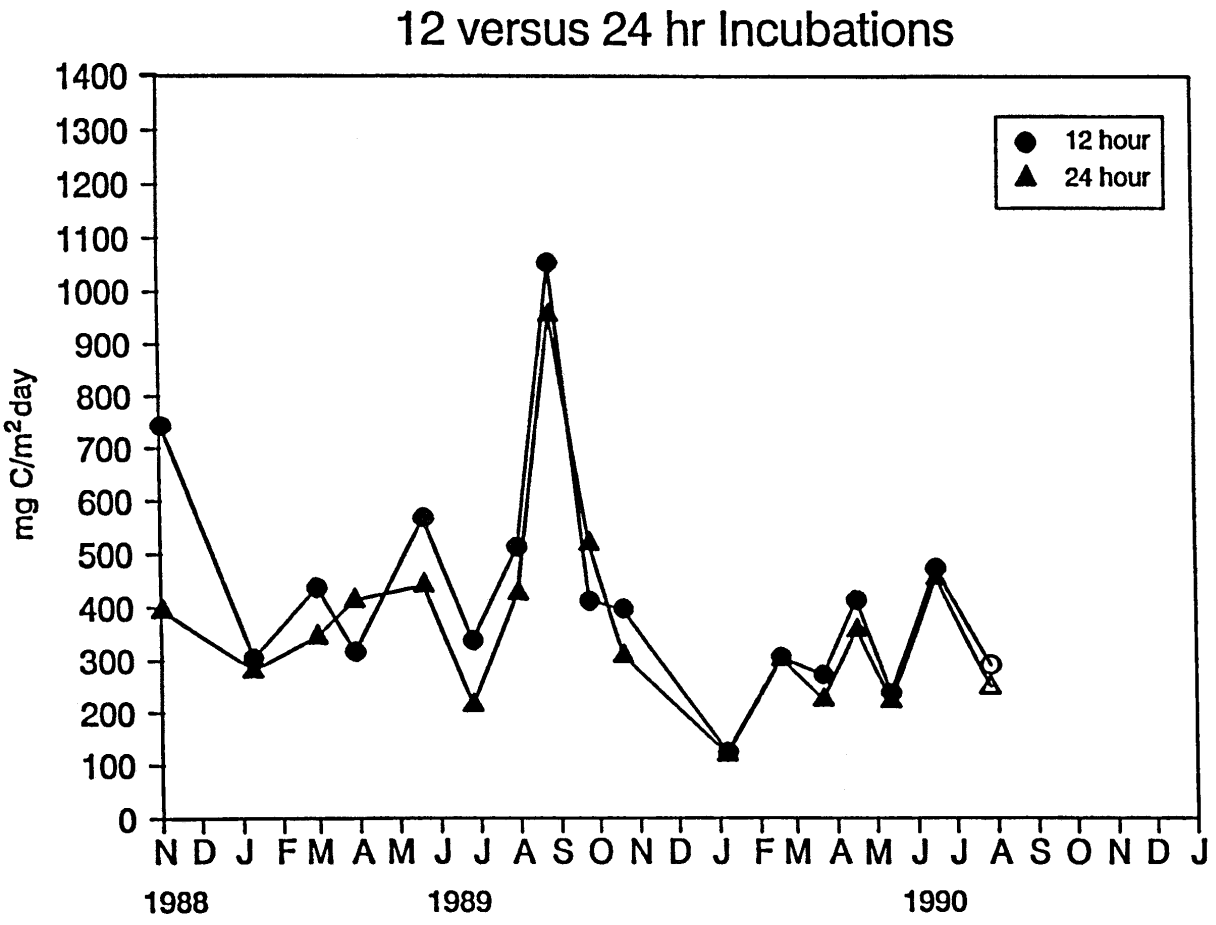
12 versus 24 hr Incubations
12 hour
24 hour
mg C/m2day
1400
1300
1200
1100
1000
900
800
700
600
500
400
300
200
100
0
N D J F M A M J J A S O N D J F M A M J J A S O N D J
1988
1989
1990

Figure 6.3.5

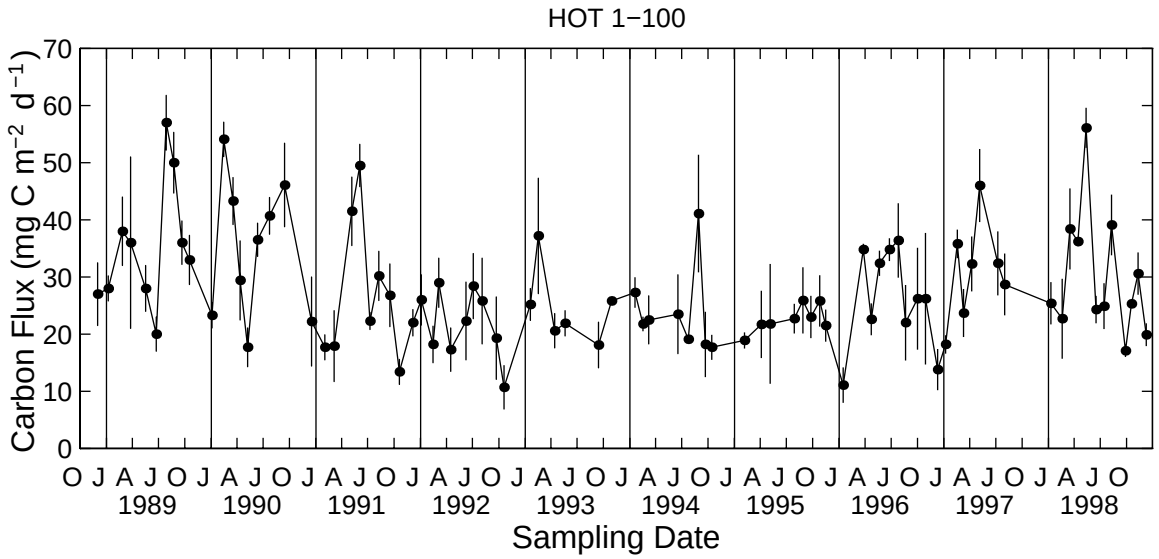

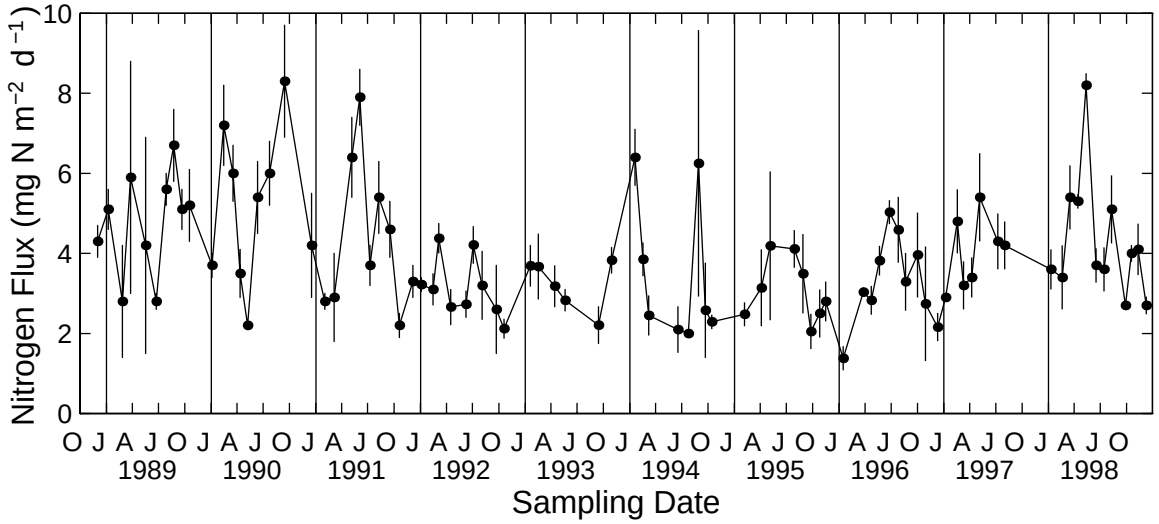

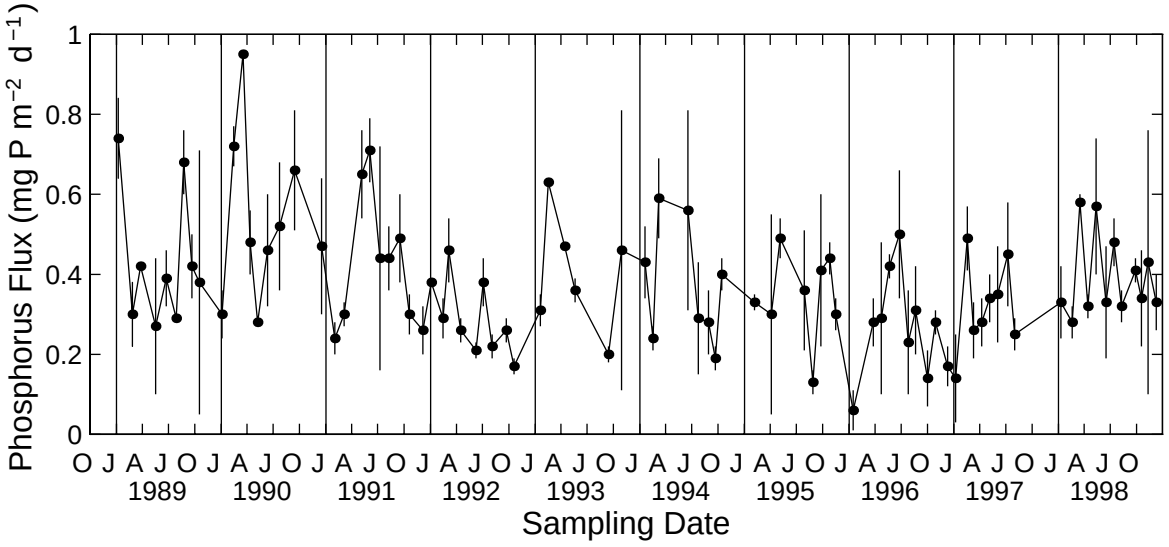

Figures 6.3.6, 6.3.7 & 6.3.8

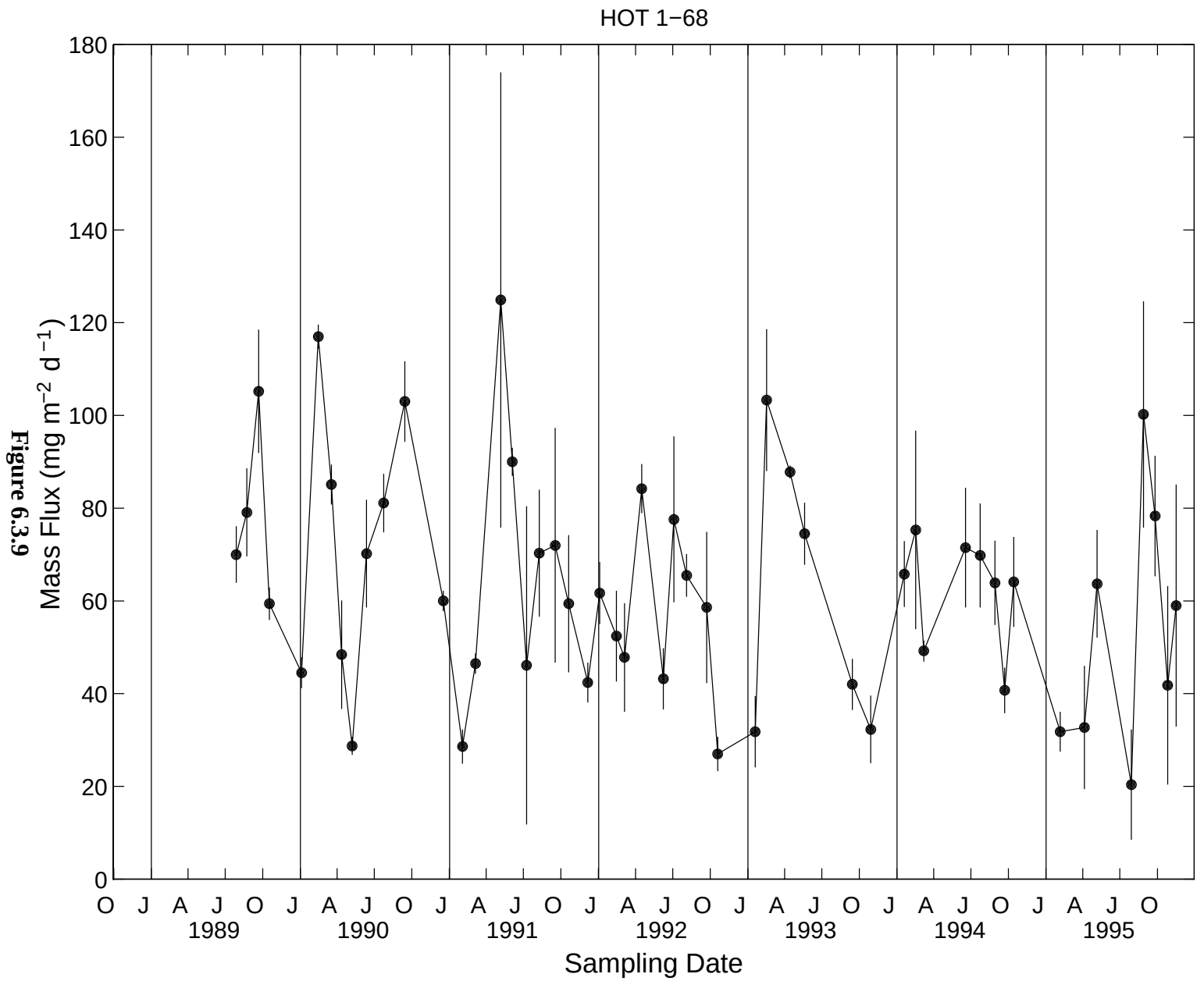
HOT 1−68
Mass Flux (mg m^{-2} d^{-1})
0
20
40
60
80
100
120
140
160
180
O J A J O J A J O J A J O J A J O J A J O J A J O J A J O
1989
1990
1991
1992
1993
1994
1995
Sampling Date

Figure 6.3.9

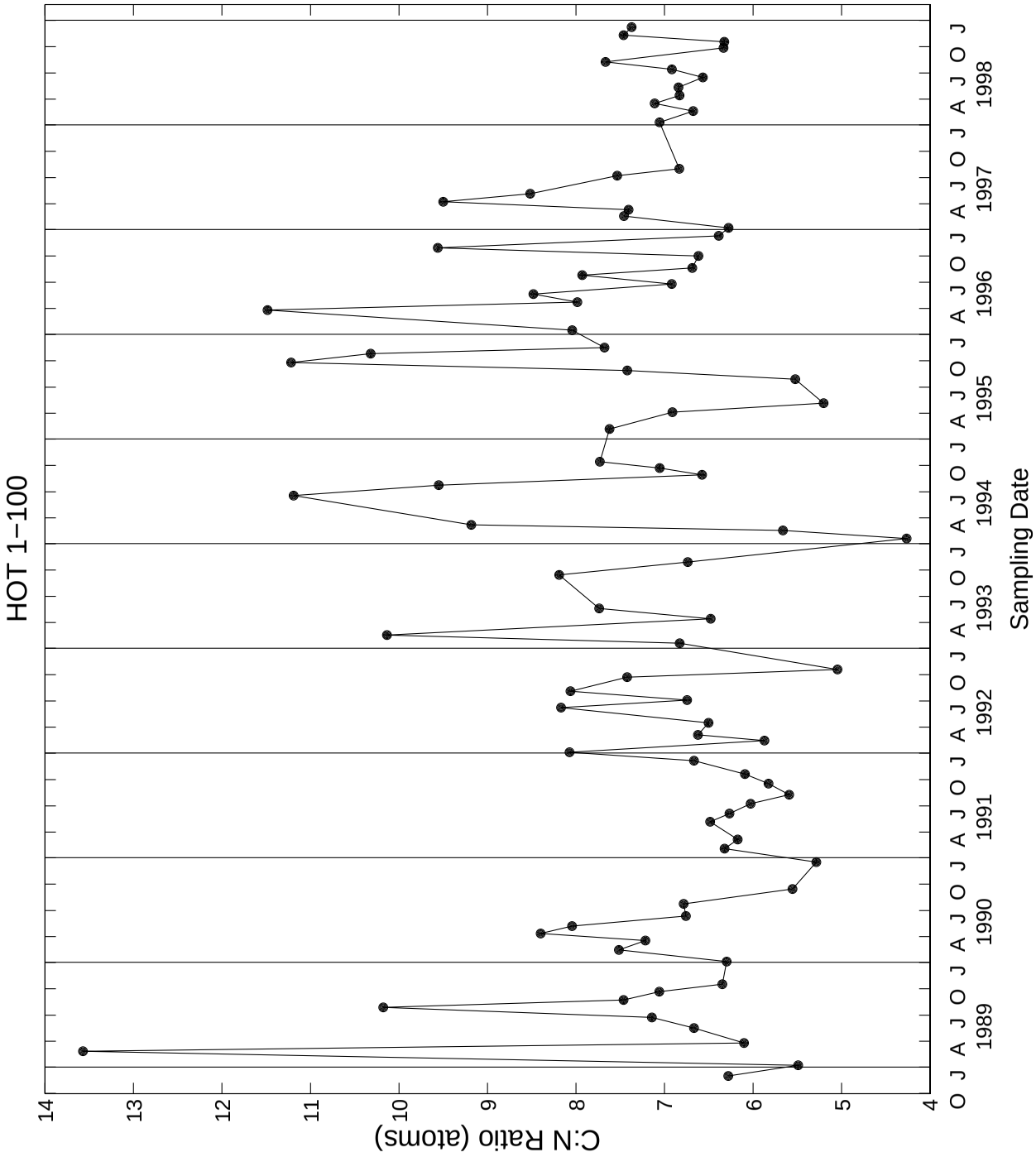
HOT 1–100
C:N Ratio (atoms)
Sampling Date
14
13
12
11
10
9
8
7
6
5
4
O J A J O J A J O J A J O J A J O J A J O J A J O J A J O J A J O J A J O J
1989
1990
1991
1992
1993
1994
1995
1996
1997
1998

Figure 6.3.10

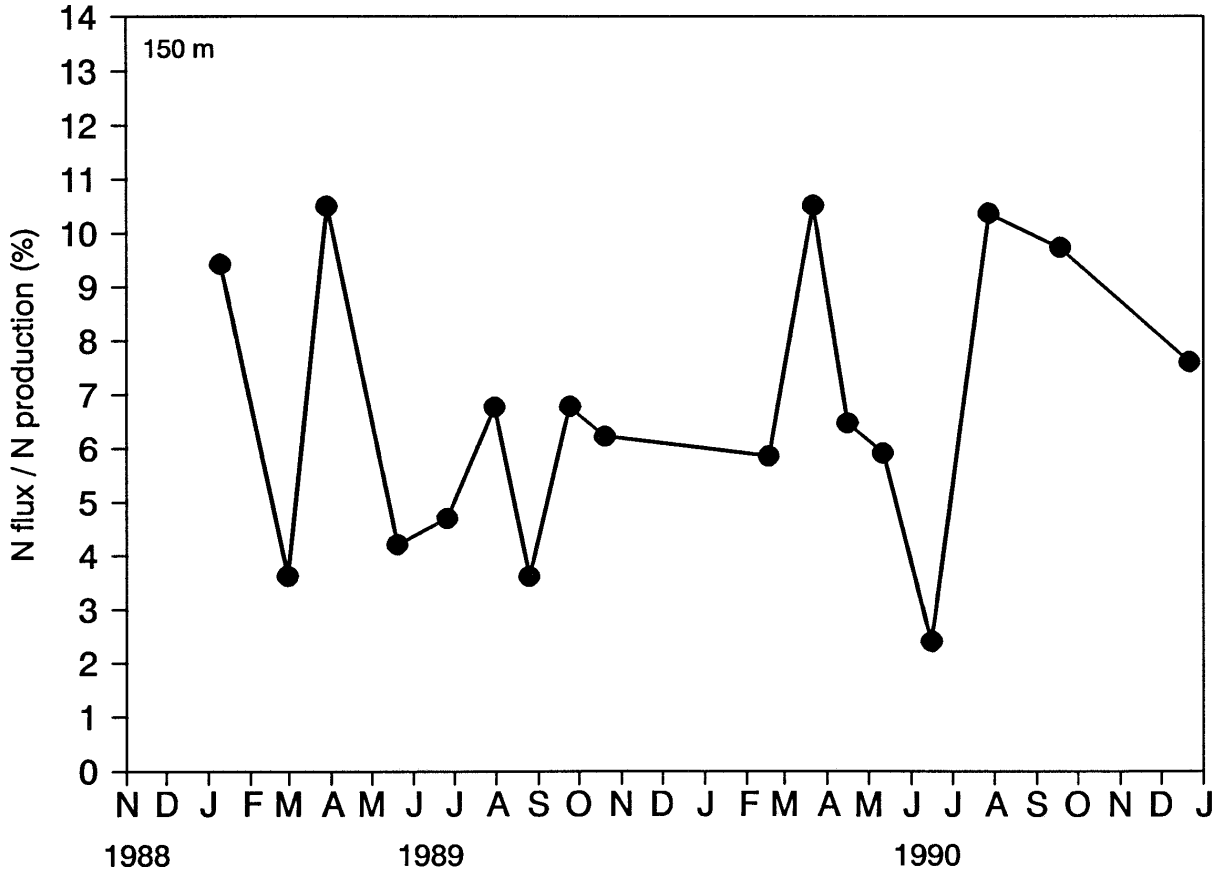
150 m
N flux / N production (%)
0
1
2
3
4
5
6
7
8
9
10
11
12
13
14
N D J F M A M J J A S O N D J F M A M J J A S O N D J
1988
1989
1990

Figure 6.3.11

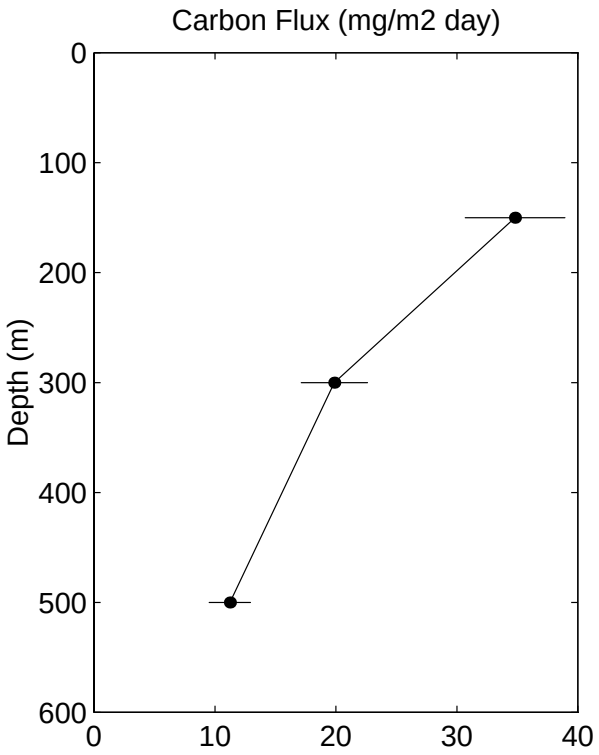
Carbon Flux (mg/m2 day)
Depth (m)
0
100
200
300
400
500
600
0
10
20
30
40

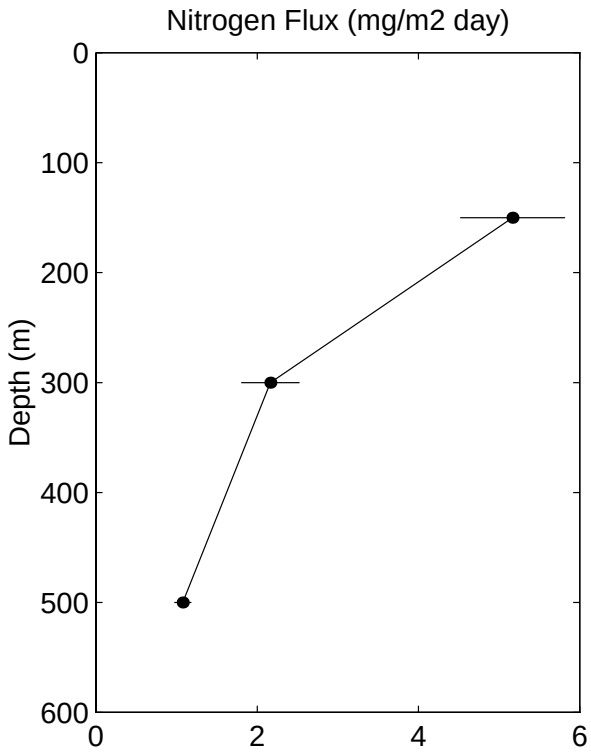
Nitrogen Flux (mg/m2 day)
Depth (m)
0
100
200
300
400
500
600
0
2
4
6

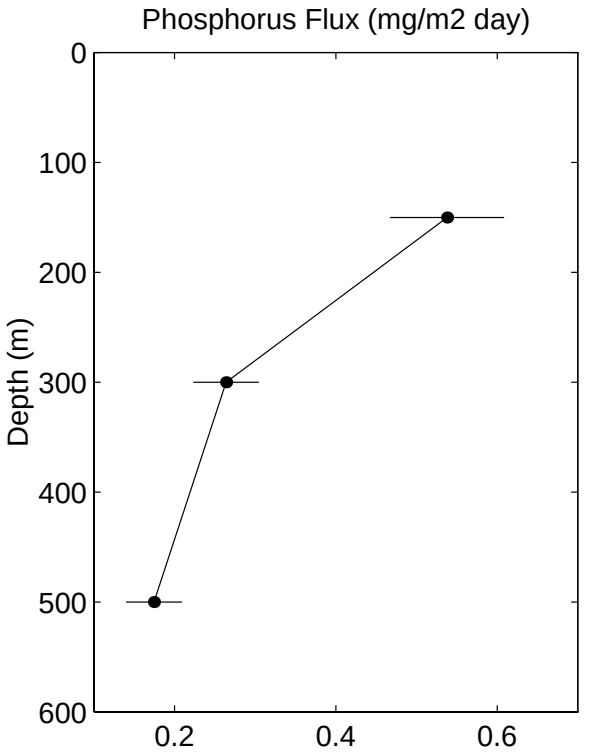
Phosphorus Flux (mg/m2 day)
Depth (m)
0
100
200
300
400
500
600
0.2
0.4
0.6

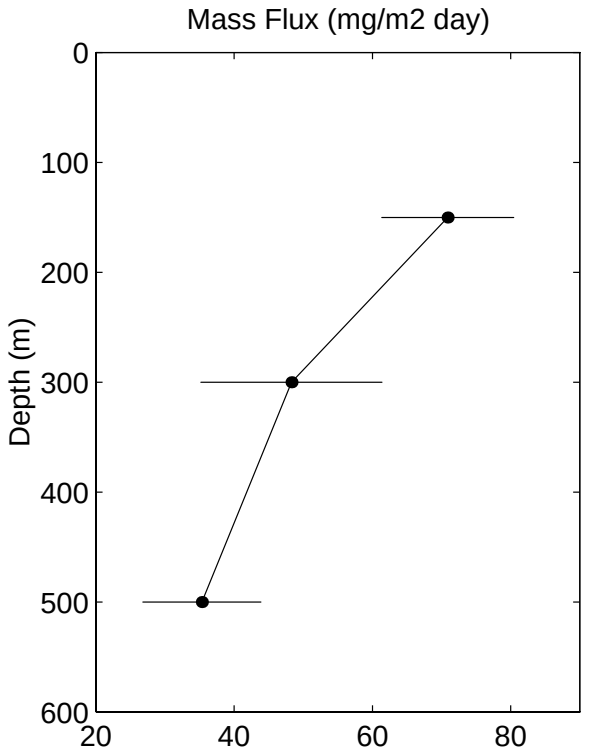
Mass Flux (mg/m2 day)
Depth (m)
0
100
200
300
400
500
600
20
40
60
80

6.4. ADCP Measurements

For each cruise with shipboard ADCP, the following figures (6.4.1-10) are provided:

Figures 6.4.1a-5c: Navigation: reference layer velocity (upper panels) and ship's longitude and latitude (lower panels) as functions of time. Time is given in days from the beginning of the year, for example, noon on January 1 is 0.5 decimal days. The reference layer velocity is shown averaged between fixes (steppy curves), and smoothed, as used in the final velocity estimates (smooth curves). Plus signs near the bottom of the reference layer velocity plots indicate ADCP data gaps. The ship's position is shown by asterisks at fixes and by a continuous curve (actually closely-spaced dots) as determined by fixes together with the ADCP data.

Figures 6.4.6a-10a: Velocity field on station: Tne top panel shows hourly averages at 20-m depth intervals while the ship was at Station ALOHA. The orientation of each stick gives the direction of the current: up is northward, to the right is eastward. The bottom panel shows the results of a least-squares fit of the hourly averages to a mean, trend, semidiurnal, and diurnal tides, and an inertial cycle. In the first column, the arrow shows the mean current, and the headless stick shows the sum of the mean plus the trend at the end of the station. For each harmonic, the current ellipse is shown in the first column. The orientation of the stick in the second column shows the direction of that harmonic component of the current at the beginning of the station, and the arrowhead at the end of the stick shows the direction of rotation of the current vector around the ellipse. Towards the end of HOT-13, the ship steamed west more than half a degree, effectively ending the time series on station. Therefore the model fit was done only on the time interval from Jan. 4 at 0830 to Jan. 6 at 0430, and the diurnal and inertial periods were excluded from the model. HOT-20 was unusual in that it consisted of a day at the station, about 1.5 days transit to Honolulu and back, and then another two days on station. The entire period has been used in the model fit.

Figures 6.4.6b-10b and 6.4.9c: Velocity field on the transits to and from the station: Velocity is shown as a function of latitude, averaged in 10-minute time intervals.

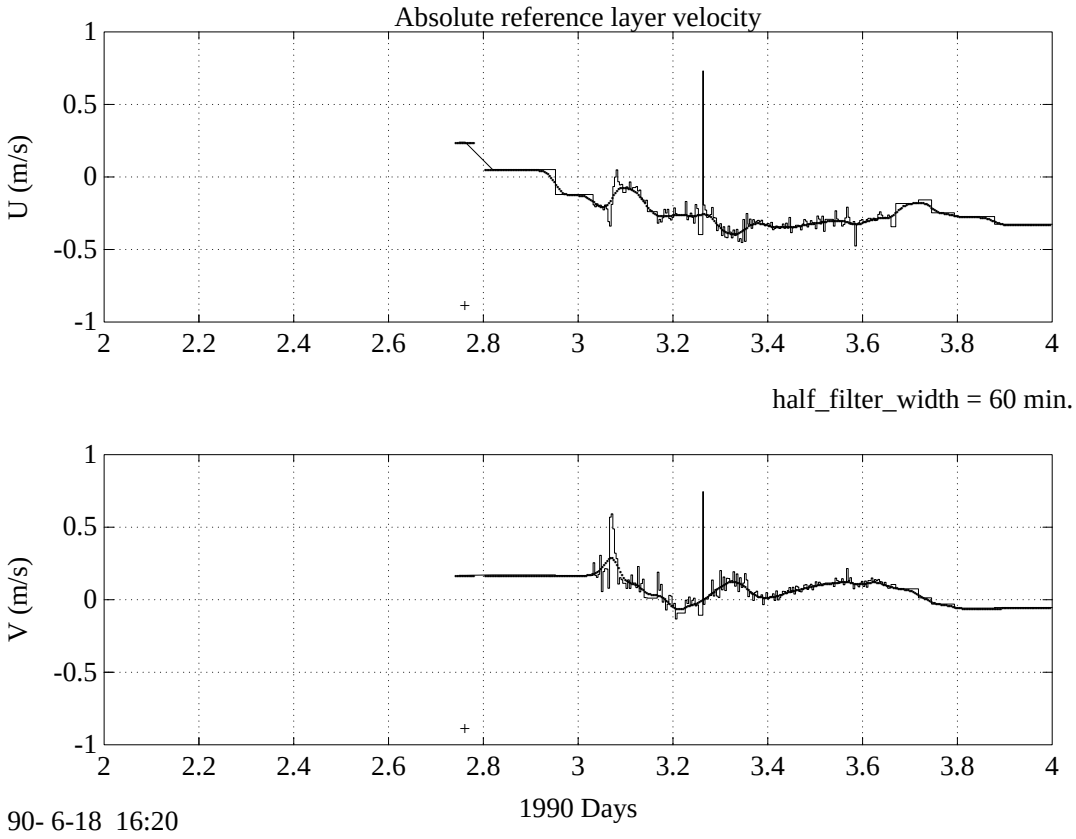
Absolute reference layer velocity
U (m/s)
V (m/s)
half_filter_width = 60 min.
1990 Days
90- 6-18 16:20

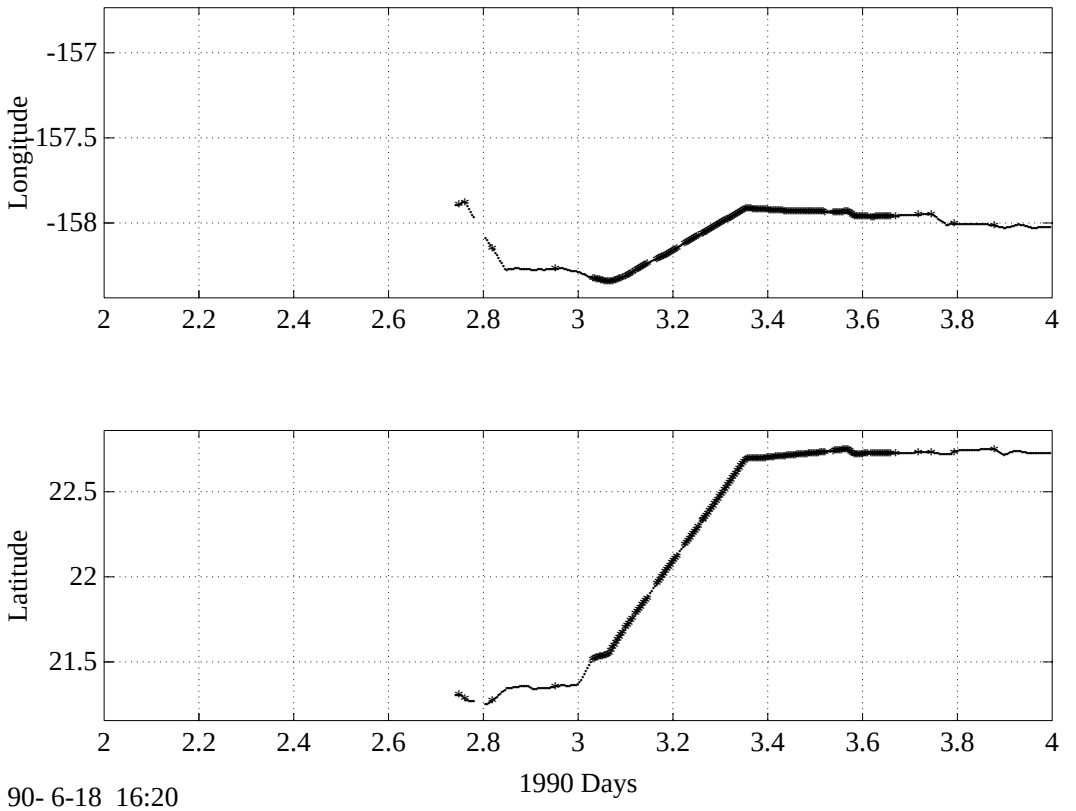
Longitude
Latitude
1990 Days
90- 6-18 16:20

Figure 6.4.1a

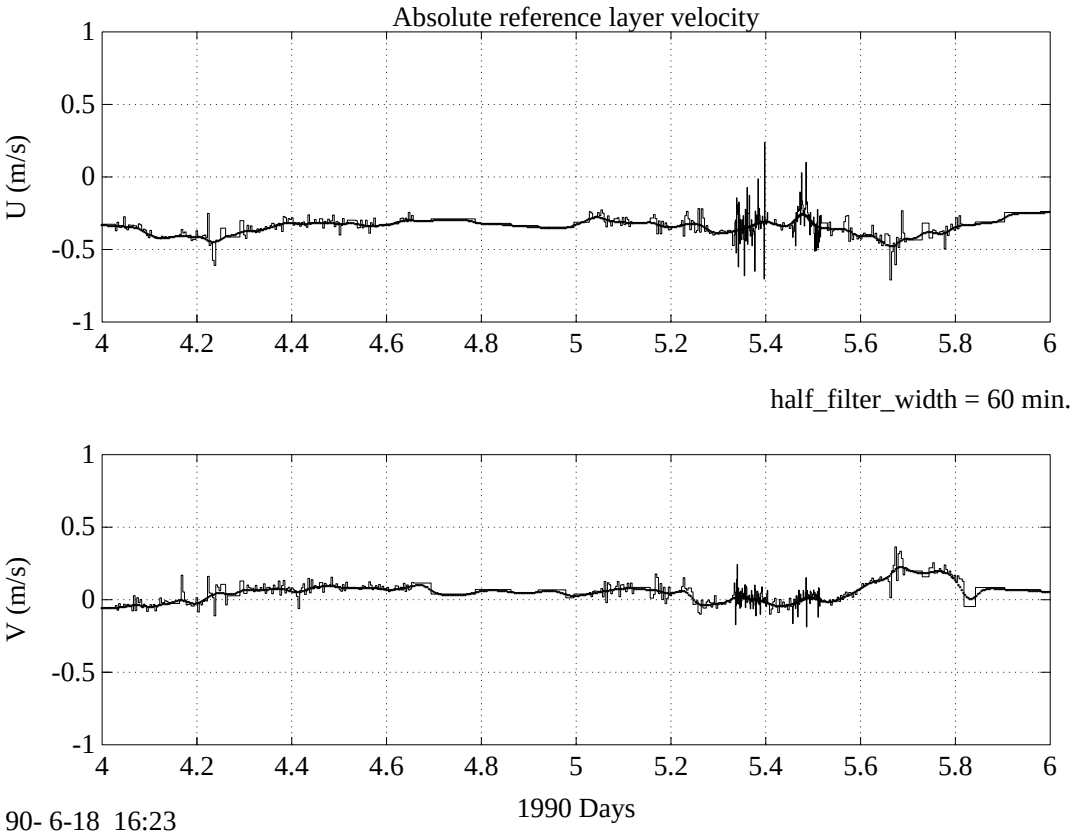
Absolute reference layer velocity
U (m/s)
V (m/s)
half_filter_width = 60 min.
1990 Days
90- 6-18 16:23

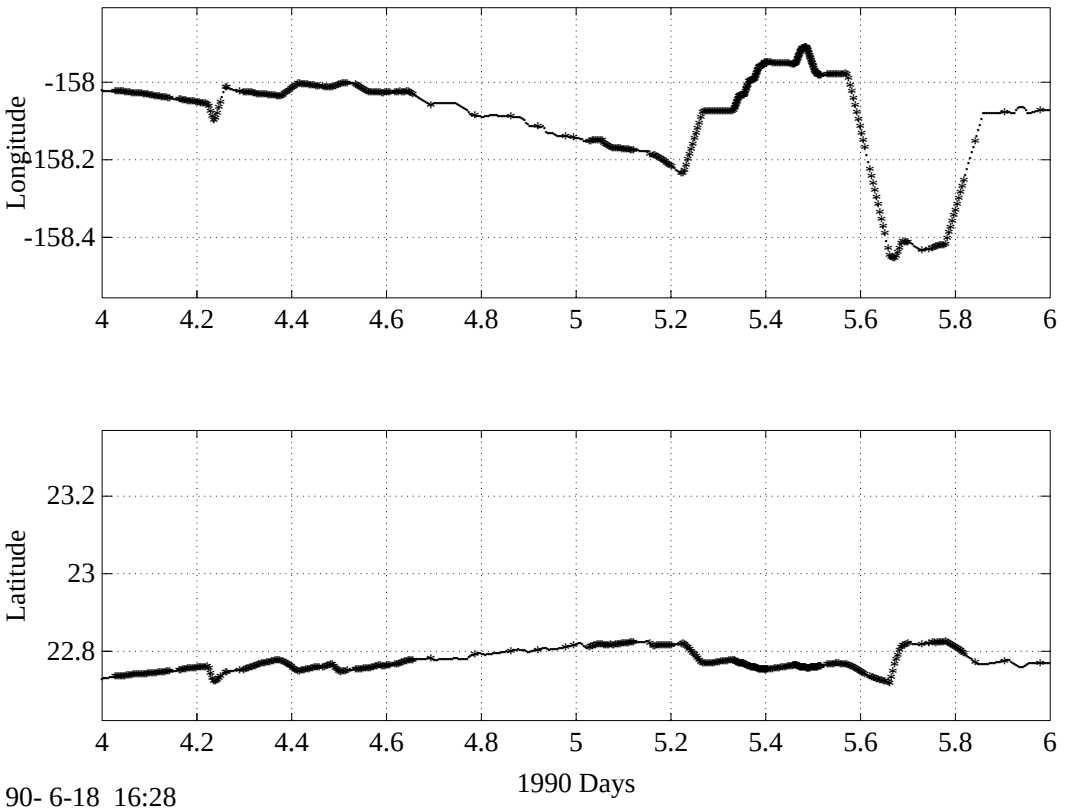
Longitude
Latitude
1990 Days
90- 6-18 16:28

Figure 6.4.1b

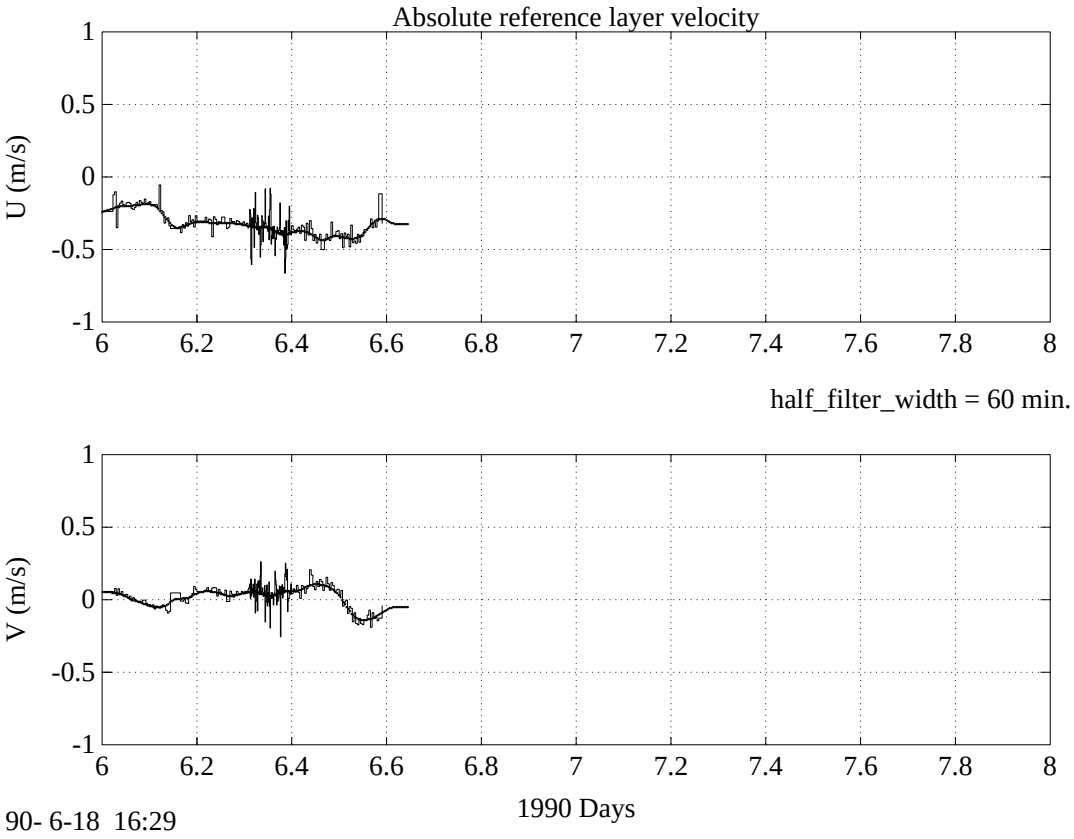
Absolute reference layer velocity
U (m/s)
V (m/s)
half_filter_width = 60 min.
1990 Days
90- 6-18 16:29

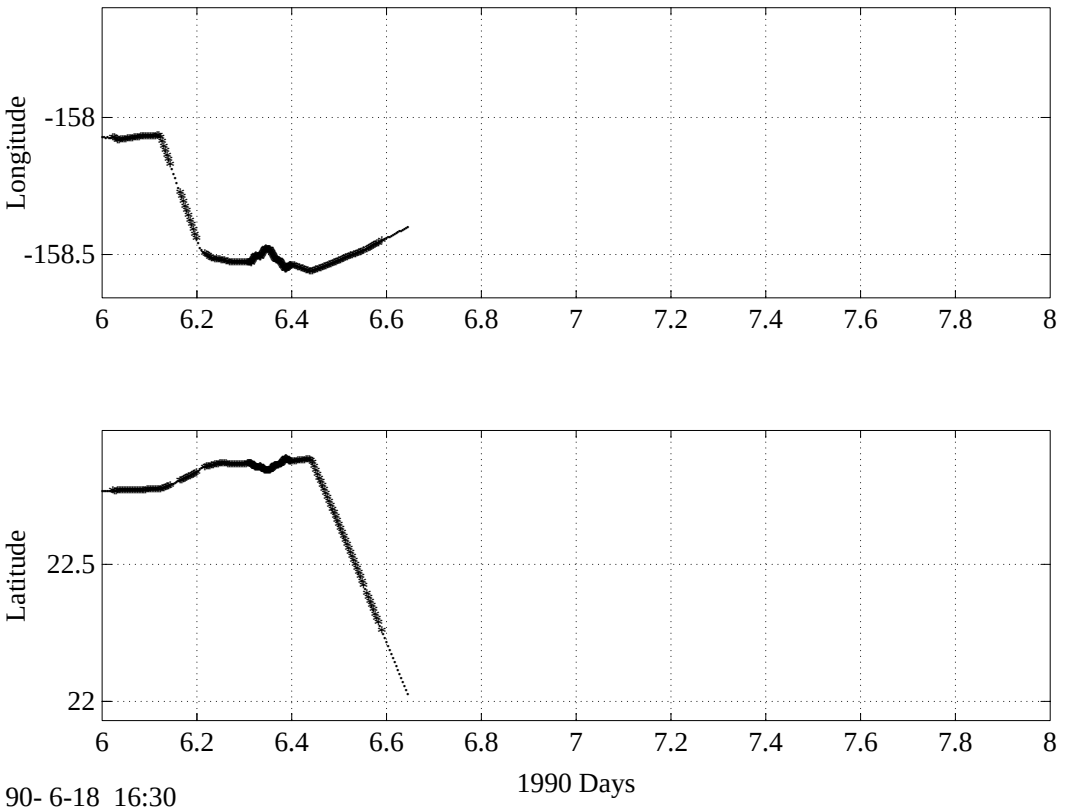
Longitude
Latitude
1990 Days
90- 6-18 16:30

Figure 6.4.1c

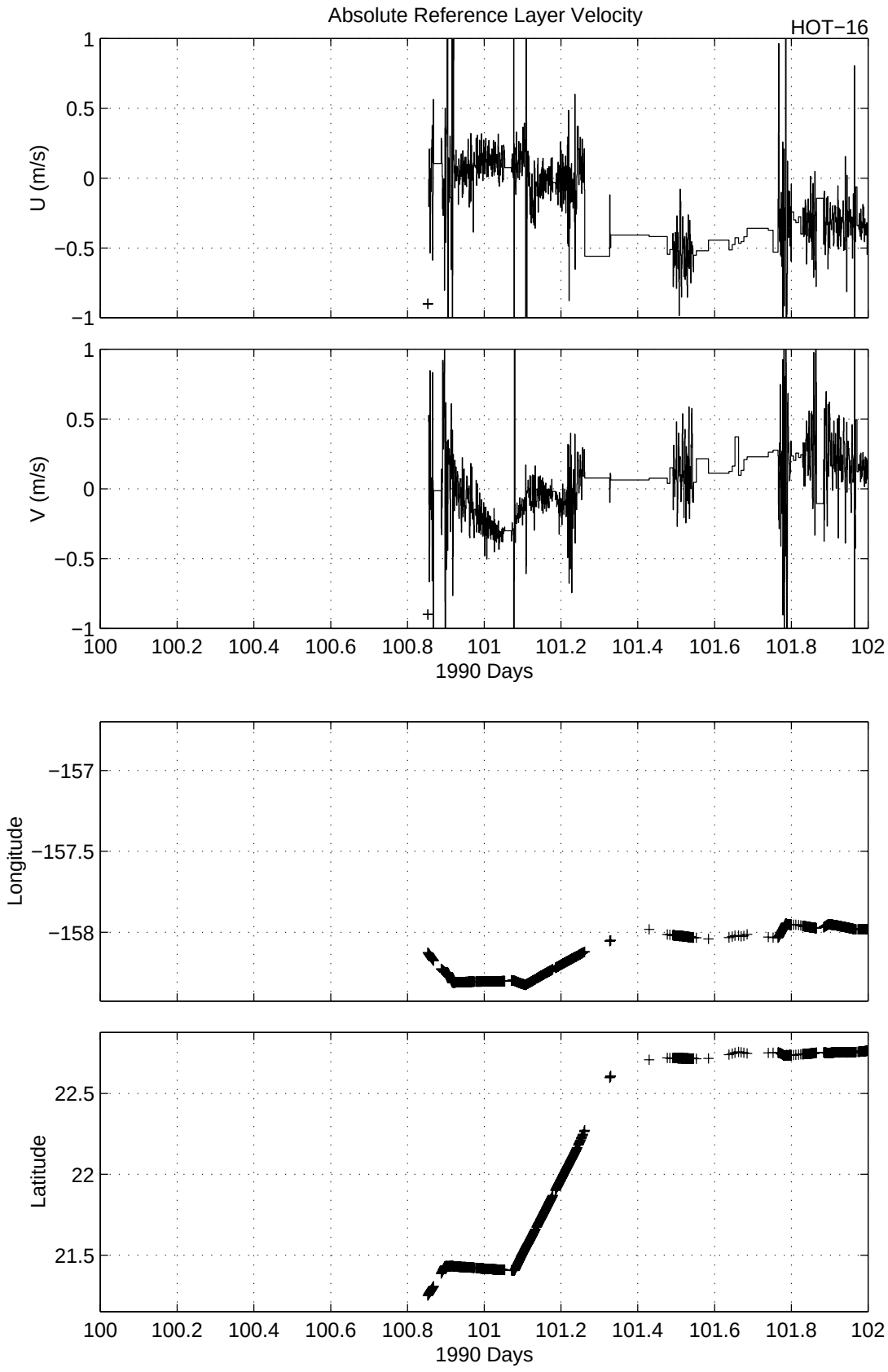

99− 8−25 11:15

Figure 6.4.2a

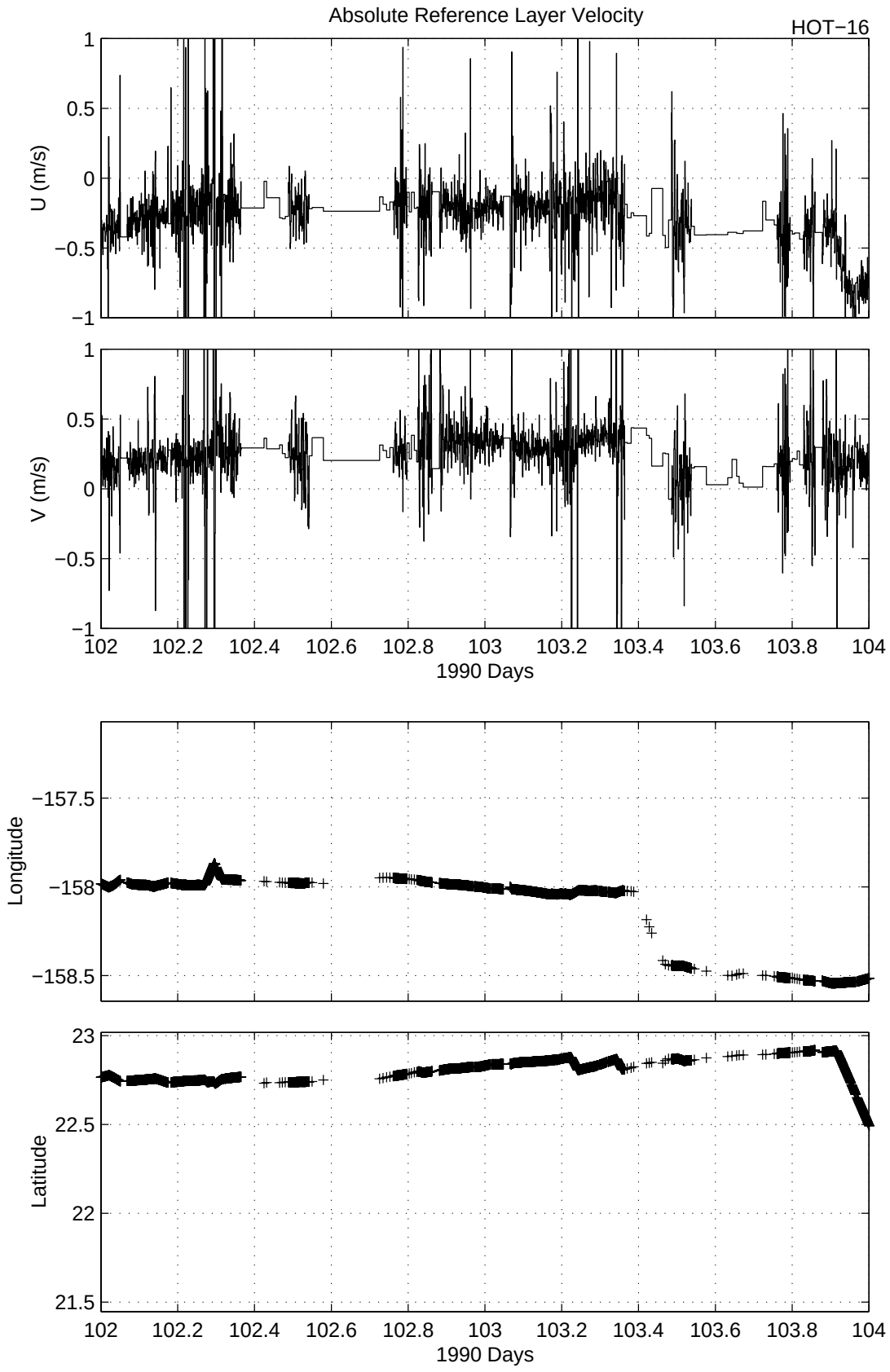

99− 8−25 11:15

Figure 6.4.2b

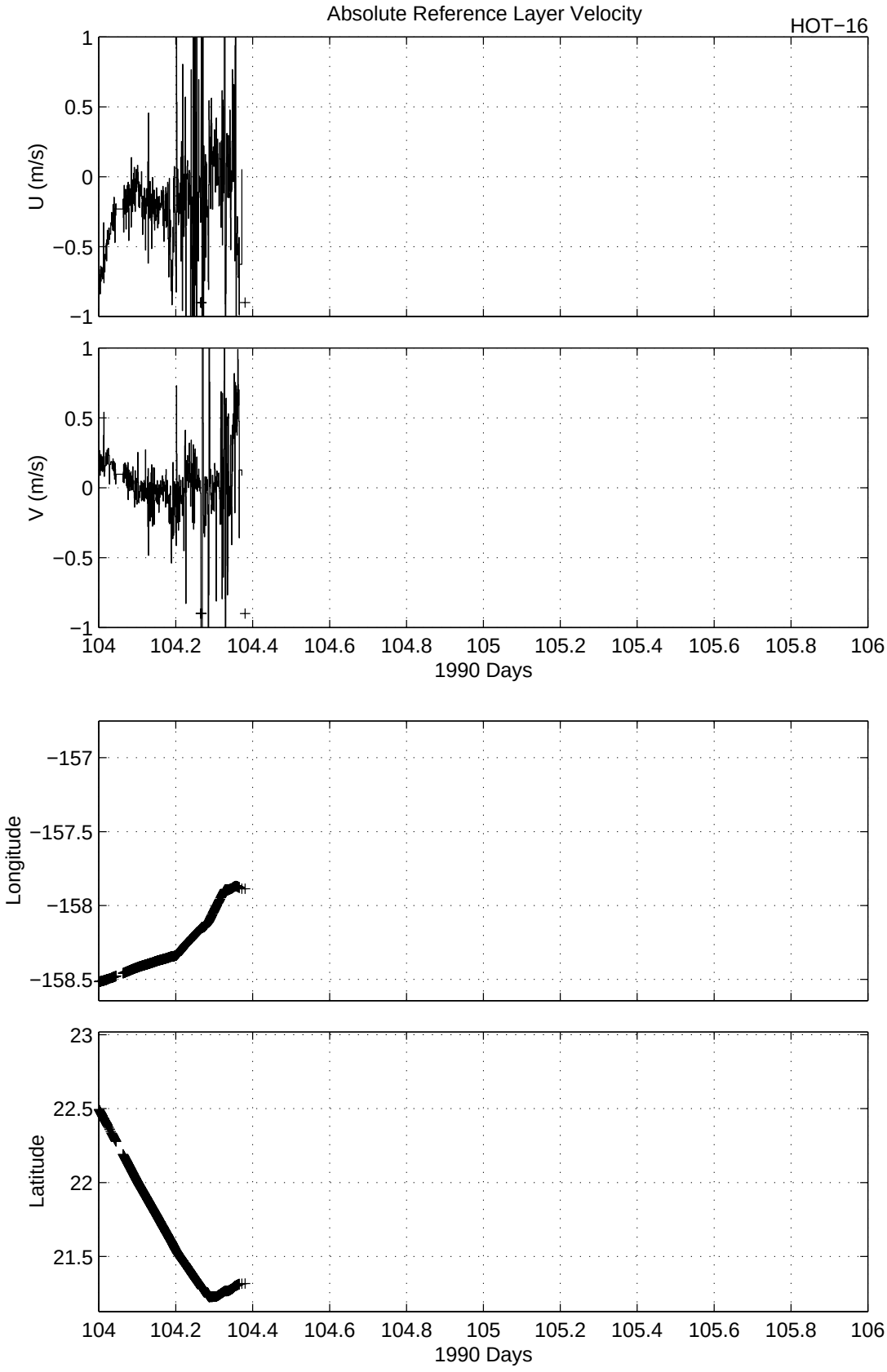
Absolute Reference Layer Velocity
HOT−16
U (m/s)
V (m/s)
1
0.5
0
−0.5
−1
104
104.2
104.4
104.6
104.8
105
105.2
105.4
105.6
105.8
106
1990 Days
Longitude
−157
−157.5
−158
−158.5
Latitude
23
22.5
22
21.5
99− 8−25 11:15

Figure 6.4.2c

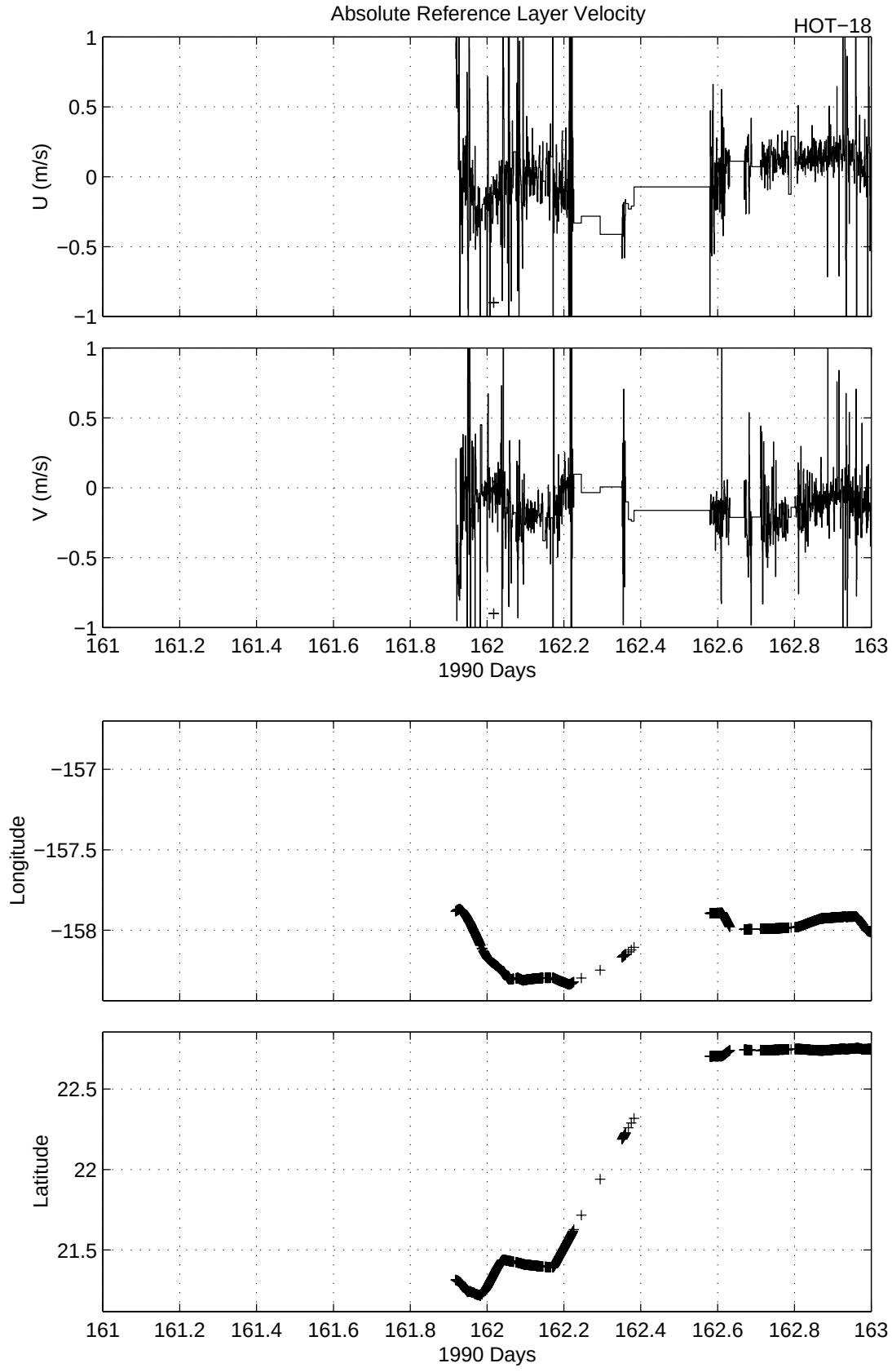
Absolute Reference Layer Velocity
HOT−18
U (m/s)
V (m/s)
1
0.5
0
−0.5
−1
161
161.2
161.4
161.6
161.8
162
162.2
162.4
162.6
162.8
163
1990 Days
Longitude
−157
−157.5
−158
Latitude
22.5
22
21.5
99− 8−25 11:24

Figure 6.4.3a

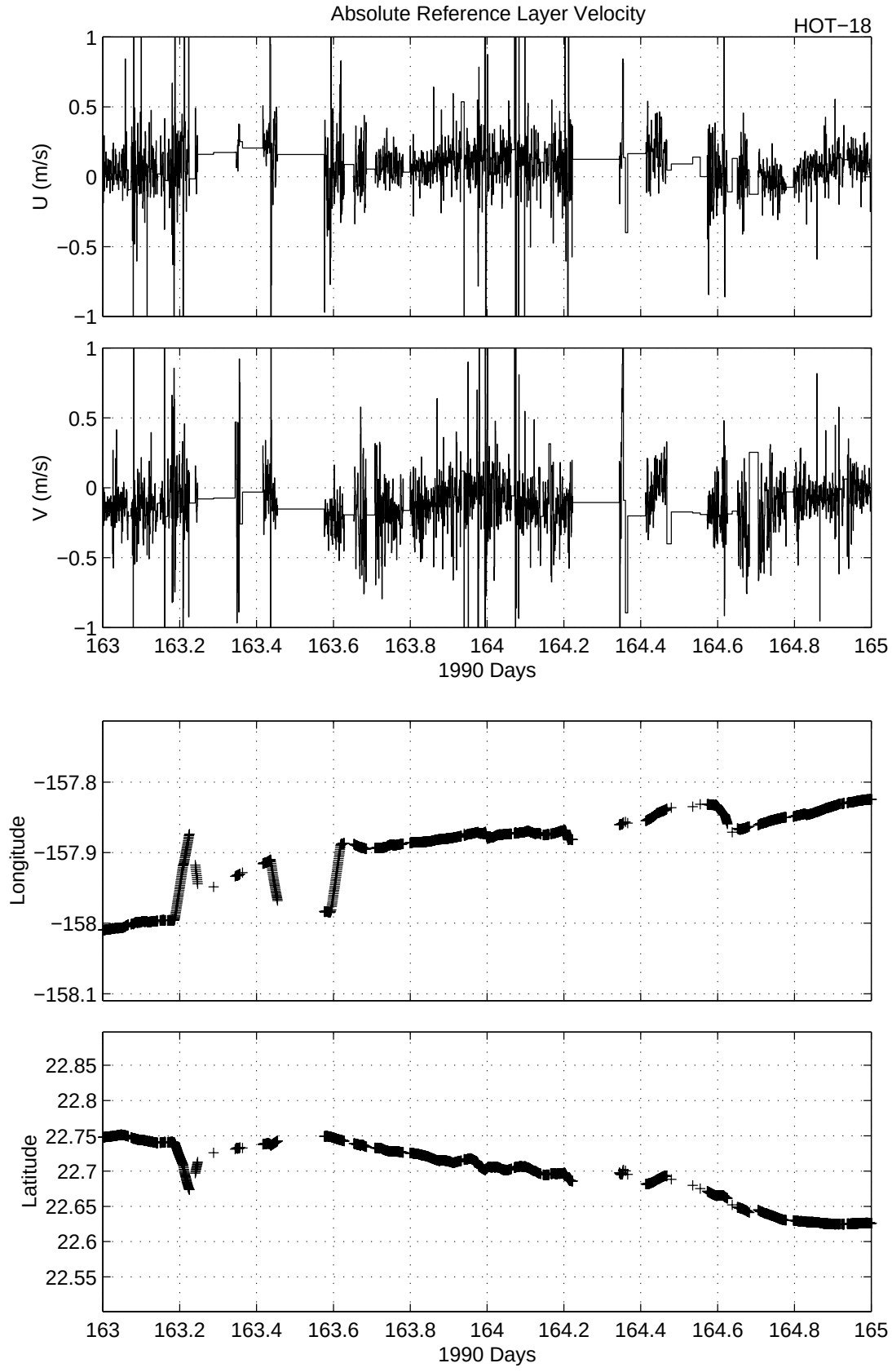
Absolute Reference Layer Velocity
HOT−18
U (m/s)
V (m/s)
1
0.5
0
−0.5
−1
163
163.2
163.4
163.6
163.8
164
164.2
164.4
164.6
164.8
165
1990 Days
Longitude
−157.8
−157.9
−158
−158.1
Latitude
22.85
22.8
22.75
22.7
22.65
22.6
22.55
99− 8−25 11:24

Figure 6.4.3b

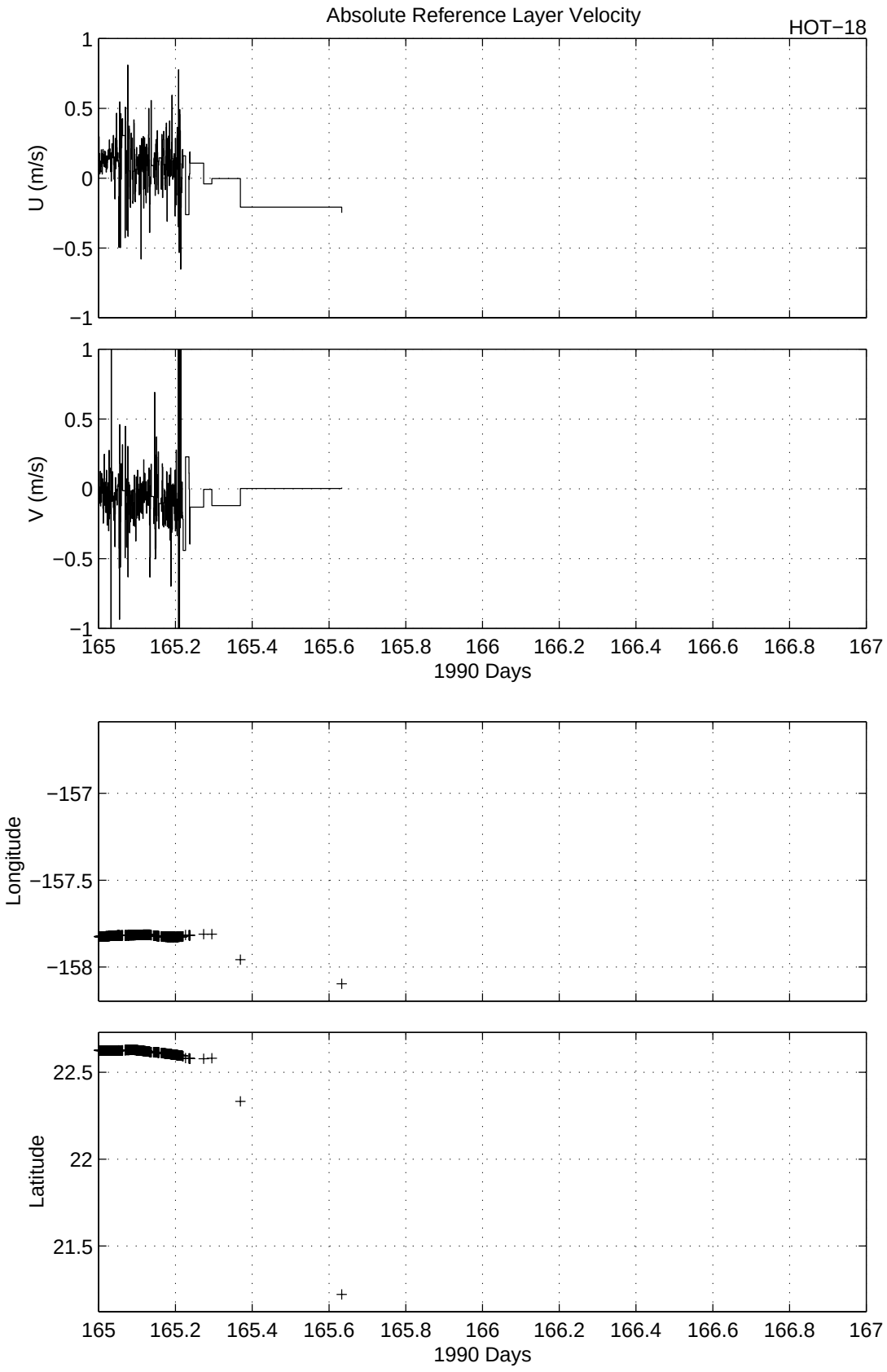
Absolute Reference Layer Velocity
HOT−18
U (m/s)
V (m/s)
1
0.5
0
−0.5
−1
165
165.2
165.4
165.6
165.8
166
166.2
166.4
166.6
166.8
167
1990 Days
Longitude
−157
−157.5
−158
Latitude
22.5
22
21.5
99− 8−25 11:24

Figure 6.4.3c

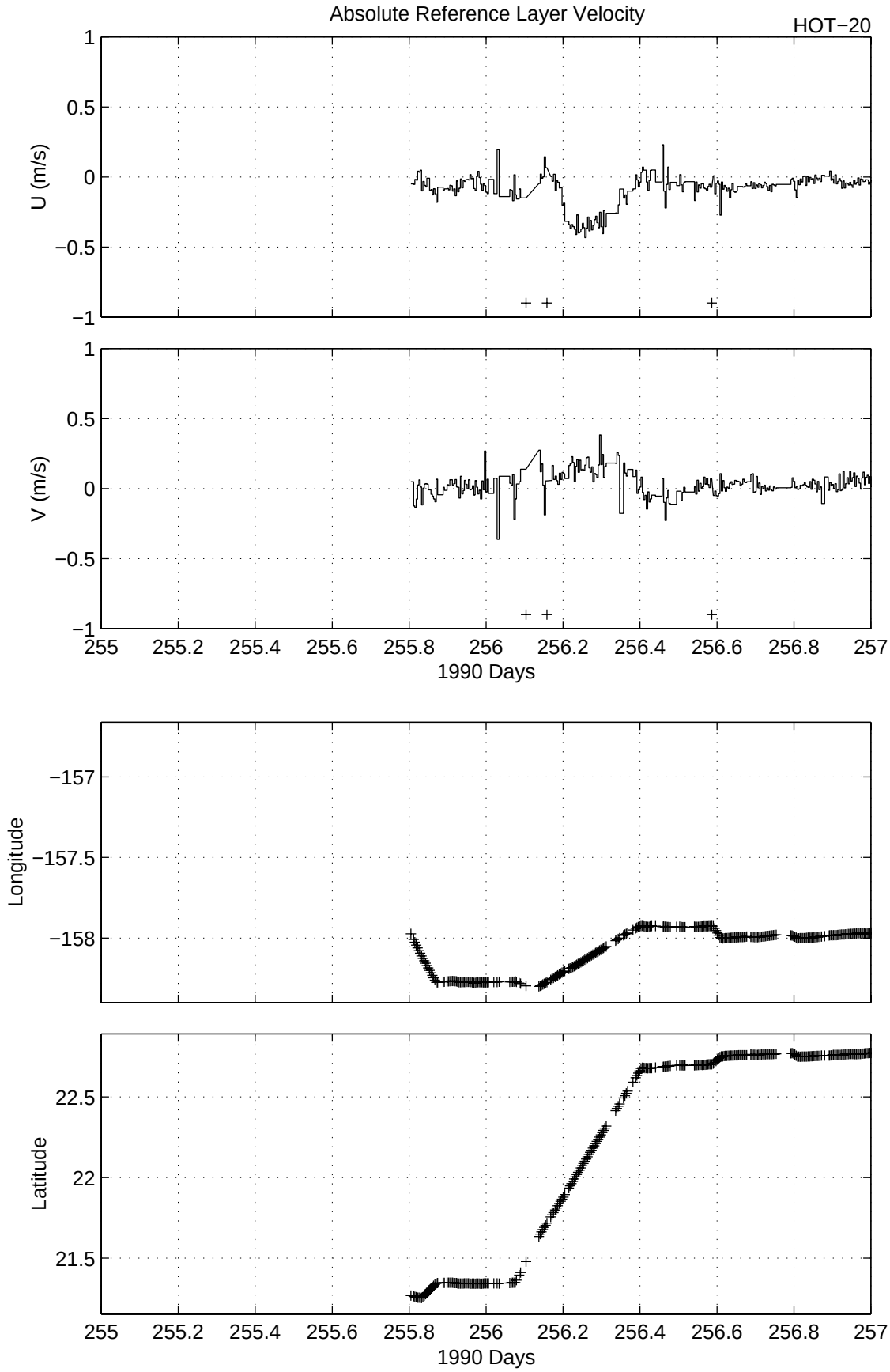
Absolute Reference Layer Velocity
HOT−20
U (m/s)
V (m/s)
1
0.5
0
−0.5
−1
255
255.2
255.4
255.6
255.8
256
256.2
256.4
256.6
256.8
257
1990 Days
Longitude
−157
−157.5
−158
Latitude
22.5
22
21.5

Figure 6.4.4a

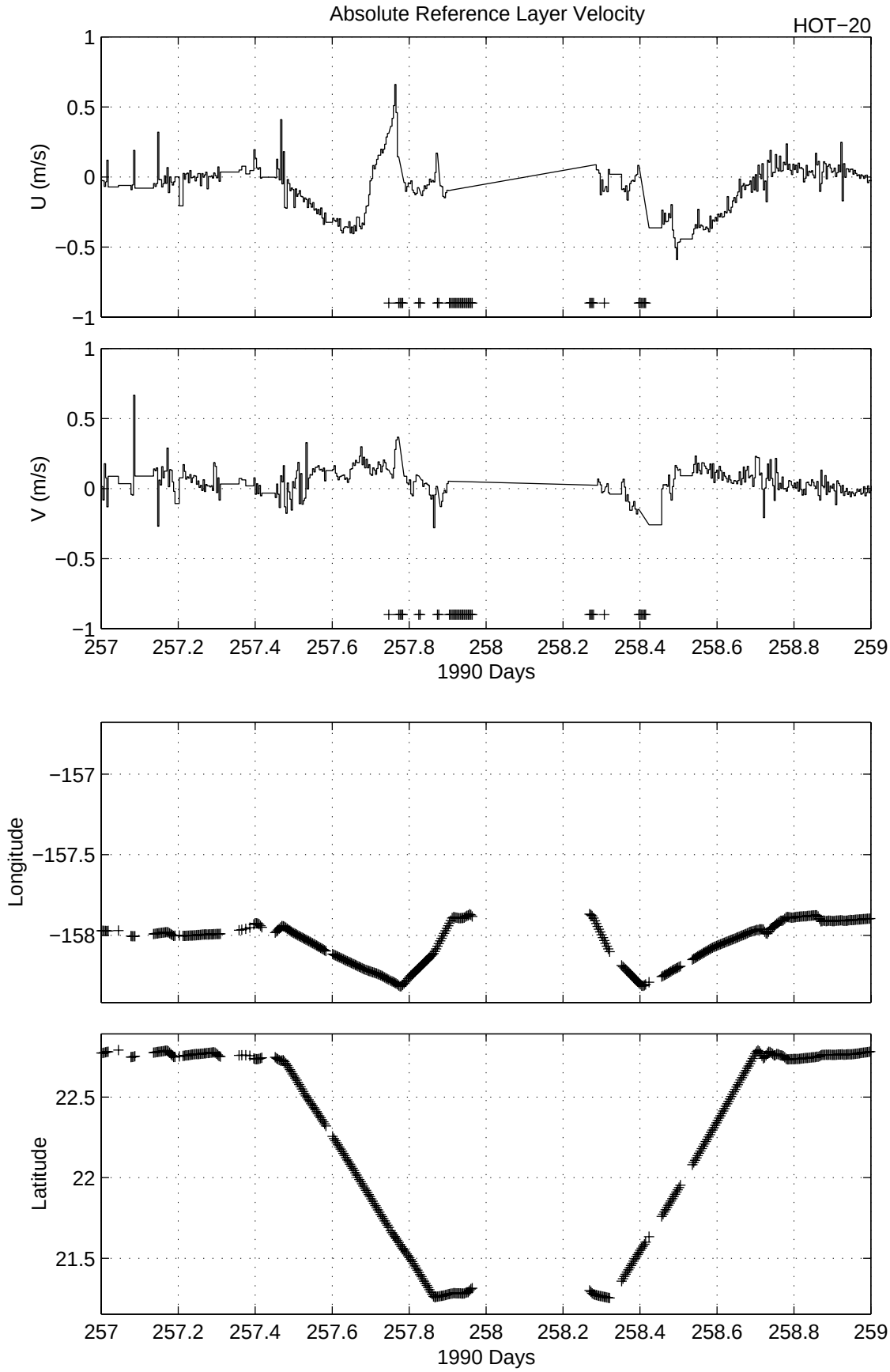
Absolute Reference Layer Velocity
HOT−20
U (m/s)
V (m/s)
1
0.5
0
−0.5
−1
257
257.2
257.4
257.6
257.8
258
258.2
258.4
258.6
258.8
259
1990 Days
Longitude
−157
−157.5
−158
Latitude
22.5
22
21.5

Figure 6.4.4b

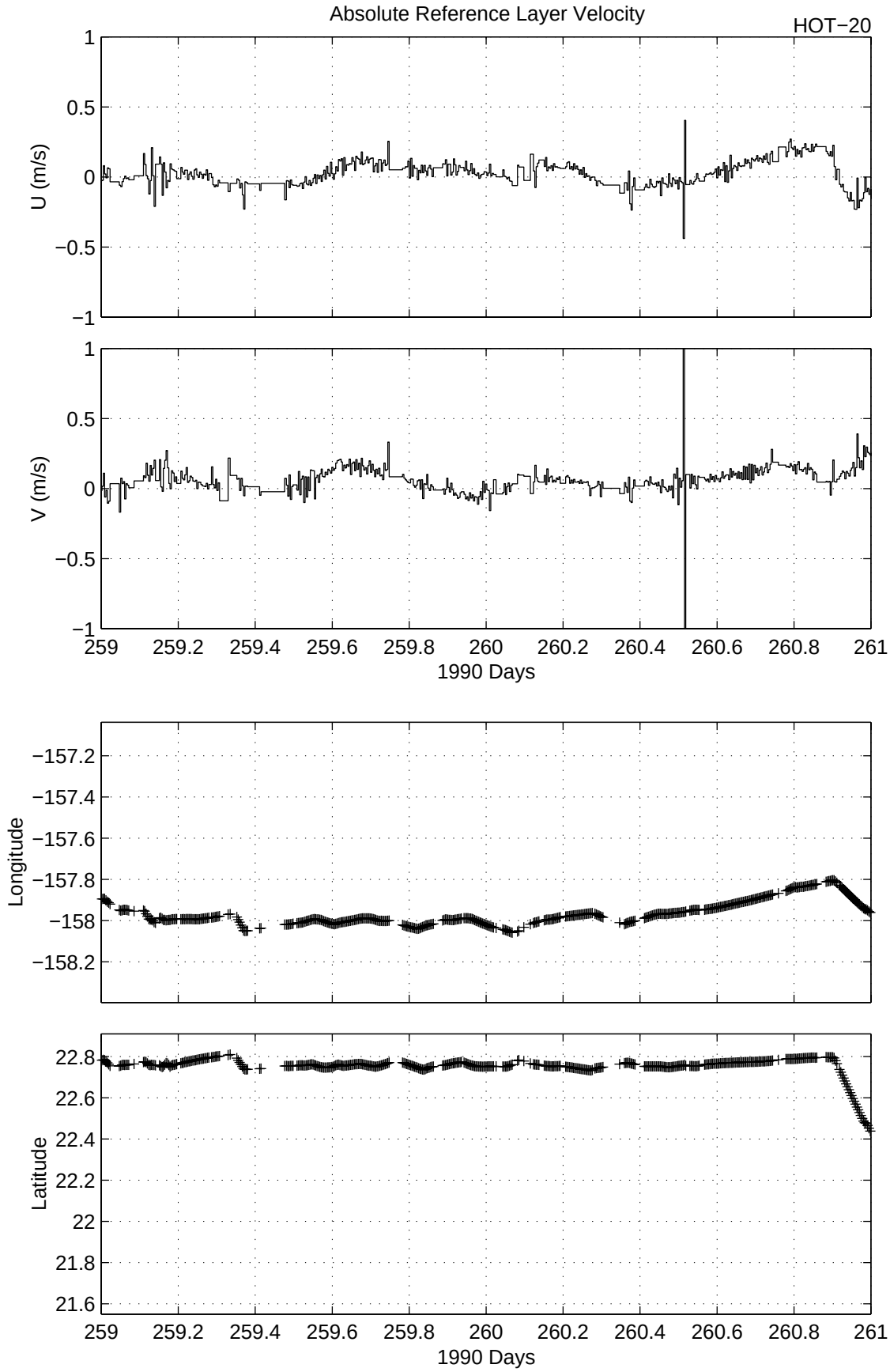
Absolute Reference Layer Velocity
HOT−20
U (m/s)
V (m/s)
1
0.5
0
−0.5
−1
259
259.2
259.4
259.6
259.8
260
260.2
260.4
260.6
260.8
261
1990 Days
Longitude
−157.2
−157.4
−157.6
−157.8
−158
−158.2
Latitude
22.8
22.6
22.4
22.2
22
21.8
21.6

Figure 6.4.4c

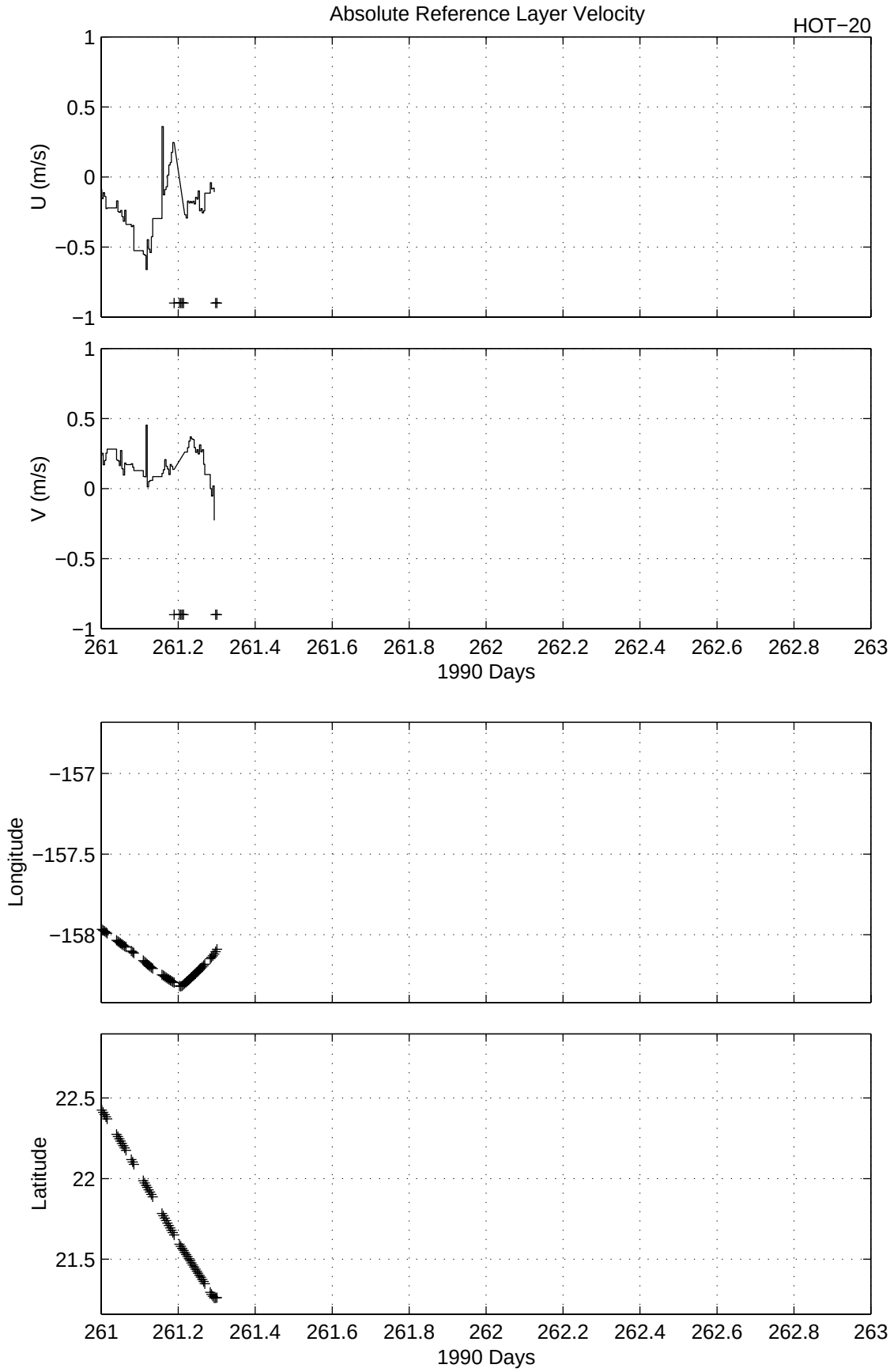
Absolute Reference Layer Velocity
HOT−20
U (m/s)
V (m/s)
1
0.5
0
−0.5
−1
261
261.2
261.4
261.6
261.8
262
262.2
262.4
262.6
262.8
263
1990 Days
Longitude
−157
−157.5
−158
Latitude
22.5
22
21.5

Figure 6.4.4d

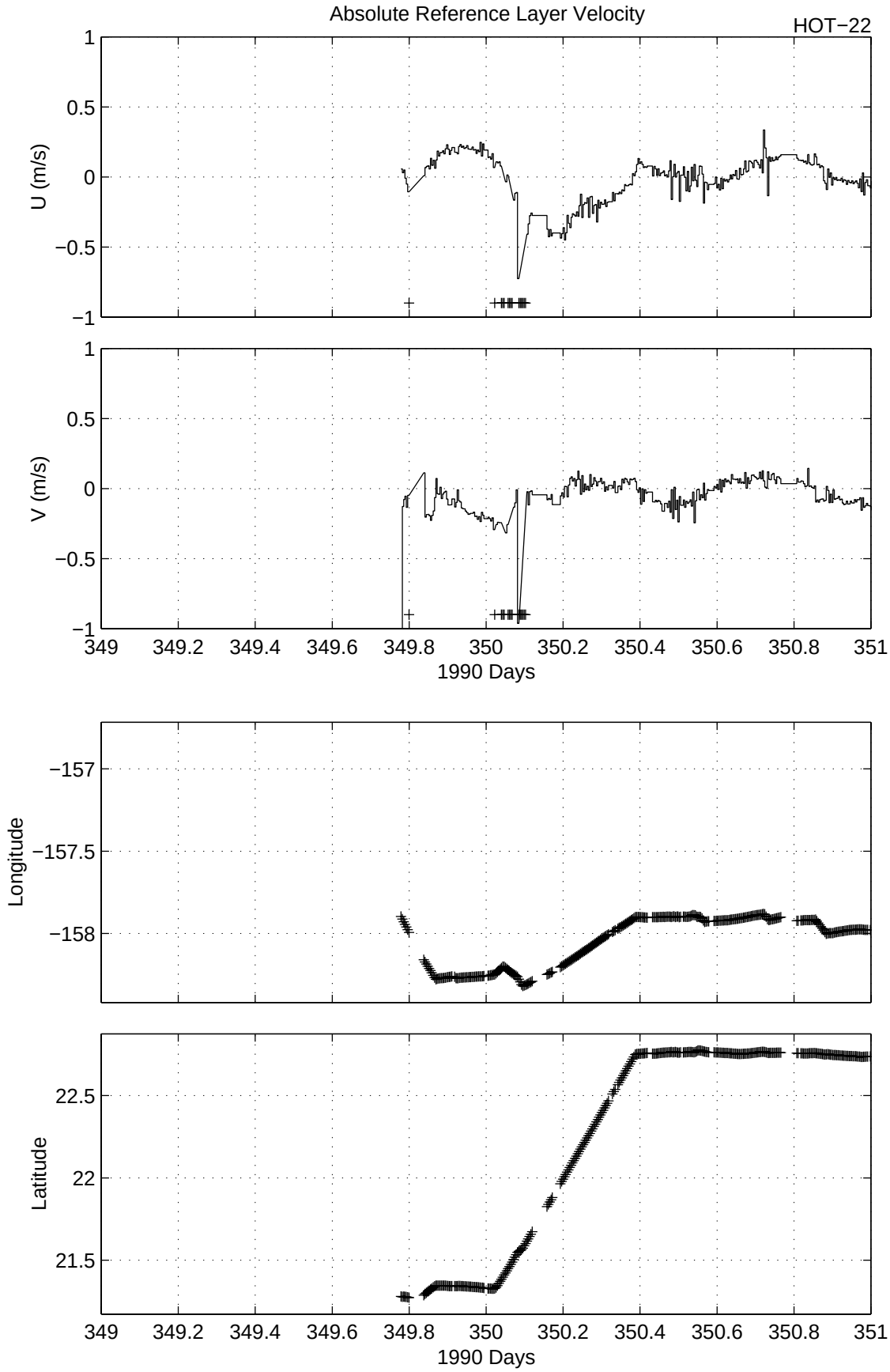
Absolute Reference Layer Velocity
HOT−22
U (m/s)
V (m/s)
1
0.5
0
−0.5
−1
349
349.2
349.4
349.6
349.8
350
350.2
350.4
350.6
350.8
351
1990 Days
Longitude
−157
−157.5
−158
Latitude
22.5
22
21.5

Figure 6.4.5a

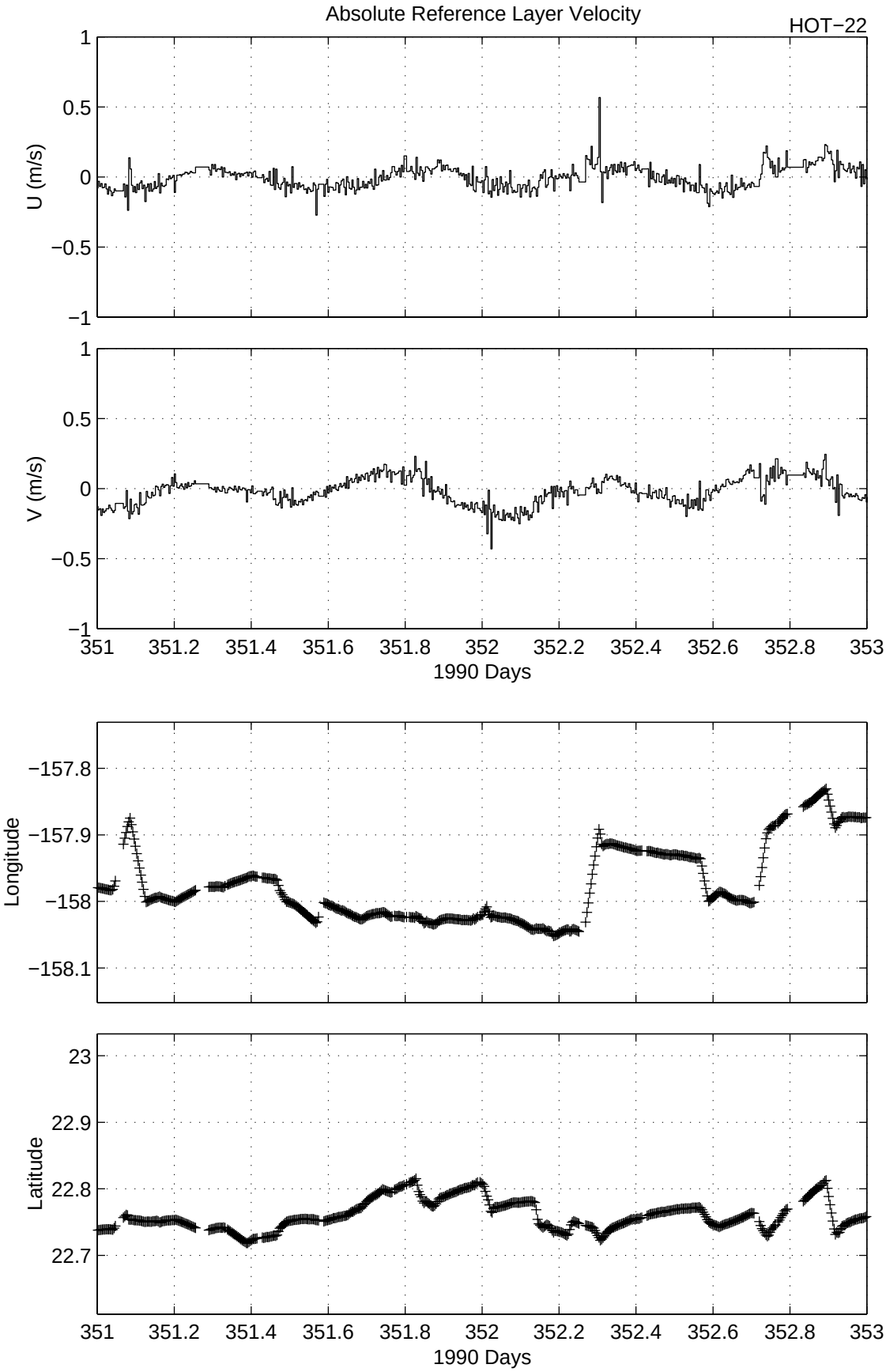
Absolute Reference Layer Velocity
HOT−22
U (m/s)
V (m/s)
1
0.5
0
−0.5
−1
351
351.2
351.4
351.6
351.8
352
352.2
352.4
352.6
352.8
353
1990 Days
Longitude
−157.8
−157.9
−158
−158.1
Latitude
23
22.9
22.8
22.7

Figure 6.4.5b

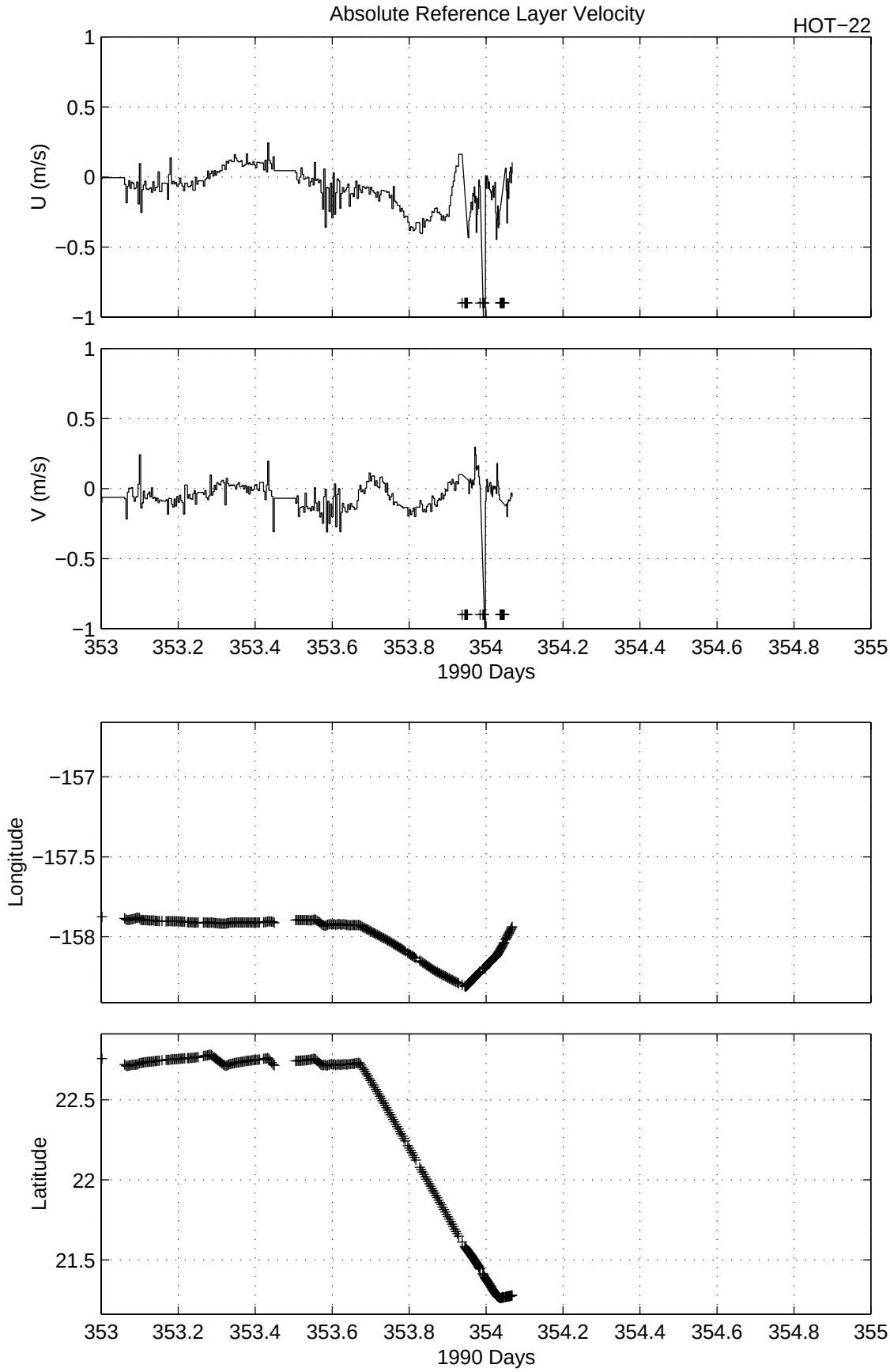
Absolute Reference Layer Velocity
HOT−22
U (m/s)
V (m/s)
1
0.5
0
−0.5
−1
353
353.2
353.4
353.6
353.8
354
354.2
354.4
354.6
354.8
355
1990 Days
Longitude
−157
−157.5
−158
Latitude
22.5
22
21.5

Figure 6.4.5c

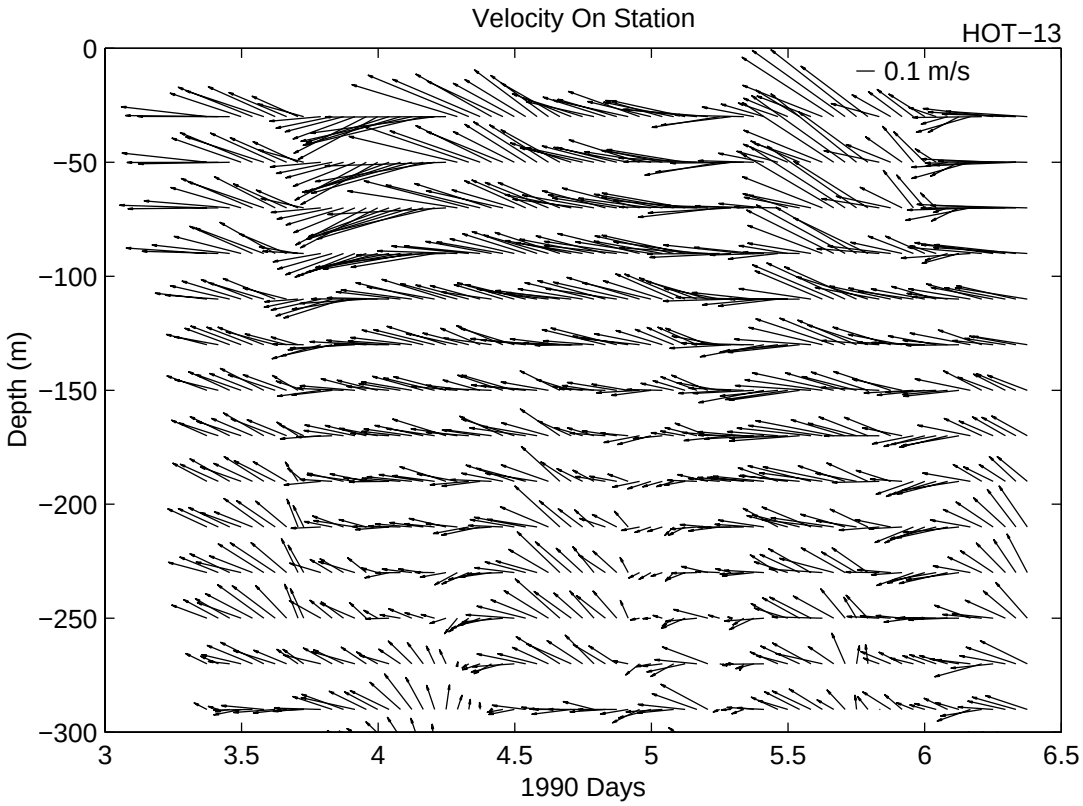
Velocity On Station
HOT−13
— 0.1 m/s
Depth (m)
0
−50
−100
−150
−200
−250
−300
3
3.5
4
4.5
5
5.5
6
6.5
1990 Days

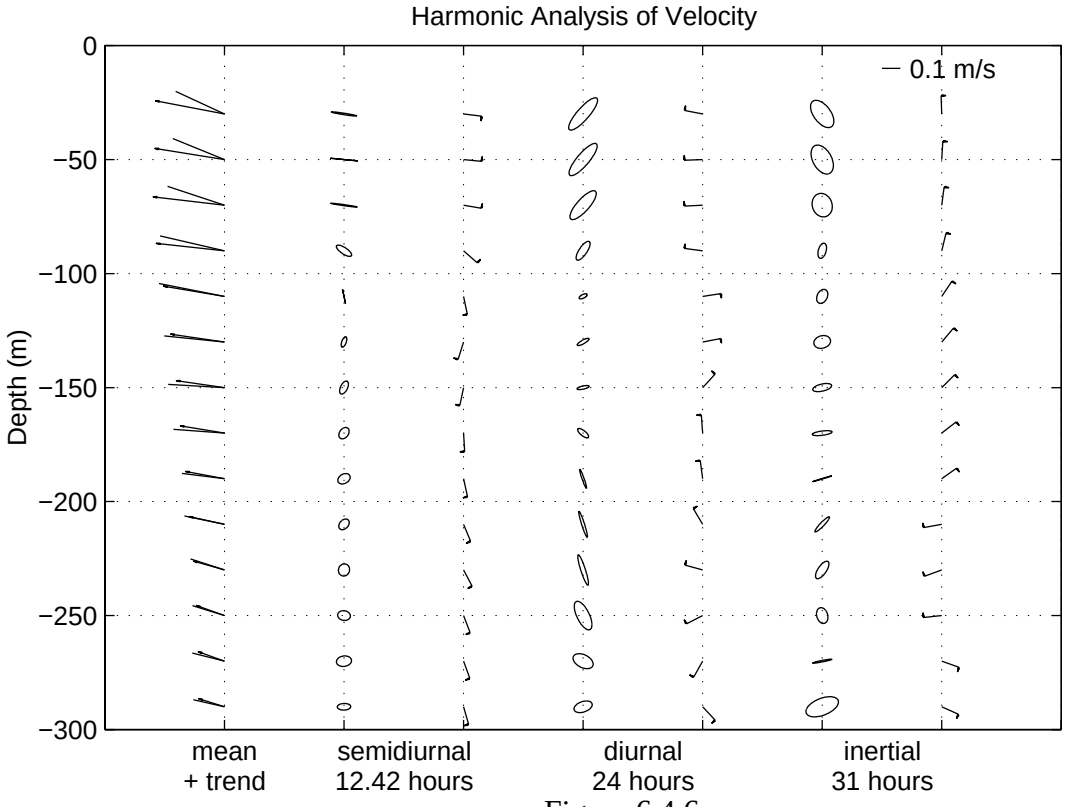
Harmonic Analysis of Velocity
— 0.1 m/s
Depth (m)
0
−50
−100
−150
−200
−250
−300
mean
+ trend
semidiurnal
12.42 hours
diurnal
24 hours
inertial
31 hours

Figure 6.4.6a

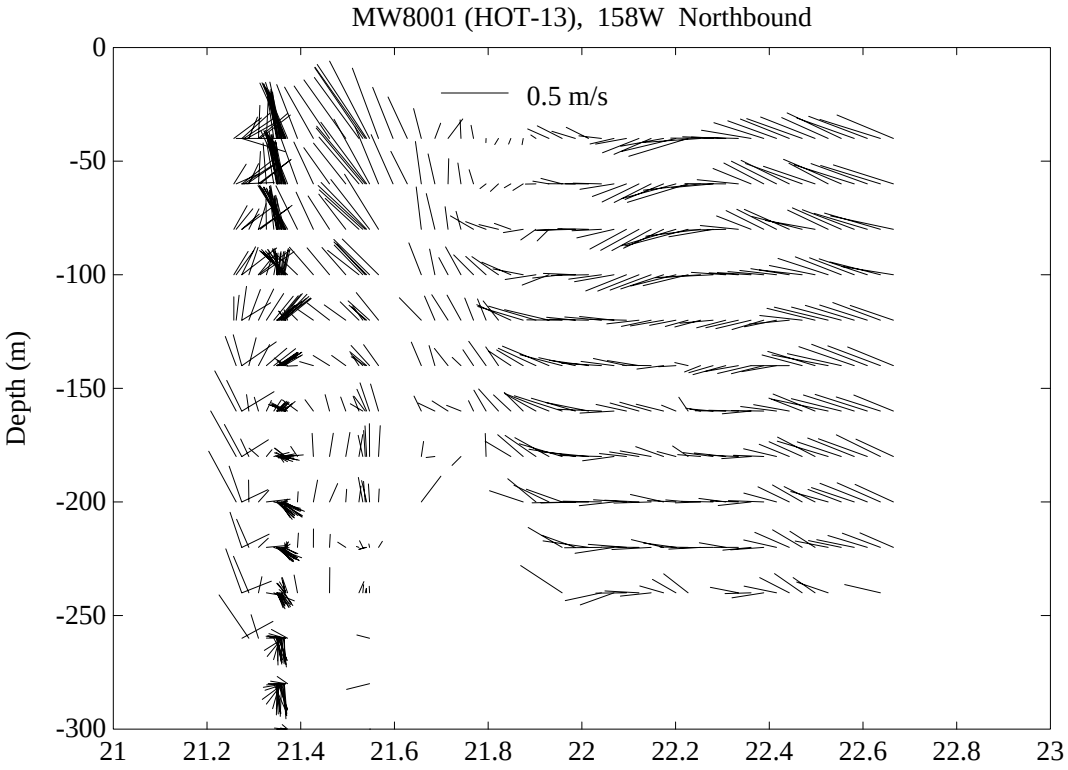
MW8001 (HOT-13), 158W Northbound
0.5 m/s
0
-50
-100
-150
-200
-250
-300
Depth (m)
21
21.2
21.4
21.6
21.8
22
22.2
22.4
22.6
22.8
23
Latitude
90- 6-19 14:34

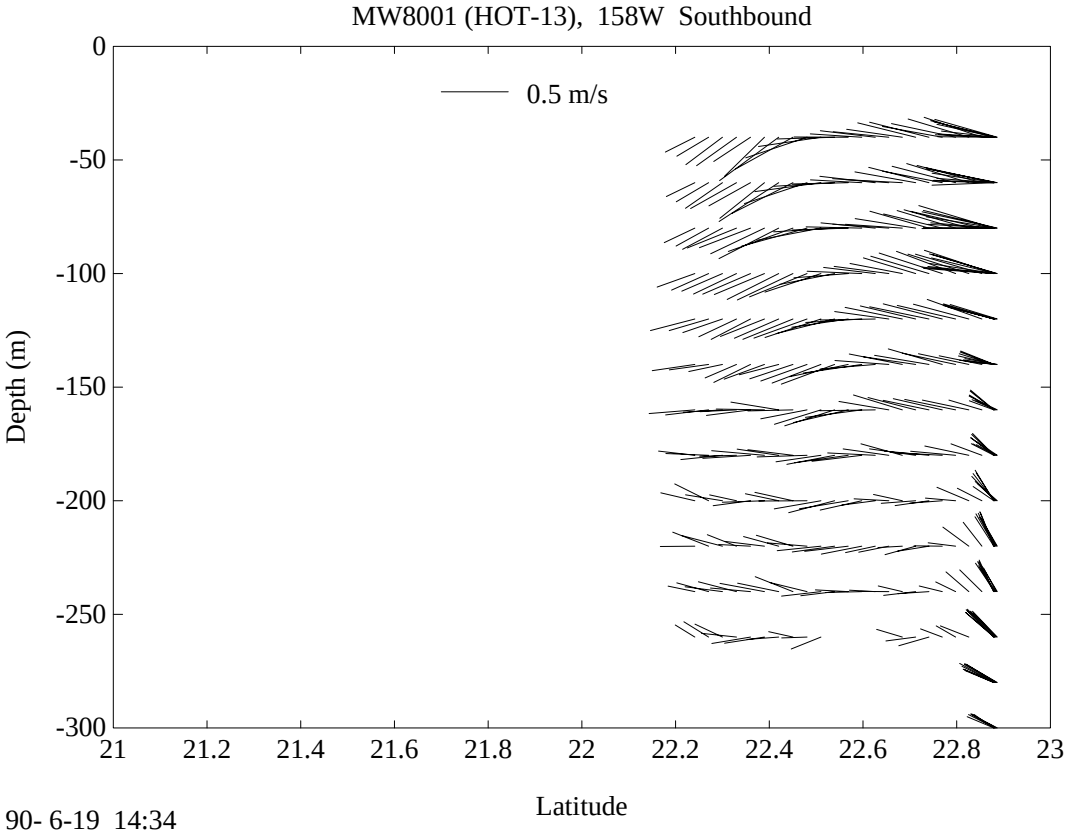
MW8001 (HOT-13), 158W Southbound
0.5 m/s
0
-50
-100
-150
-200
-250
-300
Depth (m)
21
21.2
21.4
21.6
21.8
22
22.2
22.4
22.6
22.8
23
Latitude
90- 6-19 14:34

Figure 6.4.6b

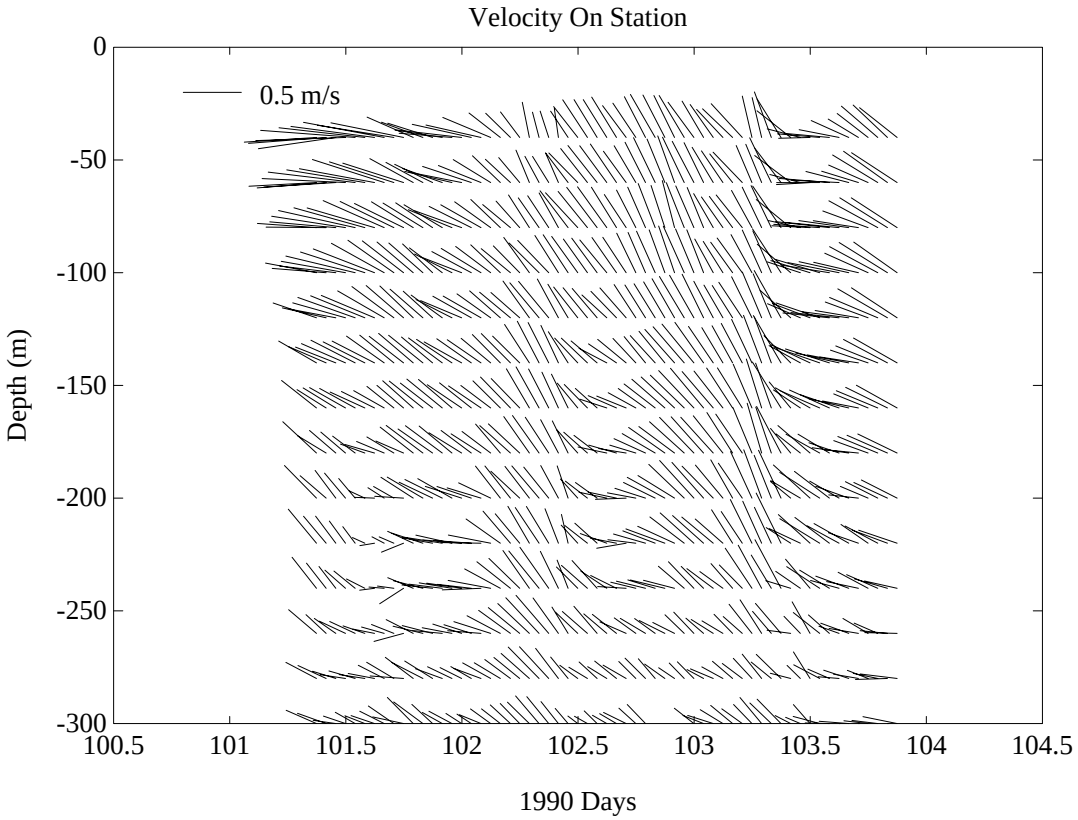
Velocity On Station
0.5 m/s
Depth (m)
0
-50
-100
-150
-200
-250
-300
100.5
101
101.5
102
102.5
103
103.5
104
104.5
1990 Days

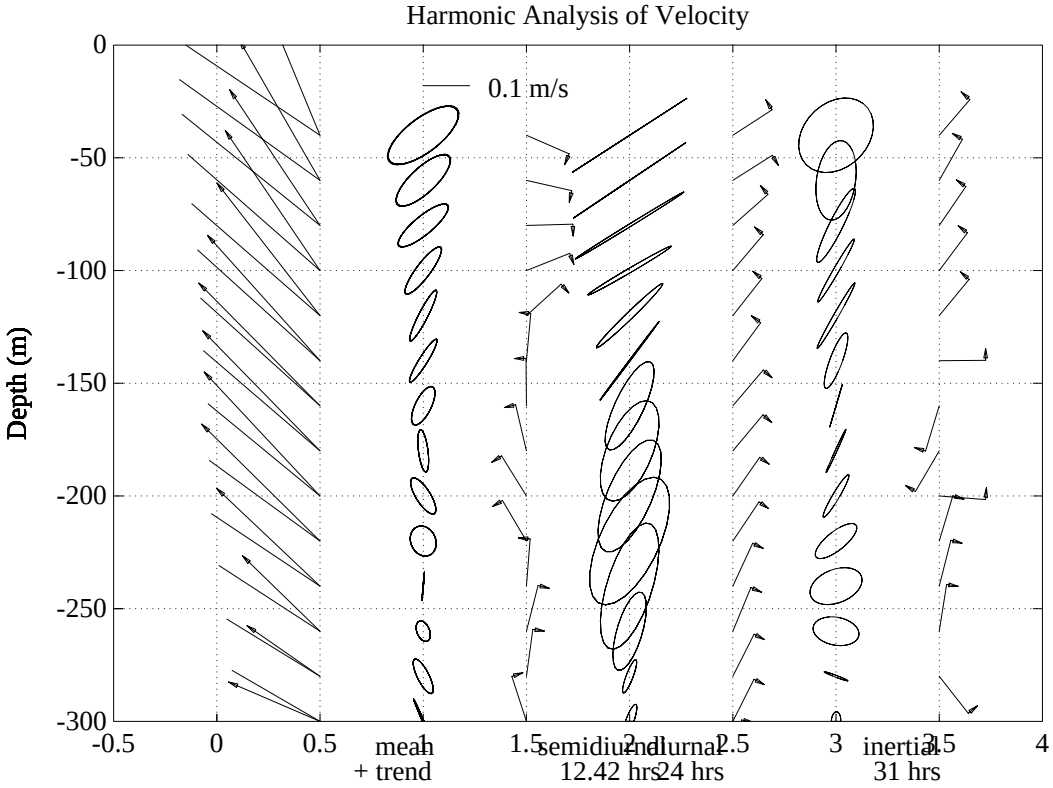
Harmonic Analysis of Velocity
0.1 m/s
Depth (m)
0
-50
-100
-150
-200
-250
-300
-0.5
0
0.5
1
1.5
2
2.5
3
3.5
4
mean
+ trend
semidiurnal
12.42 hrs
diurnal
24 hrs
inertial
31 hrs

Figure 6.4.7a

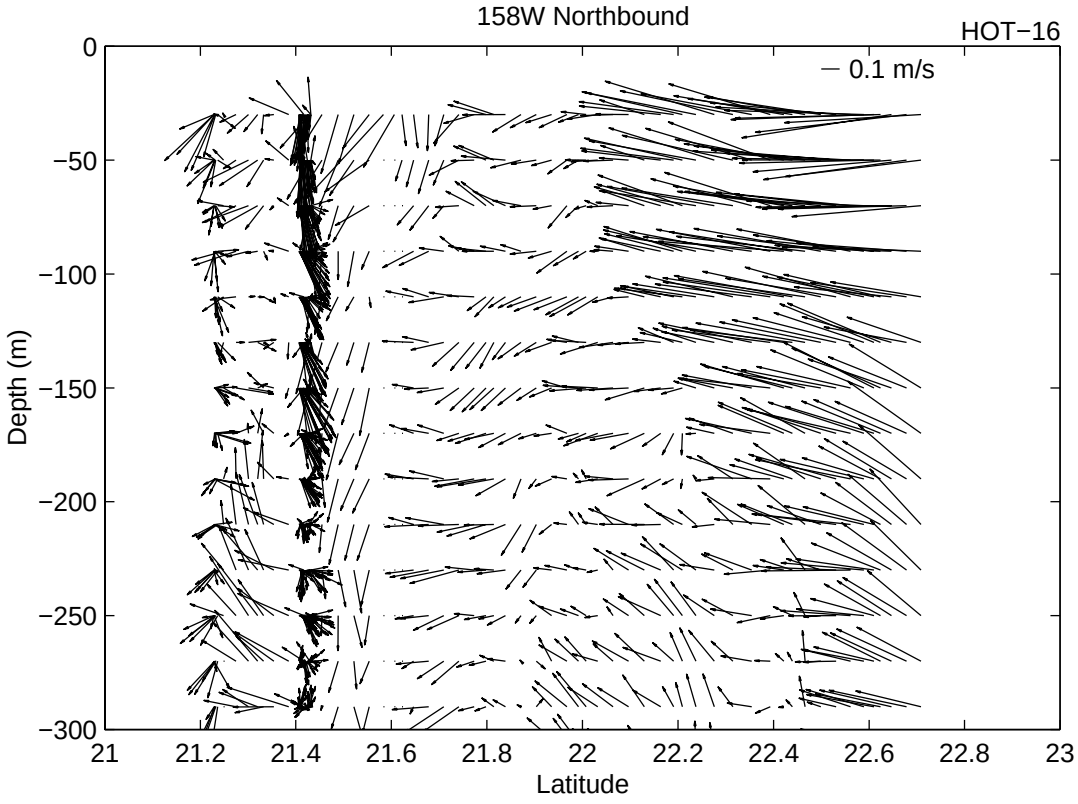
158W Northbound
HOT−16
0.1 m/s
0
−50
−100
−150
−200
−250
−300
Depth (m)
21
21.2
21.4
21.6
21.8
22
22.2
22.4
22.6
22.8
23
Latitude

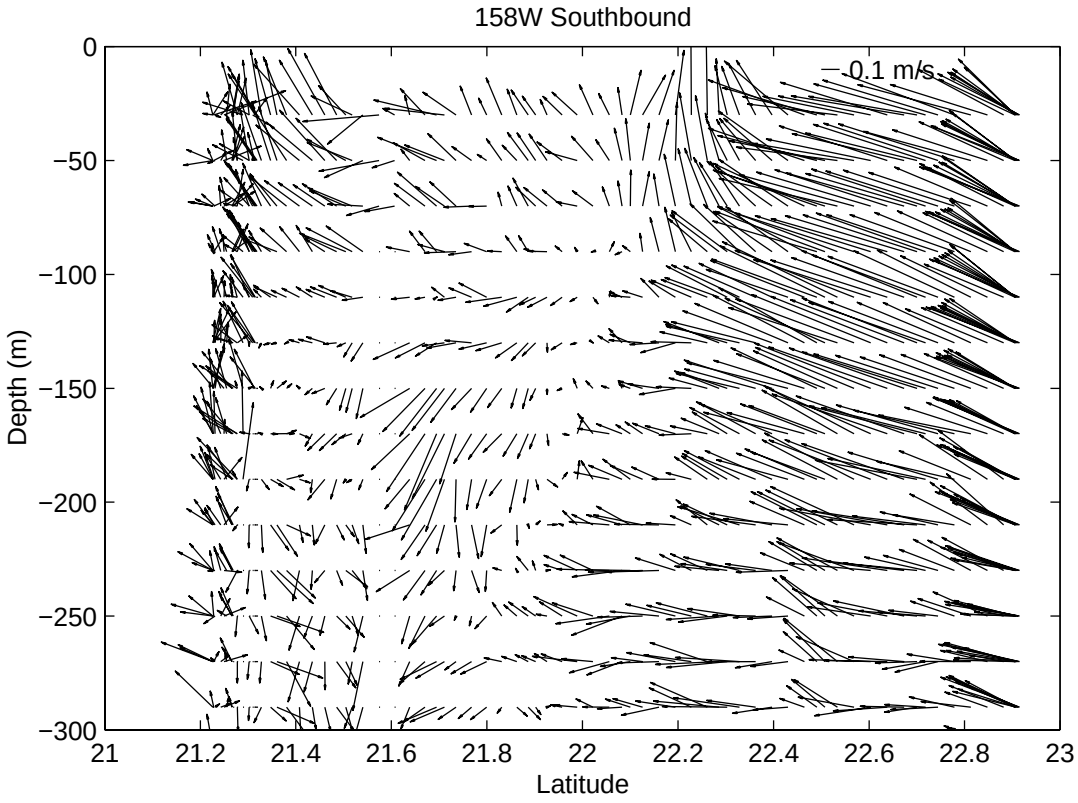
158W Southbound
0.1 m/s
0
−50
−100
−150
−200
−250
−300
Depth (m)
21
21.2
21.4
21.6
21.8
22
22.2
22.4
22.6
22.8
23
Latitude

Figure 6.4.7b

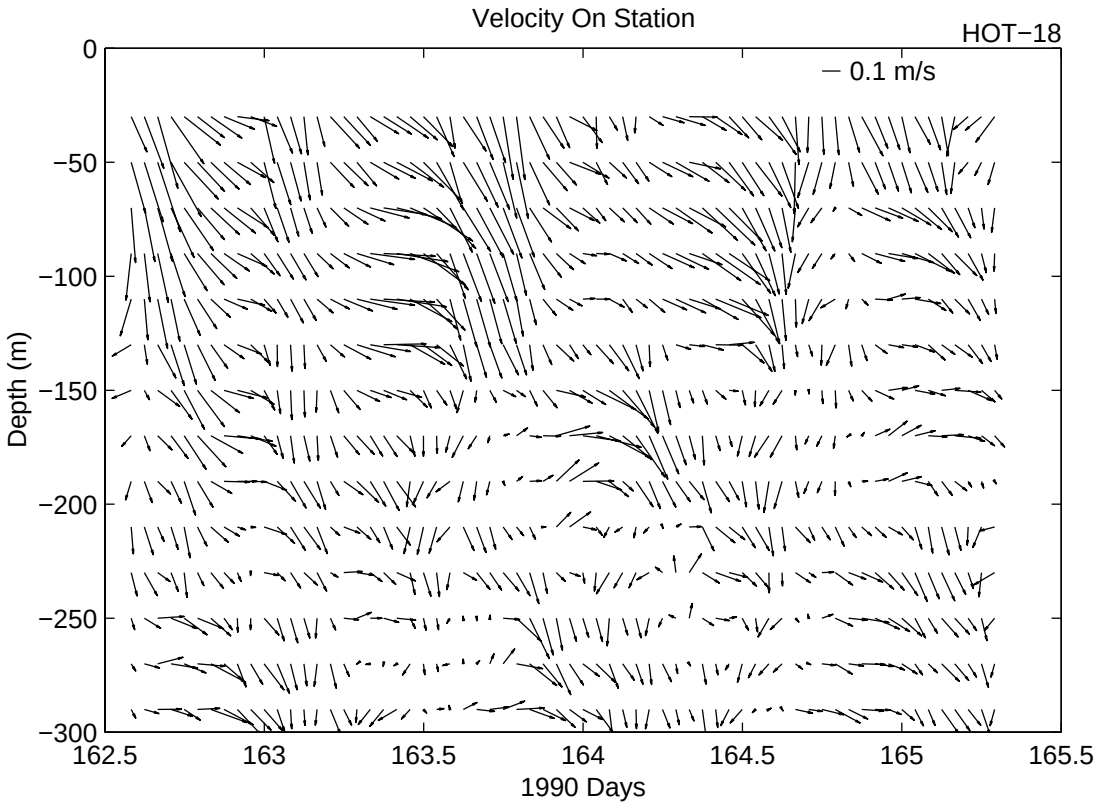
Velocity On Station
HOT−18
— 0.1 m/s
0
−50
−100
−150
−200
−250
−300
Depth (m)
162.5
163
163.5
164
164.5
165
165.5
1990 Days

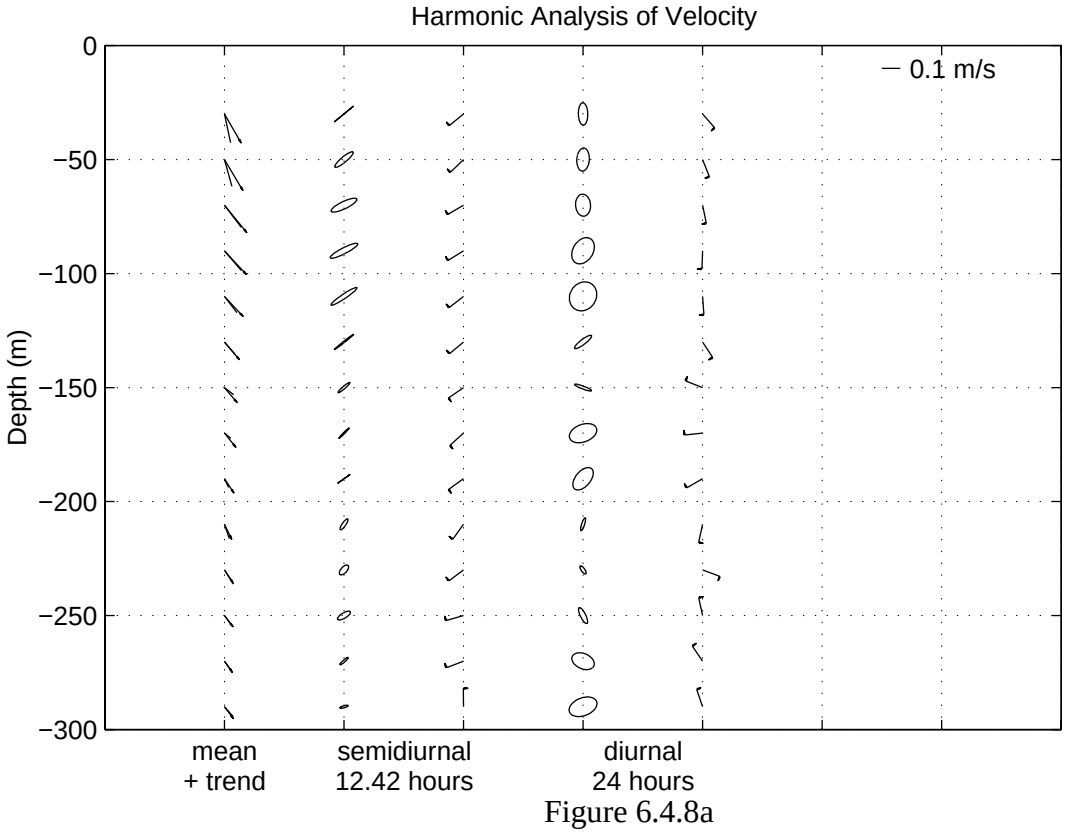
Harmonic Analysis of Velocity
— 0.1 m/s
0
−50
−100
−150
−200
−250
−300
Depth (m)
mean
+ trend
semidiurnal
12.42 hours
diurnal
24 hours

Figure 6.4.8a

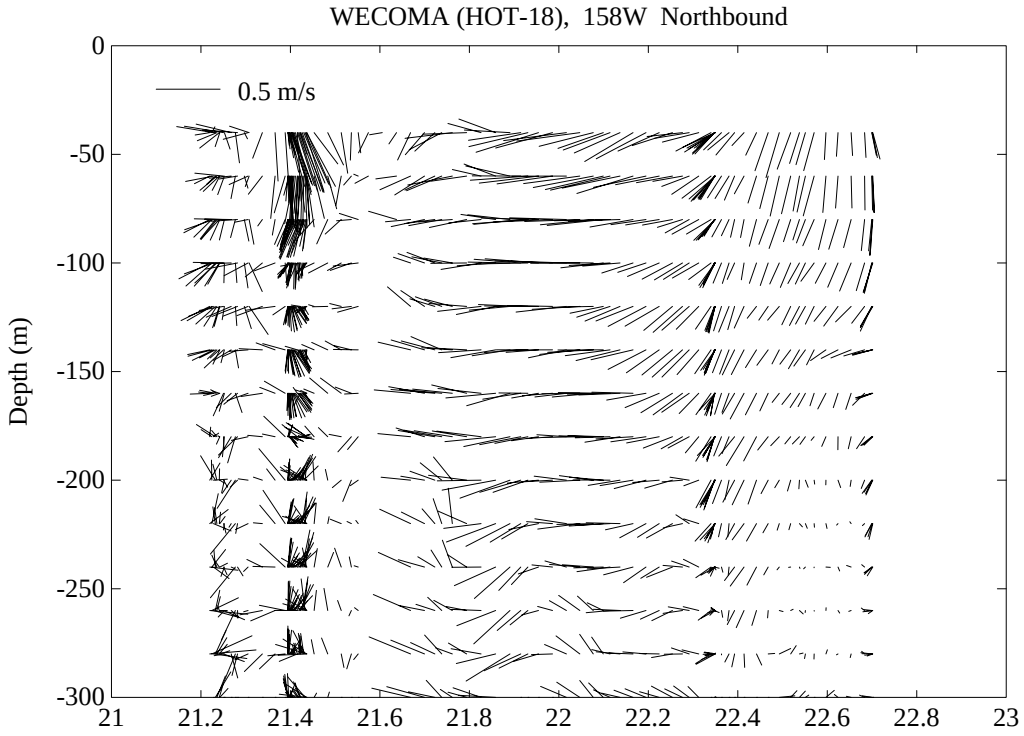
WECOMA (HOT-18), 158W Northbound
0.5 m/s
Depth (m)
0
-50
-100
-150
-200
-250
-300
21
21.2
21.4
21.6
21.8
22
22.2
22.4
22.6
22.8
23
Latitude
90-10- 3 16: 9

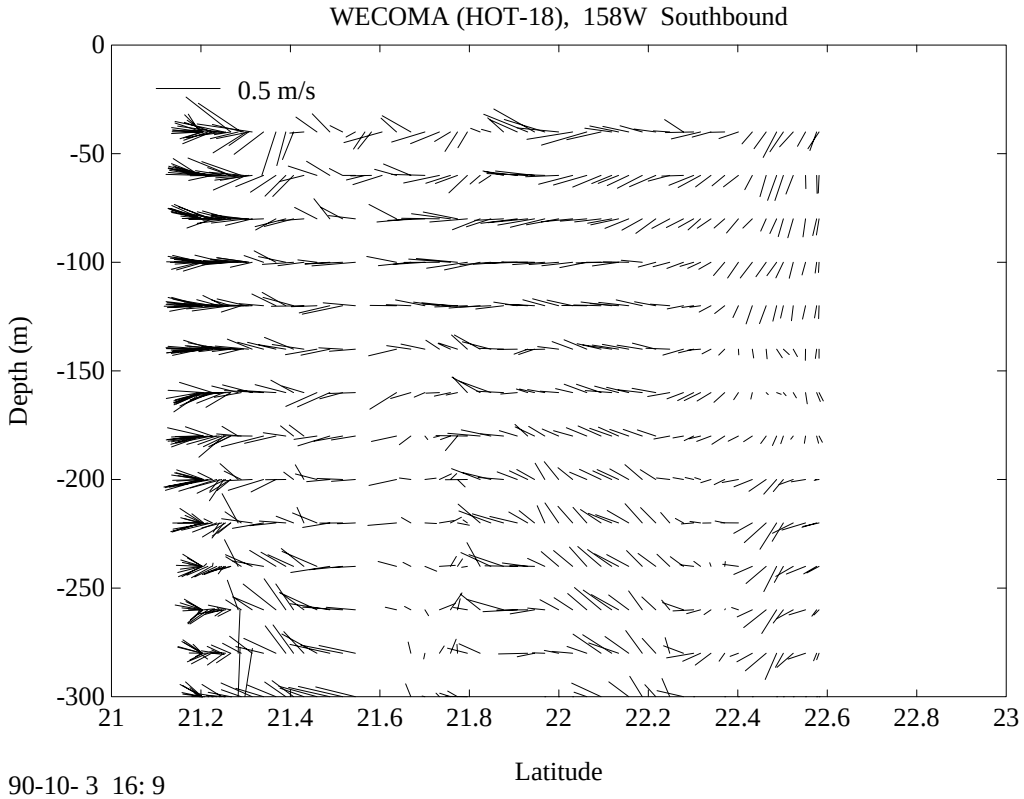
WECOMA (HOT-18), 158W Southbound
0.5 m/s
Depth (m)
0
-50
-100
-150
-200
-250
-300
21
21.2
21.4
21.6
21.8
22
22.2
22.4
22.6
22.8
23
Latitude
90-10- 3 16: 9

Figure 6.4.8b

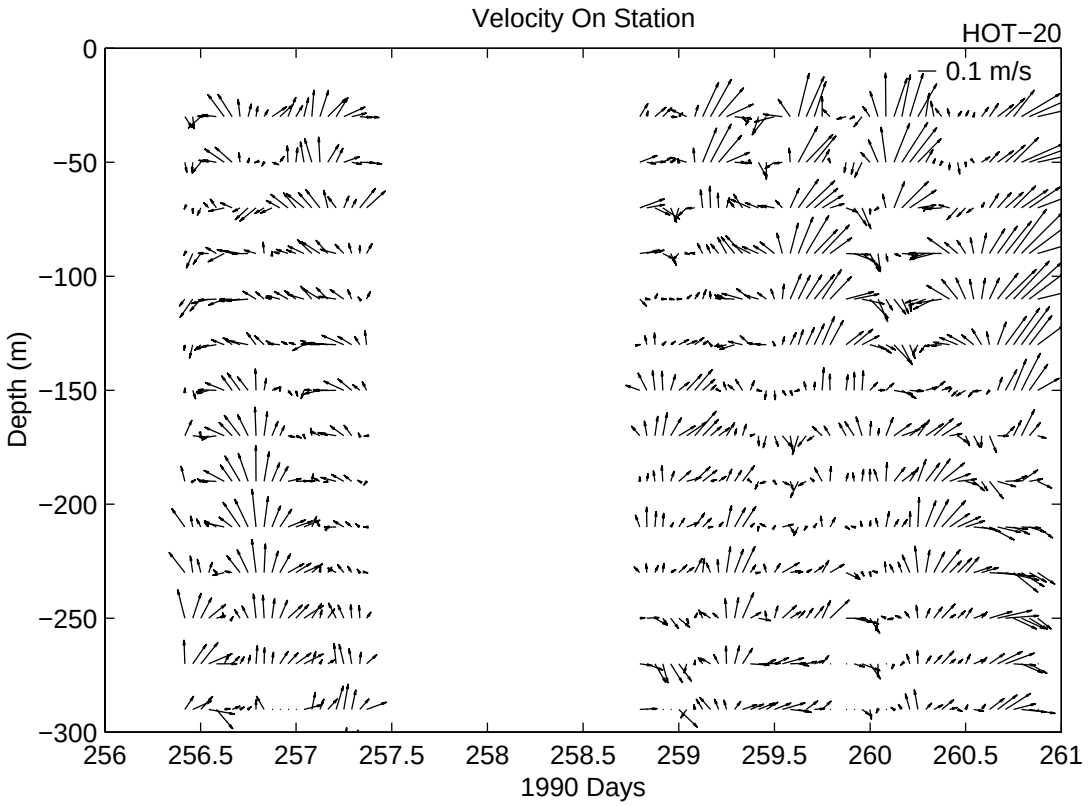
Velocity On Station
HOT−20
0.1 m/s
Depth (m)
0
−50
−100
−150
−200
−250
−300
256
256.5
257
257.5
258
258.5
259
259.5
260
260.5
261
1990 Days

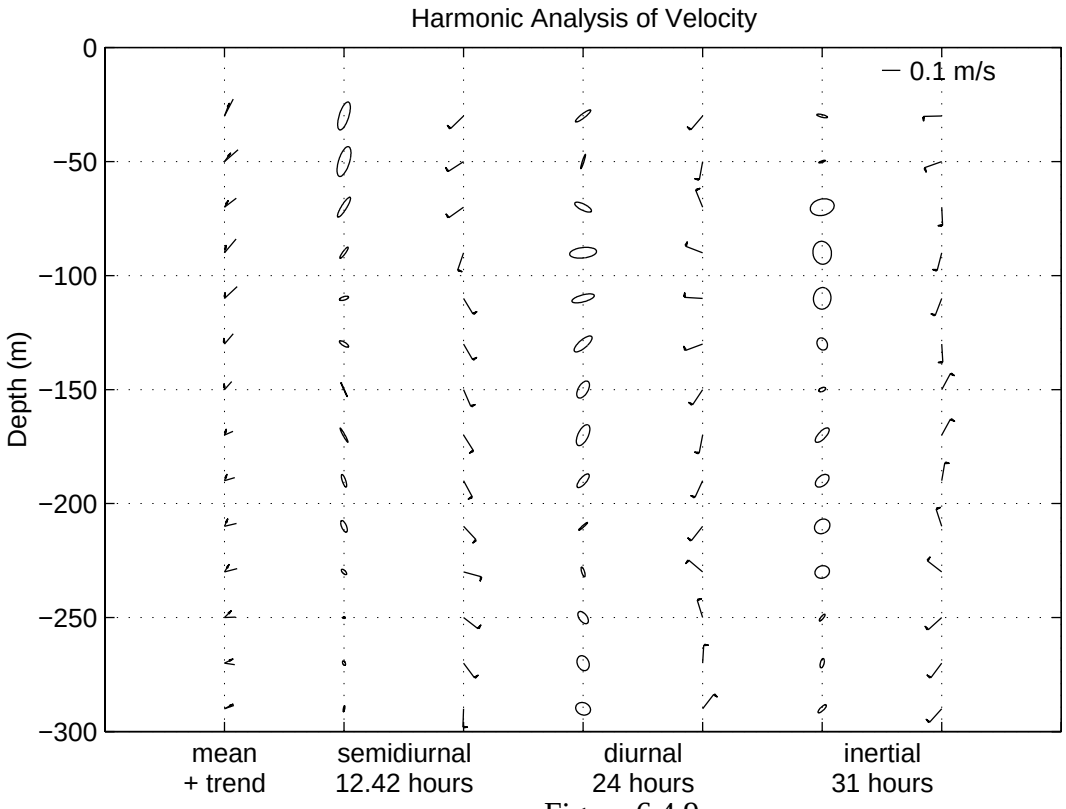
Harmonic Analysis of Velocity
0.1 m/s
Depth (m)
0
−50
−100
−150
−200
−250
−300
mean
+ trend
semidiurnal
12.42 hours
diurnal
24 hours
inertial
31 hours

Figure 6.4.9a

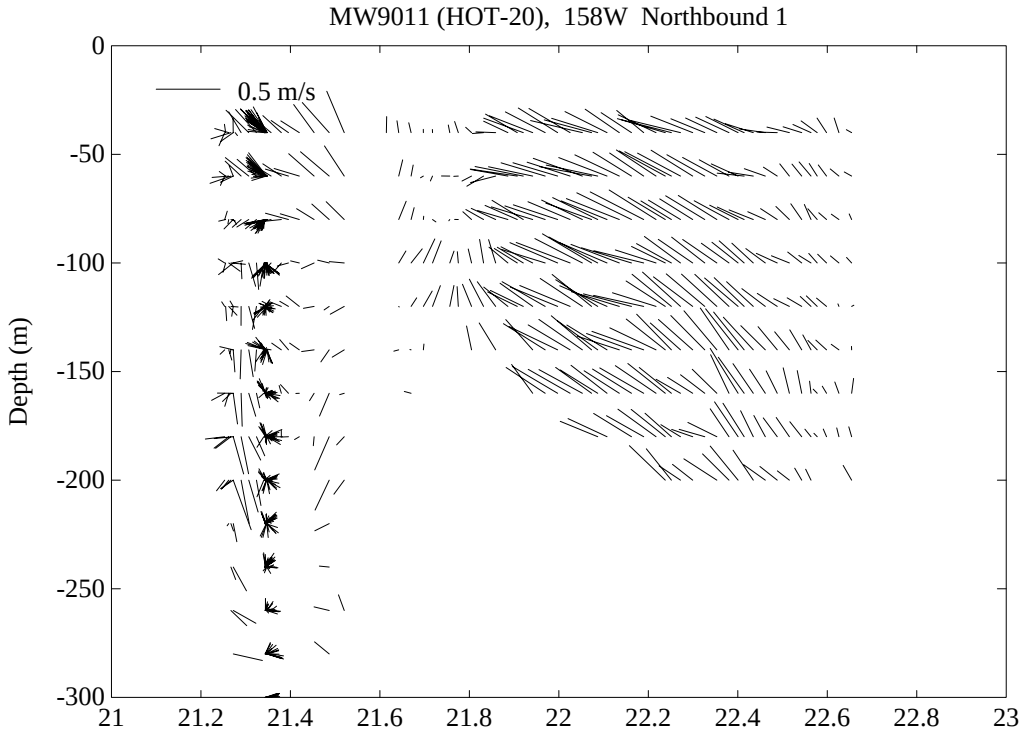
MW9011 (HOT-20), 158W Northbound 1
0.5 m/s
0
-50
-100
-150
-200
-250
-300
Depth (m)
21
21.2
21.4
21.6
21.8
22
22.2
22.4
22.6
22.8
23
Latitude
90-10-16 18:37

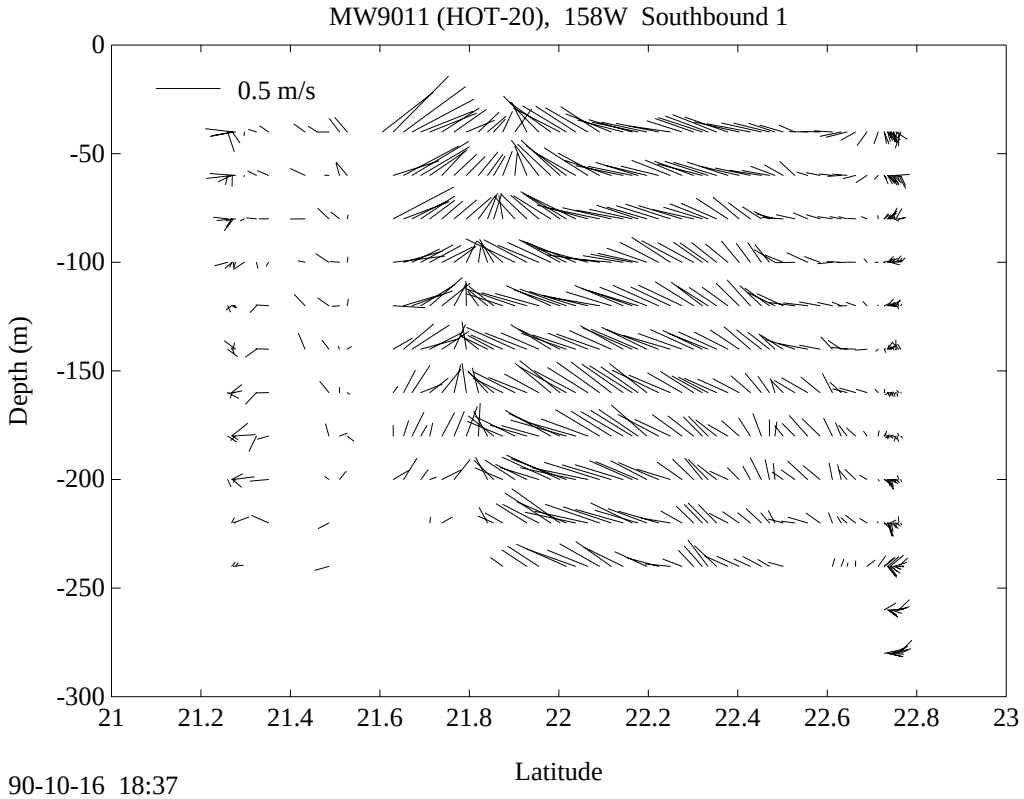
MW9011 (HOT-20), 158W Southbound 1
0.5 m/s
0
-50
-100
-150
-200
-250
-300
Depth (m)
21
21.2
21.4
21.6
21.8
22
22.2
22.4
22.6
22.8
23
Latitude
90-10-16 18:37

Figure 6.4.9b

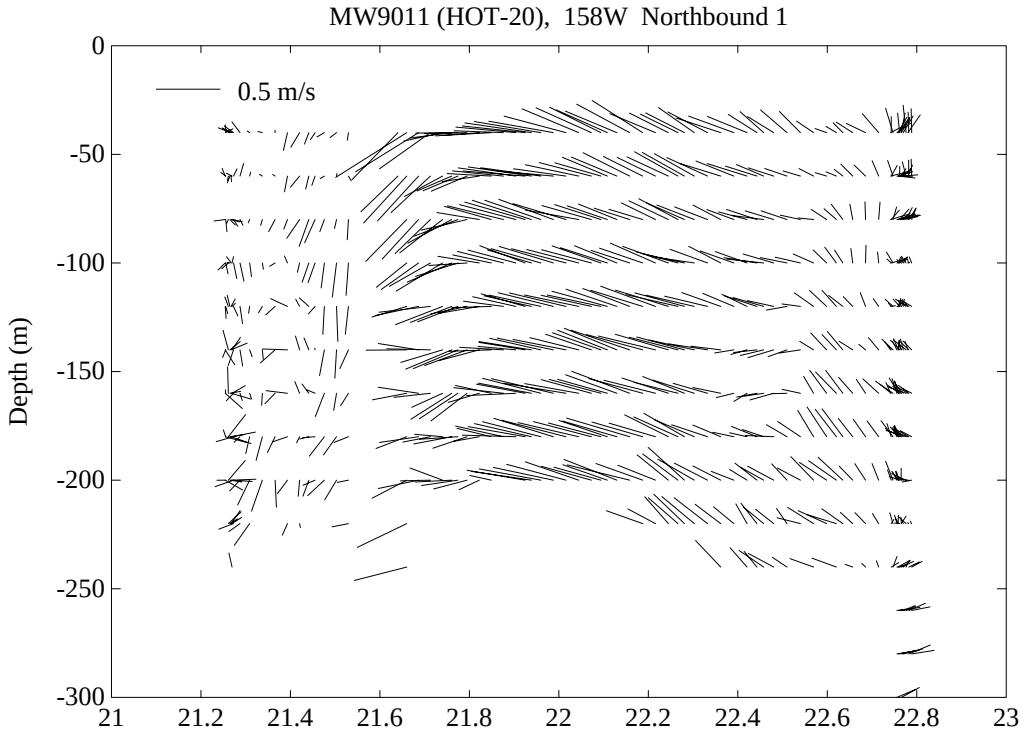
MW9011 (HOT-20), 158W Northbound 1
0.5 m/s
Depth (m)
0
-50
-100
-150
-200
-250
-300
21
21.2
21.4
21.6
21.8
22
22.2
22.4
22.6
22.8
23
Latitude
90-10-16 18:37

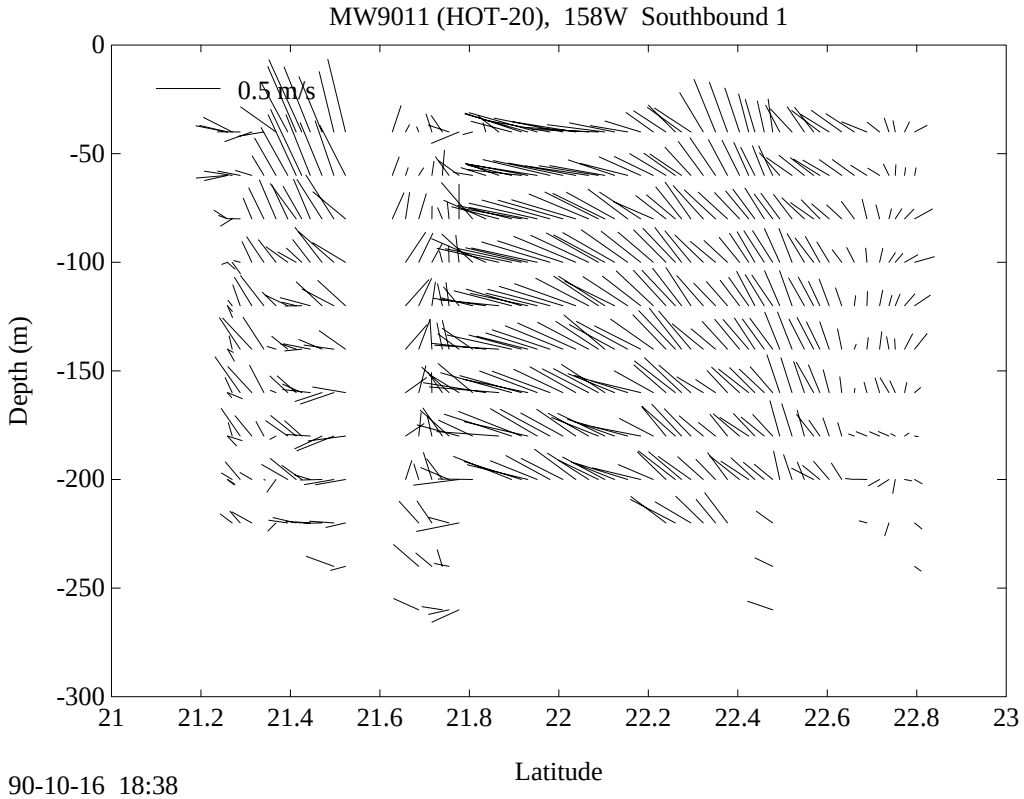
MW9011 (HOT-20), 158W Southbound 1
0.5 m/s
Depth (m)
0
-50
-100
-150
-200
-250
-300
21
21.2
21.4
21.6
21.8
22
22.2
22.4
22.6
22.8
23
Latitude
90-10-16 18:38

Figure 6.4.9c

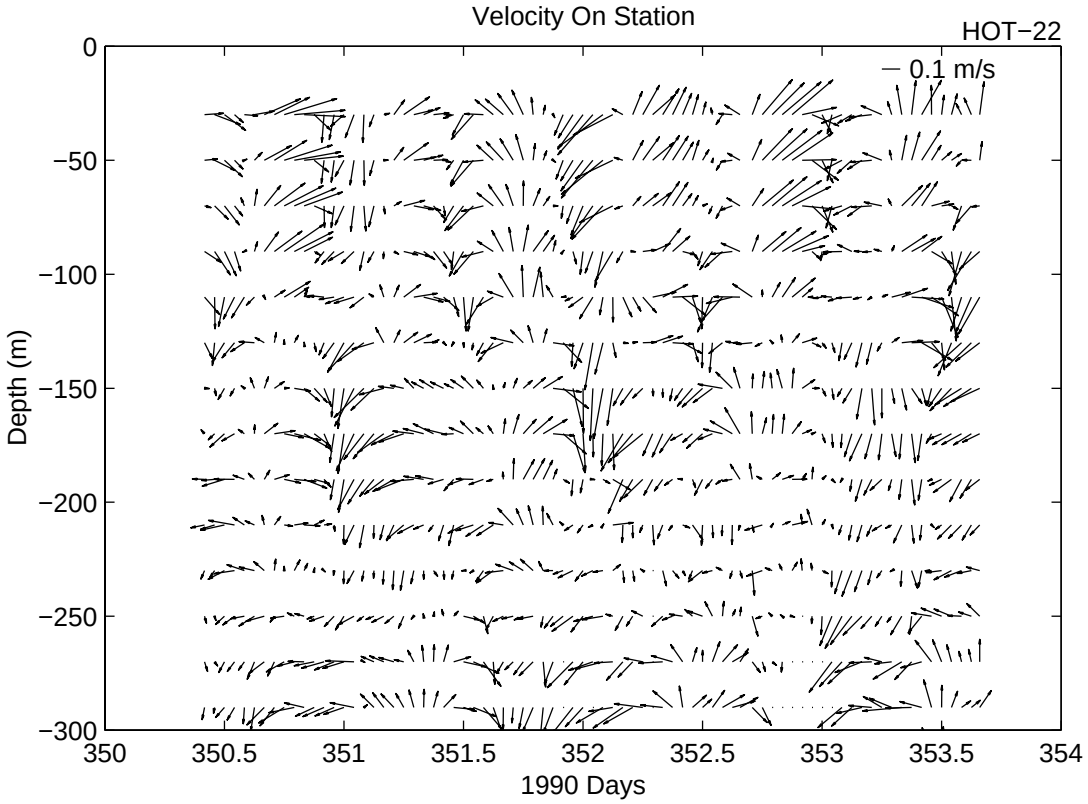

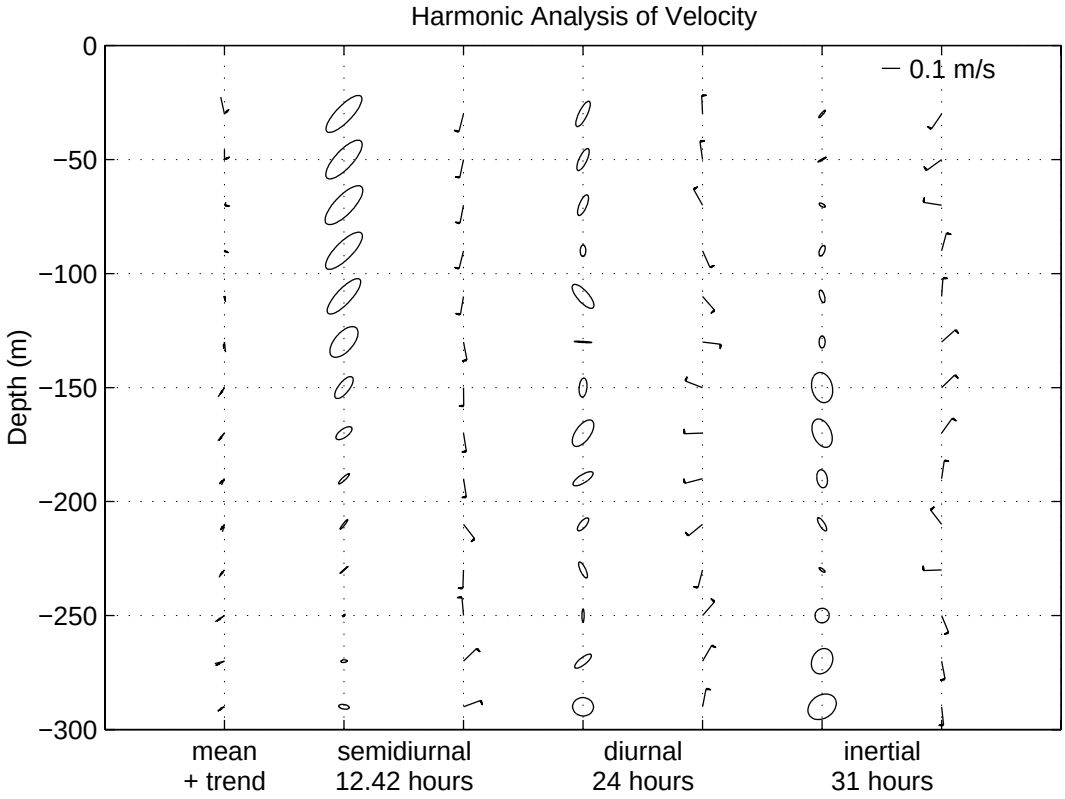

Figure 6.4.10a

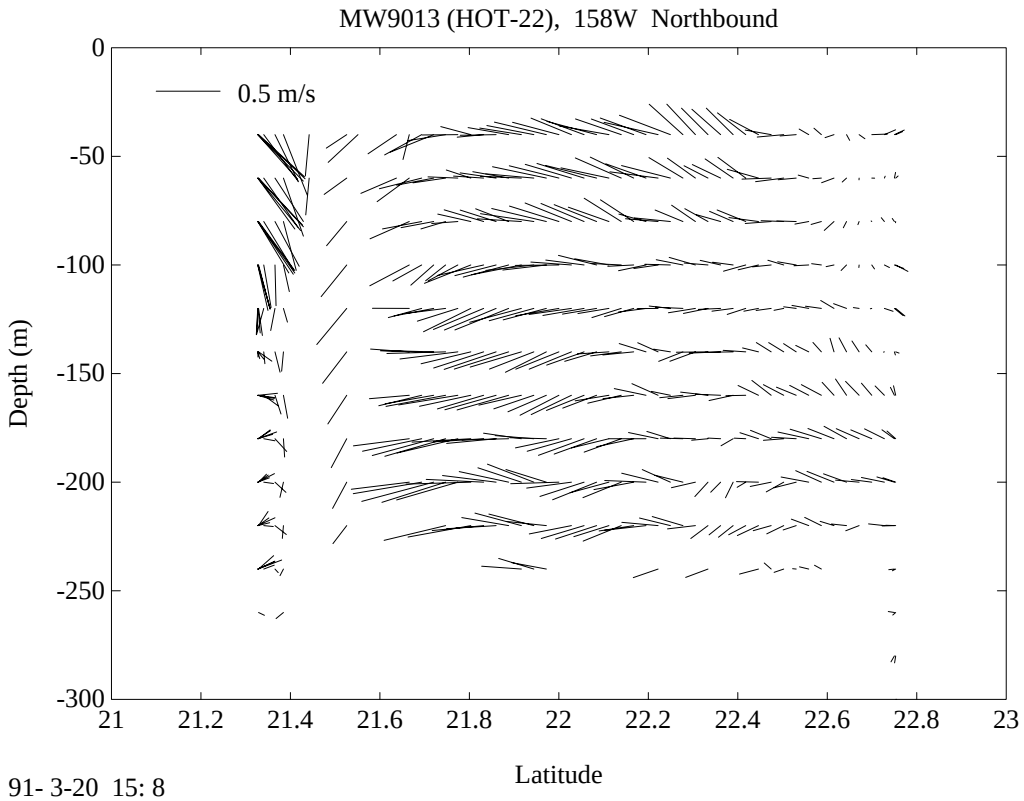

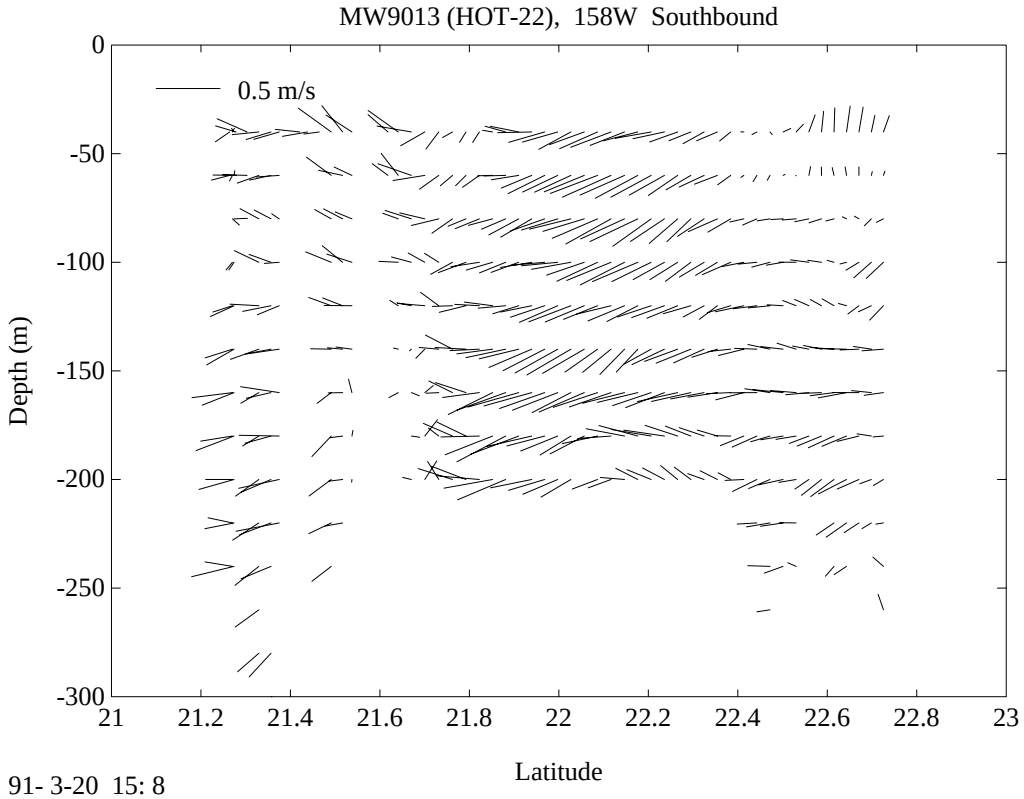

Figure 6.4.10b

6.5. Meteorology

Figure 6.5.1a: Upper panel: Atmospheric pressure measured while at Station ALOHA during 1990. Open circles represent individual measurements. Lower panel: Sea surface temperature measured while at Station ALOHA during 1990.

Figure 6.5.1b: Upper panel: Dry bulb temperature measured while on station during 1990. Lower panel: Wet bulb air temperature measure while as Station ALOHA during 1990.

Figure 6.5.1c: Upper panel: Dry air temperature measured at Station ALOHA during 1990. Dry-wet air temperature measured at Station ALOHA during 1990.

Figure 6.5.2: True winds measured at Station ALOHA on HOT-13.

Figure 6.5.3: True winds measured at Station ALOHA (upper panel) and collected by NDBC Buoy 51001 (as shown in Figure 1.1) for HOT-14.

Figure 6.5.4: As in Figure 6.5.2, except for HOT-15.

Figure 6.5.5: As in Figure 6.5.2, except for HOT-16.

Figure 6.5.6: As in Figure 6.5.2, except for HOT-17.

Figure 6.5.7: As in Figure 6.5.2, except for HOT-18.

Figure 6.5.8: As in Figure 6.5.2, except for HOT-19.

Figure 6.5.9: As in Figure 6.5.2, except for HOT-20.

Figure 6.5.10: As in Figure 6.5.2, except for HOT-22.

Figure 6.5.1a
HOT 23-32 Atmospheric Pressure

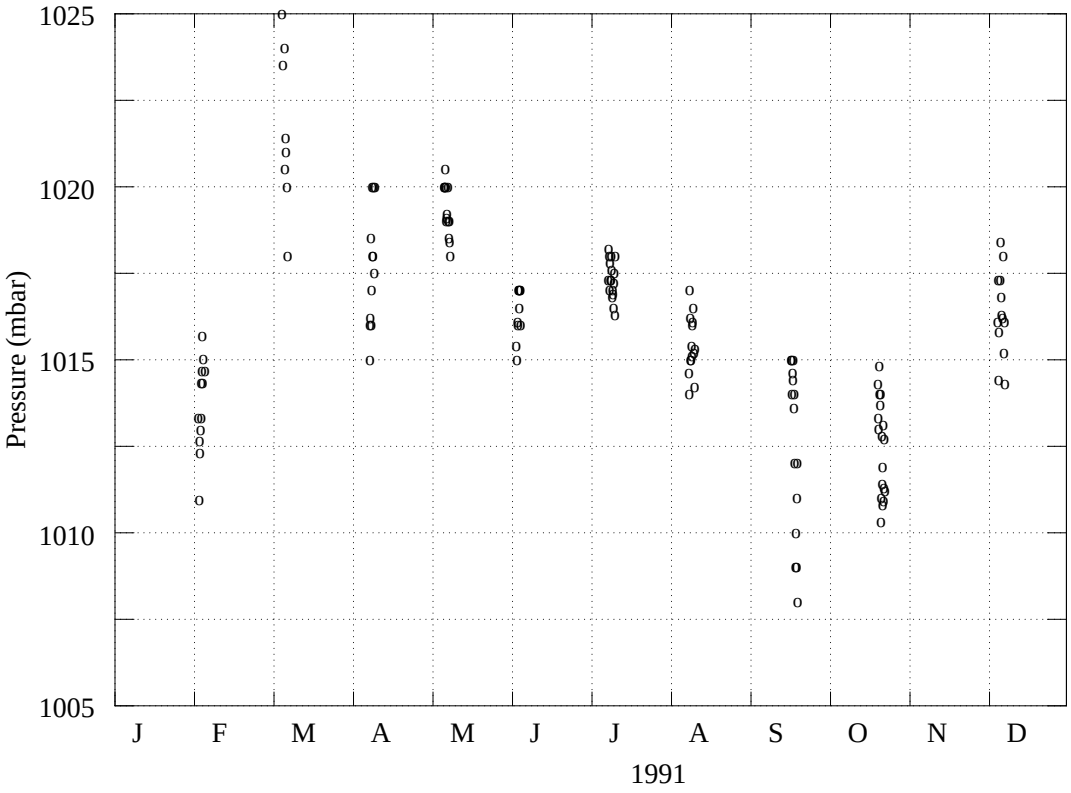

Sea Surface Temperature

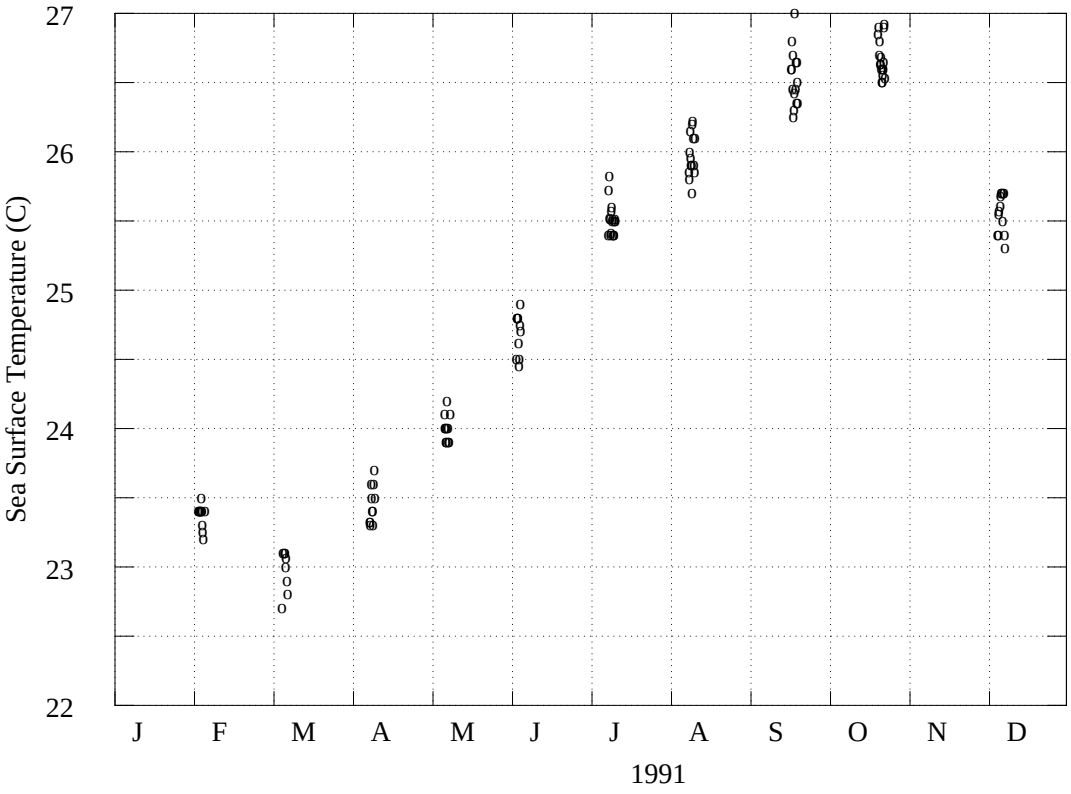

Figure 6.5.1b

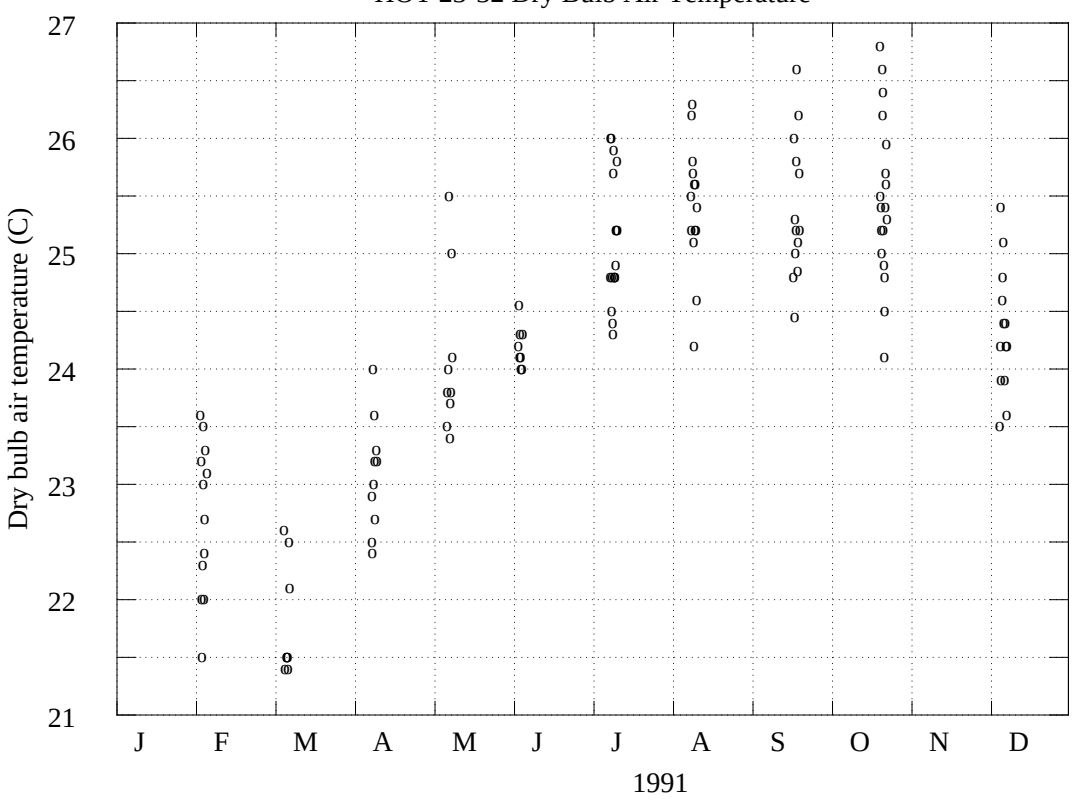
HOT 23-32 Dry Bulb Air Temperature
Dry bulb air temperature (C)
27
26
25
24
23
22
21
J
F
M
A
M
J
J
A
S
O
N
D
1991

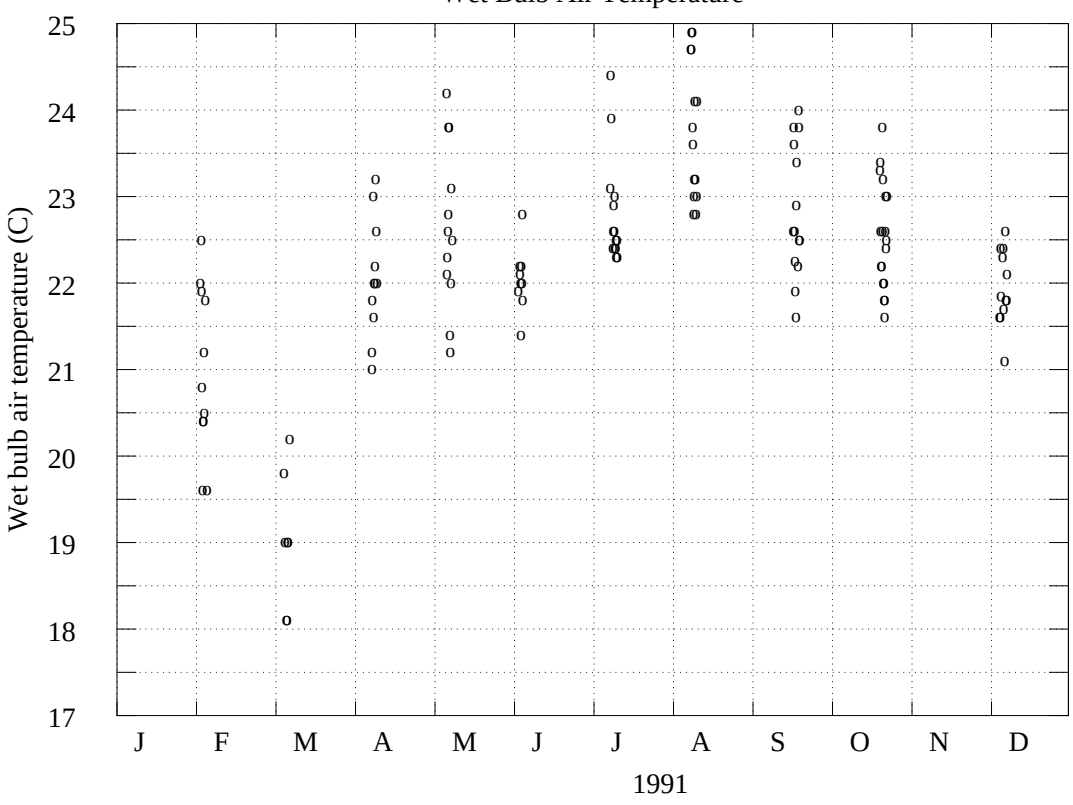
Wet Bulb Air Temperature
Wet bulb air temperature (C)
25
24
23
22
21
20
19
18
17
J
F
M
A
M
J
J
A
S
O
N
D
1991

Figure 6.5.1c

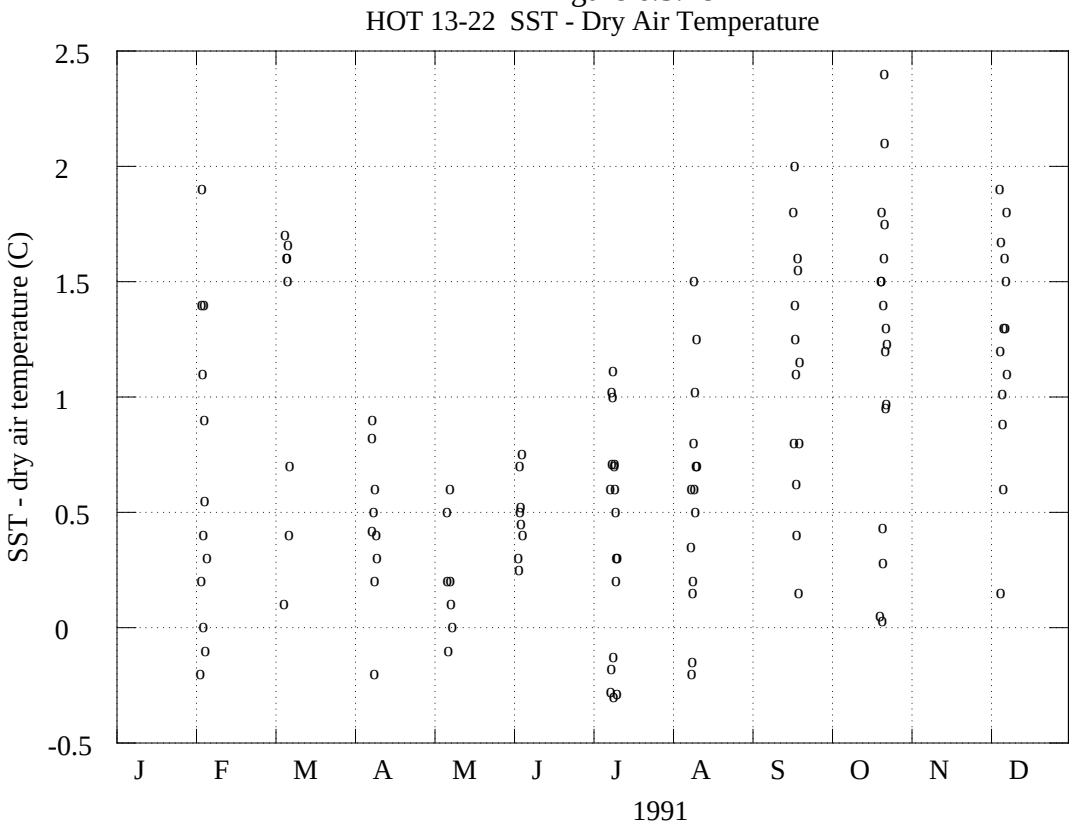
HOT 13-22 SST - Dry Air Temperature
SST - dry air temperature (C)
2.5
2
1.5
1
0.5
0
-0.5
J
F
M
A
M
J
J
A
S
O
N
D
1991

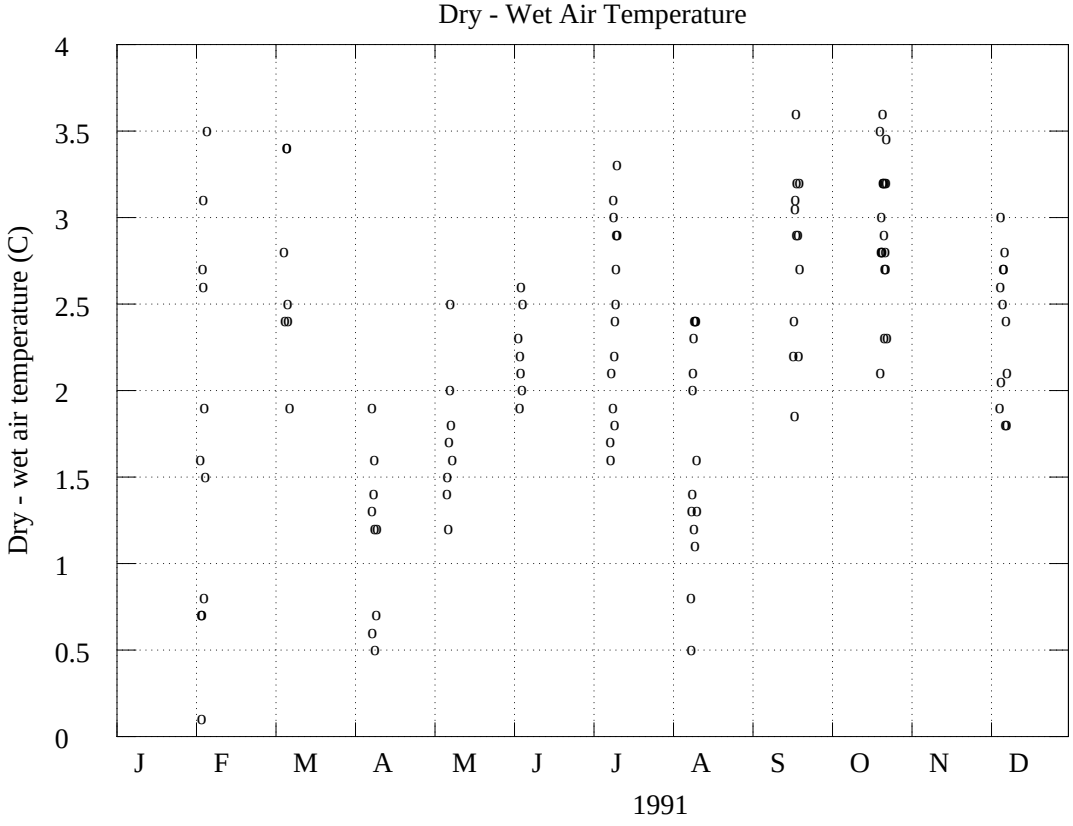
Dry - Wet Air Temperature
Dry - wet air temperature (C)
4
3.5
3
2.5
2
1.5
1
0.5
0
J
F
M
A
M
J
J
A
S
O
N
D
1991

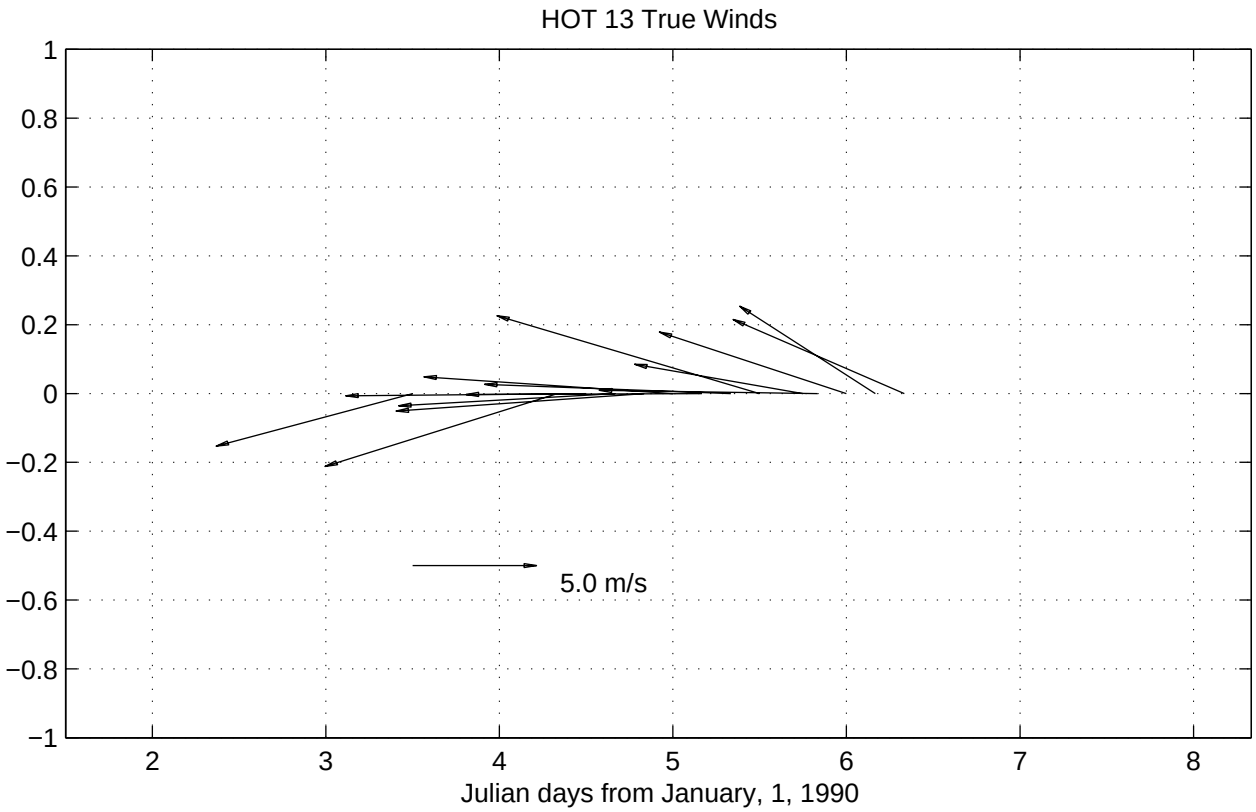
HOT 13 True Winds
1
0.8
0.6
0.4
0.2
0
−0.2
−0.4
−0.6
−0.8
−1
2
3
4
5
6
7
8
5.0 m/s
Julian days from January, 1, 1990

Figure 6.5.2

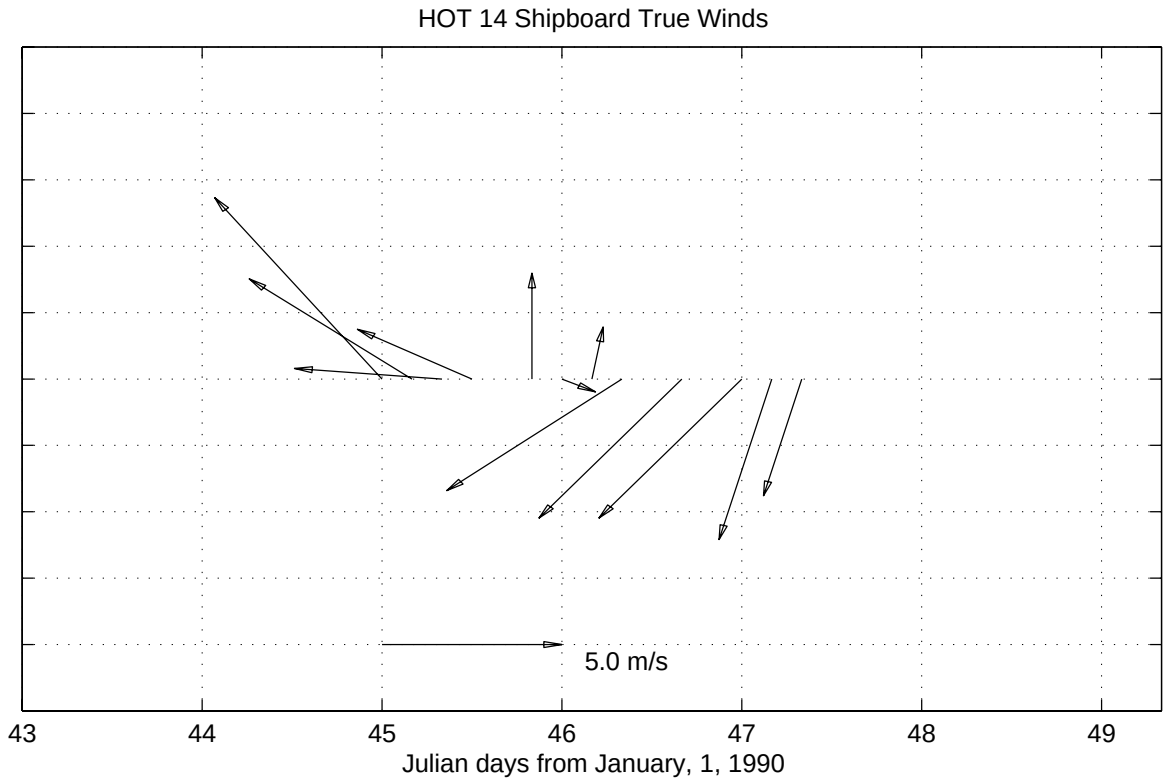
HOT 14 Shipboard True Winds
5.0 m/s
43
44
45
46
47
48
49
Julian days from January, 1, 1990

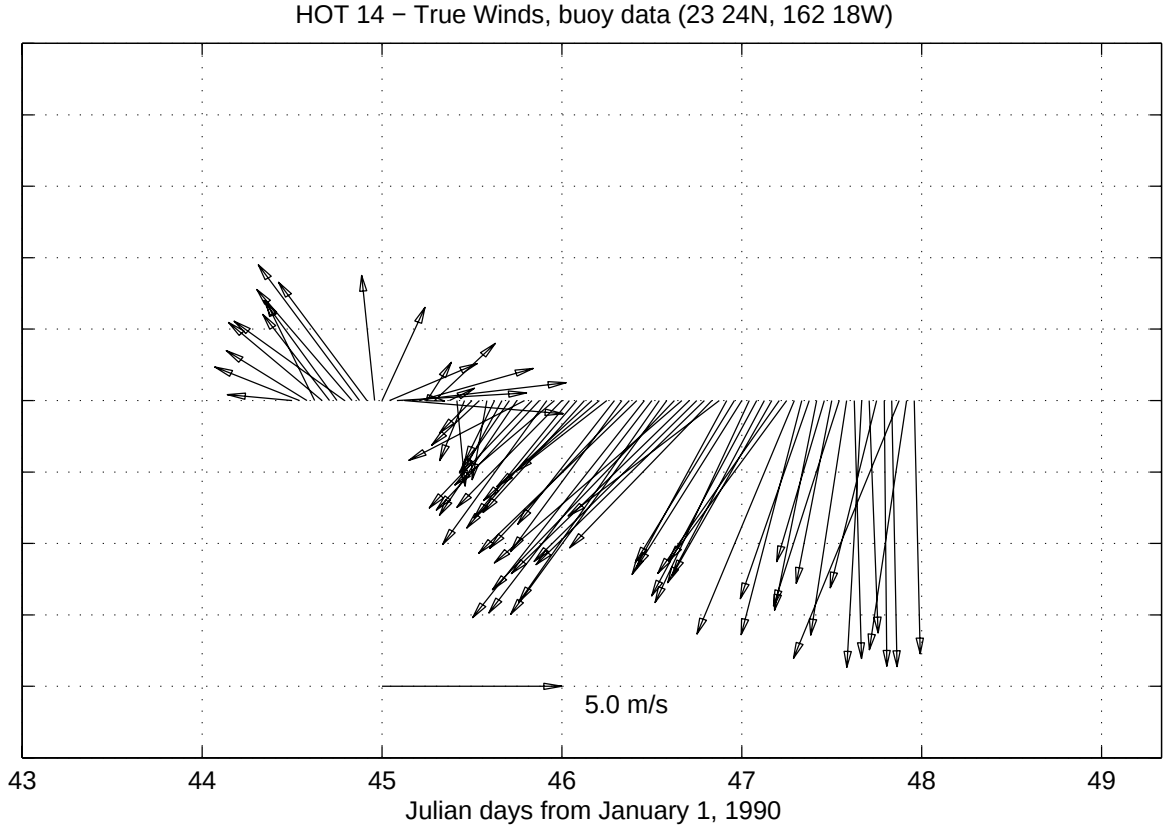
HOT 14 − True Winds, buoy data (23 24N, 162 18W)
5.0 m/s
43
44
45
46
47
48
49
Julian days from January 1, 1990

Figure 6.5.3

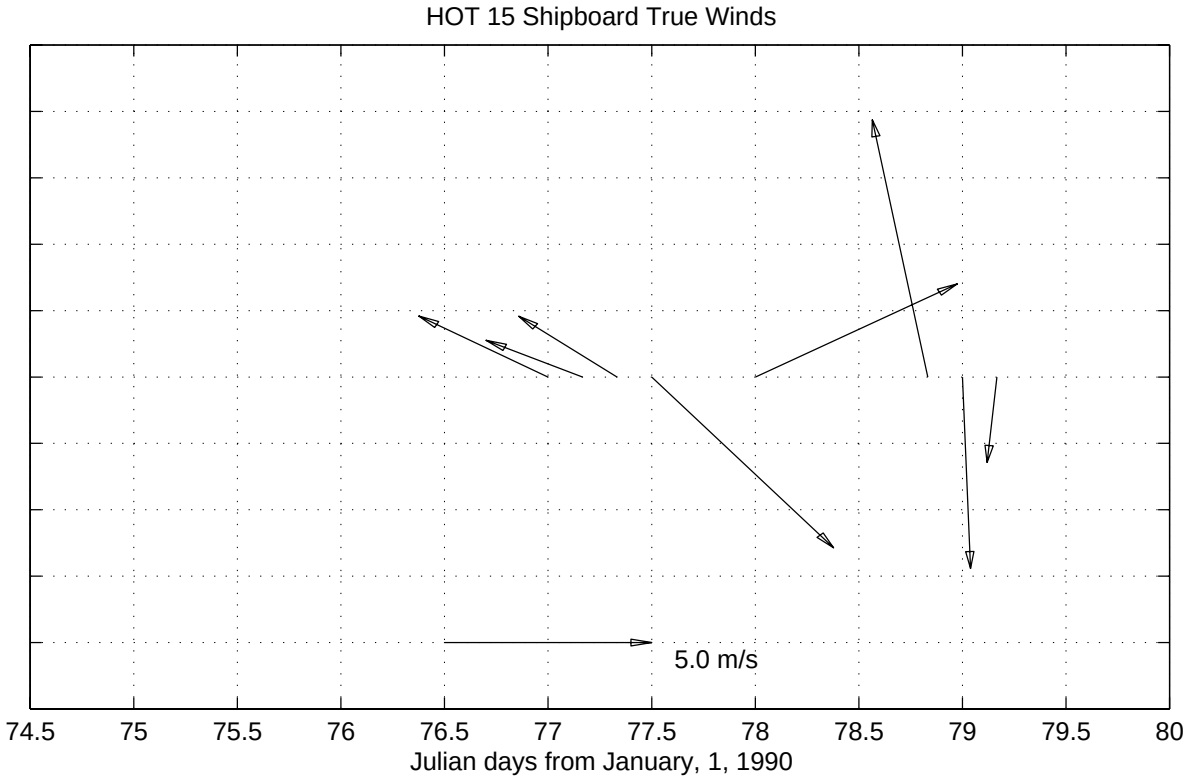
HOT 15 Shipboard True Winds
5.0 m/s
74.5
75
75.5
76
76.5
77
77.5
78
78.5
79
79.5
80
Julian days from January, 1, 1990

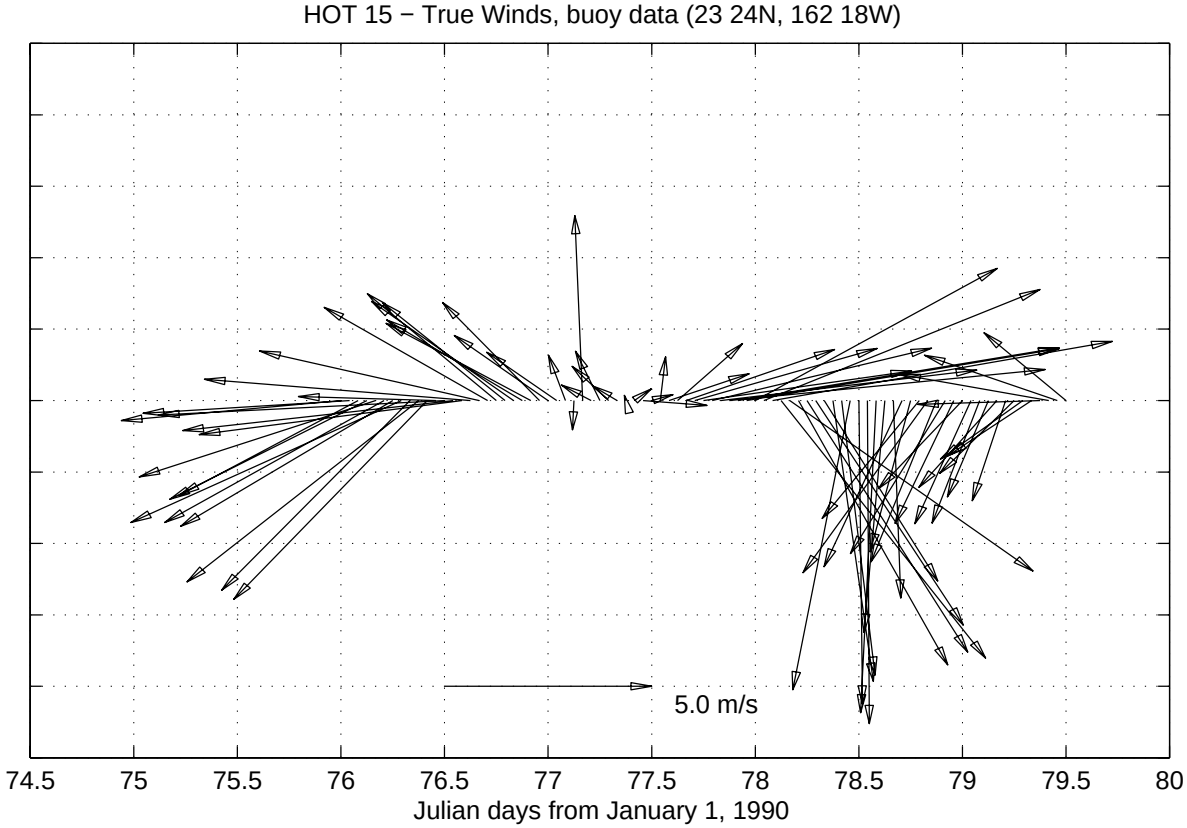
HOT 15 − True Winds, buoy data (23 24N, 162 18W)
5.0 m/s
74.5
75
75.5
76
76.5
77
77.5
78
78.5
79
79.5
80
Julian days from January 1, 1990

Figure 6.5.4

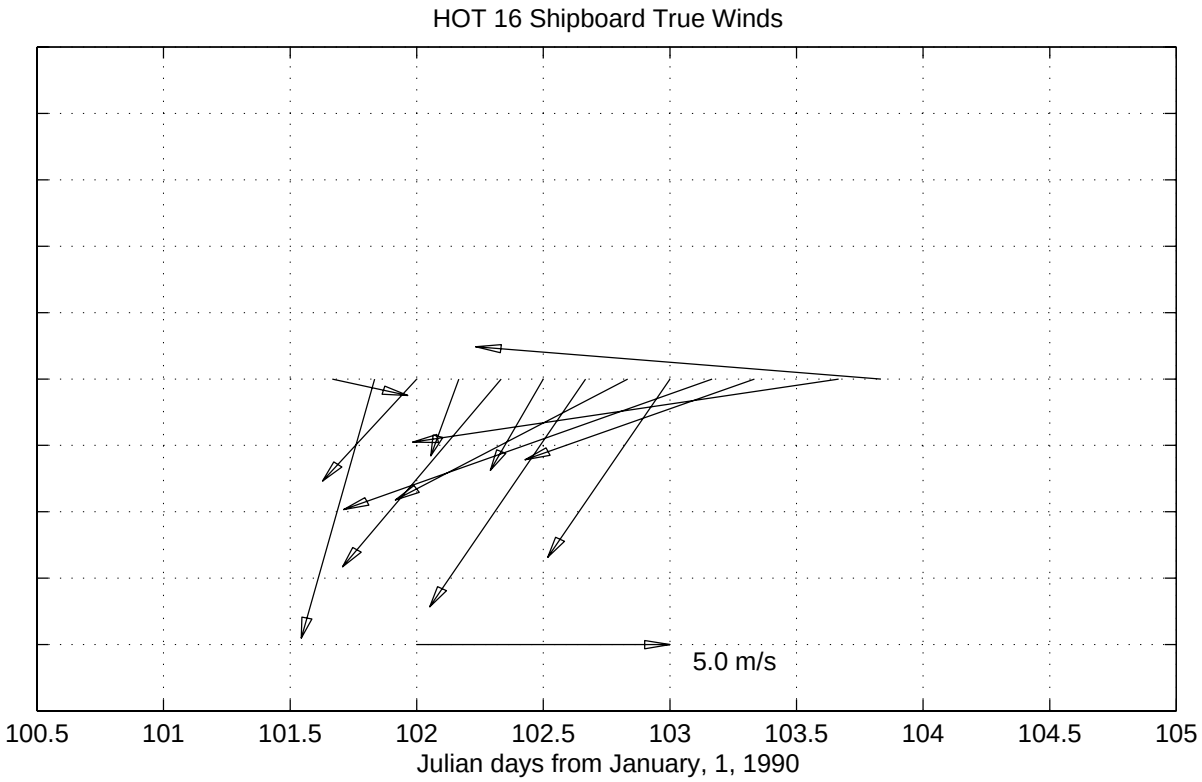
HOT 16 Shipboard True Winds
5.0 m/s
100.5
101
101.5
102
102.5
103
103.5
104
104.5
105
Julian days from January, 1, 1990

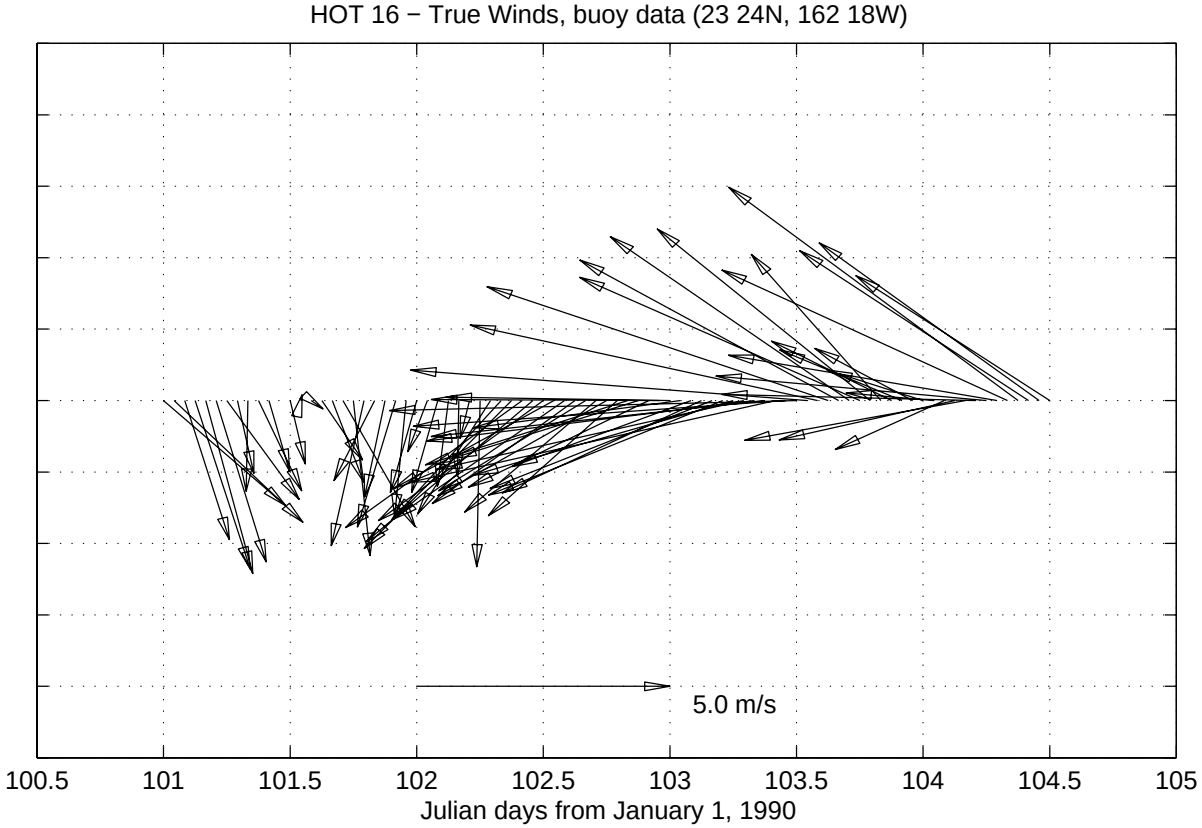
HOT 16 − True Winds, buoy data (23 24N, 162 18W)
5.0 m/s
100.5
101
101.5
102
102.5
103
103.5
104
104.5
105
Julian days from January 1, 1990

Figure 6.5.5

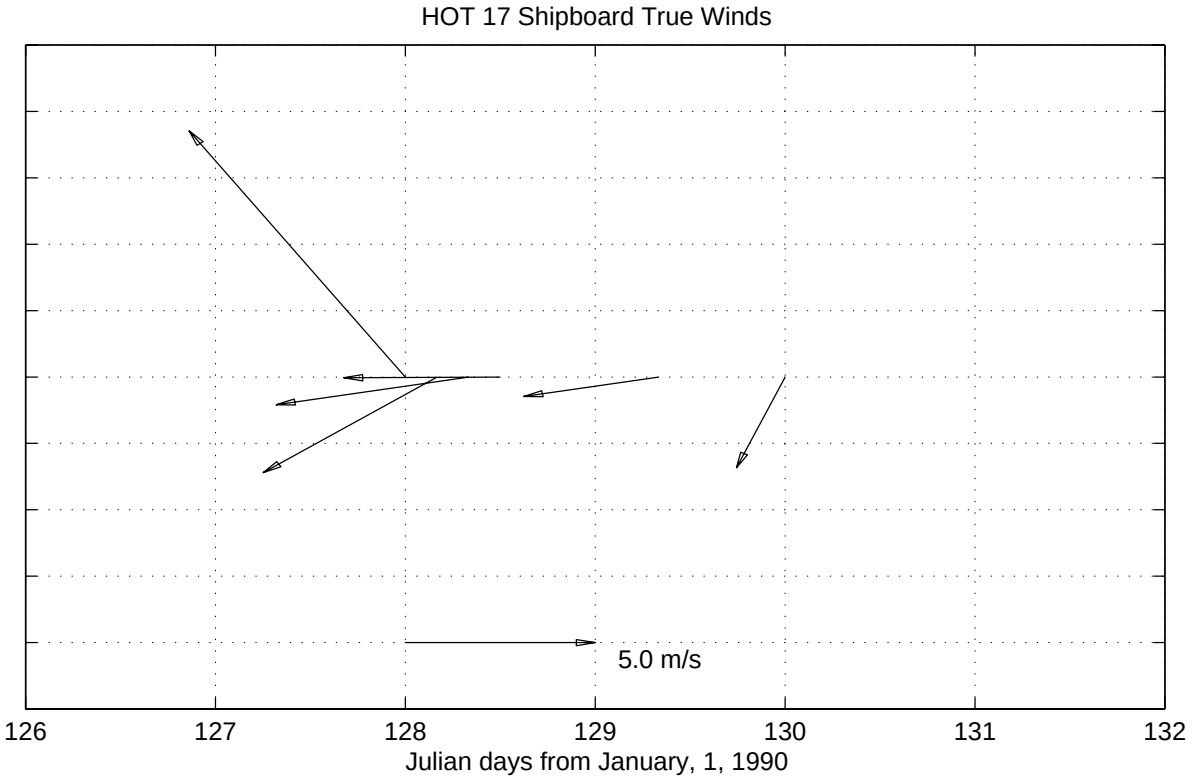
HOT 17 Shipboard True Winds
5.0 m/s
126
127
128
129
130
131
132
Julian days from January, 1, 1990

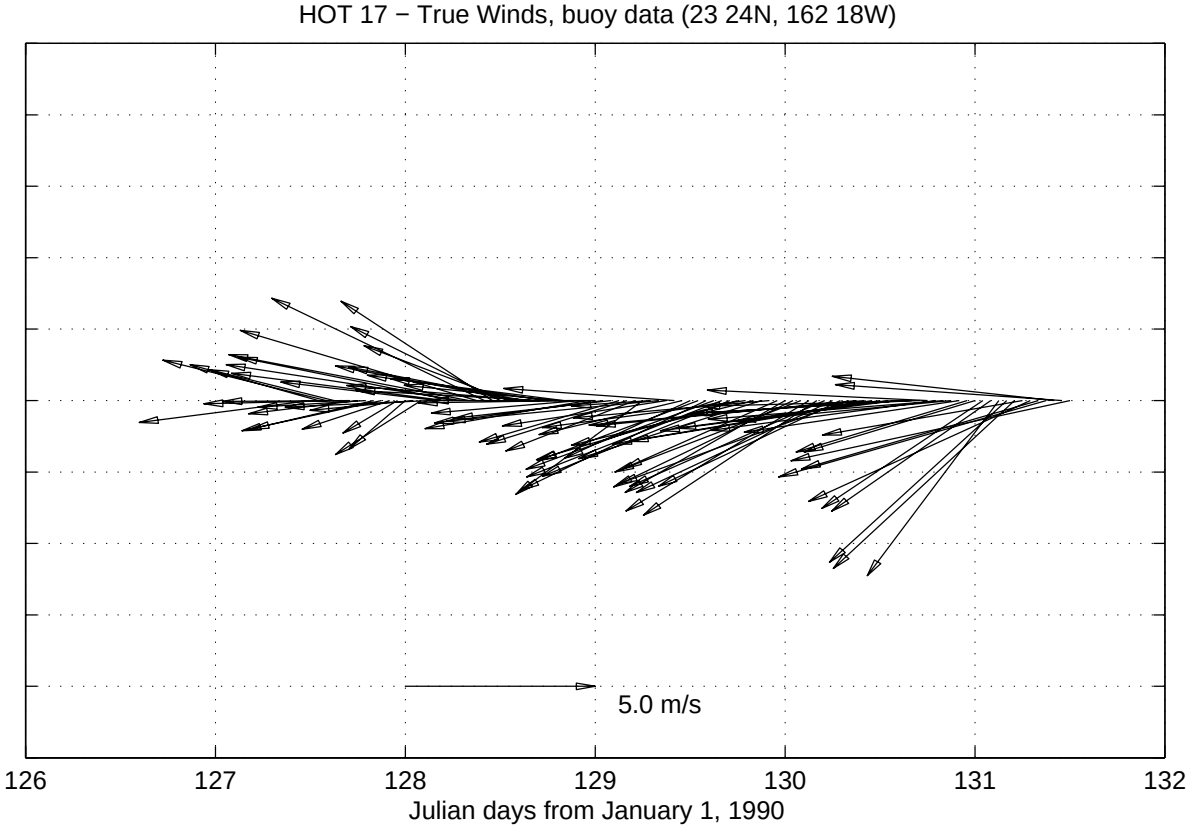
HOT 17 − True Winds, buoy data (23 24N, 162 18W)
5.0 m/s
126
127
128
129
130
131
132
Julian days from January 1, 1990

Figure 6.5.6

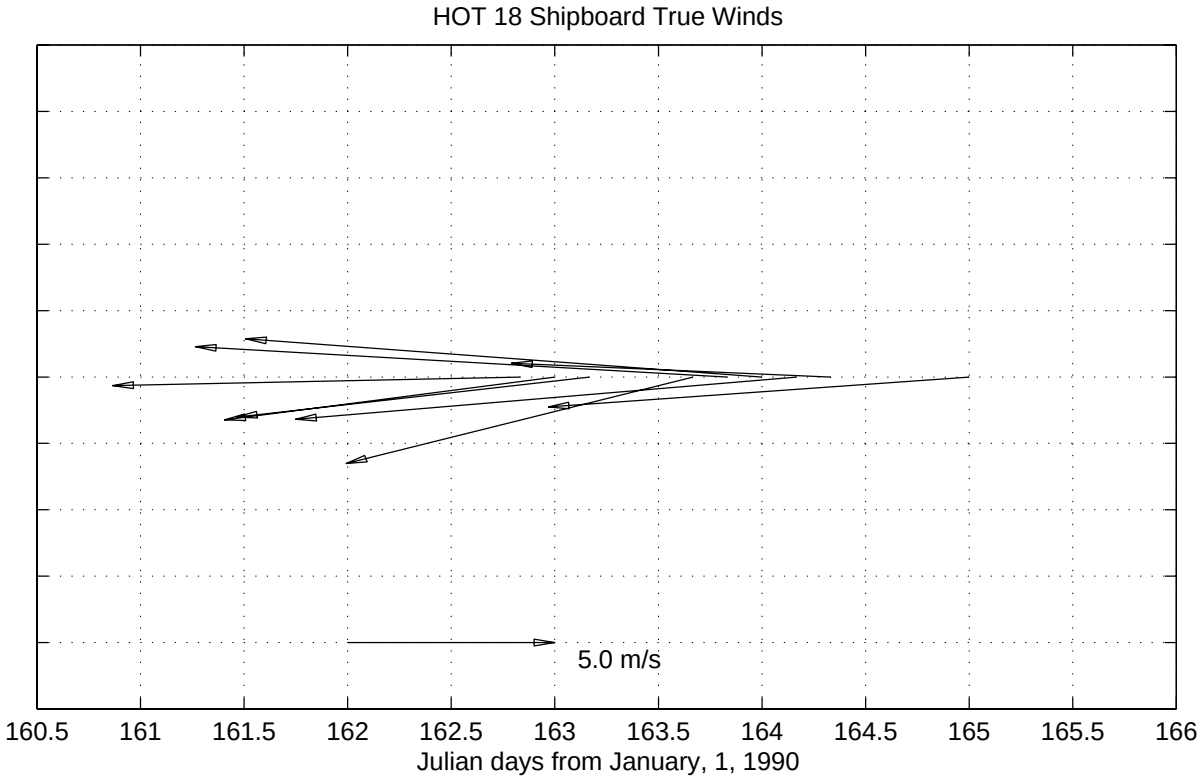
HOT 18 Shipboard True Winds
5.0 m/s
160.5
161
161.5
162
162.5
163
163.5
164
164.5
165
165.5
166
Julian days from January, 1, 1990

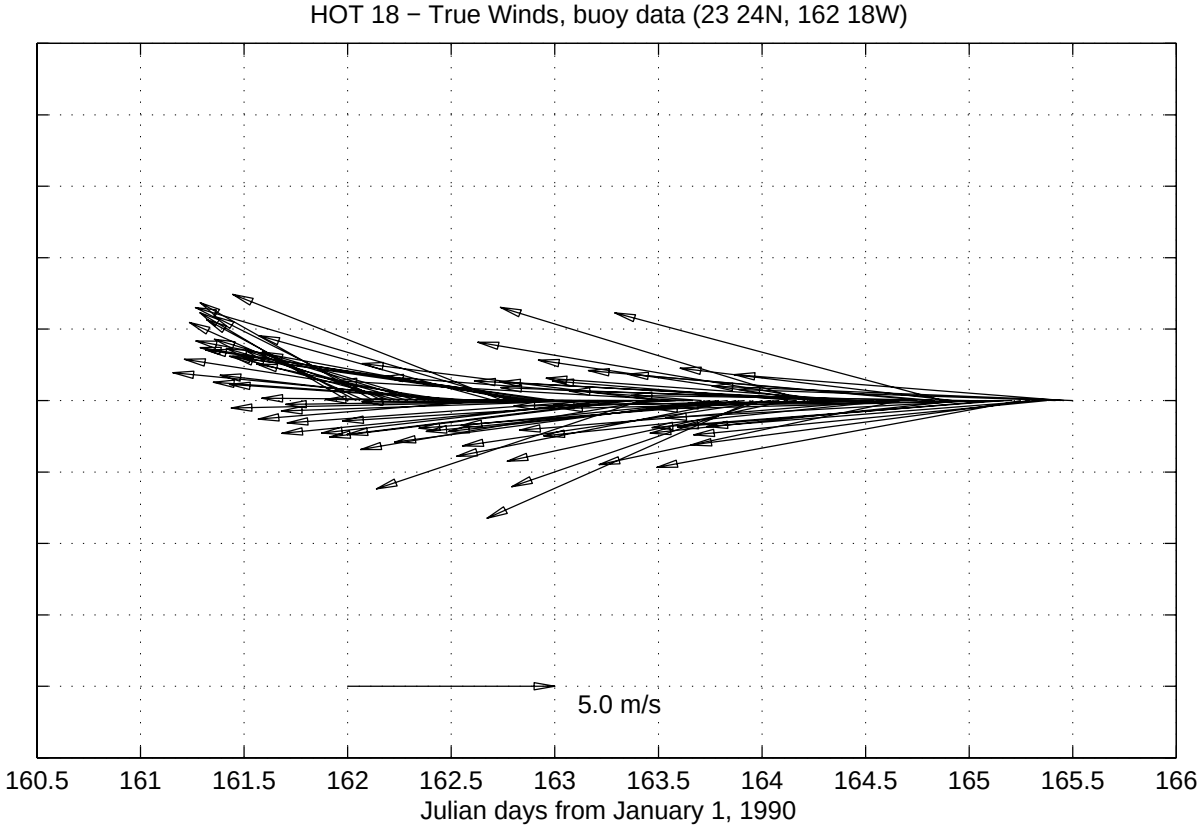
HOT 18 − True Winds, buoy data (23 24N, 162 18W)
5.0 m/s
160.5
161
161.5
162
162.5
163
163.5
164
164.5
165
165.5
166
Julian days from January 1, 1990

Figure 6.5.7

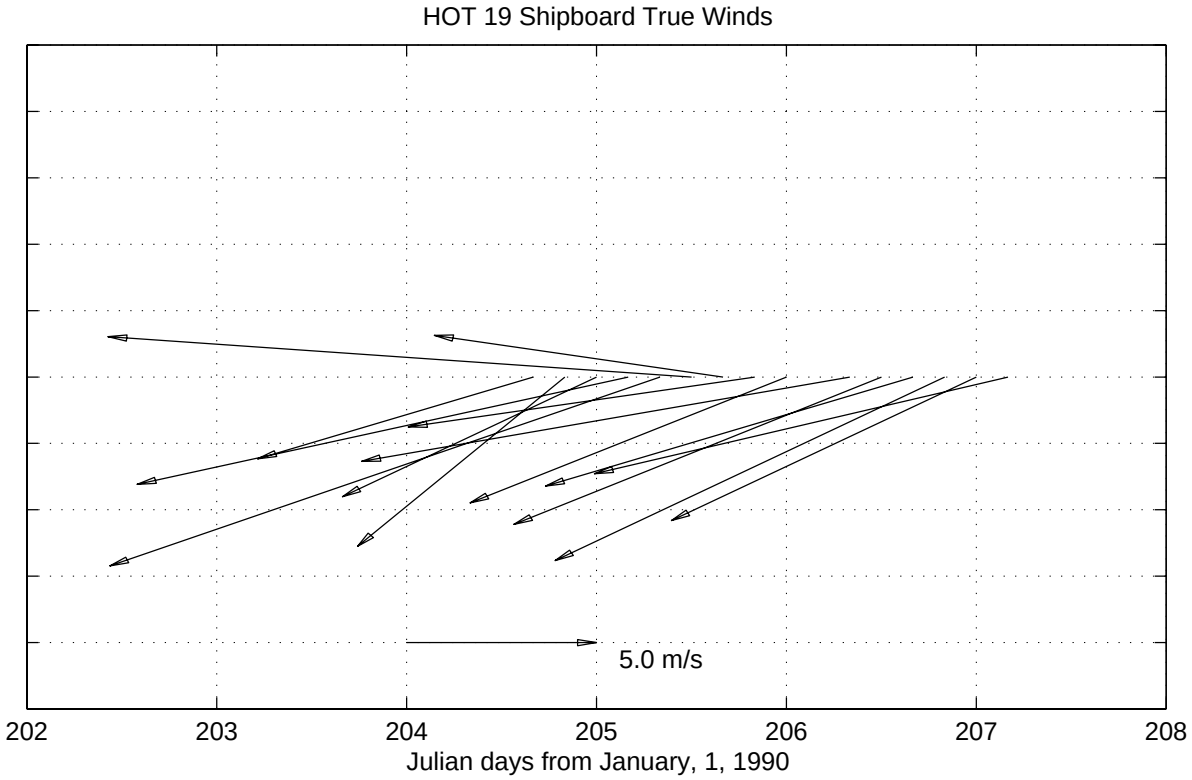
HOT 19 Shipboard True Winds
5.0 m/s
202
203
204
205
206
207
208
Julian days from January, 1, 1990

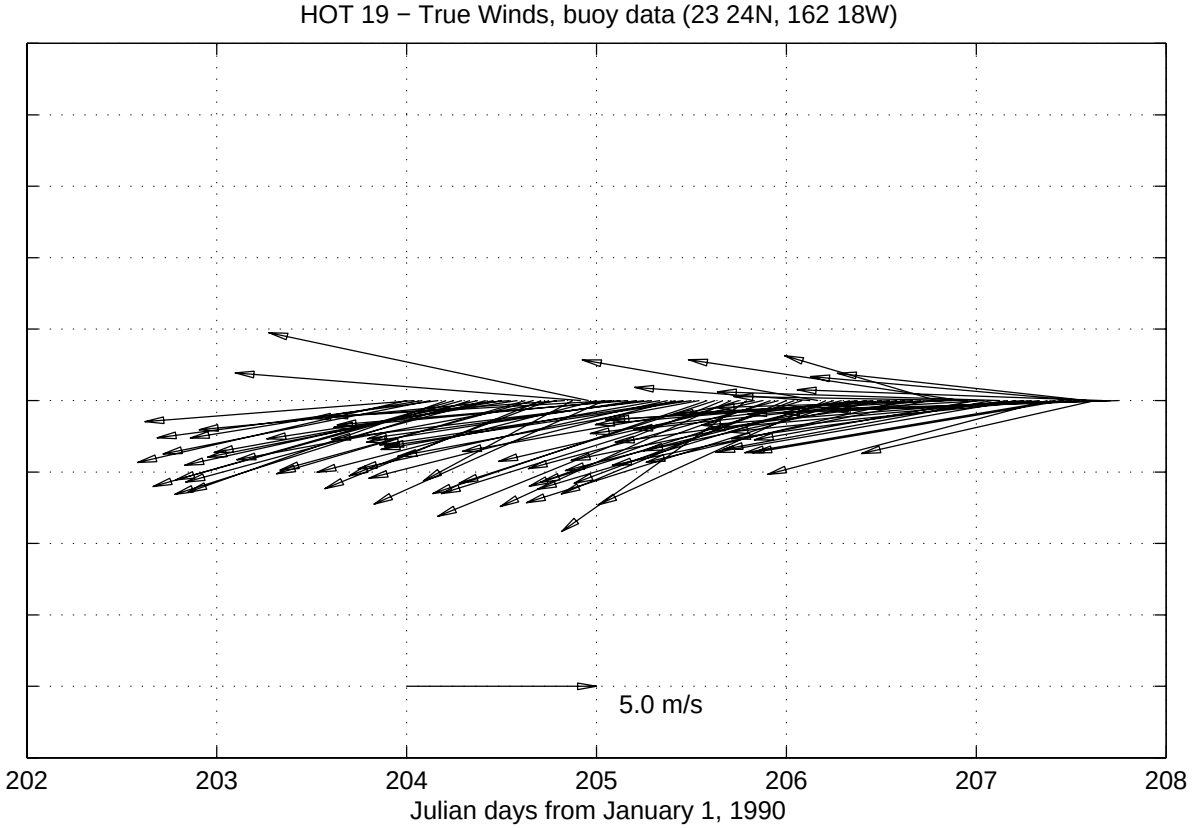
HOT 19 − True Winds, buoy data (23 24N, 162 18W)
5.0 m/s
202
203
204
205
206
207
208
Julian days from January 1, 1990

Figure 6.5.8

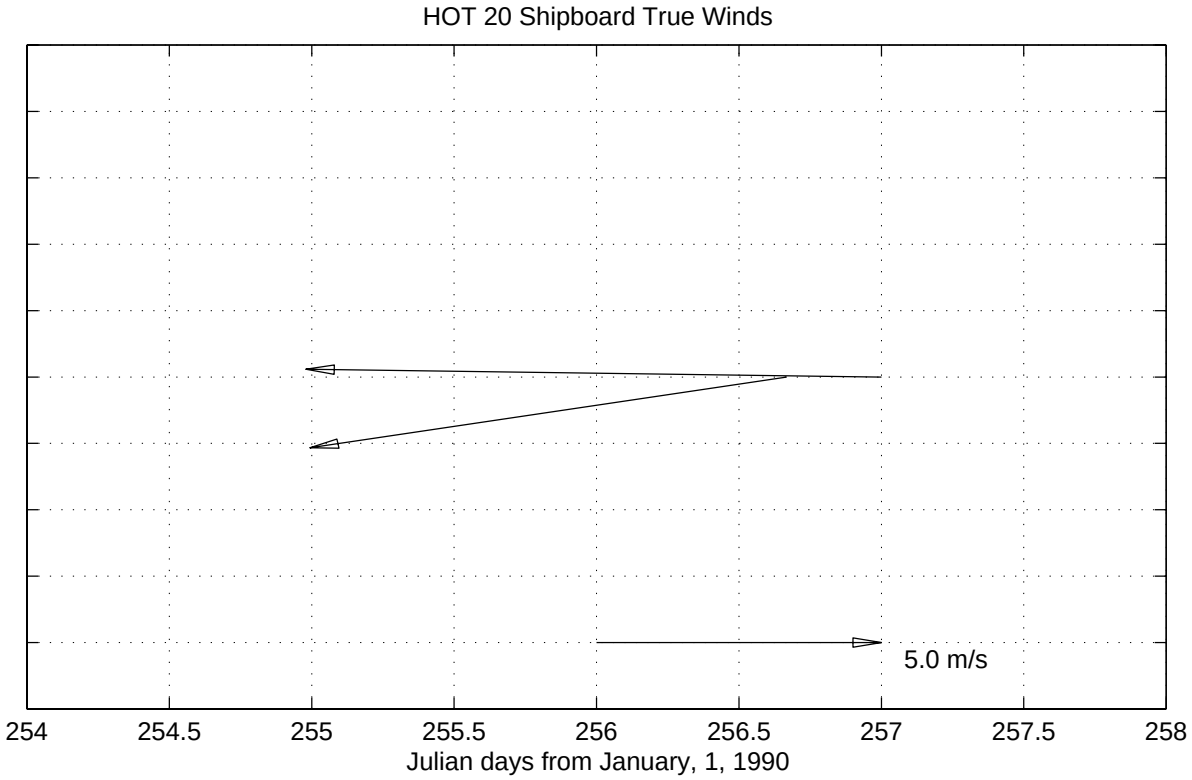
HOT 20 Shipboard True Winds
5.0 m/s
254
254.5
255
255.5
256
256.5
257
257.5
258
Julian days from January, 1, 1990

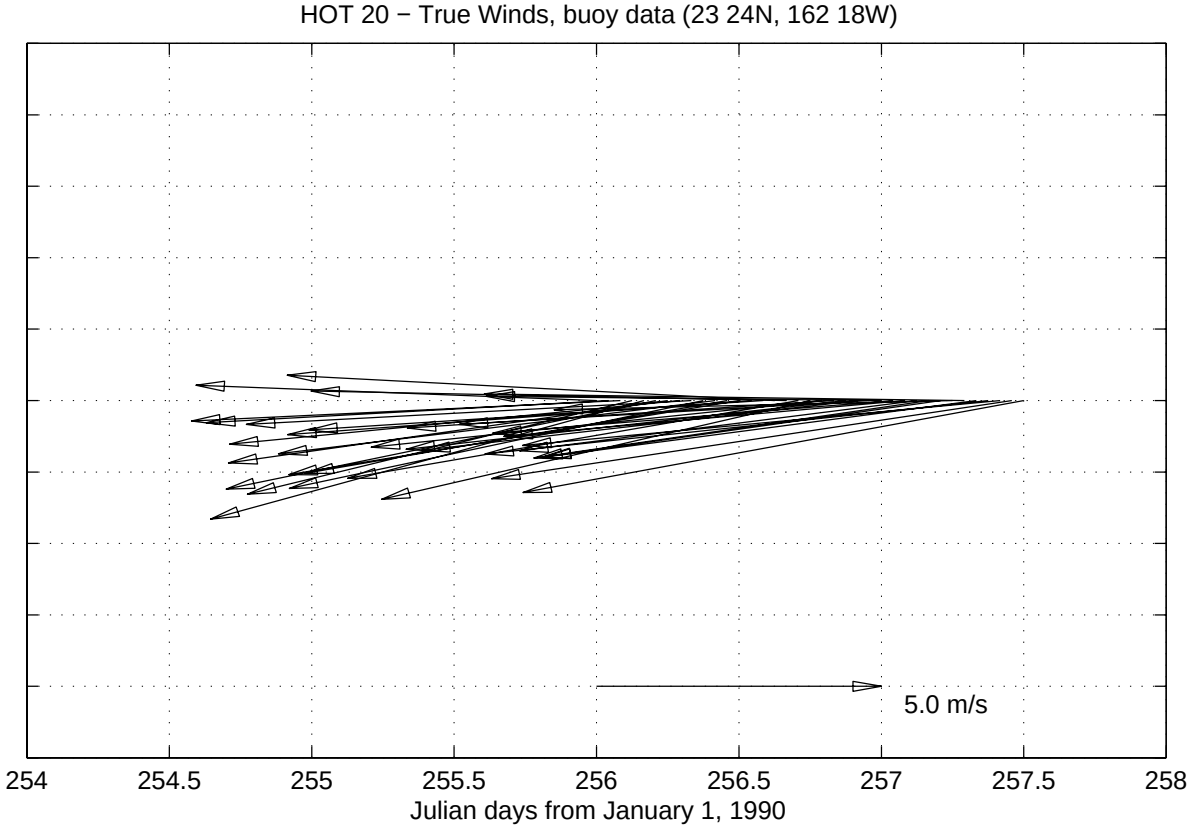
HOT 20 − True Winds, buoy data (23 24N, 162 18W)
5.0 m/s
254
254.5
255
255.5
256
256.5
257
257.5
258
Julian days from January 1, 1990

Figure 6.5.9

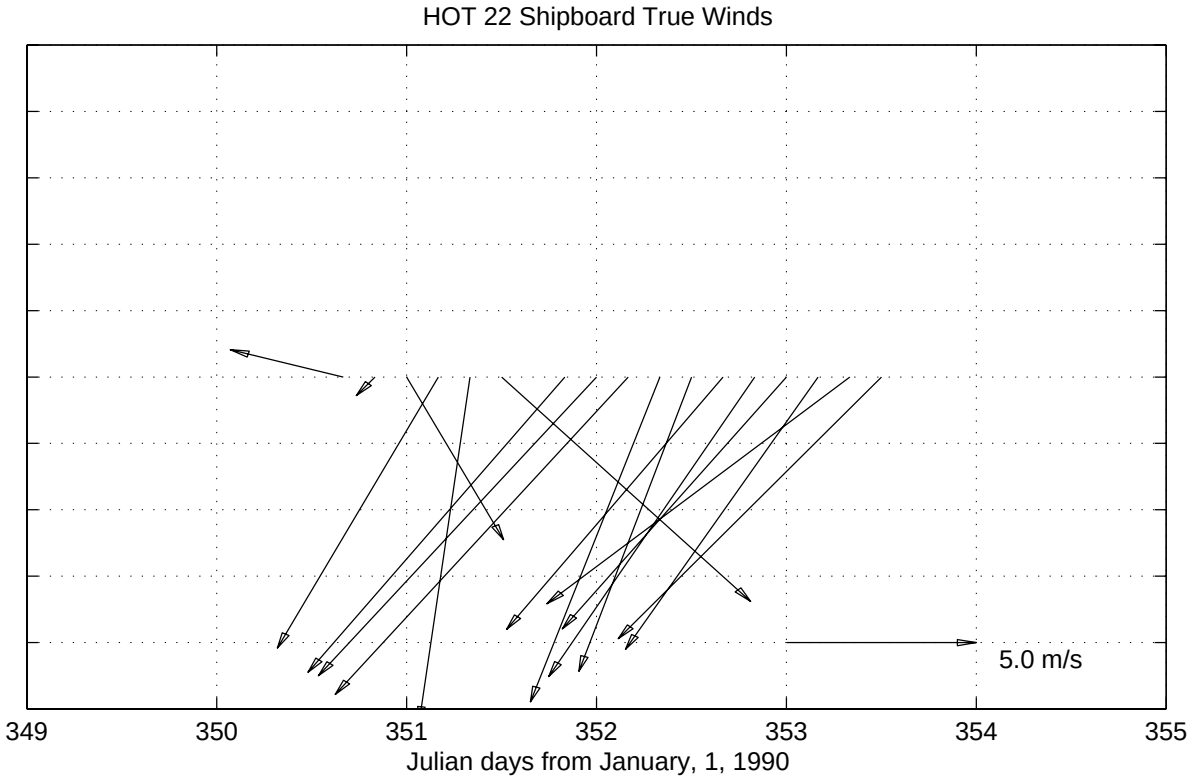
HOT 22 Shipboard True Winds
5.0 m/s
349
350
351
352
353
354
355
Julian days from January, 1, 1990

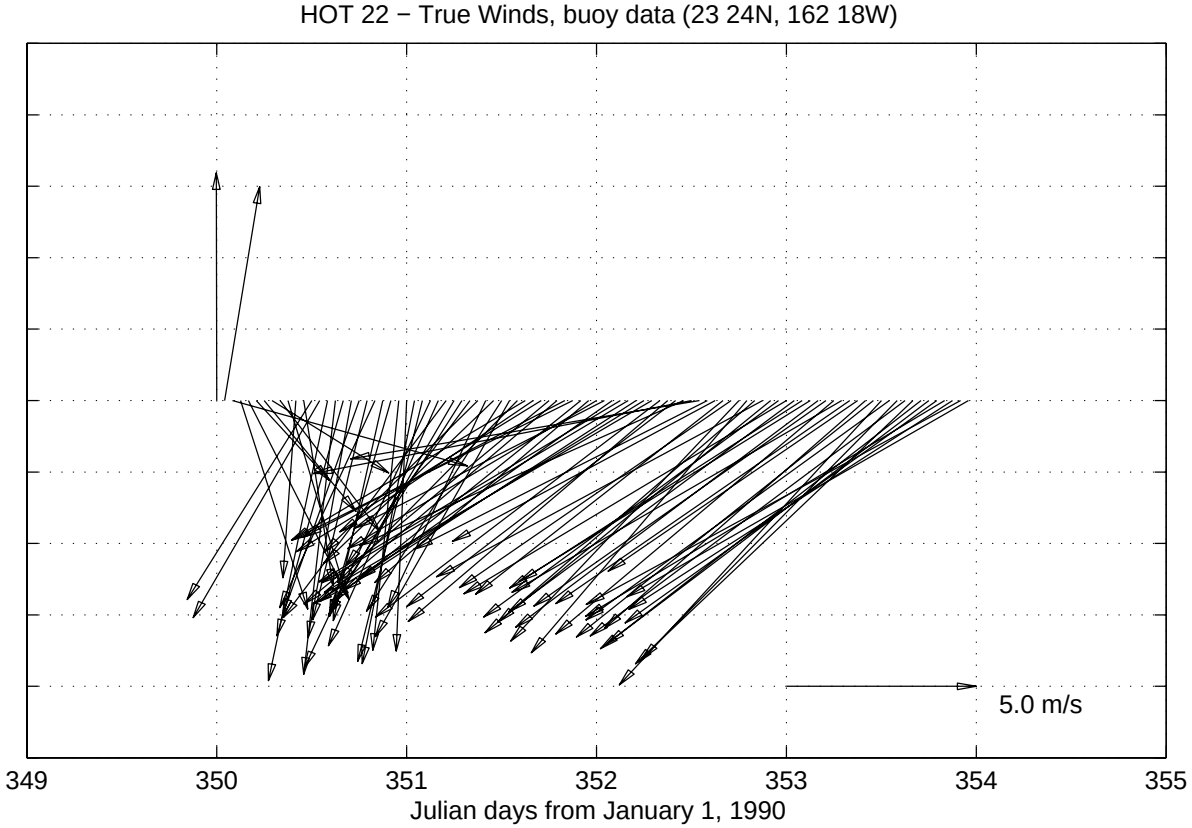
HOT 22 − True Winds, buoy data (23 24N, 162 18W)
5.0 m/s
349
350
351
352
353
354
355
Julian days from January 1, 1990

Figure 6.5.10

6.6. Optical Measurements

Figure 6.6.1a and b: Underwater irradiance expressed as a percentage of surface irradiance on HOT cruises during 1990.

Figure 6.6.1a

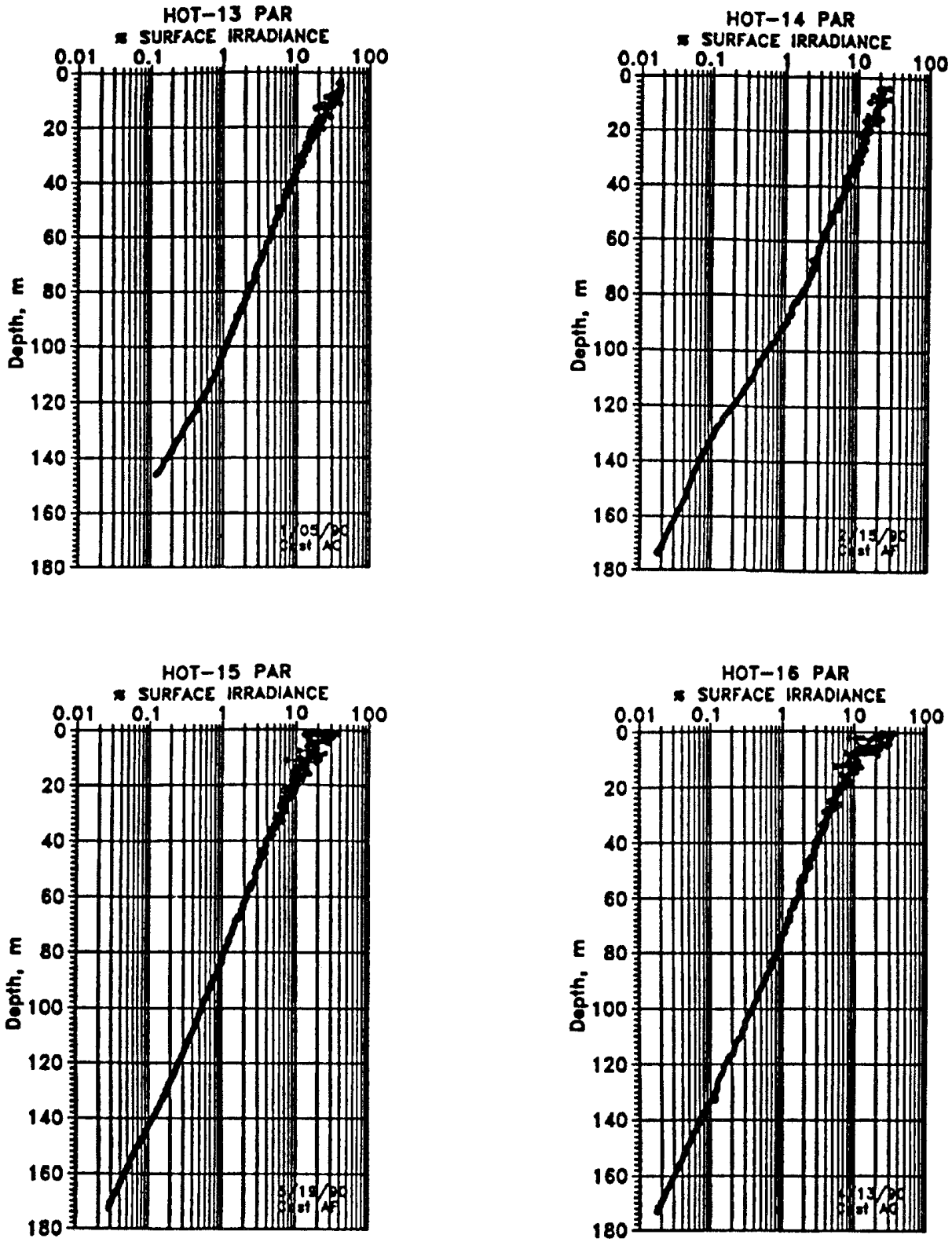
HOT-13 PAR
% SURFACE IRRADIANCE
0.01
0.1
1
10
100
Depth, m
0
20
40
60
80
100
120
140
160
180
HOT-14 PAR
% SURFACE IRRADIANCE
HOT-15 PAR
% SURFACE IRRADIANCE
HOT-16 PAR
% SURFACE IRRADIANCE

Figure 6.6.1b

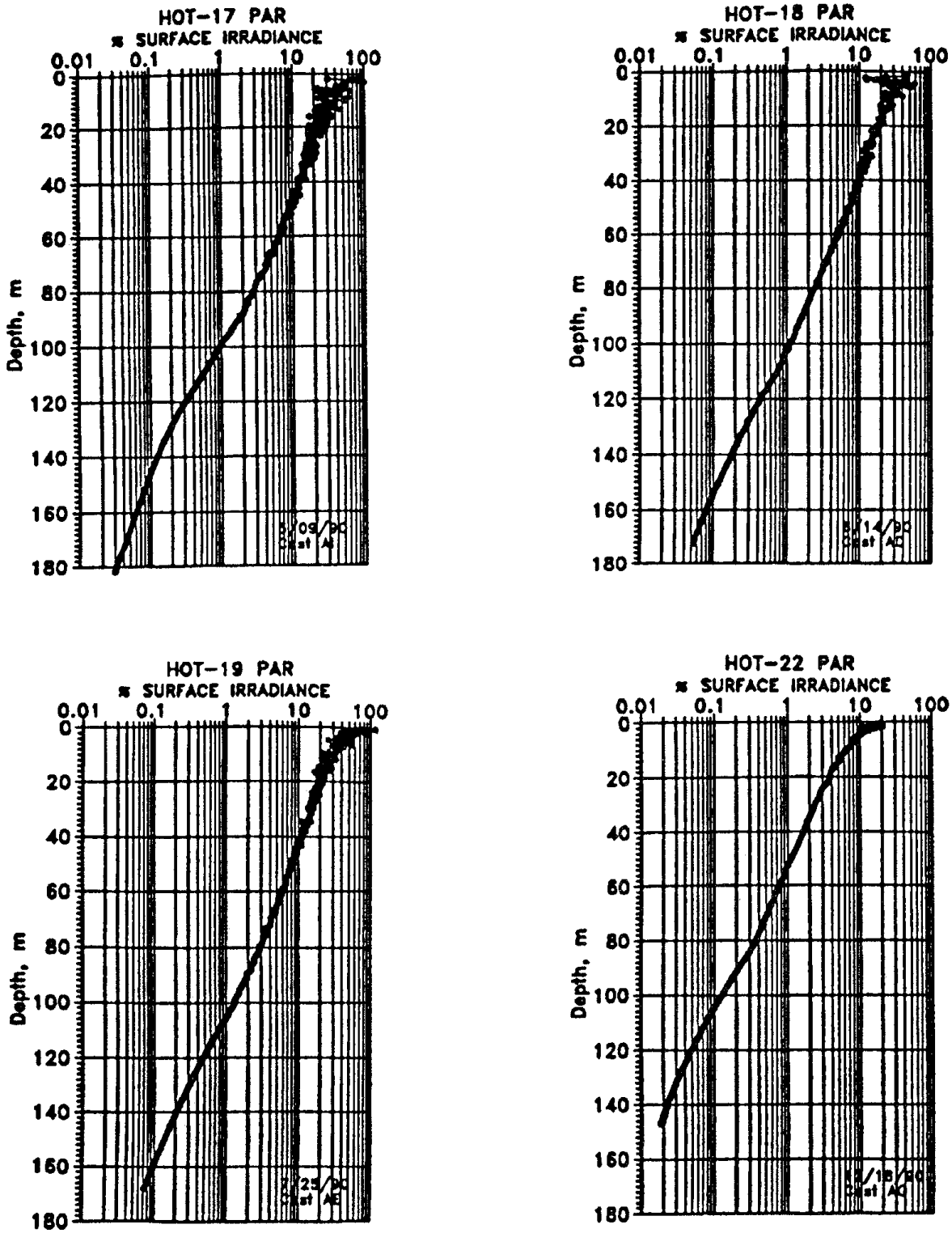
HOT-17 PAR
% SURFACE IRRADIANCE
0.01
0.1
1
10
100
Depth, m
0
20
40
60
80
100
120
140
160
180
HOT-18 PAR
% SURFACE IRRADIANCE
0.01
0.1
1
10
100
Depth, m
0
20
40
60
80
100
120
140
160
180
HOT-19 PAR
% SURFACE IRRADIANCE
0.01
0.1
1
10
100
Depth, m
0
20
40
60
80
100
120
140
160
180
HOT-22 PAR
% SURFACE IRRADIANCE
0.01
0.1
1
10
100
Depth, m
0
20
40
60
80
100
120
140
160
180

6.7. Station locations and Sediment-Trap Tracks

Figure 6.7.1: CTD station locations and sediment trap drift tracks on HOT-13. Upper panel: CTD stations represented by open circles relative to Station ALOHA. Solid lines connect casts taken in sequence and numbers show location of first and last casts. Dashed line shows area nominally defined as Station ALOHA. Lower panel: Sediment trap drift tracks. Dashed line represents drift trap assuming a direct drift between deployment and recovery location. Solid lines on subsequent figures connect positions determined from Service ARGOS.

Figure 6.7.2: As in Figure 6.7.1, except for HOT-14.

Figure 6.7.3: As in Figure 6.7.1, except for HOT-15.

Figure 6.7.4: As in Figure 6.7.1, except for HOT-16.

Figure 6.7.5: As in Figure 6.7.1, except for HOT-17.

Figure 6.7.6: As in Figure 6.7.1, except for HOT-18.

Figure 6.7.7: As in Figure 6.7.1, except for HOT-19.

Figure 6.7.8: As in Figure 6.7.1, except for HOT-20.

Figure 6.7.9: As in Figure 6.7.1, except for HOT-22.

Figure 6.7.10: Drift tracks for all sediment trap deployments during 1990.

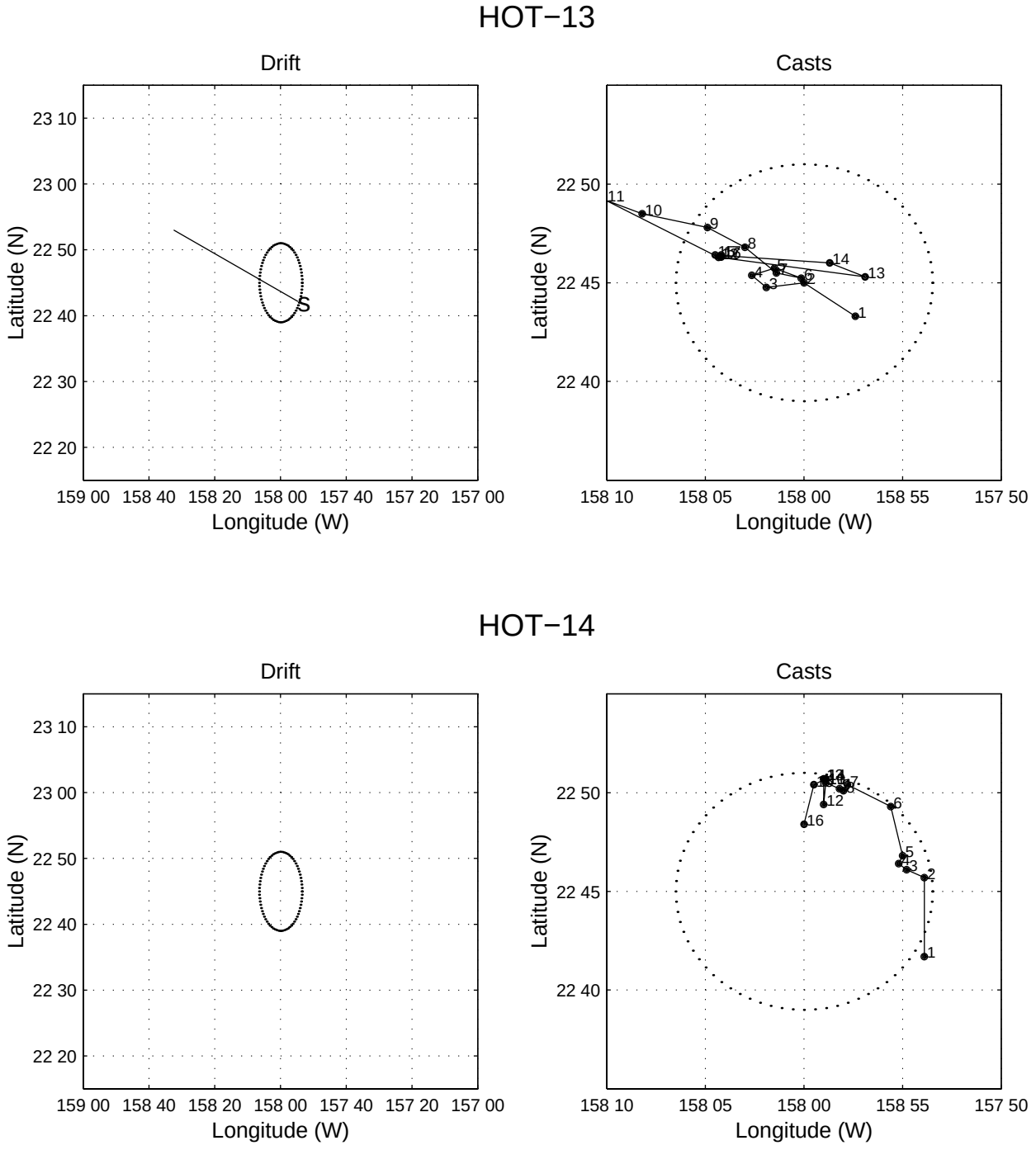

Figures 6.7.1 & 6.7.2

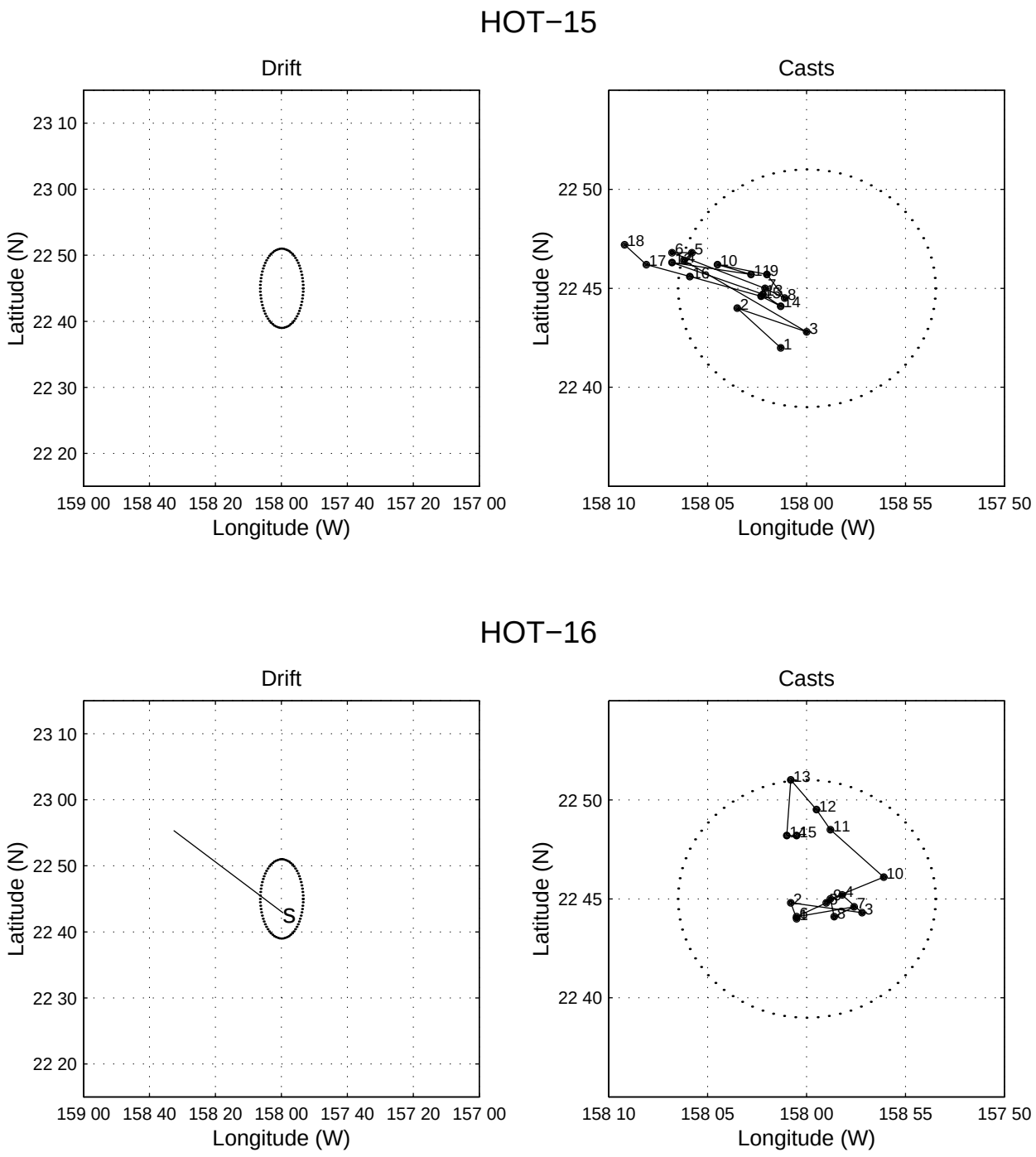

Figures 6.7.3 & 6.7.4

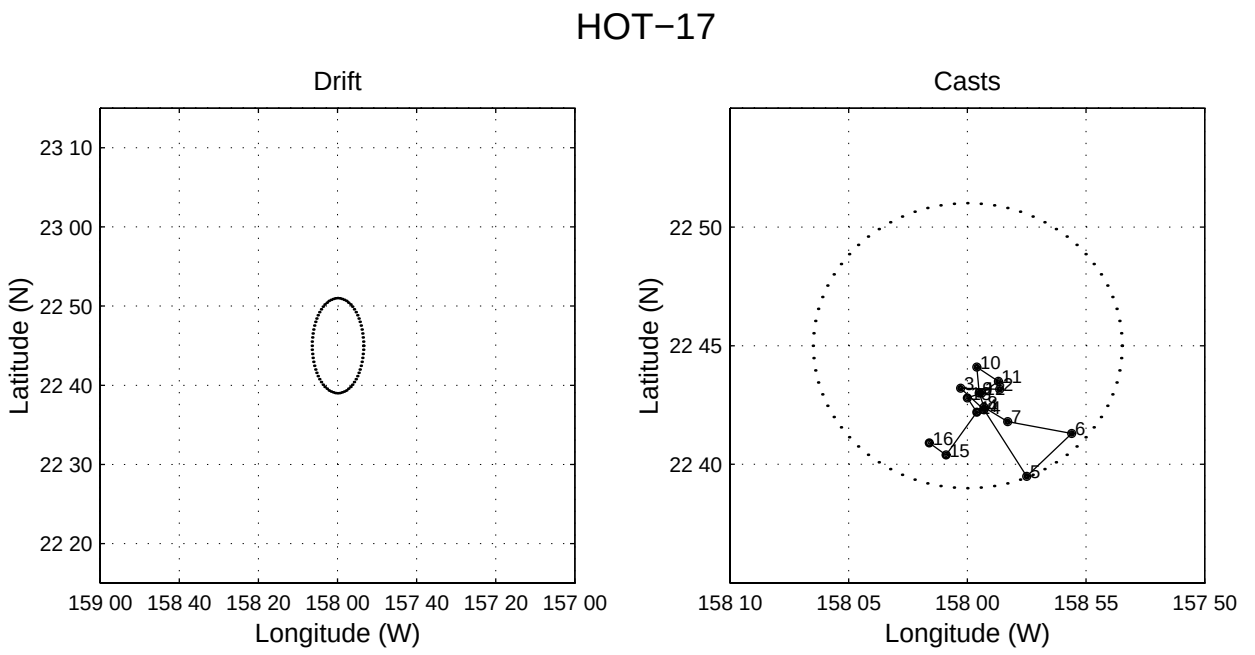

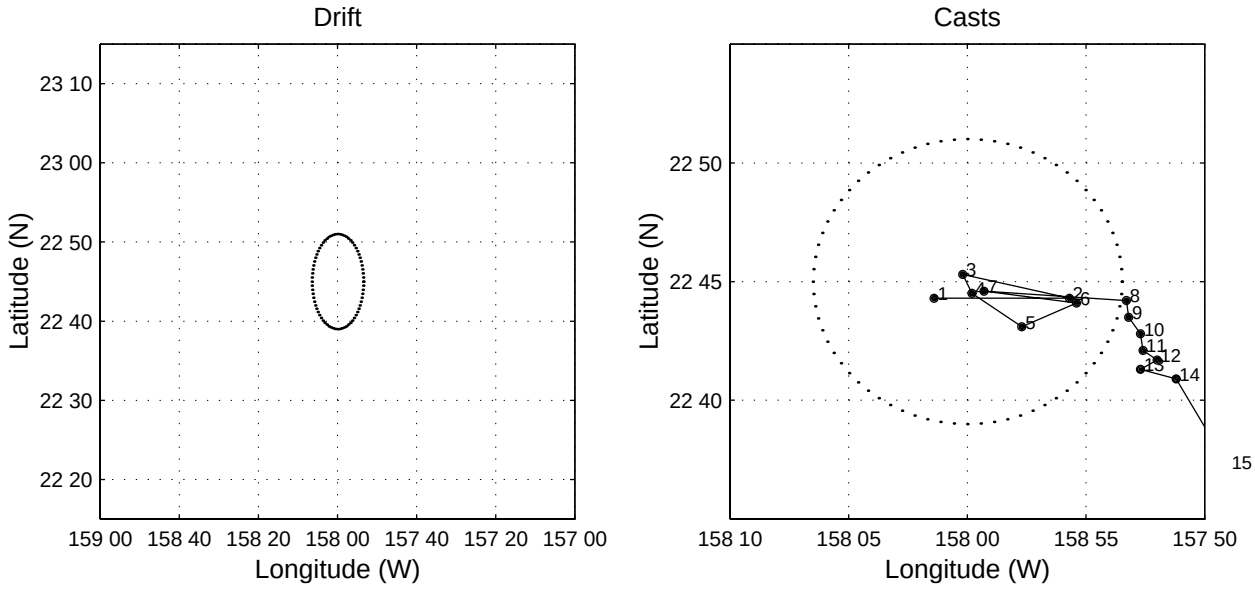

Figures 6.7.5 & 6.7.6

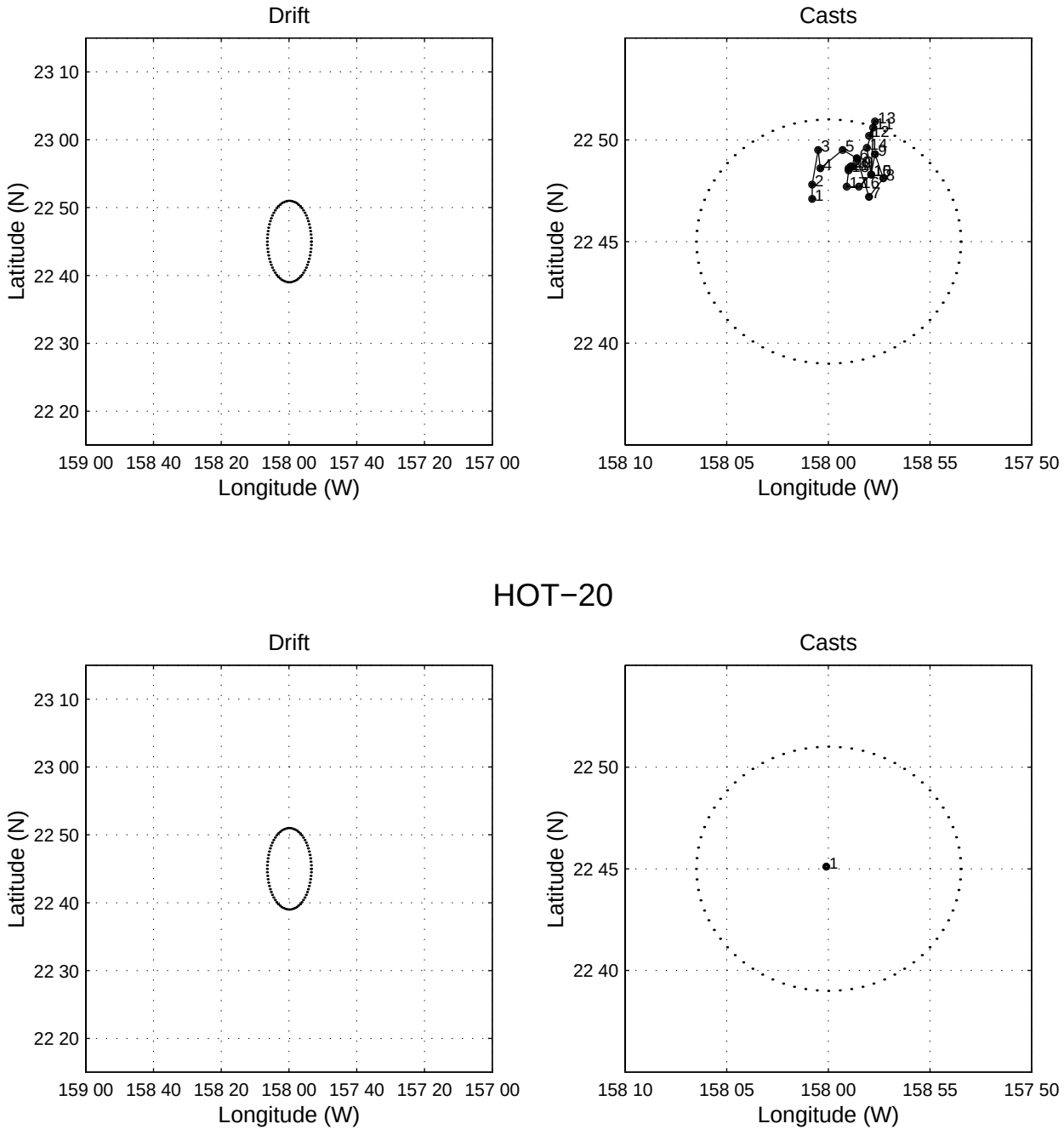

Figures 6.7.7 & 6.7.8

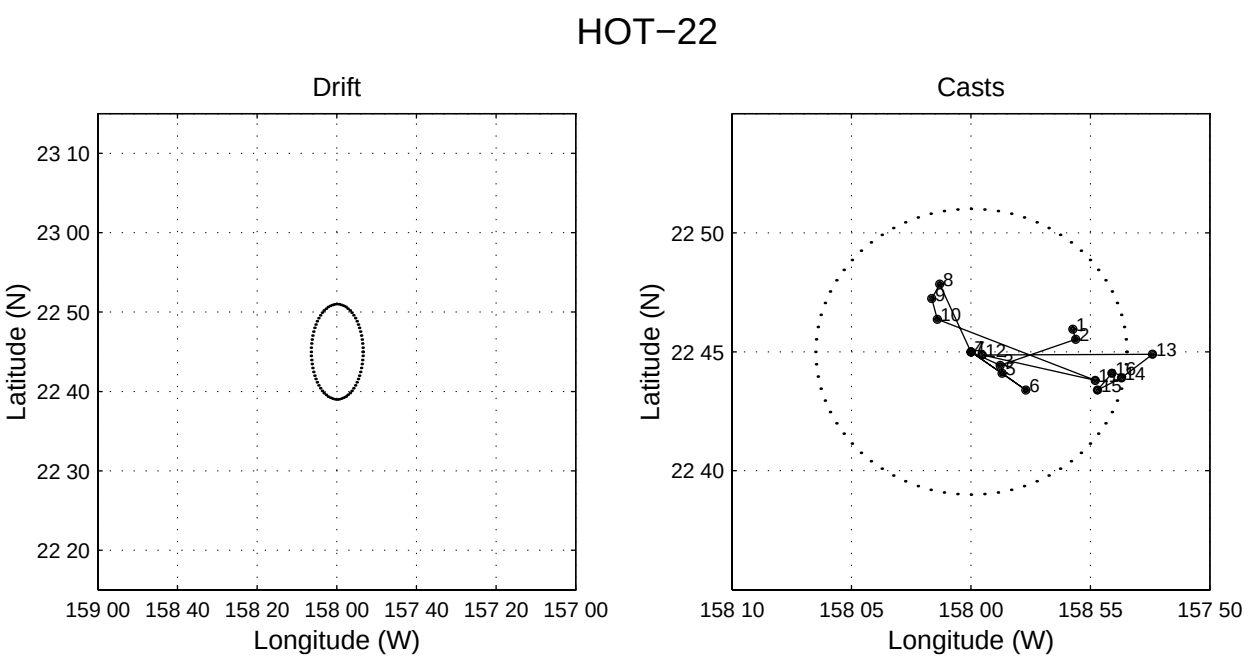
HOT−22
Drift
Casts
Latitude (N)
Longitude (W)
23 10
23 00
22 50
22 40
22 30
22 20
159 00
158 40
158 20
158 00
157 40
157 20
157 00
22 50
22 45
22 40
158 10
158 05
158 00
158 55
157 50
1
2
3
4
5
6
7
8
9
10
11
12
13
14
15
16

Figure 6.7.9

Figure 6.7.10

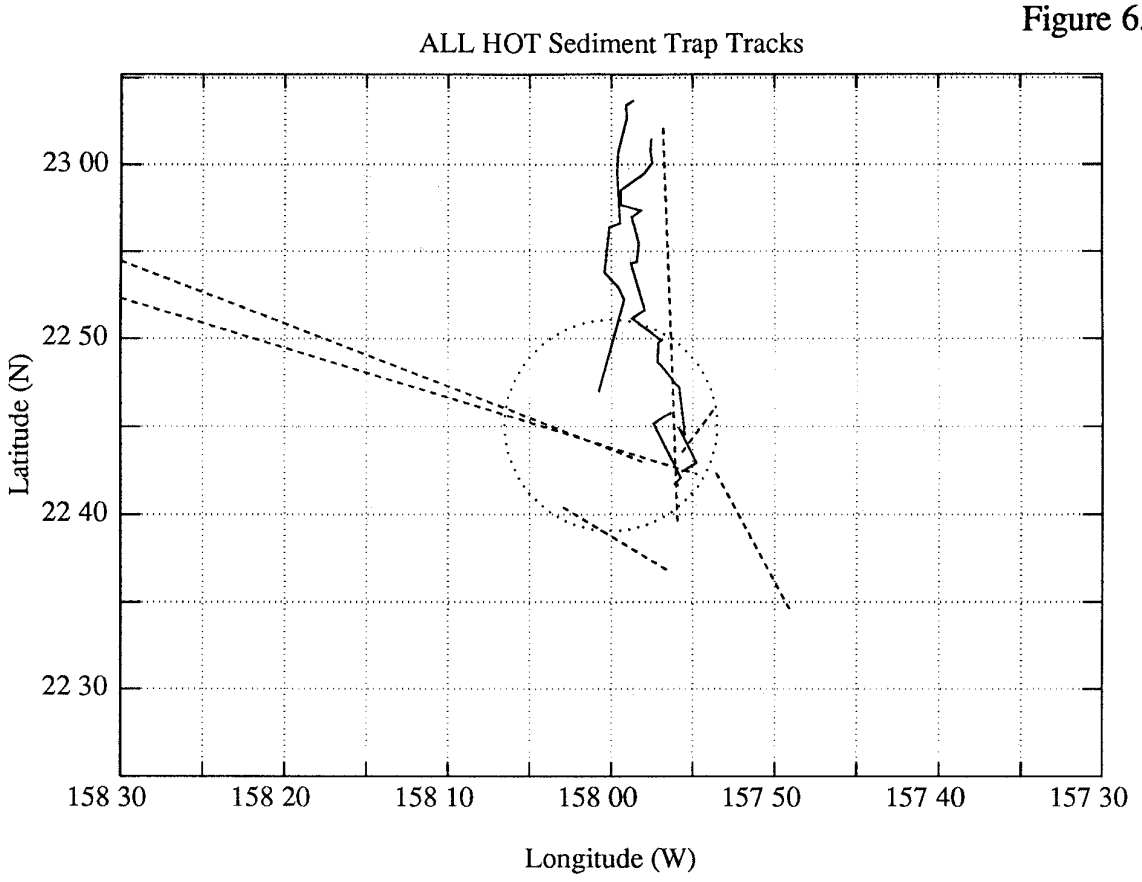

Figure 6.7.10

7. Data Availability and Distribution

Data collected by the HOT program are made available to the oceanographic community as soon after processing as possible. In order to save paper and to provide easy access to our data for prospective users, we have provided summaries of our CTD and water column chemistry data on the enclosed IBM PC 5.25" high-density floppy diskette. CTD data at NODC standard pressures for temperature, potential temperature, salinity, oxygen, and potential density are provided in ASCII files; water column chemistry data are provided in Lotus 1-2-3™ files. The pressure and temperature reported for each water column chemical measurement sample are derived from CTD temperature and pressure readings at the time of bottle trip. Densities are calculated from calibrated CTD temperature, pressure, and salinity values. Where appropriate, chemical concentrations are expressed per kilogram as described in Section 2.2. With the exception of the results of replicate analysis, all water column chemical data collected during 1990 are given in these data sets.

These data included in the Lotus 1-2-3™ files have been quality controlled and the flags associated with each value indicate our estimate of the quality of each value. The text file readme.txt gives a description of data formats and quality flags.

A more complete data set, containing data collected in both the year 1 and year 2 data HOT program data reports, as well as 2 dbar averaged CTD data, are available from two sources. The first is through NODC in the normal manner. The second source is via the world-wide Internet system. The data reside in a data base on a workstation at the University of Hawaii, and may be accessed using anonymous ftp on Internet.

In order to maximize ease of access, the data are in ASCII files. File names are chosen so that they may be copied to DOS machines without ambiguity. (DOS users should be aware that Unix is case-sensitive, and Unix extensions may be longer than 3 characters.)

The data are in a subdirectory called /pub/hot. More information about the data base is given in several files called Readme. * at this level. The file `Readme.first` gives general information on the data base; we encourage users to read it first.

The following is an example of how to use ftp to obtain HOT data. The user's command are denoted by underlined text, while the computer's responses are denoted by regular text. The workstation's Internet address is `mana.soest.hawaii.edu`, or 12 8.171.151.9 (either address should work).

prompt> ftp 128.171.151.9

Name (.....) : anonymous

Password: type your own Internet address

ftp> cd /pub/hot

ftp> ls

A directory of files and subdirectories will appear here.

ftp> get Readme.first

ftp> quit